PEPTIDES AND PROTEINS: ANTI-VIRALS TO NOVEL MATERIALS

By

Scott A. Miller

Dissertation

Submitted to the Faculty of the

Graduate School of Vanderbilt University

in partial fulfillment of the requirements

for the degree of

DOCTOR OF PHILOSOPHY

in

Chemistry

May, 2006

Nashville, Tennessee

Approved:

Professor David W. Wright

Professor James E. Crowe Jr.

Professor Brian O. Bachmann

Professor Carmello J.Rizzo

Professor Eva Harth

Dedicated to my family,

especially Mom,

who earned this as much as I did.

ACKNOWLEDGEMENTS

Well, it has been a long and winding road from the womb to Ph.D. I have had the privilege of interacting with several intriguing and helpful people along the way. The first group of people is my family. My parents, Kenneth Alan Miller and Linda Ann Miller, have always been there for my sister Karen and me. They gave me a head start and put us in contact with the right people while sacrificing themselves. One of these people is Burke 'big daddy' Swearingen, who has kept up with me and tried his best to keep me on the straight and narrow since middle school. As for this document, my dad's grammar coaching and my mother's priceless information and hard work with desktop publishing were the final pieces to the puzzle. My wife, Amanda Kelley Miller, has put up with a lot from me, but she is still here and I thank her for her incredible work ethic at her own schooling and full time job as a registered dietician at Baptist Hospital. She has bestowed upon me Nina and Bacari, our mismatched pair of dogs. Nina, our old toothless cockapoo, has literally been by my side to lend me a smile and tail wag for inspiration, and Bacari, our big weenie ridgeback, is slowly starting to join the family after two years here. My maternal grandfather Hewitt Goodman was always willing to put me to work on his boat shrimping and fishing for some much needed stress relief. The family unit owes a great deal of gratitude to my paternal grandmother Mary Belle Harvey for the good food and ability to keep us all coming together and staying in touch.

The next group of people I came across was coworkers and advisors in chemistry. I need to thank my undergraduate advisor who guided me through the minefield of chemical research. Dr. Norris Hoffman gave me my first chance to work in a lab and

learn the real art of chemistry on a budget. His additional advice and friendship has helped carry me through my post-graduate experience as well. Ah yes, and this brings me to the group most responsible for me writing this dissertation, the Wright group.

Where to begin and how to keep this short? Dr. David Wright (a.k.a. DW, bossman, *&%$, and !@#*%) has been a great preceptor, advisor, and friend during our five years together. I thank him for finding a way to get me in his first crop of Vanderbilt students when I was thinking of transferring. He gave me the opportunity to push myself as only he can: 'just figure it out, Scott!' This may have been the best advice I heard, although not at the time. I learned a lot about details and my own abilities as I tackled instrument repair, massive projects I had no business attempting, and undergraduate mentoring. He also tried his best to teach me how to write, but if I see one more 'poor transition' comment I'll scream. Finally, he introduced us to his family, the beach trips, and other events which are some of my fondest memories.

The group itself has several members worth a comment in no particular order. Dr. Crystal Miller was always there to keep me in line as required and did most of our group event planning. Clare Kenney-Carney and I have been together since our undergrad years. (If she had just told me what group she was trying to join, we could have avoided the last five years together.) Luckily, they have been fun years, and I wish her and the new baby all the best. Ah, Malgorzata Broncel – we made beautiful peptides together. She has been the best technician we could have hoped for. She put up with me teaching her peptide synthesis and for that she deserves a medal. Dr. Joe Slocik was a very simpatico conversationalist, very helpful in crystallizing nascent ideas. Dr. Marc Knecht was an early colleague whose work preceded mine, and then he was gone. Thanks to Dr.

Lisa Pasierb for teaching me some peptide synthesis and HPLC skills in the early days. Elizabeth ‘Liddy’ Bentzen has always opened her home and mind to us and has been an invaluable friend and coworker along the way. We do well together to bounce and refine ideas off of each other. Aren Gerdon was often stowed away in the Cliffel lab, but when he came out, it was a blast. Sarah Sewell tried her best to organize the lab, although we usually were not very cooperative. Stephen Reese Harry, a mighty fine worker and others of the newer members of the lab, Ryan, Alex, Kristin, Jonas, Melissa, and Leila, thanks for the fun we had in our brief time together. I will remember you, and hopefully we can generate our own stories as I am only going to the next building over.

We could not have pulled this all off without the help of collaborators. Many thanks go to the William’s lab headed by John V. Williams. Gabi was able to collect the hMPV F protein, and Sharon was critical for all her tedious and time consuming work on the fusion assays. The Crowe lab supplied us with a wealth of cell and viral knowledge. Dr. Jarrod Smith gave helpful conversations on computer modeling, Dr. Donald Stec played some softball with us in between NMR conversations and aid. Markus Voehler was kind enough to run some of the peptide NMR experiments.

Special thanks go out to Chris Rector and Mike Bowers as we always helped each other move when needed. Chris was also kind enough to pick me up on the side of the road, and Mike was kind enough to help me fix and maintain my truck.

TABLE OF CONTENTS

LIST OF TABLES

LIST OF FIGURES

CHAPTER I

GENERAL INTRODUCTION

Introduction

Biomimicry is a growing field dedicated to applying nature's successes to solve man's problems. As a model, nature may be hard to emulate but has already solved many challenges that face today's most gifted researchers and scientists. Materials experts marvel at the silk from a spider that is several times stronger than man-made steel, yet is light and flexible. Pharmaceutical companies still cannot compete with human immune systems and antibodies when it comes to specificity and potency. Recent revelations pertaining to commonly used non-steroidal anti-inflammatory drugs (NSAIDS) offer one compelling reason why nature is ahead of the science race and that is time. Billions of years of trial and error (i.e., natural selection) have produced efficient and marvelous organisms, biological systems, and materials that have passed the test of time often dismissing man's innovations.

As man encounters ever increasing amounts of resistance and friction on his way to theoretical boundaries, feasibility becomes an increasingly important factor. High temperatures, high pressures, and caustic chemicals are often employed to obtain new materials, while effective biological and pharmaceutical discoveries are hindered by complex structures and a general deficiency in understanding the details governing the system targeted. In contrast, nature's materials are often produced in aqueous environments under ambient conditions. Specific and efficient pathways have evolved to

allow a tiny frog possession and fabrication of the world's most potent toxins, while bacteria are able to construct defense systems that neutralize man's strongest antibiotics. The goal of biomimicry is to understand and utilize nature's 'old' technology. This document explores some of the tools and potential innovations of this emerging field.

Silica Oxide from Oceanic Diatoms

Evolution has provided several organisms (e.g., diatoms, sponges, radiolaria) capable of using ubiquitous monosilicic acid in the synthesis of species specific silica based endo- and exoskeletons.[1] Diatoms are unicellular eukaryotic algae that play a crucial role in silica biogenesis throughout the world's oceans. Classified under generas *Nitzschia* and *Hantzachia*, diatoms utilize amorphous silica as structural components within their cell walls, also known as a frustule,[2] to produce elaborate and complex structures arising from predominantly two different cell shapes. Pinnate diatoms present a long and narrow morphology with an axis that traverses the length of the diatom and parallel to the plane of symmetry. In contrast, centric diatoms display radial symmetry around a lengthwise axis cutting through the center of the cell **(Figure 1)**.[3]

Biomimetic research has recently focused on the biochemical pathways utilized in the production of the diatoms biogenic silica. Silicic acid ($Si(OH)_4$), which has been found in concentrations of 70 μM within the world's oceans, is thought to be the synthetic building block of biogenic silica.[4] Silica exoskeleton generation would likely require active transport and sequestering of enough silicic acid to complete the frustule synthesis. Indeed, five different transport proteins from the cell walls of *Cylindrotheca fusiformis* have been putatively identified in active silicic acid transport.[5,6,7]

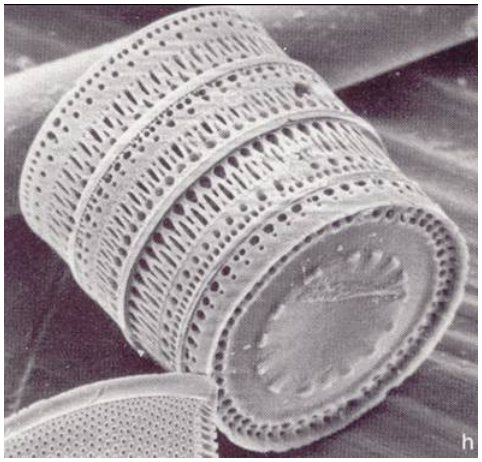

Figure 1. The diatom *P. sulcata*.[2]

The Frustule of *Coscinodiscus granii*

Frustule synthesis is unique to each diatom, which has its own unique cell wall, or frustule, structures offering a myriad of morphologies. The silica frustule protects the diatom from external forces and pressures by encapsulating the interior of the cell and is also used as a photon collector. Understanding the mechanisms involved in the biogenesis of silica is of interest to both biochemists and material scientists. The secrets of advanced material production under ambient conditions are thought to reside in the biomimicry of this process. These structures are expected to have superior properties in a wide array of applications and possibly lead to controlled nanoarchitecture.[8,9]

A group of cationic polypeptides (called silaffins) isolated from purified frustules of the diatom *Cylindrotheca fusiformis* were discovered and found to create networks of silica nanospheres within seconds of being exposed to a solution of silicic acid.[10] Also found within the frustules were several long-chain polyamines, and recent biomimetic experiments have shown that these also precipitate silica spheres *in vitro* with diameters consistent with natural diatoms.[11] A more detailed discussion of the proteins involved in

diatom biosilification and a biomimetic approach to novel materials is given below and in Chapter III.

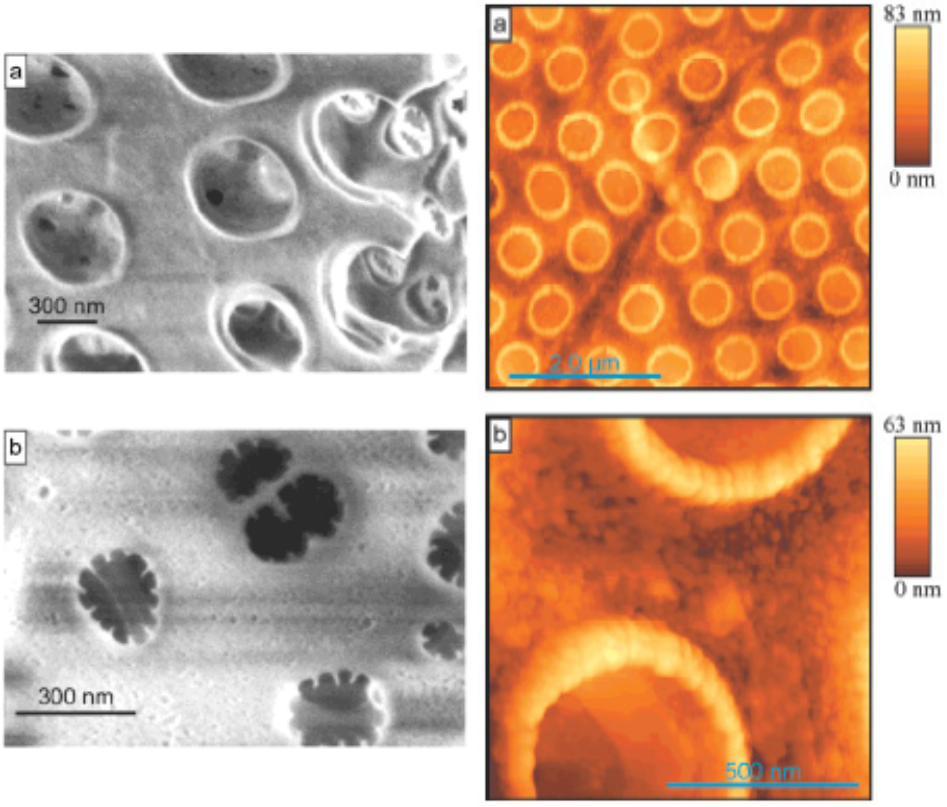

Figure 2. Imaging of the diatomic frustule. (Left) SEM images. (Right) AFM images of the inner surface of the diatomic frustule.[12]

Using scanning electron microscopy (SEM) and atomic force microscopy (AFM), Noll *et al.* studied the morphological structure of the diatom *Coscinodiscus granii* **(Figure 2)**. The general morphology of the silica is very similar in both SEM and AFM analysis. SEM analysis revealed the inner surface of the frustule to be smooth and featureless between the craters in the silica shell. The diameter of the craters is approximately 400 nm.[12] A closer look from the AFM revealed well defined structures associated with the rim of the craters. These granular structures were on the order of tens

of nanometers and located between the craters **(Figure 2)**. Starting from the surface of the frustule, the crater heights were observed to be around 80 nm.[12] This size regime and spherical shape are very similar to silica produced from the silica precipitating proteins, silaffins, thought to be crucial in the cellular division process and biosilification of the frustule.

Diatom Cell Division

Division of a rigid and amorphous metal oxide cell wall presents problems not experienced by cells with a semi-fluid phospholipid bilayer. Thus, mitotic reproduction of the diatom cell wall undergoes phases of morphogenesis not seen in most eukaryotic cells. The unique frustules of diatoms are a direct result of the biodeposition of silica resulting from cell division. Frustules are composed of two halves that fit together similar to a Petri dish **(Figure 3).** The top half of the frustule is the epitheca which overlaps the bottom half known as the hypotheca. The nascent cells retain the opposing theca from the parent cell.[3,13,14] Therefore, newly formed cells must generate a portion of the frustule, either the epitheca or the hypotheca.

An early step in the diatom division process is creating a specialized organelle known as the silica deposition vesicle (SDV) composed of organic matter and silica in which the ornate exoskeletons are created. Each daughter cell is associated with its own intracellular membrane-bound SDV organelle.[15,16] The SDV is a dynamic organelle that is manipulated and molded during formation of the frustule, and produces the

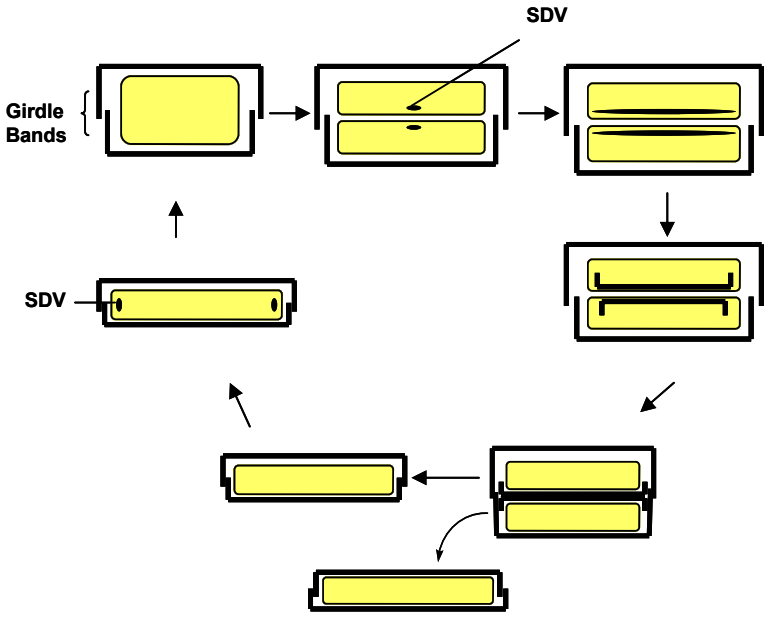

Figure 3. Diatomic cell division. Provided by Dr. Marc Knecht.

characteristic structures associated with the diatoms valves and girdle bands.[13,17] After completion, the whole silica structure is exocytosed to become an integral part of the cell wall.[13] During the exocytosis stage of cell division, the silica held within the SDV creates a hypovalve on the exterior of the daughter cells where the silica frustule is absent. With the hypovalve now developed, daughter cells separate from each other resulting in two new cells. Overlapping bands of the Petri dish structure and girdle bands continue to develop into the new frustule. At this point of division, each nascent cell utilizes two SDVs to develop the overlapping girdle bands and completing the mitotic division process **(Figure 3)**. Eventually a fresh hypotheca is spawned for each of the new cells.[3,13,14] While this specialized cell division alleviates mitosis involving a rigid outer shell, it presents the diatom with a conundrum. Each division results in a daughter cell that is smaller than the parent cell it was spawned from. Therefore, as the lineage

progresses, new members of the population will continue to diminish in size. To deal with this size reduction, diatoms participate in sexual reproduction when they reach ~30% reduction of their original cell size.[18,19] This process restores the diatoms to their original size.

Great interest exists in determining the specific process responsible for the precise nanoarchitecture achieved by diatom division. Templating appears to be the key to achieving these intricate structures. Scientists have isolated several biological macromolecules from the frustule via hydrogen fluoride digestion of biogenic silica. The products that result from the digestion are highly structured and templated from various proteins, post translationally modified peptides, and polyamines. The well orchestrated use and direction of these components plays a pivotal role in the biogenesis of silica.

Kröger *et al.* have isolated numerous proteins known as pleuralins[20] and frustulins[21] which most likely form an organic scaffold for the controlled biosilification of the diatom's frustule. Immunoelectron microscopy studies have suggested that pleuralins and frustulins are not directly responsible for silica production activity; however, they become associated with the biogenic silica following the polycondensation process.[22] This association is most likely conferred from the interaction of the multiple hydroxylated serine residues of the pleuralins and frustulins with the surface silanolate groups of the silica nanoparticles. This agglomeration results in an organic layer on the surface of the new particle leading to species specific self-assembly of the frustule. The proteins offer an organic template that holds the siliceous materials fixed during theca formation. While this material is found on the silica surface, it is not responsible for the condensation of silicic acid.

Two other organic materials isolated from silica deposits of the *Cylindrotheca fusiformis* and *Thalassiosira pseudonana* frustules are the species specific protein peptides, known collectively as silaffins,[23-28] and various polyamines.[3,11,29,30] These biological molecules have been shown to be responsible for the catalytic polycondensation reaction of silicic acid to silica. Previously, silaffins had only been characterized from *C. fusiformis,* and were found to be rich in hydroxyamino acids and lysines. Two of these species, natSil1A and -1B, are highly post-translationally modified, having phosphorylated serines and modified lysines containing ε-N-dimethyllysine, phosphorylated ε-N-trimethyl-δ-hydroxylysine, or long chain N-methyl derivatives of polypropylenimine. These phosphate groups are likely responsible for the protein self assembly resulting in a requisite primary amine concentration in order to drive the rapid polycondensation of silicic acid.[31,32]

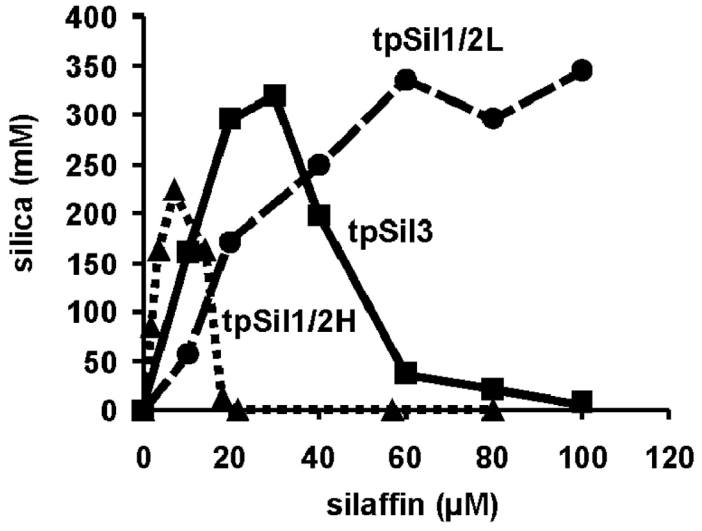

Figure 4. Varying concentrations of tpSil1/2H (▲), tpSil1/2L(●), or tpSil3 (■) were tested for silica production following a 10 min reaction time with silicic acid. All were in the presence of a constant concentration of *T. pseudonana* LCPA (0.75 g/l).[26]

A study by Poulsen and Kröger investigated the silica morphogenesis of *T. pseudonana* by alternative processing.[26] They isolated the five major silaffins (tpSil1H, -1L, -2H, -2L, and -3) and compared their abilities to precipitate silica. Interestingly, the silaffins of *T. pseudonana* share little to no sequence homology with *C. fusiformis,* but are similar in amino acid composition and post-translational modifications. As they relate to frustule formation, it was found that all of the silaffins were able to precipitate silica when accompanied by long chain polyamines, but that tpSil1/2H and tpSil3 assemblies have an inhibitory effect at higher concentrations **(Figure 4)**. This discovery provides some insight into the regulation of silica biogenesis by unmasking the role and timing of the individual silaffins. Furthermore, given the lack of homology between diatoms, residue composition and amine concentration appear to be governing factors in the formation, size, and shape of silica nanospheres.

Combined genomic and proteomic investigations into the biochemical pathway leading to modified silaffins were recently reported by Frigeri *et al.*[28] Aided by the genomic mapping of *T. pseudonana*,[27] mRNA responses were monitored during the biosilification process. These responses identified key enzymatic players **(Figure 5)** for future investigation as they relate to silaffin and polyamine synthesis. For example, Frigeri *et al.* were able to inhibit ornithine decarboxylase by utilizing the specific inhibitor 1, 3-diaminopropane dihydrochloride (DAPDH). The resulting frustule of the inhibited decarboxylase exhibited massive deformities **(Figure 6)** and confirmed the enzymes critical role in a diatoms mitosis and subsequent cell wall formation. This result is the only proteomic analysis of a diatom frustule and outlines a methodology for elucidation of the complete biochemical pathway responsible for biosilification.

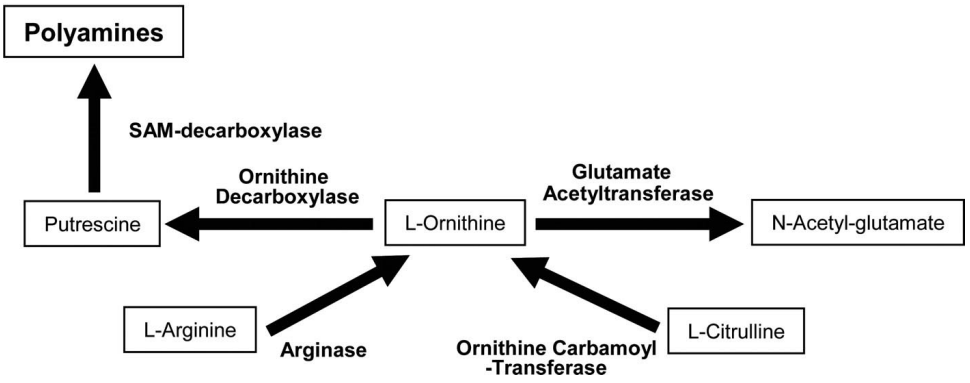

Figure 5. Polyamine biosynthesis pathway showing identified enzymes (bold) and intermediates (boxed). SAM: S-adenosylmethionine [28]

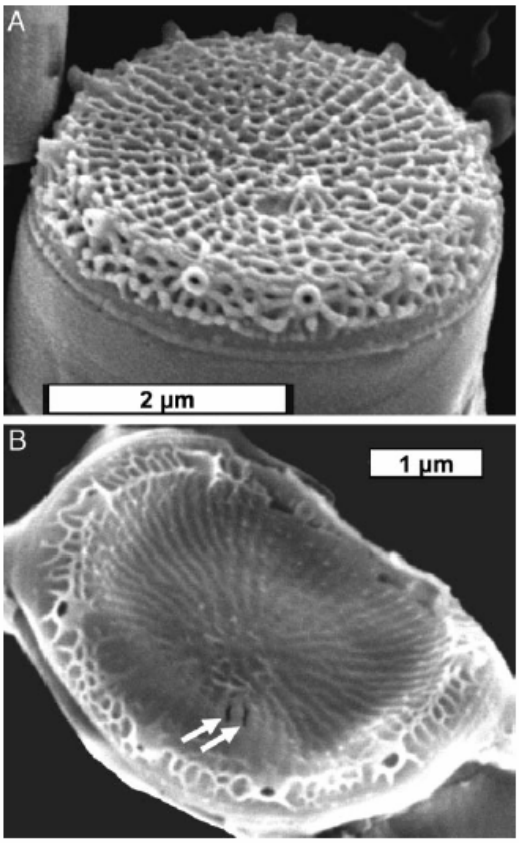

Figure 6. (A) Untreated diatom. (B) Diatom treated with 10mM 1,3-diaminopropane dihydrochloride. Arrows denote where silification is absent.[28]

The body of research on the reproduction of the ocean's diatoms is beginning to come into focus. Pathways involved in the synthesis of key players are starting to be discovered, while their specific functions are being determined. Critical analysis reveals a potential biomimetic methodology for novel materials. As mentioned previously, sequence homology suggests that only composition, in particular amine concentration, is required for condensation of monosilicic acid under ambient conditions. While the goal of specific nanoarchitecture is still hindered by a lack of knowledge pertaining to the scaffold structure employed by diatoms, novel silica composites containing biologically active materials are now a possibility. The first of these biomimetic experiments was performed with a short peptide segment of natSil1A.

The R5 Peptide

One of the most studied and utilized short chained peptides isolated from the diatomic frustules is the R5 peptide (H_2N-SSKKSGSYSGSKGSKRRIL-CO_2H) from *Cylindrotheca fusiformis*.[25,32,33] Kröger *et al.* reported that the synthetic and unmodified R5 peptide was able to rapidly condense silicic acid and precipitate silica from an ambient aqueous solution. They noted that the unmodified peptide precipitated silica at an optimal pH of 7 while the native silaffin protein was optimized to function at ~pH 5, the physiological relevant acidic conditions (**Figure 7)** of the SDV.[25]

Knecht *et al*. examined a variety of R5 mutants and determined critical residues responsible for the polycondensation of silicic acid to silica.[32] They found that the RRIL motif was critical for silica production, presumably because this motif mediated the formation of aggregates of multiple R5 peptides. Indeed, any aggregate is likely to

present a locally high amine concentration shown to be important for the condensation reaction.[31] Furthermore, it was noted that the R5 peptide was incorporated into the silica nanosphere as was evident by subsequent condensation reactions failing to reproduce the same level of silica production.

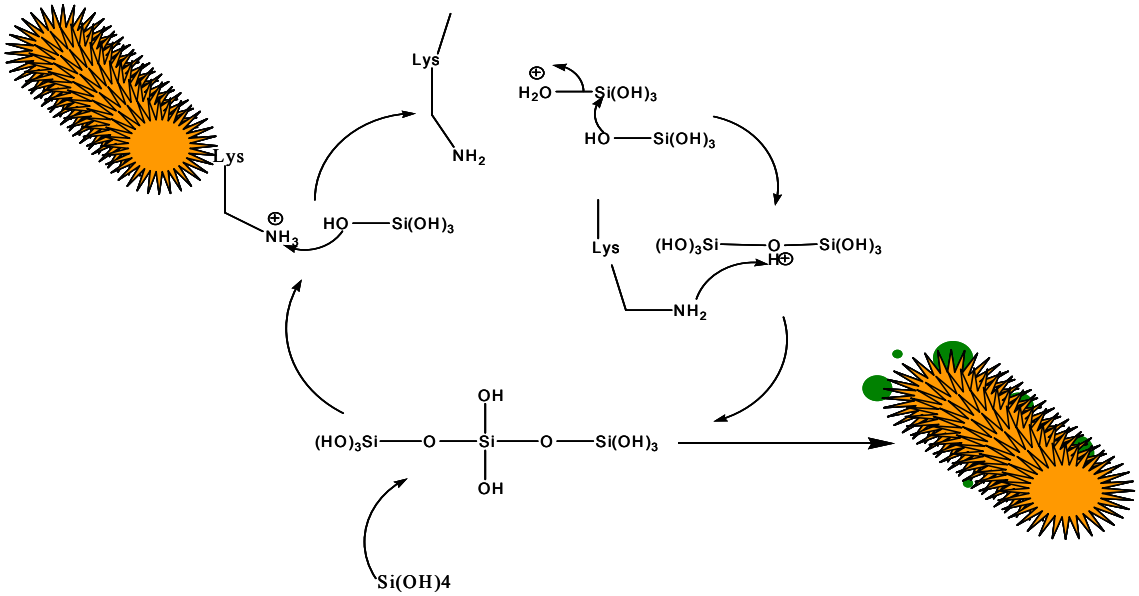

Figure 7. Amine mediated condensation of silicic acid. R5 peptide aggregate is represented in orange and nascent silica nanoparticles in green. Provided by Sarah Sewell.

The R5 mediated, rapid benchtop precipitation of silica nanospheres confirmed the hypothesis of sequence and protein mass not being the fundamental cause of biosilification. Discovery of the suprastructure and the RRIL motif allowing for R5 aggregation led to the true source of silica precipitation, the formation of a critical primary amine concentration. Luckarift *et al.* were able to utilize the R5 peptide as a component for the encapsulation of butyrylcholinesterase.[33] They were able to calculate a loading of up to 20% (wt/wt) by determining the amount of initial enzymatic activity

associated with the isolated silica nanoparticles. This was a significant improvement over traditional sol-gel encapsulation methods which are biologically limited by very low pH conditions, hydrophobicity of alkyl silicates, protein aggregation at relatively high concentrations, and denaturation via alcohol byproducts.[34-41] Thus, traditional methods restrict potential protein candidates and typically produce loadings of 0.1 – 5% (wt/wt).[34-36,38-42] Another favorable property of the enzyme containing silica nanoparticles from R5 was their stability over time. Butyrylcholinesterase was able to retain its activity over a period of 30 days from within the silica composite **(Figure 8)**.[43] A biomimetic approach to robust, stable, and biologically active nanocomposites has many potential applications

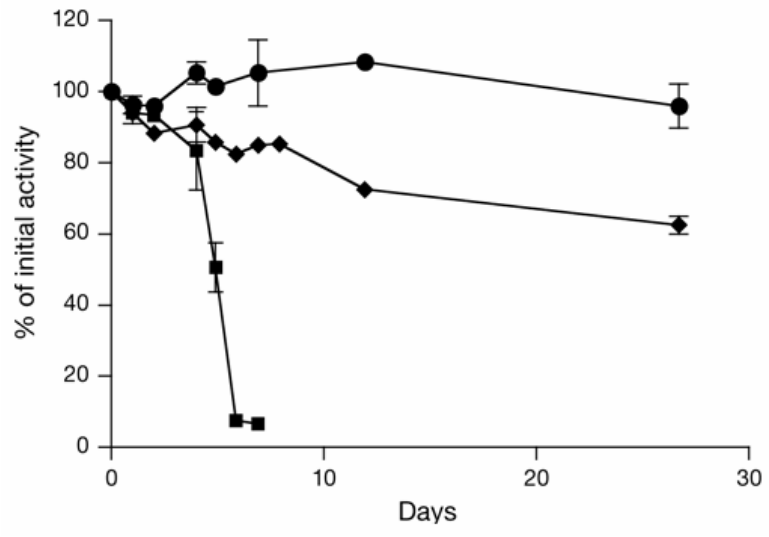

Figure 8. Stability of butyrylcholinesterase activity at 25 °C in free and biosilica-immobilized enzyme systems. free enzyme (■), free enzyme with antibiotic solution (♦) and biosilica-immobilized enzyme (●)[33]

in the medical, pharmaceutical, chemical, and agricultural fields, but the R5 peptide approach relies upon a reasonable and steady supply of peptide. Modern pharmaceutical

manufacturers and research academic labs have begun to answer the need of custom peptides by investing in the promise of chemical peptide synthesis.

Peptide Synthesis

Merrifield's solid-phase peptide synthesis (SPPS)[44] and great improvements in liquid chromatography techniques[45] opened the door for robust and widespread peptide synthesis. SPPS resolved the problem of solubility associated with the intermediates used in a more traditional solution synthesis of peptides. Simplicity and speed make SPPS amenable to mechanization which has led to the emergence of automated synthesizers to carry out the many repetitive steps **(Figure 9)**.[46] Solid support peptides make up the vast majority of synthetic peptides at the milligram scale.

The basis of peptide synthesis is founded in general organic synthesis and has been optimized to an unusually high degree. The reactions utilized in peptide synthesis require near 100% yield and efficient kinetic rates. Deviation from these requirements results in error propagation for each subsequent reaction and/or unreasonable synthesis time. This requires optimization of the inert polymeric support, protection schemes, deprotection, and coupling reagents. These strict requirements and the numerous functional groups of the amino acid residues offer a proving ground for various organic methodologies. Despite intense research and optimization, peptide synthesis presents several obstacles to even the seasoned practitioners.

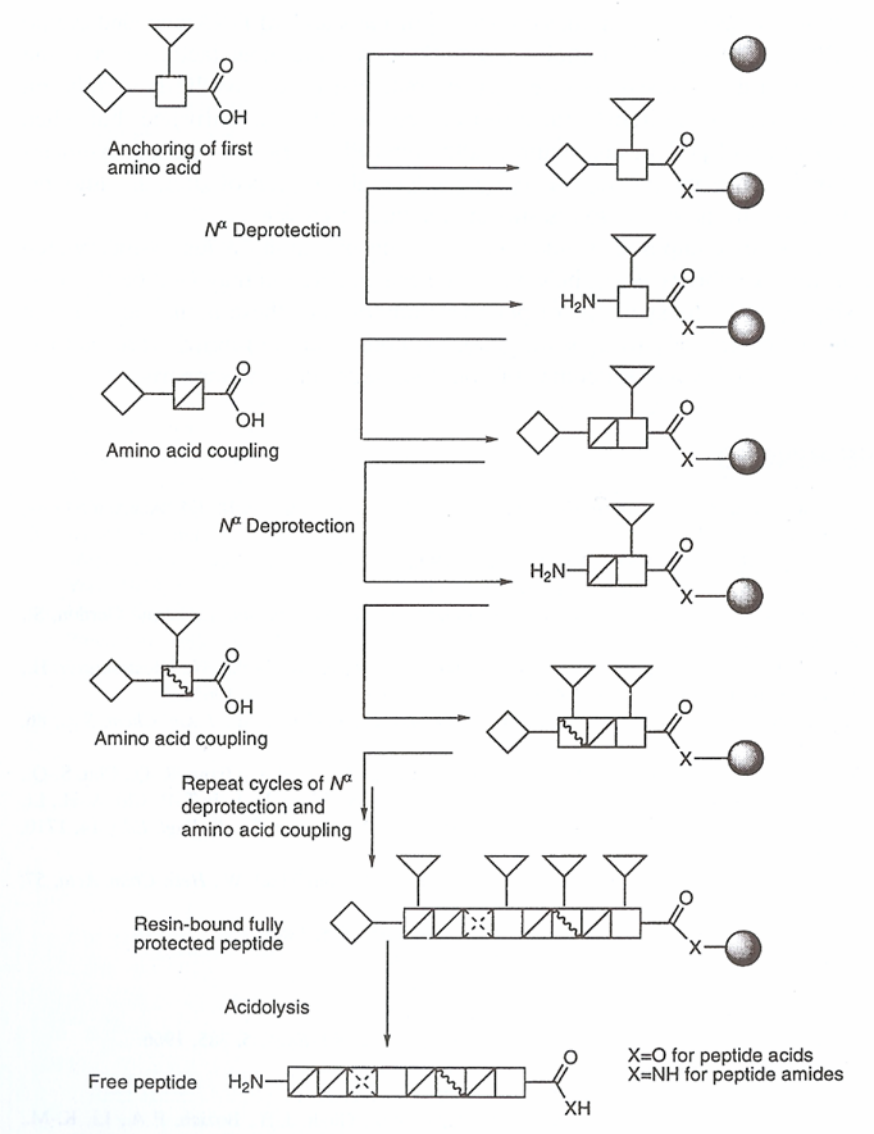

Figure 9. Standard SPPS strategy for chain elongation.[165]

Reactions and Reagents

Appropriate supports for SPPS require certain essential characteristics. Particles should not only be chemically inert, but also of particular size and shape for reactivity and rapid filtration. At the same time, potential solid support material must not interact detrimentally with itself or the growing peptide chain. Additionally, the support should

be able to accept modifications and allow for covalent bonds for first residue attachment. Finally, the material should swell in order to be penetrated by the reagents of the chemical reactions. There are two primary choices of resin support used in peptide synthesis, cross-linked polystyrene and polyethylene glycol-grafted polystyrene.

Merrifield chose a cross-linked polystyrene support, which is composed of beads between 20 and 50 μm. The mechanical stability of polystyrene based resins allows for vacuum filtration and can swell to 8 ml/gram in apoloar solvents such as dichloromethane, a desirable property to avoid peptide aggregation to be discussed below.[47,48] Friedel Crafts chloromethylation[49] and Gabriel synthesis[50] allows for aminomethyl groups and hydroxymethyl groups by displacement of chloride ions for acetate ions followed by hydrolysis.[51,52] These reactions allow for a wide array of functionalization to produce resins with a substitution level of 0.3 – 1.2 mmol/gram.

Another common support system in SPPS is the polyethylene glycol (PEG) grafted polystyrene. PEG based supports were developed in an attempt to improve the solvation of the bound peptides.[53,54] PEG of 2000 to 3000 daltons is typically attached to the base polystyrene directly to amino-functionalized[55,56] resins or by anionic copolymerization of ethylene glycol in order to produce 'tentacle polymers.'[57-61] While the PEG spacer has been shown to improve solvation, the substitution levels range from 0.15 – 0.3 mmole/gram which reduces the number of growing chains as a function of surface area. This reduction can aid in the synthesis of long peptides by lessening the steric interference and possible interaction of multiple peptide chains.

Chemical peptide synthesis revolves around repetitive amide bond formation with an orthogonal protection scheme[62,63] of sidechains and N termini within an aprotic polar

solvent (most notably N, N - dimethylformamide) in conjunction with active ester amino acid derivatives. N^{α} was traditionally protected by the Boc group.[64,65] The required hydrogen fluoride treatment to cleave Boc schemed peptides from the solid support created the need for the more commonly used 9-fluorenylmethoxycarbonyl (FMOC) protecting group.[66] FMOC is removed via a secondary amine base, most commonly piperidine, through a well characterized mechanism **(Figure 10)**.[67,68] Monitoring of this reaction can be performed via ultraviolet-visible (UV-Vis) spectrometry at 275 nm (dibenzofulvene product) or by the Kaiser test for primary amines.[69] Following N^{α} deprotection, a solution of excessive activated ester derivatives of amino acids is then added to the resin.

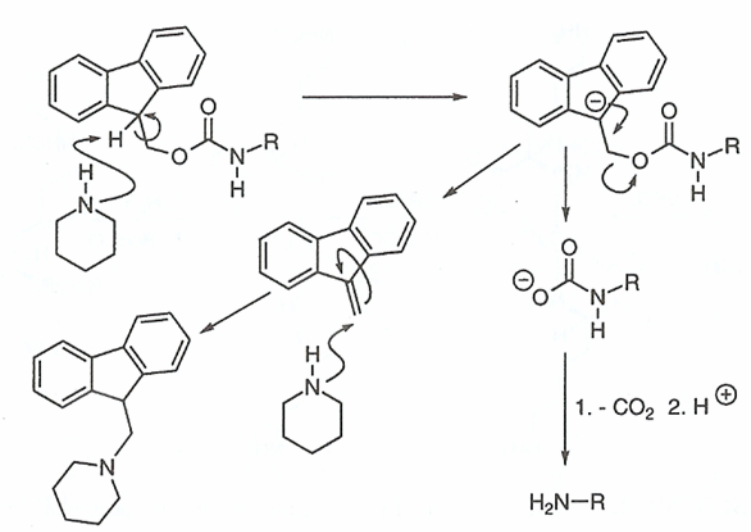

Figure 10. Piperidine mediated N-terminal FMOC removal.[101]

Two commonly used classes of reagents to achieve acid activation are the carbodiimides and aminium (uronium) salts. Dicyclohexylcarbodiimide (DCC)[70] was

introduced in 1955 and was the benchmark for many years before the introduction of diisopropylcarbodiimide (DIC)[71] which has a more soluble byproduct. Several side reactions can occur using carbodiimides, but the most important is oxazolone formation resulting in unwanted racemization of the final product.[72,73] To alleviate stereo mixing, a kinetic trap is required that displaces the diimide prior to ring formation, but generates an ester active enough to achieve rapid amide bond formation. The first additive offered was N-hydroxy-succinimide,[74,75] but has since been superseded by the extremely popular 1-hydroxybenzotriazole (HOBt).[76] Since phosphonium[77] and aminium salts[78,79] were first employed in SPPS, they have become a powerful weapon in the arsenal of peptide chemists. Activation of the carboxylic acid via these salts is base catalyzed by a tertiary base, incapable of removing FMOC, by removing the acidic proton from the C-terminus allowing for rapid activation. While aminium salts, such as *O*-(benzotriazol-1-yl)1, 1, 3, 3-tetramethyluronium hexafluorophosphate (HBTU), do not mechanistically require such an additive, HOBt is still typically utilized **(Figure 11)**. These reagents impart their greatest benefit during the coupling of sterically hindered amino acid residues known to present problems with diimide reagents.[80-83]

After the completion of peptide chain elongation to the desired length, removal of the peptide from the solid support is typically achieved from acidolysis.[84] Most of the common residue sidechain protecting groups used in FMOC synthesis, such as trityl and *tert*-butyl groups, are removed during the cleavage of the peptide from the resin with trifluoroacetic acid (TFA).[85] Additives such as alkyl silanes,[86] thiols, anisoles, and water are employed to scavenge the carbocations produced during the acidolysis to avoid unwanted alkylation of the peptide chain.[87] Following filtration of the solubilized

peptide, ethyl ether is often used to precipitate the desired product, and reverse-phase chromatography is then able to isolate desired peptides from the mixture.

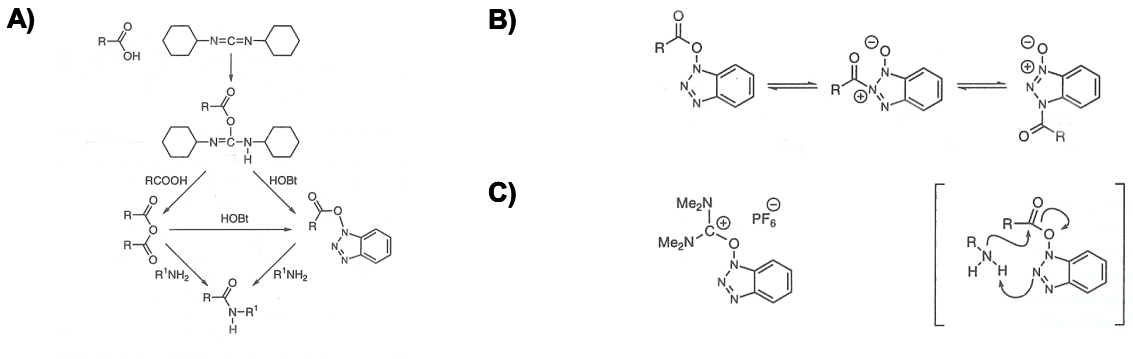

Figure 11. (A) DCC coupling utilizing HOBt to eliminate racemization. (B) Resonance structures of HOBt active ester following amino acid activation by either DCC. (C) HBTU.[165]

Solvation and Aggregation

Despite the use of optimized conditions and global protection schemes, SPPS is rife with problems. Various sidechain reactions can occur during the N^{α} deprotection and subsequent cleavage process. Furthermore, the addition of subsequent residues with bulky hydrophobic protection groups can lead to an eventual insolubility of the growing chain. The major side reaction of the various residues during synthesis is the formation of undesired cyclic species. One example of this process is formation of diketopiperazines. These rings result in auto-cleavage of the first two residues on the resin. Judicious selection of chemical linkers on the polystyrene support can alleviate diketopiperazines formation. Sidechains are also known to be reactive with the peptide backbone itself. Aspartamides present themselves during piperidine catalyzed removal of the FMOC group whenever a glutamic acid or asparagine is present. During acidolysis, the major obstacle is the formation of pyroglutamates, which creates a cyclic N-terminus.

These side reactions exacerbate the problem of low yields as well as the requirement for more refined and tedious separation techniques.

The most perilous pitfall in SPPS is the onset of aggregation of multiple peptide chains or the peptide chain with the polystyrene resin itself during the elongation. Amide bond formation during peptide synthesis is normally quantitative, unless required reagents are unable to access the exposed primary amines of the N-termini. This is often the case when aggregation of the peptide backbone occurs and either slows the kinetic rate of coupling by either involving the N^{α} hydrogens in a hydrogen bonding network or rendering the peptide chain insoluble.[88] This phenomenon has been seen as early as the fifth residue in some peptides.[89] Indeed, gel-phase nuclear magnetic resonance (NMR) of peptide-resin suspensions suggests that the on-resin intermolecular association is the result of hydrogen bonding.[90,91] The likely orientation is similar to that of a ß-sheet which causes the N-terminal amino acid inaccessible.[92,93] High Ala, Val, Ile, Asn, and Gln content peptide sequences have a greater tendency for aggregation. A peptide whose synthesis is afflicted by sluggish N^{α} deprotection and/or slow coupling times is said to be a 'difficult sequence', because the incomplete couplings will propagate as error through subsequent acid additions resulting in truncated peptide products complicating purification and lowering yields.

Solutions for Difficult Sequences

Alleviation of difficult peptide sequences has garnered much of the recent research into peptide synthesis. Two general strategies are commonly used to combat poor peptide production, change the environment in which the coupling is taking place

and structurally altering the growing chain. The first of these strategies, manipulating the environment, has found some level of success with the addition of additives such as trifluoroethanol, hexafluoroisopropanol, dimethylsulphoxide, and chaotropic salts.[94-98] While isolated cases have reported improvements by using additives, none of them have had the universal success of structurally modifying the peptide chain.

Several different structural modification strategies have been postulated as alleviants of aggregation. The most promising of these, Sheppard's 2-hydroxy-4-methoxybenzyl (Hmb) residue derivatives and Mutter's pseudoprolines, have already begun to find widespread use. Hmb protection is the substitution of the offending amide proton responsible for peptide backbone aggregation in exchange for the sterically hindering methoxybenzyl derivative.[99] Hmb derivatives are incorporated through HOBt activation of pentafluoroester derivatives of Hmb protected residues and are removed and scavenged during standard acidolysis with TFA **(Figure 12)**.[100]

Several success stories with judicious placement of Hmb residues have been documented, and one example is the improved synthesis of an HIV-1 related octadecapeptide.[101] The original 18-mer target peptide constituted the C-terminal end of a larger 44-mer target peptide. The 18-mer was originally attempted on an automated synthesizer without sidechain protection on $Asn^{3,5}$ or Gln^{11} and multiple protection groups of cysteine residues: H-Leu-Ile-Asn-Cys(Trt)-Asn-Thr(^{t}Bu)-Ser(^{t}Bu)-Val-Ile-Thr(^{t}Bu)-Gln-Ala-Cys(Acm)-Pro-Lys(Boc)-Val-Ser(^{t}Bu)-Phe-Pepsyn KA® resin. UV-Vis monitoring of the FMOC removal showed a dramatic broadening at Val^8, six residues from the ß-sheet inhibiting tertiary Pro. Subsequent couplings were kinetically slow and failed to reach quantitative results as shown by the Kaiser test.[69] The resulting crude

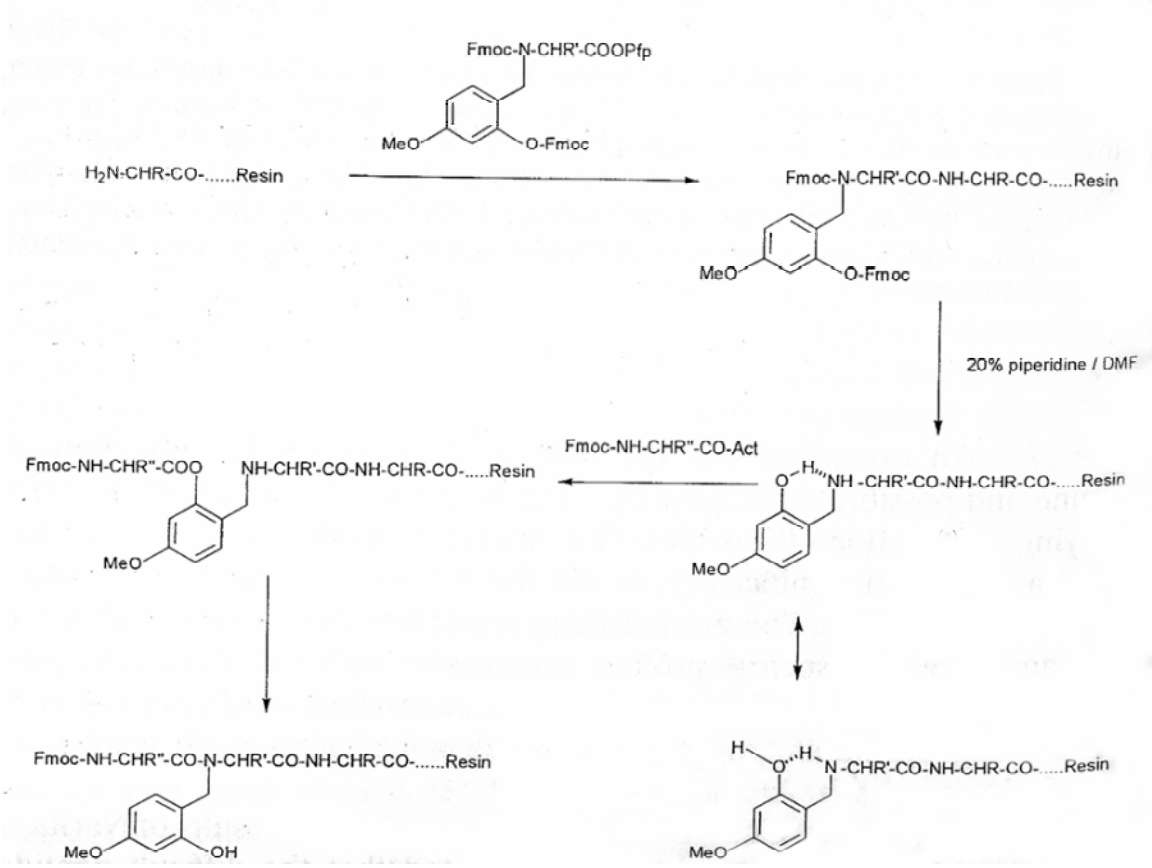

Figure 12. Scheme for the incorporation of Hmb residues via pentafluoroester activation.[101]

mixture was found to only contain 33% of the desired product **(Figure 13).** The introduction of the bulky trityl protecting group to Gln[11] delayed the onset of aggregation by two residues, but was unable to significantly improve the final purity. The optimal point for Hmb insertion was Val[8] which was expected to offset aggregation by six residues and allow for a majority of the assembly to be completed. No further synthetic obstacles were encountered and a significant improvement of the resulting crude mixture was observed via HPLC **(Figure 13)**. This 18-mer and other cases demonstrate the power of backbone protection schemes in offsetting peptide aggregation. Unfortunately,

as discussed in Chapter IV, the insertion of Hmb protection schemes is not a universal solution.[100,102,103]

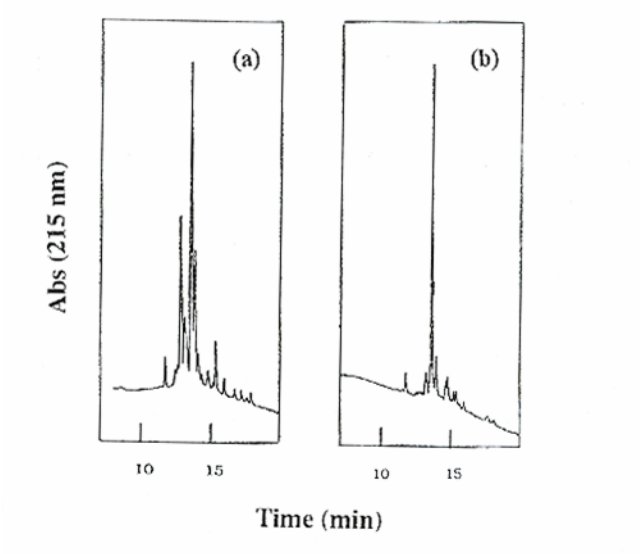

Figure 13. HPLC profiles of the HIV-related octadecapeptide. (A) Standard assembly showing the effects of aggregation on crude product. (B) Introduction of both Gln(Trt)[11]and (Hmb)Va[18] shows very little aggregation during assembly.[101]

Nature uses the amino acid residue proline, which lacks the amide bond hydrogen and is constrained in its angles, to either initiate a loop or turn in a protein structure or disrupt α-helix formation and ß-sheet structure. Manfred Mutter reasoned that inserting a proline, or similar structure, into the peptide chain would have a negative effect on the suspected ß-sheet structure at the root of aggregation **(Figure 14)**.[104-106] To mimic biology, the method developed involves reversible conversion of Cys, Ser, and Thr into a 'pseudoproline' via formation of an oxazolidine dipeptide. The result is a more soluble peptide chain that is structurally reluctant to engage in ß-sheet formation. The

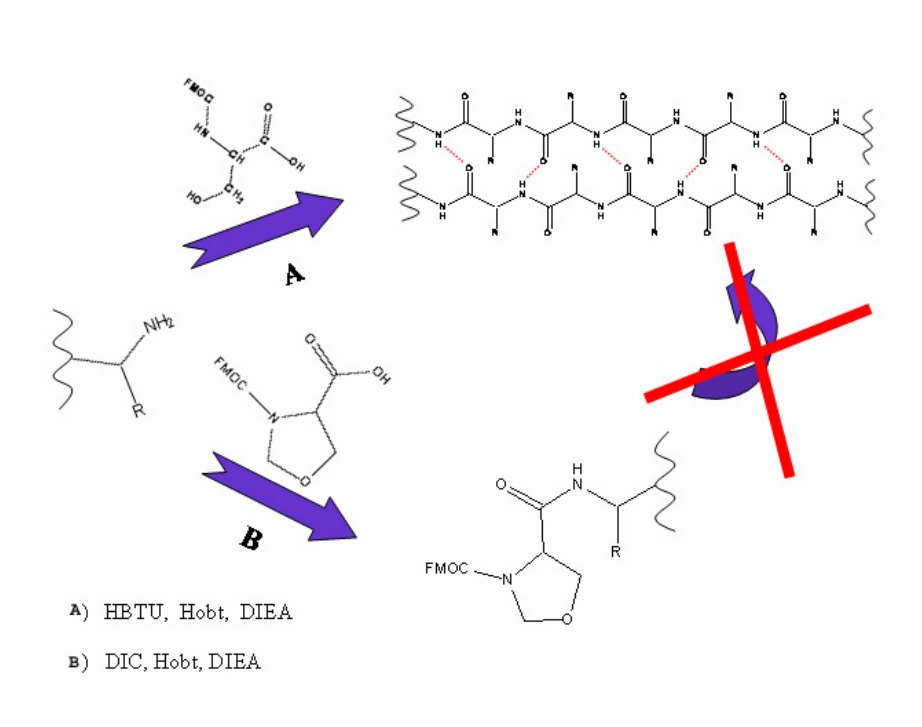

Figure 14. (A) Insertion of standard amino acid residues allows for ß-sheet hydrogen bonding network. (B) Pseudoproline residues disrupt secondary structure.

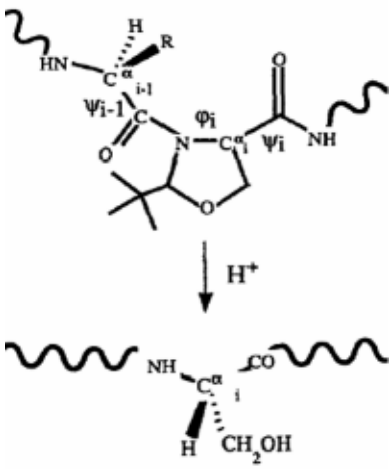

Figure 15. Acidolysis of pseudoproline derivatives.[106]

pseudoproline residues are converted to the natural residues Cys, Ser, and Thr via typical acidolysis treatment **(Figure 15)**. As discussed in Chapter IV, pseudoprolines have found general use and success, but are still limited in their ability to resolve many difficult peptide sequences. The primary limitation is the requirement of a Ser, Thr, or Cys in a sequence position prior to the onset of aggregation and with a four to six residue distance from the trouble region. As is the case with the previouly discussed Hmb protection scheme, use of pseudoprolines often requires prior knowledge of the peptide in terms of where aggregation occurs.

Judicious use of solvent mixtures and backbone protection schemes in peptide synthesis has enabled investigators to not only synthesize entire proteins such as ribonuclease A,[107] but also individual domains and functional motifs in a wide array of biologically relevant proteins. One of the achievements owing to peptide synthesis is the study of conformational switching peptides.

Amphiphilic Peptides

An area of major theoretical and practical interest is the *de novo* design of peptides displaying well-characterized structural and functional properties.[108-111] A sound understanding of the conformational properties of amphiphilic peptides, where secondary structure is often governed by the formation of multimeric aggregates, is of great importance in the construction of novel proteins. Knowledge of these peptides will allow for the development of model systems for the investigation of protein mechanisms and function. Separate from the natural tendencies associated with amino acids and peptides towards particular secondary structures, peptide aggregates are manipulated by

hydrophobic interactions in an aqueous solution. By studying and manipulating these forces, mimics for globular protein folding can be achieved for investigation.[108-110,112-115]

Previously, peptide folding and refolding has been studied as a function of solvent and temperature.[115,116] Mutter *et al.* designed and studied a short series of peptides that were found to switch between α-helix and β-sheet secondary motifs as a function of pH in a purely aqueous environment.[117] To create amphiphilic sequences, the repetitive pattern of an amphiphilic β-sheet (i.e., alternating hydrophobic and hydrophilic residues) was mutated such that hydrophobic residues that would become the hydrophilic face of the α-helical bundle were now indifferent, thus neither polar nor hydrophobic. This design resulted in a general sequence for peptides that were amphiphilic in nature for both α-helix and β-sheet **(Figure 16)**.

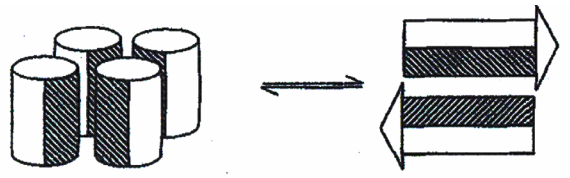

Figure 16. (Top) Schematic of the conformational transition between α-helical bundles and β-sheet structure. (Bottom) General amphiphilic sequence where P=polar, H=hydrophobic, and N=neutral amino acid residues.[117]

Circular dichroism (CD) revealed that all four peptides (Ac-EAALEAALELAAELAA-NH_2, Ac-KAALKAALKLAAKLAA-NH_2, Ac-KAALEAALKLAAELAA-NH_2, Ac-EAALKAALELAAKLAA-NH_2) were able to switch conformations **(Figure 17)**. For example, peptide 1 was clearly in a β-sheet conformation at pH 4, but was ~23% helical (as determined against a

poly-L-Lysine reference) at ≥ pH 7. The transition region of pH 5 – 6 displays intriguing spectra not previously seen for simple helix-coil or β-structure-coil transitions. Peptide 3 was found to have three transitional pH values. At pH 3 and 9, peptide 3 was predominantly helical with contents of 60% and 53% respectively. However, spectra obtained at pH 7 and 11 are consistent with a predominantly β-sheet structure. These findings begin to allude to motifs found revolving around conformational protein changes often seen in nature. Of particular interest is the class of proteins implemented by viruses to achieve entry into target cells. These fusion proteins are known to undergo significant conformational changes during the fusion event, and one of the most well-characterized fusion proteins, influenza's hemagglutinin, has been found to be activated via a change in pH (see below).

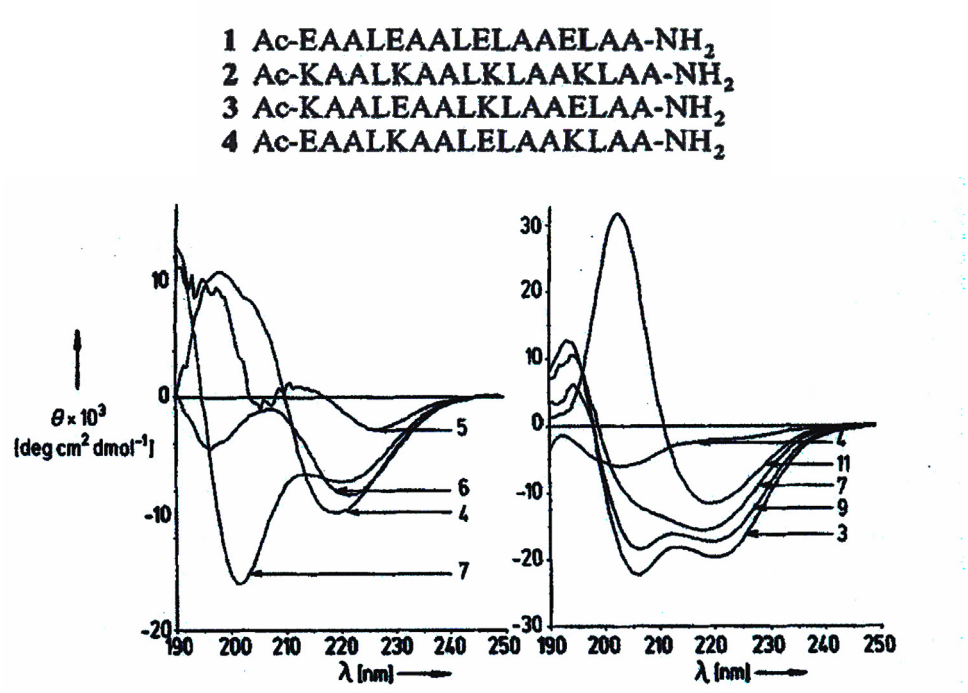

Figure 17. (Top) Amino acid sequences of amphiphilic peptides. (Bottom left) CD-spectra of peptide 1 (0.5 mg/mL). (Bottom right) Cd-spectra of peptide 3 (0.5 mg/mL) in aqueous solution at varying pH.[117]

Membrane Fusion

A critical element of many biological processes is specific membrane fusion.[118] The obligatory first step of any fusion event is the close proximity of potential fusion partners. Derjaguin-Landau-Verwey-Overbeek (DLVO) theory estimates the likelihood of surfaces coming in to such close contact. DLVO theory was developed for colloidal particle aggregation and is derived from interaction of attractive van der Waals and repulsive electric double layer forces between the charged surfaces of particles in solution. Consequently, the free energy (ΔG) can be directly related to the separation distance, h, between the two potential fusion partners. The ratio of the number of particles at distance h to an infinite separation is offered by the Boltzmann equation, $\exp[-\Delta G(h)/kT]$, where k is the Boltzmann constant and T is absolute temperature. For two vesicles to be fusion partners, $\Delta G/kT >> 1$, i.e., the inter-membrane energy of interaction is large enough to overcome Brownian motion. DLVO has its critics and is often insufficient in explaining short distance electrostatic interactions amongst more biologically relevant lipid bilayers, thus several other methods have been developed to study the fusion process of vesicles that better simulate close contact interactions and fusion of biological membranes. Some of these techniques include lipid dye exchange,[119] electron microscopy (EM),[120,121] and fluorescent contents mixing.[122]

These techniques reveal that the source of the large energy necessary for fusion is the massive conformation perturbations and high energy intermediates of the monolayers involved in fusion. The fusion event involves the merging of two separate organelles and the mixing of the aqueous components within **(Figure 18)**. Two vesicles in close enough proximity come together to form a prefusion complex. The current paradigm has the

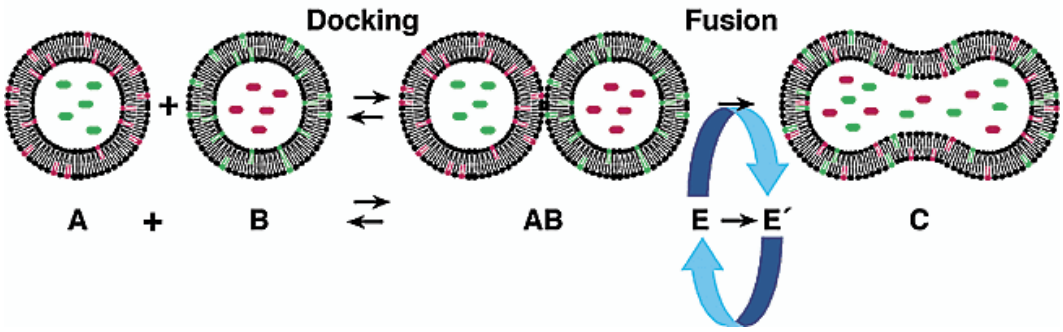

Figure 18. The membrane fusion reaction. Two lipid vesicles (A and B) come into close contact, "docking" (AB) juxtaposed vesicles fuse membranes into a single unit (C). The mixing of lipid and aqueous markers (green and red) indicate the progress of the compartmental mixing process. The fusion process can proceed spontaneously, via catalysis, or by specific proteins. These proteins are sometimes involved in both "docking" and fusion. In the latter case, a conformational change of the protein catalyst (E⟶E') is coupled with transitions of the lipids.[164]

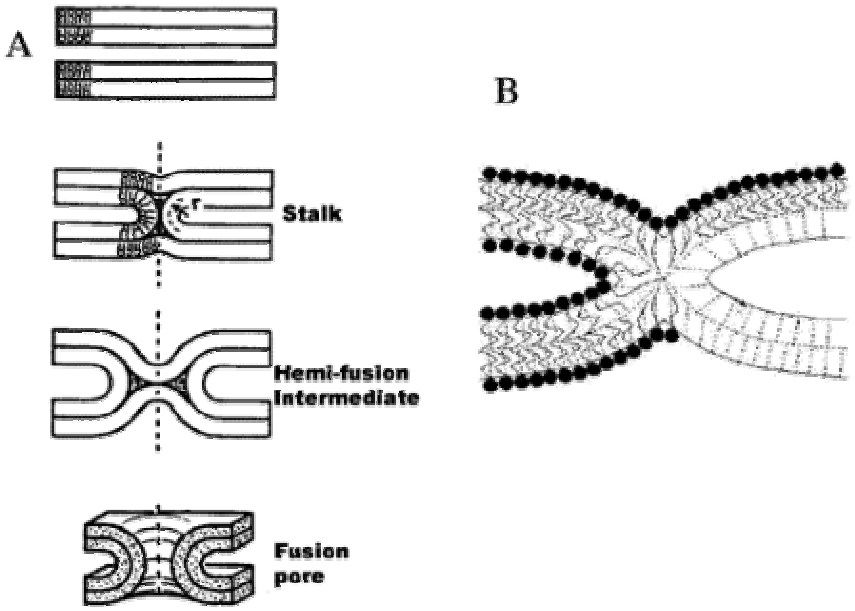

Figure 19. Schemes for membrane fusion. (A) Top drawing represents two juxtaposed bilayers prior to fusion. The stalk illustrates the intermediate with the (cis) monolayers in close contact obtaining negative curvature with radius r. Juxtaposition of the two trans monolayers creates a hemifusion intermediate. A fusion pore represents the first intermediate to allow mixing of aqueous contents. (B) Membranes are void of hydrocarbons filling voids, as shown by the stippled black areas in the stalk and hemifusion intermediates in section A.[164]

fusion reaction proceeding in at least two stages. First, the contacting outer monolayers (often referred to as 'cis') leaflets fuse, but interior distal (called 'trans') leaflets remain in tact. This 'stalk' continues to change as the distal monolayers become juxtaposed and begin to fuse into the hemi-fusion intermediate. This intermediate then ruptures to form a fusion pore, the first intermediate that allows for content mixing, and completes the coalescence of interior contents **(Figure 19)**. The reaction could proceed spontaneously if the reactants are inherently unstable. For example, it is possible to produce ~20 nm in diameter unilamellar lipid vesicles by ultrasonication, thus introducing energy into the system. These vesicles have a high degree of positive curvature in their outer layer and a large amount of negative curvature associated with the distal layer **(Figure 20)**. Spontaneous fusion will occur if the lipids comprising the layers experience stress from

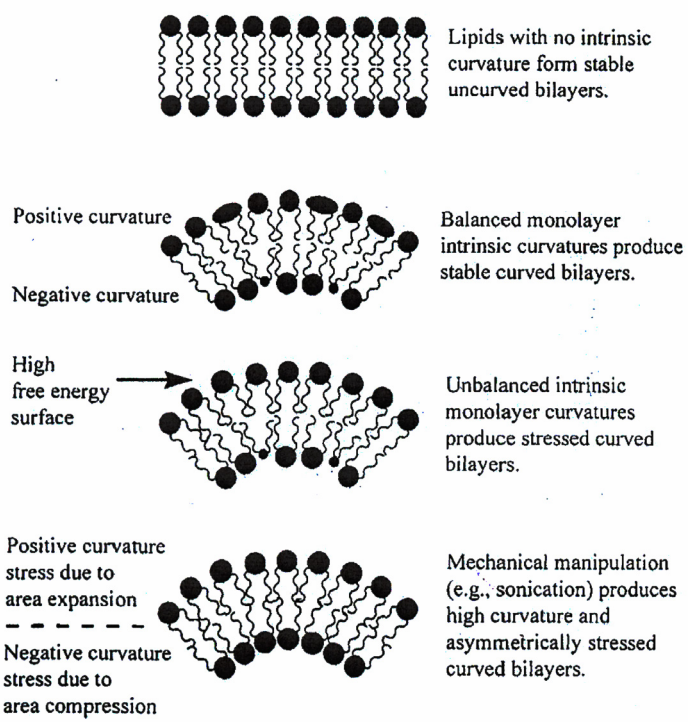

Figure 20. Concepts of intrinsic lipid curvature and stress.[119]

these curved environments. If the vesicles do not spontaneously fuse, then small perturbations, such as divalent ions, peptides, sonication, or PEG are needed to trigger fusion. This conversion of relatively flat lipid bilayers into fusion intermediates is a costly energetic process involving a range of chemical chain tilts and lipid remodelling **(Figure 21)**.

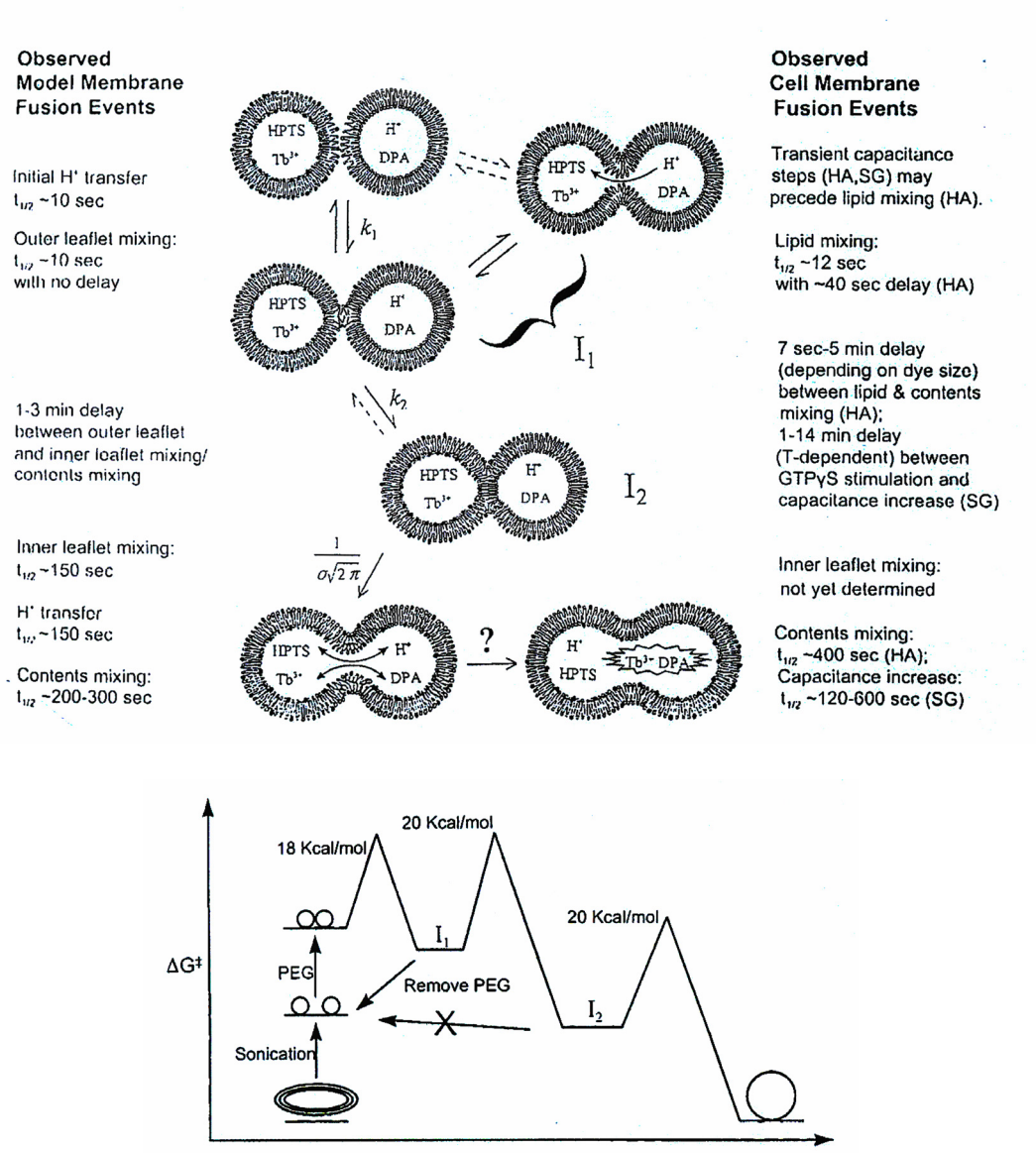

Figure 21. (Top) Hypothetical membrane fusion events based upon biophysical measurements of PEG mediated SUV, secretory granule (SG), and HA mediated fusion. (Bottom) Concept of energetics for fusion. Measured activation energies are listed in **Table 1.** [119]

By utilizing sonication and PEG-mediated fusion techniques, Lentz and Lee, were able to study the time, energy, and structural intermediates associated with fusion.[119] Sonicated vesicles (SUV) are known to have perturbed outer lipid layers causing them to be metastable and easily prompted into fusing. PEG is a hydrophilic polymer that is able to dehydrate membrane surfaces forcing lipophilic membranes together by overcoming the hydration repulsion between membranes that is thought to be an initial step in the fusion process.[123] Lentz and Lee were able to create vesicles that were easily coerced into fusing via exposure to ultasonication or PEG. EM and fluorescent studies elucidated times and energies that showed a close relationship between SUV fusion and observed cell membrane fusion events **(Figure 21).** They observed that initial outer leaflet mixing occurred in less than 10 seconds followed by a delay of up to 3 minutes before content mixing occurred. This initial outer leaflet mixing requires an activation energy of ~ 18 kcal/mol and is followed by another energy barrier of ~20 kcal/mol to achieve inner leaflet mixing. These times, and likely energies, correspond with known protein mediated fusion events.

From a macroscopic view, there is a significant similarity between PEG mediated model membrane fusion, discussed above, and the sequence of events observed for viral fusion. Electrophysical measurements of biological membranes have suggested the creation of transient pores in the early stages of protein mediated fusion.[124-126] Pore formation occurs either just prior or simultaneously with lipid mixing, which takes place up to 5 minutes prior to content mixing. The activation energy for the first step of PEG mediated fusion and that of vesicular stomatitis virus (VSV) fusing with ghost erythrocytes (42kcal/mol pH 5.85)[127] was found to be comparable **(Table 1)**. While the

morphology of intermediates and activation energies of SUV and biological membrane fusion are similar, nature must overcome the associated high energy barrier by means other than ultrasonication and a high concentration of PEG.

Table 1. Thermodynamics of fusion intermediates. Rates were determined at 35°C.[119]

Process	Rate (s^{-1})	$\Delta H^{\ddagger}$ (kcal/mol)	$\Delta G^{\ddagger}$ (kcal/mol)	$T\Delta S^{\ddagger}$ (kcal/mol)	$\Delta S^{\ddagger}$ (cal/mol)
*I*1 formation	2.43	37	18	19	63
*I*2 formation	0.044	27	20	7	23
Pore formation	0.020	21	20	1	3
Lipid mixing in viral fusion	4.21	42	17	25	81
Pore opening in secretory fusion	~ 0.010	23	21	2	7

Biological vesicles, in contrast to studied lipid vesicles, are intrinsically stable and their fusion often occurs at salt concentrations and distances (typically nanometer scale) not adequately explained by DLVO theory[128] or metastable lipid models. Nature has evolved specific and well orchestrated events and proteins to deal with energetic concerns related to membrane fusion. Biological membrane fusion events are stringently regulated and often involve a mediator commonly referred to as 'docking' or 'fusion' proteins. These protein catalysts are often required for the docking and coalescing of fusion partners. One of the hallmarks of protein mediated docking and fusion is large, often irreversible, conformational changes of the protein responsible for making membrane fusion energetically favorable. The most studied of these proteins are the membrane fusion proteins from envelope viruses such as influenza.

Viral Fusion Proteins

Enveloped viruses have evolved two distinguished, yet conceptually similar, classes of viral fusion proteins to mediate membrane fusion.[129,130] Class I is utilized by orthomyxo-, retro-, filo-, and paramyxoviruses. Following release from the ribosome, these fusion proteins are proteolytically cleaved by a host protease to give a membrane-anchored subunit with an amino-proximal fusion peptide. Three identical copies aggregate into a metastable fusion primed protein, which is subsequently triggered (either by receptor binding or acid exposure) to undergo the requisite conformational change. The result is the postfusion structure with a characteristic triple-stranded coiled-coil complex.[131,132] This coiled-coil structure has been found to be extremely thermal stable and is thus suspected to provide the free energy required to overcome the energetic barriers associated with the fusion process.[133]

Class II viral fusion proteins are utilized by flavi- and alphaviruses. Class II fusion proteins possess internal fusion peptides in contrast to the amino-proximal fusion peptides of Class I. Class II fusion proteins are not enzymatically cleaved following synthesis, rather they are associated with a second membrane glycoprotein or accessory protein. The activation event is the subsequent cleavage of this accessory protein.[134] X-ray structures of the fusion E proteins from Semliki forest virus[135] and tick-borne encephalitis[136] reveal several motifs unrelated structurally to Class I proteins. Given the crucial role of membrane fusion in the viral life cycle, understanding and manipulating these proteins can result in new strategies for fighting viral infection.

Influenza Hemagglutinin

Over the past two decades many studies have shown a complex and orchestrated pathway by which influenza hemagglutinin (HA) mediates viral and cellular membrane fusion.[129,137] HA is the sole protein required for viral fusion with the host cell. HA is initially synthesized as an incompetent precursor, called HA0. HA0 is then proteolytically cleaved into two subunits, a transmembrane and a surface subunit. This cleavage results in the metastable or fusion primed glycoprotein. The surface subunit, HA1, remains covalently attached to the transmembrane subunit, HA2, through a single disulphide bond. HA1 is responsible for recognition of sialic acid, the specific receptor on the host cell. HA2 contains the fusion peptide region at the amino terminus and is anchored in the viral membrane via hydrophobic helices. Following sialic acid binding, the influenza virus is endocytosed. The endosome has an acidic interior, and this low pH exposure triggers fusion (the optimal pH for fusiogenic activity has been determined via monitoring of spike morphology changes, and is found to be 5.0 at 37˚C).[138-140] This fusion process consists of enormous conformational changes of HA which results in the influenza virus escaping the endosome to content mix with the interior of the host cell. The fusion process of HA is often referred to as the 'spring-loaded model' owing to the notion of a primed protein ready for fusion.

The Spring-Loaded Model

Wilson and coworkers provided the first high-resolution view of a viral envelope glycoprotein.[141] The crystal structure showed a large portion of the native HA ectodomain that was cleaved from the viral surface by bromelain. The result is a

structure that lacks the hydrophobic region anchoring the protein to the viral membrane. The HA is a long homotrimer that extends 135 Å. The top of the structure is comprised of three exposed globular head domains responsible for sialic acid binding. This head sits above the remainder of HA1 and HA2 oriented as a long stalk containing a trimeric coiled-coil at its core. The coiled-coil is composed strictly of HA2 which also contains the buried fusion peptide. This configuration was perceived to be the native pre-fusion state, because the protein was never exposed to acidic conditions. Wilson's crystal provided insight into influenza's fusion machinery, but left several unanswered questions such as how a buried fusion peptide ended up in a cell membrane almost 100 Å away.

Insights into the conformational rearrangement of HA have been elucidated from synthetic peptides, computer models, and isolated post-fusion ectodomain structures in neutral and low pH conditions.[142,143] Sequencing of the HA protein reveals critical regions involved in the fusion process. The glycine rich fusion peptide which eventually finds itself inserted into the target membrane is located at the N-terminus of the HA2 subunit. Furthermore, computer analysis suggested a region in HA2 would have a strong propensity for forming a coiled-coil similar to the stalk already seen. However, the available crystal structure of HA was at a neutral pH and showed these residues (54-81) to be an extended loop (residues 55-75). Indeed, it was concluded from biophysical studies that the synthetic peptides from this region do form a loop to coiled-coil transformation in solution. This led to the notion of a 'spring-loaded' protein to highlight the notion of a metastable protein primed for action. The result of the identified peptides forming a helix, later confirmed by X-ray crystallography, is the extension of the central helical stalk and the movement of the fusion peptide over 100 Å to the N-terminal end of

the stalk in order to interact with a target membrane **(Figure 22)**. This theory was supported by evidence of proline substitutions at residues 55 and 71 allowing HA expression but disabling fusiogenic activity. While this rearrangement brings the fusion

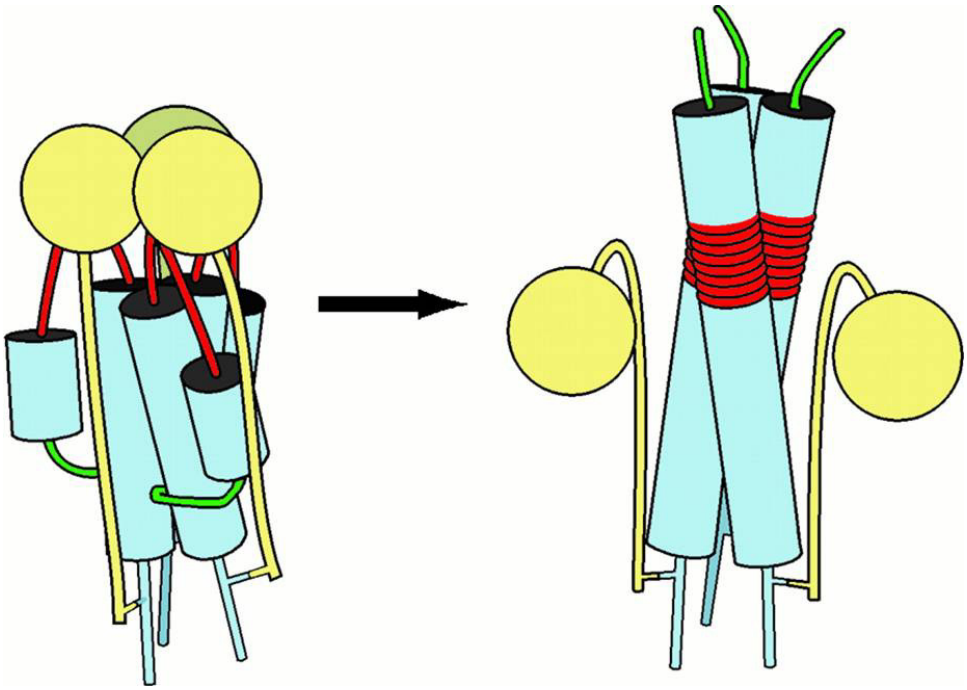

Figure 22. The spring-loaded mechanism for HA mediated fusion. (Left) The native conformation of HA; HA1 subunits (yellow) occupy the distal end of the protein, sitting above a trimeric coiled-coil domain of HA2 (blue). The fusion peptide (green) is sequestered within the core. (Right) Following exposure to low pH, conformational changes occur that trigger the fusion event. Noncovalent interactions between HA1 and HA2 are perturbed allowing the loop regions of HA2 (red) to "spring" into an extension of the central trimeric coiled-coil, thus propelling the fusion peptides to the top of the structure to interact with the target membrane.[142]

peptide in contact with the host membrane, the viral membrane is only brought into close proximity of the host membrane following a transition of residues 112-128 from each of the three members of the HA homotrimer. These residues move to fill grooves along the triple stranded stalk in an anti-parallel fashion. The result is a meshing of the viral and host cell membranes as discussed above. The resulting hexameric coiled-coil of the

transitional peptide segments found in several Class I fusion proteins have demonstrated unusually high melting temperatures.[144-152] The tension and thermal stability of this fusion core formation is thought to provide the driving force and energy needed to achieve the energetically costly fusion process.[146,153,154]

Peptides to Inhibit HIV gp41

One of the modern day plagues is the blood borne human immunodeficiency virus (HIV). HIV1-gp41 is the Class I fusion protein employed by HIV to merge the viral and cellular membranes. Structurally and functionally, gp41 is very similar to HA, but is triggered by the binding of the CD4 receptor on the surface of the target cell membrane in contrast to the low pH trigger of HA. Post-fusion gp41 was subjected to proteolysis, an enzymatic dissection performed to expose stable domains, and only a trimeric helical domain survived.[155] The trimeric unit was found to be comprised of two discontinuous peptides, one from each of two 4, 3 heptad repeat domains (HR). One of two 4, 3 heptad repeat regions is located C-proximal to the fusion protein (HR-1), and the other is N-proximal to the transmembrane anchor (HR-2). Crystallography of both HIV and the closely related simian immunodeficiency virus (SIV) confirmed the presence of the coiled-coil structure in a post-fusion state. The HR-2 peptides were packed in an anti-parallel fashion in the grooves of the triple stranded helical bundle of the HR-1 peptides **(Figure 23)**. Formation of this structure would require a folding of the pre-fusion gp41. This folding would have the HR-2 peptide looping around to the same end of the molecule as the HR-1 peptides resulting in the fusion peptide and transmembrane anchor being in close proximity to promote fusion of the attached membranes.

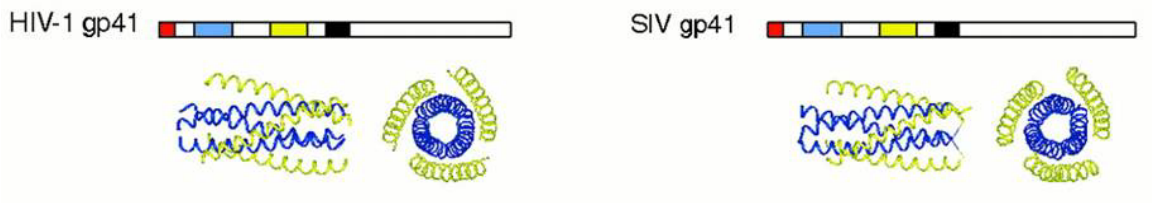

Figure 23. Hexameric coiled-coil crystal structures isolated from HIV and SIV. The top schematic protein sequence displays the fusion peptide (red), HR-1 region (blue), HR-2 region (yellow), and transmembrane domain (black). Adapted from reference 146.

The combined HA and gp41 data suggests a common fusion mechanism amongst members of different viral families. This process has been hypothesized by several groups.[129,131,156,157] It follows that the envelope fusion glycoprotein is expressed as an inactive precursor only able to promote fusion following proteolytic cleavage. The cleavage event locks the protein in a metastable state blocked from fusion by a kinetic barrier. The kinetic barrier theory is supported by experiments that reveal HA can be triggered not only by acidic conditions, but also high temperature and urea denaturation.[158] Once exposed to fusion-activating events, the fusion protein overcomes the kinetic barrier to initiate the required conformational changes for fusion. In the case of HA, HA1 domains lose some of their trimeric contacts and the fusion peptide is liberated from its buried position and is sprung to the amino terminus of the central triple-stranded coiled-coil. This allows the fusion peptide to mesh with host cell membrane. It is unknown in HIV if there is a spring-loaded mechanism involved or if CD4 binding uncovers the fusion peptide, but the fusion peptide and central triple-stranded coiled-coil stalk become exposed. For both viruses, the transmembrane subunit is spanning both the viral and host cell membranes following fusion peptide insertion. Interactions amongst

helical peptides promote the formation of a hexameric coiled-coil that concludes with both membranes at the same end of the folded molecule.

The massive conformation changes required for the Class I fusion proteins leaves the possibility of relatively long lasting intermediates exposed. These intermediates could be exploited as potential fusion inhibiting drug targets. A biomimetic approach that shows promise is the use of synthetic peptides from the HR regions responsible for the coiled-coil domain. Synthetic peptides from both HR-1 and HR-2 have demonstrated effective fusion inhibition.[155,159-161] HR-2 peptides are known to function at the nanomolar range, and are much more potent than the HR-1 peptides, which typically

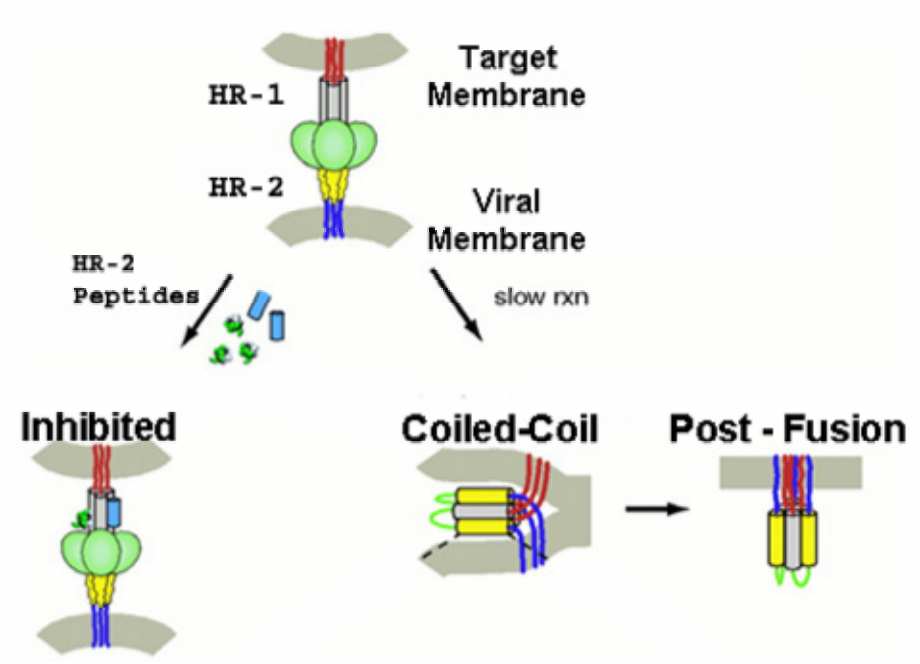

Figure 24. Schematic representation of the current working model for viral membrane fusion. Following exposure to activating conditions, the fusion peptide (red) is inserted into the target membrane exposing the two HR regions. The HR-1 peptide helical stalk, and likely the HR-2 peptide region, is exposed, vulnerable to inhibitory molecules, at least for HIV-1. This 'prehairpin intermediate' of HIV-1 constrains gp41 such that the HR regions cannot interact. In the absence of inhibitors, the prehairpin intermediate resolves into the hexameric coiled-coil, and membrane fusion occurs. Adapted from reference 146.

require a micromolar concentration. The current paradigm has the HR-2 peptides working in a dominant-negative manner where the synthetic peptides compete for binding in the grooves presented by the HR-1 helical stalk **(Figure 24)**. The effectiveness of the unmodified synthetic peptides has lead to several other biomimetic peptide based inhibitors against HIV fusion.[162,163]

The success of HIV inhibiting peptides illustrates a biomimetic success. The use of proteases, computer modeling, and natural peptides has provided a powerful new weapon against a viral killer responsible for thousands of death a year. Furthermore, the target of the HR peptides is proposed to be a common intermediate throughout the Class I fusion proteins thus allowing for similar studies to understand and fight a plethora of viruses.

Research Aims and Goals

The increasing demand for novel weapons in the war against infectious agents and new biologically active materials is at the core of the research presented:

- Excluding vaccines, viruses have historically been out of reach for the pharmaceutical industry. Several drugs are available to combat the symptoms of viral infection, but few actually attack the virus itself. Paramyxoviruses are the leading cause of respiratory distress, and kill thousands of children worldwide every year. The Paramyxoviridae family includes all four parainfluenza strains, measles, mumps, respiratory syncytial virus, and human metapneumovirus. While vaccines are available for a few of these agents such as measles and mumps, most have no known treatment against the virus itself. Chapter II discusses a biomimetic approach to studying and

inhibiting the fusion protein of the human metapneumovirus by utilizing homology modeling techniques and synthetic peptides.

- Unique biologically active materials have potential application in clinical diagnostics, pharmaceuticals, electronic devices, etc. Building upon work done previously in our laboratory, Chapter III explores the synthesis and characterization of silica nanocomposite materials which encase functional enzymes.
- Difficult peptide sequences present the danger of terminating a line of research. Complicated solvent regiments, Hmb protection, and pseudoprolines provide viable options for overcoming the low solubility and aggregation associated with these sequences; however, they are not universally applicable. Chapter IV investigates room temperature ionic liquids (RTILs) as potential new solvents that may have universal application in peptide synthesis.

REFERENCES

(1) Simpson, T. L. V., B.E. *Silicon and Siliceous Structures in Biological Systems*; Springer: New York, 1981.

(2) Round, F. E.,Crawford, R. M.,Mann, D. G. *The Diatoms: Biology & Morphology of the Genera*; Cambridge University Press: Cambridge, 1990.

(3) Kröger, N.,Sumper, M. In *Biomineralization: From Biology to Biotechnology and Medical Applications*; Baeuerlein, E., Ed.; John Wiley and Sons: Weinheim, 2000, pp 151.

(4) Tréguer, P.,Nelson, D. M.,Van Bennekom, J. V.,DeMaster, D. J.,Leynaert, A.,Quéguiner, B. *Science* **1995**, *268*, 375.

(5) Hildebrand, M.,Dahlin, K.,Volcani, B. E. *Mol. Gen. Genom.* **1998**, *260*, 480.

(6) Bhattacharyya, P.,Volcani, B. E. *Proc. Nat'l. Acad. Sci.* **1980**, *77*, 6386.

(7) Sullivan, C. W. *J. Phycol.* **1976**, *12*, 390.

(8) Parkinson, J.,Gordon, R. *Trends Biotechnol.* **1999**, *17*, 190.

(9) Mann, S.,Ozin, G. *Nature* **1996**, *382*, 313.

(10) Kröger, N., Deutzmann, R. & Sumper, M. *Science* **1999**, *286*, 1129.

(11) Kröger, N.,Deutzmann, R.,Bergsdorf, C.,Sumper, M. *Proc. Nat'l. Acad. Sci.* **2000**, *97*, 14133.

(12) Noll, F.,Sumper, M.,Hampp, N. *Nano Lett.* **2002**, *2*, 91.

(13) Pickett-Heaps, J.,Schmid, A. M. M.,Edgar, L. A. In *Prog. Phyc. Res.*; Round, F. E., Chapman, D. J., Eds.; Biopress: Bristol, U.K., 1990; Vol. 7, pp 1.

(14) Zurzolo, C.,Bowler, C. *Plant. Physiol.* **2001**, *127*, 1339.

(15) Crawford, R. M.,Schmid, A. M. In *Biomineralization in Lower Plants and Animals*; The Systematics Society: London, 1986.

(16) Drum, R. W.,Pankratz, H. S. *J. Ultrastruct. Res.* **1964**, *10*, 217.

(17) Edgar, L. A.,Pickett-Heaps, J. D. *J. Phycol.* **1984**, *20*, 47.

(18) Mann, D. G. *Hydrobio.* **1993**, *269/270*, 11.

(19) Van Den Hoak, C.,Mann, D. G.,Jahns, H. M. *Algae: An Introduction to Phycology*; Cambridge University Press: New York, 1997.

(20) Kröger, N.,Wetherbee, R. *Protist* **2000**, *151*, 263.

(21) Kröger, N.,Bergsdorf, C.,Sumper, M. *Eur. J. Biochem.* **1996**, *239*, 259.

(22) Van de Poll, W. H.,Vrieling, E. G.,Gieskes, W. W. C. *J. Phycol.* **1999**, *35*, 1044.

(23) Kröger, N.,Deutzmann, R.,Sumper, M. *J. Biol. Chem.* **2001**, *276*, 26066.

(24) Kröger, N.,Lorenz, S.,Brunner, E.,Sumper, M. *Science* **2002**, *298*, 584.

(25) Kröger, N.,Deutzmann, R.,Sumper, M. *Science* **1999**, *286*, 1129.

(26) Poulsen, N.,Kroger, N. *J. Bio. Chem.* **2004**, *279*, 42993.

(27) Armbrust, E. V.,al., e. *Science* **2004**, *306*, 79.

(28) Frigeri, L. G.,Radabaugh, T. R.,Haynes, P. A.,Hildebrand, M. *Mol. Cell. Prot.* **2006**, *5.1*, 182.

(29) Sumper, M. *Angew. Chem. Int. Ed.* **2004**, *43*, 2251.

(30) Sumper, M.,Lorenz, S.,Brunner, E. *Angew. Chem. Int. Ed.* **2003**, *42*, 5192.

(31) Knecht, M. R.,Wright, D. W. *Langmuir* **2004**, *20*, 4728

(32) Knecht, M. R.,Wright, D. W. *Chem. Comm.* **2003**, *24*, 3038.

(33) Luckarift, H. R.,Spain, J. C.,Naik, R. R.,Stone, M. O. *Nat. Biotech.* **2004**, *22*, 211.

(34) Dave, B. C., Miller, J.M. & Dunn, B., Valentine, J.S. & Zink, J.I. J. *Sol-Gel Sci. Technol.* **1997**, *8*, 629.

(35) Gill, I., Ballesteros, A. *J. Am. Chem. Soc.* **1998**, *120*, 8587.

(36) Mann, S. J. *J. Mater. Chem.* **1995**, *5*, 935.

(37) Monnier, A. et al. *Science* **1993**, *261*, 1299.

(38) Oliver, S., Kuperman, A., Coombs, N., Lough, A. & Ozin, G. *Nature* **1995**, *378*, 47.

(39) Ying, J. Y., Mehnert, C.P. & Wong, M.S. *Angew. Chem. Int. Ed.* **1999**, *38*, 56.

(40) Zhao, D. Y. e. a. *Science* **1998**, *279*, 548.

(41) Kresge, C. T., Lenowicz, M.E., Roth, W.J., Vartuli, J.C. & Beck, J.S. *Nature* **1992**, *359*, 710.

(42) Monnier, A., Schuth, F., Huo, Q., Kumar, D., Margolese, D., Maxwell, R.S., Stucky, G.D., Krishnamurty, M., Petroff, P., Firouzi, A., Janicke, M., Chmelka, B.F. *Sciernce* **1993**, *261*, 1299.

(43) Luckarift, H. R., Spain, Jim C, Naik, Rajesh R & Morley O Stone *Nat. Biotech.* **2004**, *22*, 211.

(44) Merrifield, R. B. *J. Am. Chem. Soc.* **1963**, *85*, 2149

(45) Hearn, M. T. W. *Methods Enzymol.* **1984**, *104*, 190.

(46) Merrifield, R. B. *in Peptides. Synthesis, Structures, and Applications*; Academic Press: New York, 1995.

(47) Sarin, V. K.,Kent, S. B. H.,Erickson, B. W.,Merrifield, R. B. *J. Am. Chem. Soc.* **1980**, *102*, 5463.

(48) Live, D.,Kent, S. B. H. *in Elastomers and Rubber Elasticity*; American Chemical Society: Washington, D.C., 1982.

(49) Feinberg, R. S.,Merrifield, R. B. *Tetrahedron* **1974**, *30*, 3209.

(50) Mitchell, A. R.,Kent, S. B. H.,Erickson, B. W.,Merrifield, R. B. *Tetrahedron Lett.* **1976**, 3795.

(51) Erickson, B. W.,Merrifield, R. B. *J. Am. Chem. Soc.* **1973**, *95*, 3757.

(52) Wang, S. S. *J.Org.Chem.* **1975**, *40*, 1235.

(53) Becker, H.,Lucas, H. W.,Maul, J.,Pillai, V. N. R.,Mutter, M. *Makromol. Chem. Rapid Commun.* **1982**, *3*, 217.

(54) Hellerman, H.,Lucas, H. W.,Maul, J.,Pillai, V. N. R.,Mutter, M. *Makromol. Chem.* **1983**, *184*, 2603.

(55) Zalipsky, S.,Albericio, F.,Barany, G. In *Peptides. Structure and Function. Proceedings of the 9th American Peptides Symposium*; Deber, C. M., Hruby, V. J., Kopple, K. D., Eds.; Pirece Chemical Company: Rockford, IL, 1985, p 257.

(56) Zalipsky, S.,Chang, J. L.,Albericio, F.,Barany, G. *React. Polym.* **1994**, *22*, 243.

(57) Bayer, E.,Hemmasi, B.,Albert, K.,Rapp, W.,Dengler, M. In *Peptides. Structure and Function. Proceedings of the 8th American Peptides Symposium*; Hruby, V. J., Rich, D. H., Eds.; Pierce Chemical Company: Rockford, IL., 1983, p 87.

(58) Bayer, E.,Dengler, M.,Hemmasi, B. *Int. J. Pept. Protein Res.* **1985**, *25*, 178.

(59) Hellstern, H.,Hemmasi, B. *Biol. Chem. Hoppe-Seyler* **1988**, *369*, 289.

(60) Bayer, E. *Angew. Chem. Int. Ed. Engl.* **1991**, *30*, 113.

(61) Bayer, E.,Rapp, W. *in Poly(Ethylene) Glycol Chemistry: Biotechnological and Biomedical Applications*; Plenum Press: New York, 1992.

(62) Englebretsen, D. R.,Harding, D. R. K. *Int. J. Pept. Protein Res.* **1992**, *40*, 487.

(63) Eichler, J.,Beyermann, M.,Bienert, M. *Coll. Czech. Chem. Commun.* **1989**, *54*, 1756.

(64) Carpino, L. A. *J. Am. Chem. Soc.* **1957**, *79*, 4427.

(65) McKay, F. C.,Albertson, N. F. *J. Am. Chem. Soc.* **1957**, *79*, 4686.

(66) Carpino, L. A.,Han, G. A. *J. Org. Chem.* **1972**, *37*, 3404.

(67) O'Ferrall, R. A. M.,Slae, S. *J. Chem. Soc.* **1970**, *(B)*, 260.

(68) O'Ferrall, R. A. M. *J.Chem.Soc.* **1970**, *(B)*, 274.

(69) Kaiser, E.,Colescott, R. L.,Bossinger, C. D.,Cook, P. I. *Analyt. Biochem.* **1970**, *34*, 595.

(70) Sheehan, J. C.,Hess, G. P. *J. Am. Chem. Soc.* **1955**, *77*, 1067.

(71) Sarantakis, D.,Teichman, J.,Lien, E. L.,Fenichel, R. *Biochem. Biophys. Res. Comm.* **1976**, *73*, 336.

(72) Benoiton, N. L. *Biopolymers (Pept. Sci.)* **1996**, 245.

(73) Bergmann, M.,Zervas, L. *Biochem.* **1928**, 280.

(74) Wunsch, E.,Drees, F. *Chem. Ber.* **1966**, *99*, 110.

(75) Weygand, F.,Hoffman, D.,Wunsch, E. *Naturforsch* **1966**, *21b*, 426.

(76) Konig, W.,Geiger, R. *Chem. Ber.* **1970**, *103*, 788.

(77) Gawne, G.,Kenner, G.,Sheppard, R. C. *J. Am. Chem. Soc.* **1969**, *91*, 5669.

(78) Dourtoglou, V.,Ziegler, J. C.,Gross, B. *Tetrahedron Lett.* **1978**, 1269.

(79) Dourtoglou, V.,Gross, B.,Lambropoulou, V.,Ziodrou, C. *Synthesis* **1984**, 572.

(80) Coste, J.,Dufour, M. N.,Pantaloni, A.,Castro, B. *Tetrahedron Lett.* **1990**, *31*, 669.

(81) Frerot, E.,Coste, J.,Pantaloni, A.,Dufour, M. N.,Jouin, P. *Tetrahedron* **1991**, *47*, 259.

(82) Schnolzer, M.,Alewood, P.,Jones, A.,Alewood, D.,Kent, S. B. H. *Int. J. Pept. Protein Res.* **1992**, *40*, 180.

(83) Wiijkmans, J. C. H. M.,Blok, F. A. A.,van der marel, G. A.,van Boom, J. H.,Bloemhoff, W. *Tetrahedron Lett.* **1995**, *36*.

(84) Tam, J. P.,Merrifield, R. B. *in The Peptides, Analysis, Synthesis, Biology*; Academic Press: New York, 1987; Vol. 9.

(85) Atherton, E.,Sheppard, R. C. *Solid Phase Peptide Synthesis*; IRL Press: Oxford, 1989.

(86) Pearson, D.,Blanchette, M.,Baker, M. L.,Guidon, C. A. *Tetrahedron Lett.* **1989**, *30*, 2739.

(87) King, D. S.,Fields, C. G.,Fields, G. B. *Int. J. Pept. Protein Res.* **1990**, *36*, 255.

(88) Atherton, E.,Woolley, V.,Sheppard, R. C. *J. Chem. Soc. Chem. Comm.* **1980**, 970.

(89) Bedford, J.,Hyde, C.,Johnson, T.,Jun, W.,Owen, D.,Quibell, M.,Sheppard, R. C. *Int. J. Pept. Protein Res.* **1992**, *9*, 106.

(90) Epton, R.,Goddard, P.,Ivin, K. J. *Polymer* **1980**, *21*, 1367.

(91) Giralt, E.,Rizo, J.,Pedroso, E. *Tetrahedron* **1984**, *40*, 4141.

(92) Narita, M.,Ishikawa, K.,Chen, J. Y.,Kim, Y. *Int. J. Pept. Protein Res.* **1984**, *24*, 580.

(93) Narita, M.,Ishikawa, K.,Nakano, H.,Isokawa, S. *Int. J. Pept. Protein Res.* **1984**, *24*, 14.

(94) Yamashiro, D.,Blake, J.,Li, C. H. *Tetrahedron Lett.* **1976**, 1469.

(95) Westall, F. C.,Robinson, A. B. *J. Org. Chem.* **1970**, *35*.

(96) Milton, S. C. F.,Milton, R. C. d. L. *Int. J. Pept. Protein Res.* **1990**, *36*, 193.

(97) Stewart, J. M.,Klis, W. A. *in Innovation and Perspectives in Solid Phase Synthesis and Related Technologies. Peptides, Polypeptides, Oligonucleotides. Macro-Organic Reagents and Catalysts*; SPCC (U.K.) Ltd.: Birmingham, U.K., 1990; Vol. 1.

(98) Hendrix, J. C.,Halverson, K. J.,Jarrett, J. T.,Lansbury, P. T. *J. Org. Chem.* **1990**, *55*, 4517.

(99) Johnson, T.,Quibell, M.,Sheppard, R. C. *J. Pept. Sci.* **1995**, *1*, 11.

(100) Nicolas, E.,Pujades, M.,Bacardit, J.,Giralt, E.,Albericio, F. *Tetrahedron Lett.* **1997**, *38*.

(101) Quibell, M.,Johnson, T. *Fmoc Solid Phase Peptide Synthesis: A Practical Approach*; Oxford University Press, Inc.: New York, 2000.

(102) Quibell, M.,Turnell, W. G.,Johnson, T. *J. Chem. Soc., Perkin Trans. 1* **1995**, 2019.

(103) Zeng, W.,Regamey, P. O.,Rose, K.,Wang, Y.,Bayer, E. *Int. J. Pept. Protein Res.* **1997**, *49*, 273.

(104) Mutter, M.,Nefzi, A.,Sato, T.,Sun, X.,Wahl, F.,Wohr, T. *Pept. Res.* **1995**, *8*, 145.

(105) Wohr, T.,Wahl, F.,Nefzi, A.,Rohwedder, B.,Sato, T.,Sun, X.,Mutter, M. *J. Am. Chem. Soc.* **1996**, *118*, 9218.

(106) Haack, T.,Mutter, M. *Tetrahedron Lett.* **1992**, *33*, 1589.

(107) Gutte, B.,Merrifield, R. B. *J. Am. Chem. Soc.* **1969**, *91*, 501.

(108) Mutter, M. *Angew. Chem.* **1985**, *97*, 639.

(109) Degrado, W. F.,Wasserman, Z. R.,Lear, J. D. *Science* **1989**, *243*, 622.

(110) Mutter, M.,Vuilleumier, S. *Angew. Chem. Int. Ed.* **1989**, *28*, 535.

(111) Richardson, J. S.,Richardson, D. C. *Trends Biochem. Sci.* **1989**, *14*, 904.

(112) Kaiser, E. T.,Kezdy, F. J. *Science* **1984**, *223*, 249.

(113) Eisenberg, W.,Wilcox, S. M.,Eshita, P. M.,Pryciak, P. M.,Ho, S. P.,Degrado, W. F. *Proteins* **1986**, *1*, 16.

(114) Ho, S. P.,Degrado, W. F. *J. Am. Chem. Soc.* **1987**, *109*, 6751.

(115) Mutter, M.,Hersperger, R. *Angew. Chem. Int. Ed.* **1990**, *29*, 185.

(116) Greenfield, N.,Davidson, B.,Fasman, G. D. *Biochemistry* **1967**, *6*, 1630.

(117) Mutter, M.,Gassman, R.,Buttkus, U.,Altman, K. H. *Angew. Chem. Int. Ed.* **1991**, *30*, 1514.

(118) Blumenthal, R.,Dimitrov, D. S. *Handbook of Physiology*; Oxford University Press: New York, 1985.

(119) Lentz, B. R.,Lee, J. K. *Mol. Membr. Biol* **1999**, *16*, 279.

(120) Weber, T.,Zemelman, B. V.,Mcnew, J. A.,Westermann, B.,Gmachl, M.,Parlati, F.,Sollner, T. H.,Rothman, J. E. *Cell* **1998**, *92*, 759.

(121) Rand, R. P.,Kachar, B.,Reese, T. S. *Biophys. J.* **1985**, *47*, 483.

(122) Baker, T. S.,Olson, N. H.,Fuller, S. D. *Microbiol. Mol. Biol. Rev.* **1999**, *63*, 862.

(123) Rand, R. P.,Parsegian, V. A. *in Molecular Mechanisms of Membrane Fusion*; Plenum Press Publishing Corporation: New York, 1988.

(124) Tse, F. W.,Iwata, A.,Almers, W. *J. Cell Biol.* **1993**, *121*, 543.

(125) Spruce, A. E.,Iwata, A.,Almers, W. *Proc. Nat'l. Acad. Sci.* **1991**, *88*, 3623.

(126) Zimmerberg, J.,Blumenthal, R.,Sarkar, D. P.,Curran, M. *J. Cell Biol.* **1994**, *127*, 1885.

(127) Clague, M. J.,Schoch, C.,Zech, L.,Blumenthal, R. *Biochemistry* **1990**, *29*, 1303.

(128) Bostrom, M.,Williams, D. R. M.,Ninham, B. W. *Phys. Rev. Lett.* **2001**, *87*, 168103.

(129) Hernandez, L. D., *et al. Annu. Rev. Cell Dev. Biol.* **1996**, *12*, 627.

(130) Stiansy, K.,Allison, S. L.,Schalich, J.,Heinz, F. X. *J. Virol.* **2002**, *76*, 3784.

(131) Chan, D. C.,Kim, P. S. *Cell* **1998**, *93*, 681.

(132) Skehel, J. J.,Wiley, D. C. *Cell* **1998**, *95*, 871.

(133) Gruenke, J. A.,Armstrong, R. T.,Newcomb, W. W.,Brown, J. C.,White, J. M. *J. Virol.* **2002**, *76*, 4456.

(134) Kielian, M.,Chatterjee, P. K.,Gibbons, D. L.,Lu, Y. E. *Subcell. Biochem.* **2000**, *34*, 409.

(135) Lescar, J.,Roussel, A.,Wien, M. W.,Navaza, J.,Fuller, S. D.,Wengler, G.,Rey, F. A. *Cell* **2001**, *105*, 137.

(136) Rey, F. A.,Heinz, F. X.,Mandl, C.,Kunz, C.,Harrison, S. C. *Nature* **1995**, *375*, 291.

(137) Wiley, D. C.,Skehel, J. J. *Annu. Rev. Biochem.* **1987**, *56*, 365.

(138) Puri, A.,Booy, F.,Doms, R. W.,White, J. M.,Blumenthal, R. *J. Virol.* **1990**, *64*, 3824.

(139) Korte, T.,Ludwig, K.,Booy, F. P.,Blumenthal, R.,Herrmann, A. *J. Virol.* **1999**, *73*, 4567.

(140) Stegmann, T.,Booy, F. P.,Wilschut, J. *J. Biol. Chem.* **1987**, *262*, 17744.

(141) Wilson, I. A.,Skehel, J. J.,Wiley, D. C. *Nature* **1981**, *289*, 366.

(142) Carr, C. M., and Kim, P.S. *Cell* **1993**, *73*, 823.

(143) P.A., B.,Hughson, F. M.,Skehel, J. J.,Wiley, D. C. *Nature* **1994**, *371*, 37.

(144) Charles J. Russell, T. S. J. a. R. A. L. *EMBO Journal* **2001**, *20*, 4024.

(145) Dutch, R. E.,Leser, G. P.,Lamb, R. A. *Virology* **1999**, *254*, 147.

(146) Eckert, D. M.,Kim, P. S. *Annu. Rev. Biochem.* **2001**, *70*, 777.

(147) Lamb, R. A.,Joshi, S. B.,Dutch, R. E. *Mol. Mem. Bio.* **1999**, *16*, 11.

(148) Lambert, D. M.,Barney, S.,Lambert, A. L.,Guthrie, K.,Medinas, R.,Davis, D. E.,Bucy, T.,Erkckson, J.,Merutka, G.,Petteway, S. R., Jr. *Proc. Nat'l. Acad. Sci.* **1996**, *93*, 2186.

(149) Lawless-Delmedico, M. K. *Biochemistry* **2000**, *39*, 11684.

(150) Malashkevich, V. N., Kim, P.S., et al. *Proc. Nat'l. Acad. Sci.* **1998**, *95*, 9134.

(151) Reay G. Paterson, C. J. R., and Robert A. Lamb *Virology* **2000**, *270*, 17.

(152) Xun Zhao, *e. a. Proc. Nat'l. Acad. Sci.* **2000**, *97*, 14172.

(153) Melikyan, G. B.,Markosyan, R. M.,Hemmati, H.,Delmedico, M. K.,Lambert, D. M.,Cohen, F. S. *J. Cell Bio.* **2000**, *151*, 413.

(154) Blumenthal, R.,Michael, J. C.,Stewart, R. D.,Epand, R. M. *Chem. Rev.* **2003**, *103*, 53.

(155) Lu, M.,Blacklow, S. C.,Kim, P. S. *Nat. Struct. Bio.* **1995**, *2*, 1075.

(156) Hughson, F. M. *Curr. Biol.* **1997**, *7*, R565.

(157) Chernomordik, L. V.,Leikina, E.,Kozlov, M. M.,Frolov, V. A.,Zimmerberg, J. *Mol. Membr. Biol* **1999**, *16*, 33.

(158) Carr, C. M.,Chaudhry, C.,Kim, P. S. *Proc. Nat'l. Acad. Sci.* **1997**, *94*, 14306.

(159) Jiang, S. B.,Lin, K.,Strick, N.,Neurath, A. R. *Nature* **1993**, *365*, 113.

(160) Wild, C., et al. *Proc. Nat'l. Acad. Sci.* **1992**, *89*, 10537.

(161) Wild, C.,Shugars, D. C.,Greenwell, T. K.,McDanal, C. B.,Matthews, T. J. *Proc. Nat'l. Acad. Sci.* **1994**, *91*, 9770.

(162) Samuel K. Sia, P. A. C., Andrea G. Cochran, Vladamir N. Malashkevich, and Peter S. Kim *Proc. Nat'l. Acad. Sci.* **2002**, *99*, 14664.

(163) Eckert, D. M.,Kim, P. S. *Proc. Nat'l. Acad. Sci.* **2001**, *98*, 11187.

(164) Blumenthal, R., Clague, M.J., Durell, S.R., Epand, R.M. *Chem. Rev.* **2003**, *103,* 53

(165) P.L.Williams, *et al. Chemical Approaches to the Synthesis of Peptides and Proteins,* CRC Press, New York 1997, p.15

CHAPTER II

THE HUMAN METAPNEUMOVIRUS FUSION PROTEIN MEDIATES FUSION THROUGH A COILED-COIL COMPLEX THAT CAN BE INHIBITED BY SYNTHETIC HEPTAD REPEAT REGION 1 PEPTIDES

Introduction

Viruses are a leading cause of lower respiratory tract infection in children worldwide, with significant associated morbidity and mortality. Previously identified major pathogens include respiratory syncytial virus (RSV), parainfluenza viruses (PIV), influenza and measles viruses, all of which are associated with clinical syndromes of severe lower respiratory tract disease, such as bronchiolitis, pneumonia, and laryngotracheobronchitis. In 2001, a new member of this viral group, the human metapneumovirus (hMPV), was discovered by Dutch scientists.[1] Samples collected longitudinally from 1976 to 2001 at the Vanderbilt Vaccine Clinic showed that 12% of lower respiratory tract diseases were attributable to hMPV.[2] Subsequent genetic analysis classified hMPV as a member of the pneumovirus subgroup within the paramyxoviridae family.[3]

The paramyxoviridae family includes two subfamilies: the paramyxoviruses and the pneumoviruses. Paramyxoviruses include all the parainfluenza types, sendai virus, mumps virus, hendra virus, Newcastle disease virus, simian type 5 virus, the morbilliviruses measles virus, canine distemper virus and others. The pneumovirus subfamily consists of the pneumoviruses RSV and pneumonia virus of mouse, the metapneumoviruses avian metapneumovirus, and hMPV.[4] Paramyxoviruses contain two major surface glycoproteins critical for viral replication and survival. The attachment

protein (G, HN, or H) first locates and binds to the cellular target. After binding, multiple trimers of the fusion (F) protein take part in anchoring the viral membrane to the host cell membrane, allowing viral entry to the cell.

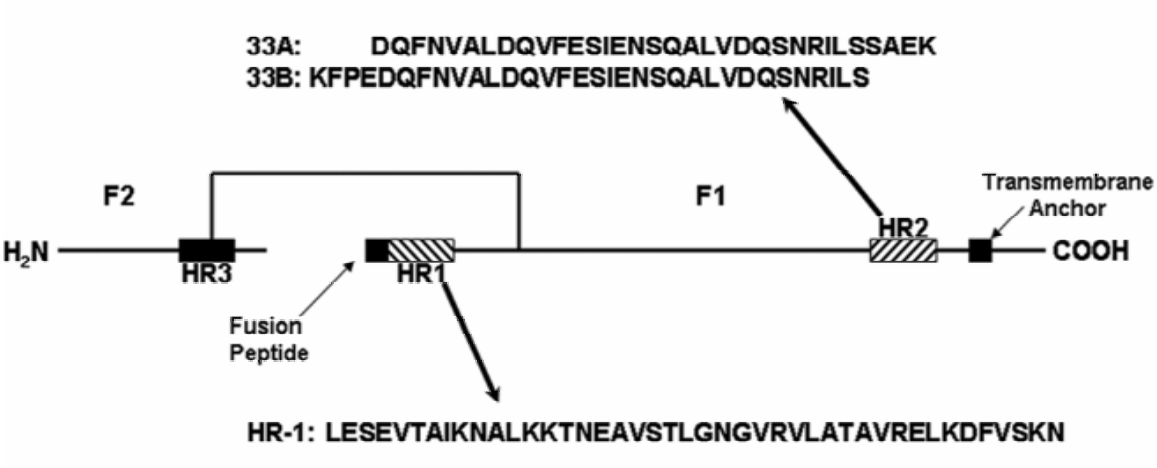

Figure 25. Schematic view of the fusion protein (F protein). The ectodomain of the hMPV F1 and F2 subunits. The relative positions of the heptad repeat regions, fusion peptide, and transmembrane anchor are illustrated. The synthetic peptides used in this study are from the HR-1 and HR-2 regions, and their sequences are listed. Peptides do not have modified N or C termini.

F protein Domains: Paramyxovirus F proteins are type I integral membrane viral fusion proteins that are synthesized as inactive precursors (F_0) and then cleaved by host-cell proteases into the biologically fusion-active F_1 and F_2 domains **(Figure 25)**. F_2 is extracellular and disulfide-linked to F_1. These type I glycoproteins span the membrane once and are a common feature among a variety of other viruses including influenza virus,[5] simian immunodefiency virus (SIV),[6] human immunodeficiency virus (HIV),[7] and Ebola virus.[8] Following cleavage, three units of fusion protein form homotrimers embedded in the viral membrane. There are two 4-3 heptad repeat domains at the N- and C-regions of the protein (designated HR-1 and HR-2 respectively), which form coiled-coil α-helices (discussed in detail below) following target cell binding. A hydrophobic

fusion peptide N-proximal to the N-terminal heptad repeat is thought to insert into the target cell membrane. At their C-terminus, a hydrophobic trans-membrane (TM) domain anchors the F protein in the plasma membrane, leaving a short cytoplasmic tail. The end result of the fusion process is the eventual association of the heptad repeats, bringing the TM domain and viral membrane into juxtaposition with the cellular membrane inducing membrane fusion.[9] Indeed, the process of hexameric coiled-coil formation has been postulated to provide ample energy to drive fusion in HIV infection, due to the large energy gain by the increase in stability afforded by the hexameric coiled-coil structure.[10] Thus, F proteins are thought to promote membrane fusion by coupling irreversible folding to membrane juxtaposition.

F protein Structure: Yin *et al.* recently solved the structure of both the pre-fusion F protein of parainfluenza virus 5 F and the cleaved ectodomain of the PIV3 F protein in a post-fusion state.[11,12] Combined, these two structures offer a view of the paramyxovirus F protein before and after fusion. In the pre-fusion conformation, the F protein is broken down into several key domains. The pre-fusion structure contains a globular head fixed to the trimeric helical bundle comprised of HR-2 peptides **(Figure 26)** reminiscent of a lollipop. The end of the HR-2 stalk has the TM domain inserted into the viral membrane. The globular head itself contains three domains, denoted DI – DIII.[12,13] DI and DII fold into rigid scaffolding molecules during the fusion event, while much of the conformational changes occur in the DIII domain (amino acids 42-278). The top of the head has three spikes formed by peptidyl loops (60-65 and 178-185), which project upwards from the globular domains of each subunit. Each of the three units of the F homotrimer contains their own DI-DIII domains wrapping around the trimeric axis,

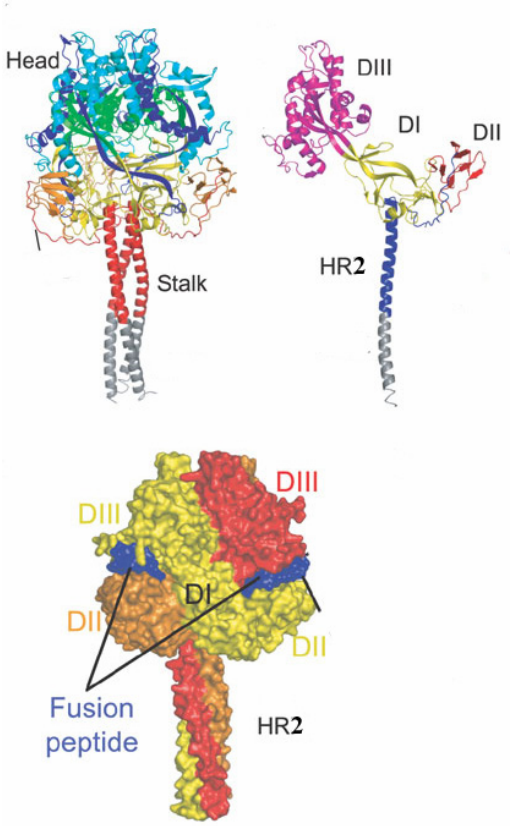

Figure 26. The pre-fusion structure of parainfluenza virus 5. (Top Left) Ribbon diagram of the homotrimer responsible for fusion. The head region undergoes massive conformation changes during the fusion event. The stalk is comprised of the HR-2 segments and terminates in the TM domain inserted into the viral membrane. Grey areas indicated an engineered non-native coiled-coil to simulate the full length stalk. (Top Right) Ribbon diagram of a single monomer of the F protein. The domains are labeled and color coded. DIII contains the helical loops and subunits which undergo stalk extension to generate the HR-1 trimeric coiled-coil. (Bottom) Color coded surface map of the pre-fusion trimeric structure. The fusion peptide eventually is inserted into the target cellular membrane. This requires the fusion peptide to travel ~ 115 Å to the N-terminus of the HR-1 trimeric stalk. Adapted from ref. 11.

creating several intersubunit contact points. Units DI and DII form the bottom side of a large cavity present at the base of the head. DIII covers the top of the cavity and contains the important spikes comprised of HR-1 and the fusion peptide (residues 103-128). HR-1 is composed of two sets of six helices forming rings which cover the top of the head, while the HR-2 three helices bundle from underneath. The fusion peptide located in DIII is in three different parts: part extended, part ß-sheet, and part α-helix. It is

pressed between DIII of its own subunit and DII of another subunit. The F protein is likely to maintain this structure until triggered by binding of a cellular targeting protein, such as hemagglutinin neuramidase (HN) in SV5, upon which the refolding into the metastable pre-fusion hairpin occurs.

At the time of this writing, crystallographic data pertaining to the metastable pre-fusion structure is absent from the literature; however, the post-fusion structure reveals the final structure resulting from PIV3 F protein mediated fusion. The massive conformational shifts of fusion result in a final F protein structure containing a predominately ß-sheet globular head, a neck region consisting of both ß-sheet and α-helix, and an elongated stalk region (monomer dimensions are ~ 27 X 160 Å) comprised of mostly α-helix **(Figure 27).** The crystal is formed by three elongated monomers that utilize their C-terminal regions (residues 428-484) to span across the trimeric axis to interact with the adjacent monomers.

The most intriguing element of the post-fusion PIV3 F protein structure is the hexameric coiled-coil bundle associated with the long stalk. The bundle is a joining of each monomer's HR-1 and HR-2 regions. The three HR-1 domains form an interior trimeric helical bundle that exposes long hydrophobic grooves along its surface and contains the familial 3-4-4-4-3 stutter pattern (residues 172-187). This stutter is necessary for the HR-1 segment to avoid a kink in the long hydrophobic groove. The hydrophobic faces of the HR-2 domains pack into the hydrophobic grooves of the HR-1 trimeric bundle. Missing from the structure are residues (95-135) which are N-terminal to HR-1 and which include the fusion peptide (starting at residue 110). Computer

modeling of the missing residues suggests that the fusion peptide is located at the tip of the hexameric coiled-coil analogous to influenza's HA (Chapter I).

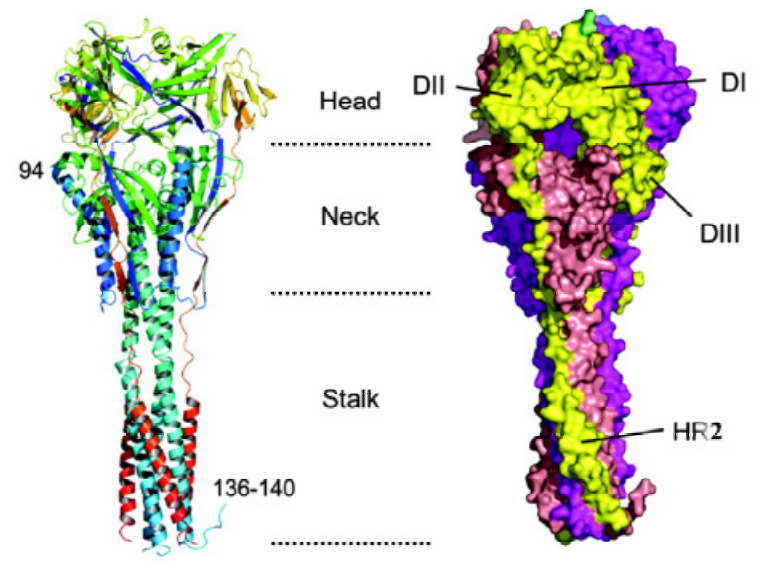

Figure 27. (Left) Ribbon diagram of the trimeric hPIV3 F protein in a post-fusion conformation. Residues 95-135 are disordered in all monomeric units. (Right) The surface image of the hPIV3 F protein. The individual F protein monomers are distinctly colored. Adapted from ref. 12.

In order to mediate viral and target cell membrane fusion, a significant refolding process must occur to achieve the post-fusion conformation seen for PIV3's F protein that started from the pre-fusion structure analogous to that of parainfluenza virus 5 F. The overall transition revolves around flipping the stalk and transmembrane domains relative to the F protein head. The globular head region is significantly compacted in the post-fusion form compared to the pre-fusion configuration. The DI domains turn slightly inwards, disrupting intersubunit contacts, while the DII domains swing around to make new contacts with other monomers. Overall, however, DI and DII domains remain close to their starting positions. Indeed, superimposing these regions in their pre- and post-

fusion positions reveals an average root-mean-square (RMS) deviation of 1.97 Å and 1.5 Å, respectively.

DIII experiences extensive refolding between the pre- and post-fusion structures, resulting in the hexameric coiled-coil projecting upwards from the head and away from DI, the pre-fusion stalk, and the viral membrane. The fusion peptide moving ~ 115 Å from its pre-fusion position to allow for DII repositioning is illustrative of the extreme refolding achieved by type I F proteins. The extension of a HR-1 stalk away from the viral membrane requires DIII to rotate and collapse inwards, further compacting the globular head **(Figure 28)**.

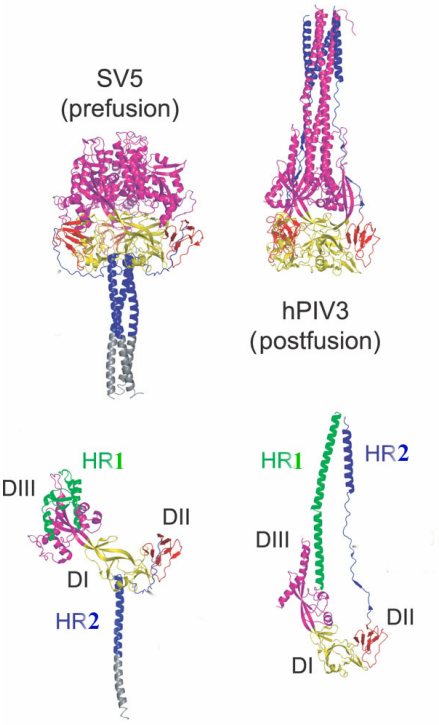

Figure 28. (Top) Side by side comparison of two type I F proteins in the pre- and post-fusion configurations. The DII elements orchestrating stalk extension are colored magenta. The HR-2 region is blue, and the DI and DII domains are yellow. (Bottom) Single monomer of the F proteins discussed above. The HR-1 region is highlighted in green and converts from well compacted helical and loop regions into an elongated stalk in a coiled-coil configuration. The HR-2 sequence migrates to pack into the hydrophobic grooves presented on the surface of the HR-1 stalk. Adapted from ref. 11.

All of the HR-1 post-fusion contacts are absent from the pre-fusion structure. The pre-fusion crystal has HR-1 divided up into four helices, two ß-strands, and five loop or kink segments. Therefore, no fewer than 11 distinct segments must undergo refolding in the DIII region to form a single elongated α-helical stalk. The hydrophobic grooves exposed on the surface of this stalk are eventually filled by HR-2 segments. In the prefusion structure, the HR-2 segments are located at the base of the head region and terminate with the TM domain inserted into the viral membrane. During the conversion to the post-fusion conformation, these HR-2 segments separate and relocate to the base of the nascent HR-1 stalk extending towards the target cellular membrane. The result is the TM domain fixed to the viral membrane moving near the fusion peptide, which is inserted into the target cellular membrane at the base of the HR-1 stalk **(Figure 29)**.

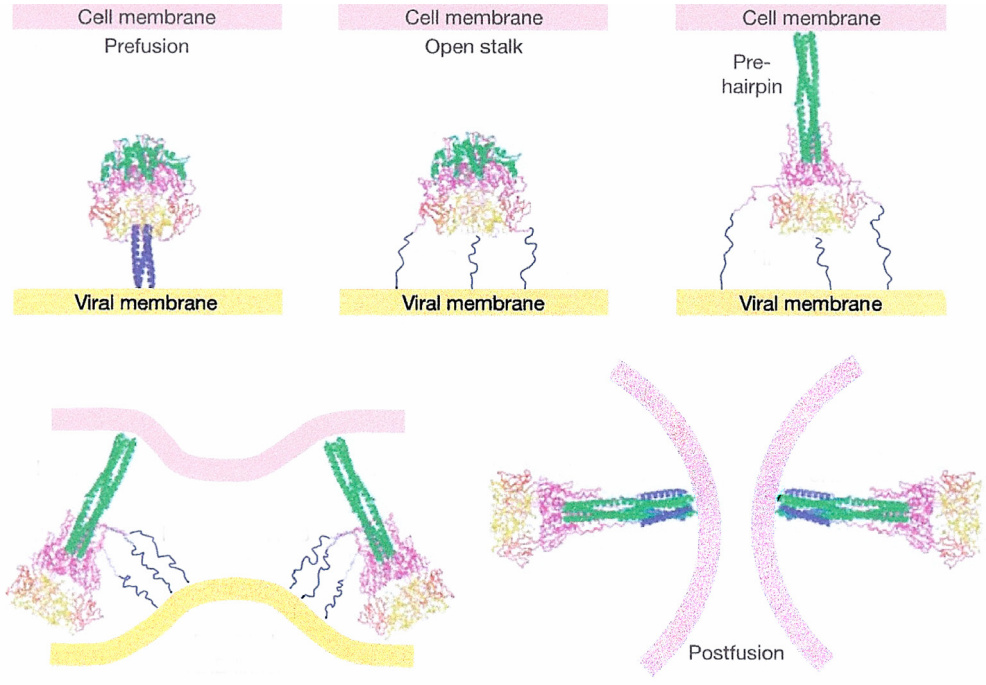

Figure 29. Proposed fusion based upon structural literature. The pre-hairpin comprised of the HR-1 stalk (green) following extension is labeled. The hydrophobic grooves along the surface of the pre-hairpin structure are packed by the HR-2 peptides (blue) in order to bring the cellular membrane and viral membrane in close proximity. Adapted from ref. 11.

Synthetic Peptides to Study Fusion: Initial structural studies of type I F proteins focused on the important hexameric coiled-coil comprised of the HR-1 and HR-2 protein segments. Peter Kim and associates used enzymatic digestion to determine the specific sequences associate with the HIV gp41 fusion core.[14] They isolated two peptides that each contain a 4, 3 heptad repeat, a 51 residue segment from HR-1 (N51; residues 540 – 590) and a 43 residue piece from HR-2 (C43; residues 624 – 686). Biophysical examination of synthetic N51 and C43 demonstrate distinct differences. The CD spectra of N51 contain a strong minimum at 222 nm indicative of α-helical conformation. The uneven 210 and 222 nm minima indicate aggregation into non-discrete formations. Furthermore, the signal was found to be concentration dependent. Also, N51 solutions experienced thermal denaturation and were shown to be proteinase-resistant, completing the profile of a strong tendency towards self-aggregation **(Figure 30)**. In contrast, the C43 peptide displayed little secondary structure. C43 was also found to be vulnerable to proteinase, but was unaffected upon addition of N51 up to a 1:1 stoichiometry.

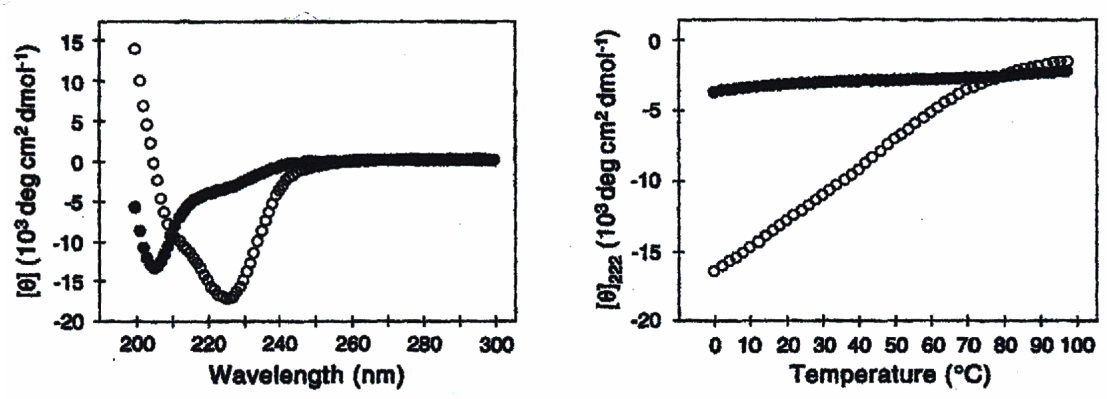

Figure 30. (Left) CD spectra of N51 (open circles) and C43 (filled circles). (Right) Thermal response for N51 and C43.[14]

The 1:1 molar mixture of N51 and C43 was of particular importance. CD analysis of the mixture resulted in a strong helical spectrum. The helical content was found to be greater than the additive spectrum of the two individual peptide spectra. This is indicative of peptide interaction, in particular, tertiary structure formation of predominately α-helical conformation. The even minima at 210 and 222 nm are indicative of a discrete structure. Indeed, sedimentation measurements revealed a mass consistent with a 1:1 ratio of six peptides of N51 and C43. Evidence supporting the hypothesis that formation of such a hexameric structure was the source of energy to drive fusion was obtained by determining the melting point of the N51 and C43 complex to be 93 °C **(Figure 31)**. Furthermore, specialized proteolysis of the N51 and C43 complex with a shortened N51 missing 12 residues from the N-terminus was performed. This experiment resulted in two peptide fragments, the 12 residue shortened N51 and a 30 residue peptide from C43. The shortened C43 peptide was truncated from the C-terminus indicating that N51 and C43 are aligned anti-parallel in the hexameric complex.

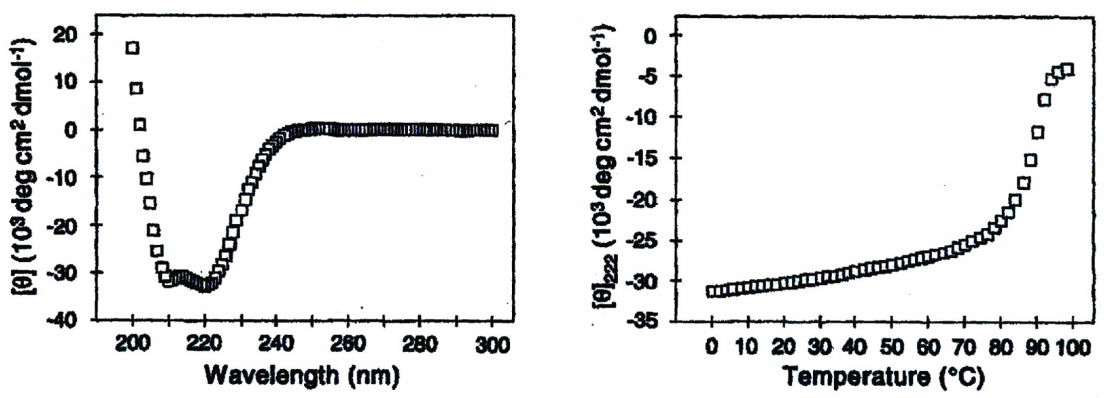

Figure 31. (Left) CD spectra of 1:1 molar mixture of N51 and C43. (Right) Melting curve for coiled-coil complex.[14]

Five years later, Lambert and associates conducted similar experiments with the HR sequences of RSV that demonstrate the similarity between type I F proteins across viral families despite poor sequence homology.[15] The peptides used in the study were

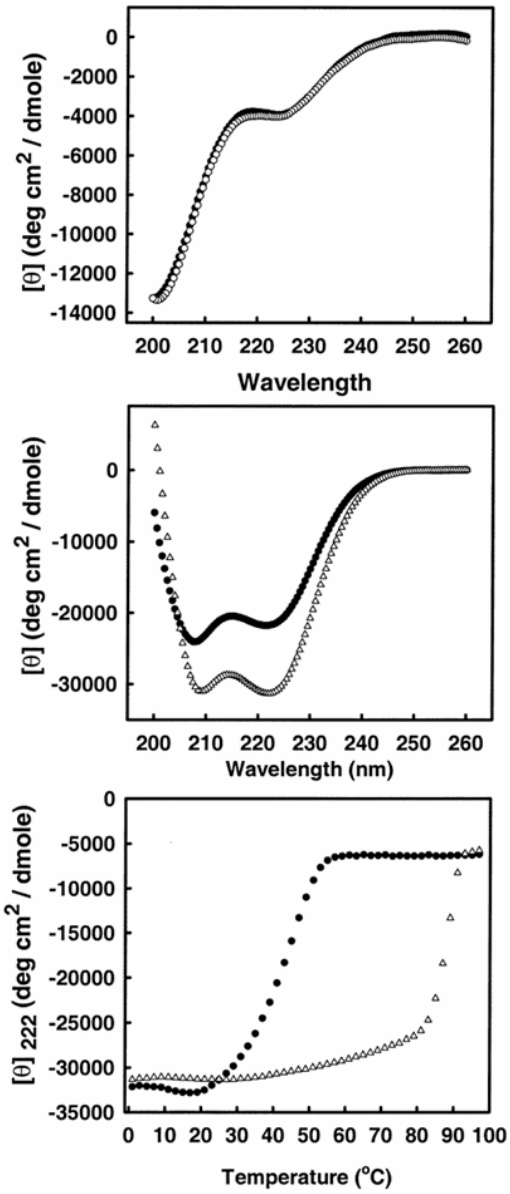

Figure 32. (Top) CD spectra of HR-2 peptide at 10 μM (filled circles) and 50 μM (open circles). (Middle) CD spectra of 1:1 mixture of the RSV HR-1 and HR-2 peptides (open circles) and the predicted spectrum assuming no interaction (filled circles). (Bottom) Melting temperature data of the HR peptides mixture (open circles) and HR-1 peptide (filled circles).[15]

also derived from proteinase-K experiments. The sequences used consisted of a 50-mer from HR-1 and a 35-mer from HR-2. The CD studies on HR-1 suggested helical self-association. The self-assembled homotrimer was confirmed by sedimentation studies and was found to have a thermal melting point of 42 °C. Simliar to C43 of HIV, the HR-2 peptide of RSV displayed random-coil monomeric secondary structure. Upon mixing both peptides, an increase in helicity content was observed (86%) that was greater than the predicted additive spectra (55%) **(Figure 32)**. The thermal stability of this complex was discovered to be ~ 87 °C. Sedimentation equilibrium experiments of the solution mixture were employed to confirm that the peptides were in a 1:1 ratio.

The striking similarities between the HIV and RSV HR peptides and their interactions was further demonstrated when the crystal structures of their respective fusion cores were solved by Peter Kim and coworkers.[16,17] While the exact sequences used for crystallographic measurements were not completely identical to the previous biophysical work on HR peptides for HIV and RSV, the sequences used were from the same domain and determined via proteolysis. HIV's core structure consisted of a 36-mer from the HR-1 region (N36; residues) and a 34-mer from the HR-2 region (C34; residues). RSV's structure was composed of a HR-1 peptide of 57 residues (residues 153-209) and a HR-2 peptide of 45 amino acids (HRSV-C45; residues 476-520). Both structures are of three HR-1 peptides forming a parallel, interior coiled-coil while three HR-2 peptides pack into hydrophobic grooves along the interior coiled-coil's surface in an anti-parallel fashion **(Figure 33)**. Numerous electrostatic contact points line the hydrophobic grooves and interact with the complementary HR-2 peptide. Another intriguing feature common to both structures is a hydrophobic pocket located near the

C-terminal area of the HR-1 interior core. This deep channel is filled by bulky hydrophobic sidechains from the corresponding HR-2 peptide (I635, W631, and W628 for HIV; F488 and F483 for RSV). This cavity and the corresponding HR-2 sidechains were later shown to be critical for fusion in HIV, thus presenting an attractive target for non-biomimetic small molecule drug design.[18]

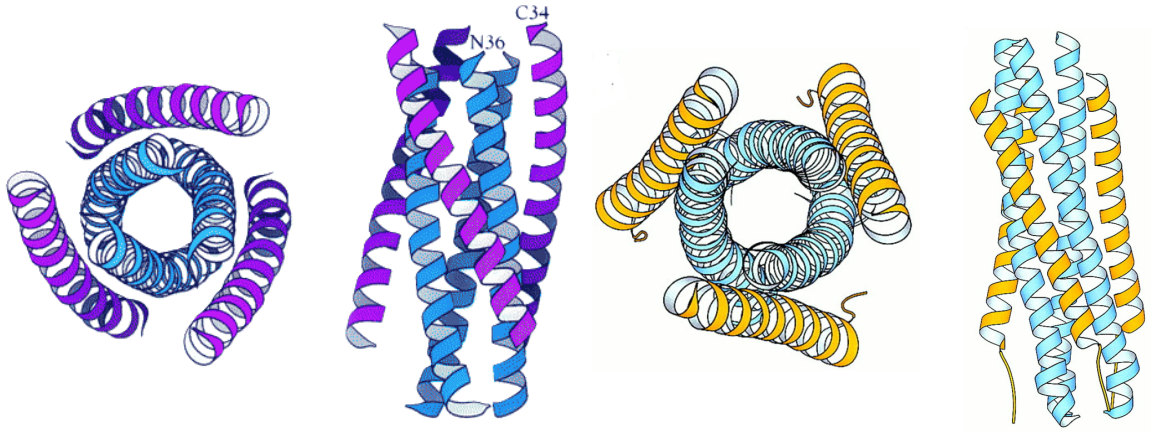

Figure 33. (Left) Ribbon diagram from the solved hexameric fusion core crystal of HIV-1. The HR-1 peptides are blue and the HR-2 peptides are in purple. (Right) Ribbon diagram from the solved hexameric fusion core crystal of RSV. The HR-1 peptides are light blue and the HR-2 peptides are in yellow.[16,17]

Given the putative role of the F protein in type I viral membrane fusion, an attractive strategy to probe the function of the coiled-coil motif and design new antiviral inhibitors is to create antagonists that bind one of the heptad repeat regions and trap the structure prior to bundle formation, as discussed in Chapter I. Indeed, synthetic peptides corresponding to both HR 1 and 2 of the HIV gp41 protein have been shown to inhibit viral fusion.[19-21] Due to the relatively high potency of HR-2 peptides, this approach has been extended to peptides derived from the fusion proteins of several viruses, including

RSV,[22] hPIV-3,[22,23] avian pneumovirus (APV),[24] Newcastle Disease virus (NDV),[25] measles virus [22] and simian virus 5 (SV5).[26] It was also noted that the HR peptides were virus-specific; no peptide has been shown to inhibit multiple viruses.

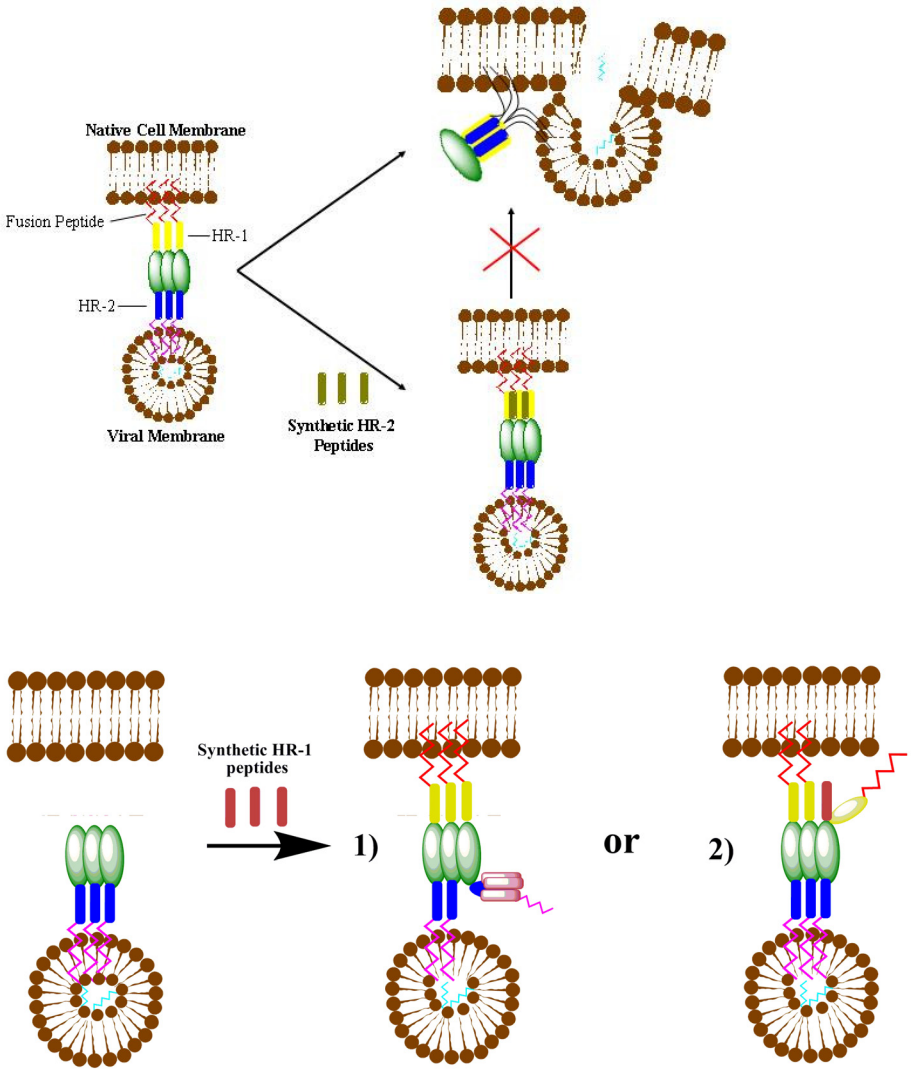

Figure 34. (Top) Suspected mechanism of HR-2 inhibition. (Bottom) Current paradigm for HR-1 peptide inhibition (1), and a possible pathway for monomeric HR-1 inhibition (2).

These peptides are thought to function by ensnaring the complementing HR peptide segments in the native F protein **(Figure 34)**. HR-1 peptides show a strong tendency to self aggregate and the current paradigm has them forming homotrimeric bundles and then capturing a native HR-2 segment in one of the hydrophobic grooves along its surface. This requirement of forming a homotrimer, as well as potential steric issues, may be the causes for the reported effectiveness of HR-1 peptides as fusion inhibitors being many times less effective than their HR-2 counterparts.[14,27-30] The inhibition studies mentioned above all found that the HR-2 based peptides were effective in nanomolar concentrations. This may be due to the HR-2 peptides working as single monomeric units, an hypothesis supported by the biophysical measurements of the individual peptides.

The effectiveness of HR-2 peptides to disrupt viral fusion is encouraging for the design of biomimetic weapons against disease. However, two drawbacks to such a strategy are the difficult peptide synthesis required and the potential loss of anti-fusion activity because of the lack of helical content shown in CD experiments. The latter issue is an intriguing academic problem. The lack of secondary structure likely prevents the HR-2 peptides from aggregating, but all previous studies suggest that the peptides adopt a helical structure in order to bind the hydrophobic grooves presented by the interior HR-1 coiled-coil. Sia *et al.* attempted to solve both problems in 2002 by chemically modifying short constrained HR-2 peptides from HIV-1.[31] They experimented with a 14-mer (residues 626-639) thought to bind the above mentioned hydrophobic cavity of the fusion core structure. They investigated several helix inducing strategies and found a significant increase in anti-fusion activity for C-14linkmid **(Figure 35)**. They found that

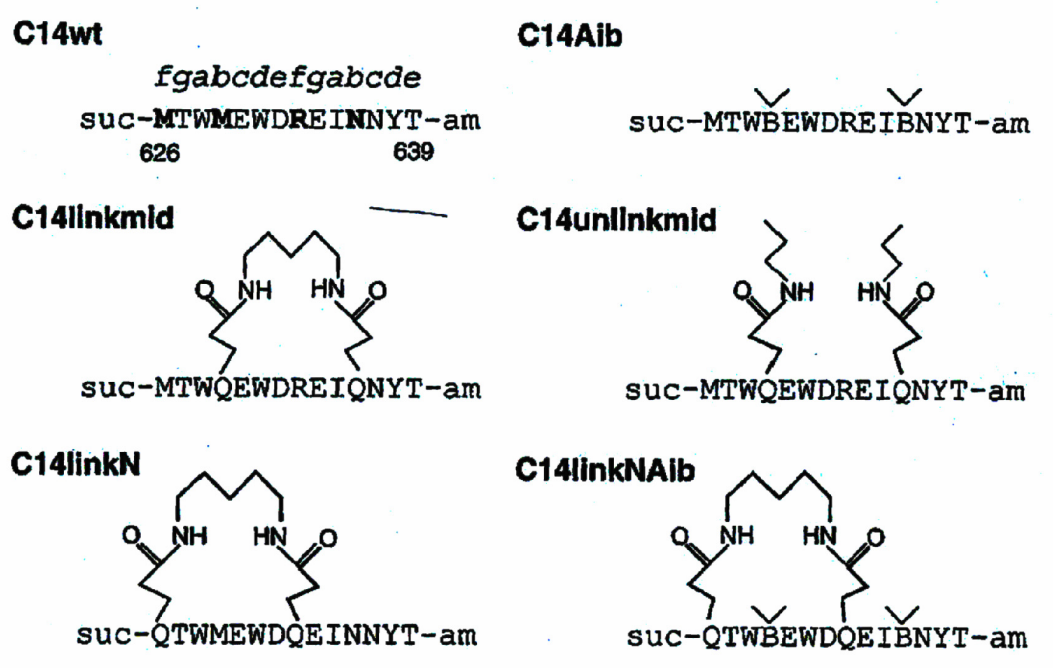

Figure 35 Peptides used by Kim and associates to test short, constrained peptides as potential inhibitors to HIV-1. C14wt is the wild type 14-mer,C14Aib have mutations M629Aib and N636Aib, C14linkmid is crosslinked at positions 629 and 636, C14unlinkmid is designed to mimic change in hydrophobicity of C14linkmid without the covalent constraint, C14linkN crosslinked at the N-terminus residues 626 and 633, and C14linkNAib is a combination of C14linkN and C14aib. "am" denotes amidated carboxy termini and "suc" represents a succynil modification to the N-termini. The heptad repeat sequence is shown above C14wt and the mutated residues are bold.[31]

C-14linkmid had the greatest propensity for forming an α-helix via TFE titrations and CD analysis. Furthermore, nuclear magnetic resonance (NMR) was utilized to follow tryptophan residues associated with the HR-1 peptide during exposure to HR-2 based inhibitors. They concluded that C-14linkmid did indeed bind the hydrophobic pocket of HIV-1 **(Figure 36)**. This was later confirmed via X-ray crystallography. The IC_{50} value of 35 μM (**Table 2, p. 71**) is still ~ 1000 times higher than the values associated with the proteolytically derived HR-2 peptides, but it demonstrates chemical avenues for optimizing biomimetic, peptidyl fusion inhibitors of type I F proteins.

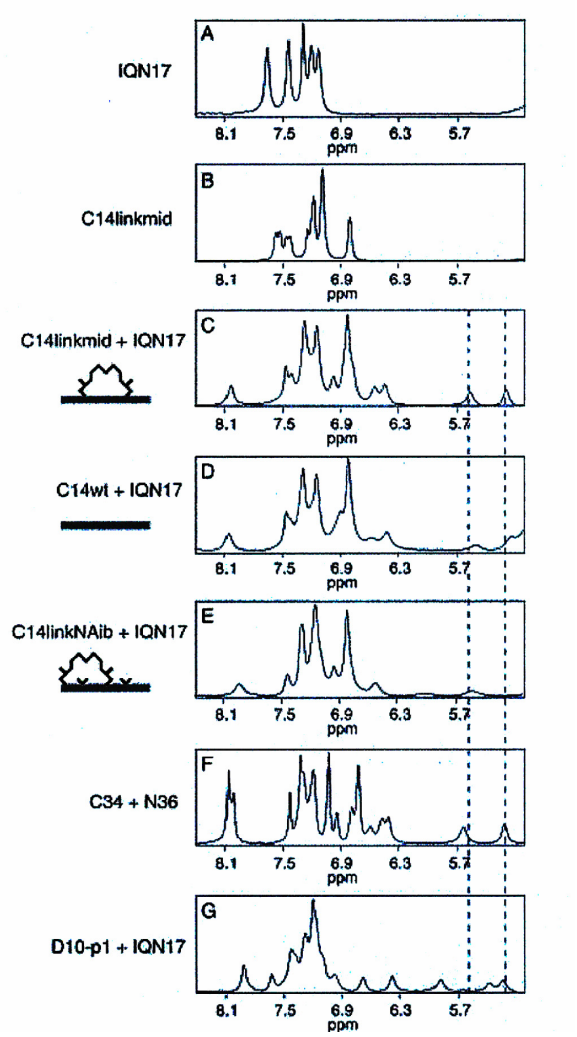

Figure 36 One dimensional proton NMR of the short, constrained peptides exposed to IQN17, a synthetic peptide containing the HIV-1 hydrophobic pocket sequence. The dashed lines highlight the resonance signals for the tryptophans in the hydrophobic pocket. A-F are discussed in the text and G is a HR-1 peptide inhibitor containing d-isomers.[31]

Recently several other fusion core crystal structures have been solved.[6,8,12,32,33] These structures also revealed the important structural features of a hydrophobic pocket within grooves on the surface of the inner HR-1 trimer, and key contact points lining the pockets and grooves. These two features likely are responsible for the extraordinary binding strength of HR peptides and their specificity. This chapter reports the first structural studies of the hMPV F protein hexameric core, inhibition of hMPV using

synthetic peptides, and evidence that HR-1 peptides can exhibit inhibitory potency comparable to that of HR-2 peptides.

Table 2 Inhibition of membrane fusion via C14 peptides.[31]

Peptide	IC_{50} for cell–cell fusion, μM*
C14linkmid	35
C14Aib	144
C14wt	>500
C14unlinkmid	>500
C14linkN	No activity
C14linkNAib	No activity

*C14wt and C14unlinkmid display very weak inhibition; the lower boundaries of their IC_{50} values are estimated.

Experimental

Coiled-Coil Model: The F protein sequences of 12 paramyxoviruses were compared using a global PAM250 scoring matrix with a gap start of 10 (MOE 2005.06). Heptad repeat (HR) regions of viruses with available coiled-coil crystal structures were aligned further with hMPV using a Blosum80 matrix for the HR regions. RSV (PDB ID: 1G2C) was found to be the most homologous sequence with 50% identity in HR-1 and 35% in HR-2, and was chosen as a template. 50 models were generated and evaluated based upon probability density function and overall energy using the modeler package within InsightII (Accelyrs). The best model was refined further in AMBER 7 in a generalized Born solvent model minimization. Minimization involved 2500 cycles with protein backbone atoms fixed allowing sidechains to relax followed by 2500 cycles allowing all atoms to relax and produce the final structure. CARNAL was used to convert the AMBER structure to PDB.

Peptide Synthesis: Peptides were synthesized on an Apex 396 (Advanced Chemtech) equipped with a 96 well reaction block capable of vortex mixing. Customized tentagel resin was swollen in Dichloromethane (Fisher) prior to synthesis. 9-Fluorenylmethoxycarbonyl (FMOC) amino acids (Synpep) were coupled using O-Benzotriazole-N,N,N',N'-tetramethyl-uronium-hexafluor-phosphate (HBTU; 5 eq with respect to resin; Synpep), 1-hydroxybenzatriazole (Hobt; 5 eq; Synpep), diisopropylethylamine (DIEA; 10eq; Advanced Chemtech) in N,N-dimethylformamide (DMF; Fisher). Peptides were cleaved with 95% (v/v) trifluoroacetic acid and 5% triisopropylsilane and desalted on a G-25 sephadex column before final purification on a C4 semi-prep reverse phase HPLC column using water and acetonitrile gradients.

Circular Dichroism: Fusion core complexes were made at 12.5 μM total peptide in 0.15 M PBS at pH 7.4 (Invitrogen) by mixing equimolar amounts of each HR peptide followed by addition of TFE or a freeze/thaw cycle. Spectra were collected on an Aviv 215 CD spectrophotometer equipped with variable temperature control over the wavelength range of 190 nm to 260 nm with a resolution of 0.5 nm and a bandwidth of 1 nm. The spectrometer is equipped with variable temperature control, automatic titration system and pH probe. Samples were analyzed in a 300 μL strain-free quartz cell with a 1.5 s averaging time. The coiled-coil complex was examined for thermal stability by CD every 5 °C from 25 °C to 100 °C.

Plaque Inhibition Assay: Serial dilutions of the 1:1 peptide solutions in OPTI-MEM medium (Invitrogen) were added to plates containing 50-60 plaque-forming units of hMPV per well. Concentrations tested were 25, 12.5, 6.25, 3.12, 1.56, 0.781, 0.390, 0.195, 0.0977, 0.0488, 0.0244, and 0.0122 μM. Additional HR-1 peptide testing was

performed at 6, 3, 1.5, 0.76, 0.38, 0.19, .0095, and 0.0048 nM. Peptide and virus mixtures were incubated for 1 hour at 37 ºC. Subconfluent cell monolayers of LLC-MK2 cells were washed twice with PBS, and 100 µl of the peptide-virus mixtures were added to the cells. Cells were incubated for 1 hour at 37 ºC with gentle rocking every 15 minutes, then overlaid with methyl cellulose, maintaining the peptide concentration. Cells were incubated for 4 days at 37 ºC. Cells were fixed with formalin at room temperature for 1 hour Plates were rinsed with running water followed by incubation for 30 minutes at 37 ºC with blocking buffer (PBS/0.1% Tween/5% nonfat dried milk). Blocking buffer was removed and the plates were incubated with a 1:1000 dilution of guinea pig anti-hMPV serum at 37 ºC for 2 hours. The plates were washed and incubated with goat anti-guinea pig Ig-horseradish peroxidase conjugate (Southern Biotech) at 1:1000 at 37 ºC for 2 hours. Secondary antibody was removed by washing, followed by the addition of TrueBlue peroxidase substrate (Kierkegarard Perry Laboratories) and incubation for 10 minutes. Plates were rinsed with water and dried overnight. Plaques were counted using a dissecting microscope and the average between triplicate wells calculated.

Size Exclusion Chromatography: The molecular weight of the coiled-coil complex was examined by size exclusion chromatography (SEC). Peptides from both HR regions were mixed equimolar and their coiled-coil formation was confirmed by CD spectroscopy. Coiled-coil complex and sodium polystyrene sulfonate weight standards were run in triplicate isocratically in 0.15 M PBS at pH 7.4 on a Waters Ultrahydrogel HPLC size exclusion column with a flow rate of 0.3 mL/min. Standards had average masses (g/mol) of 4,950, 7,950, 16,600, 34,700, and 57,500. Eluants were monitored at

wavelengths 210, 220, and 257 nm. Coiled-coil complex elution peak masses were determined from linear calibration of the logarithmic weight values.

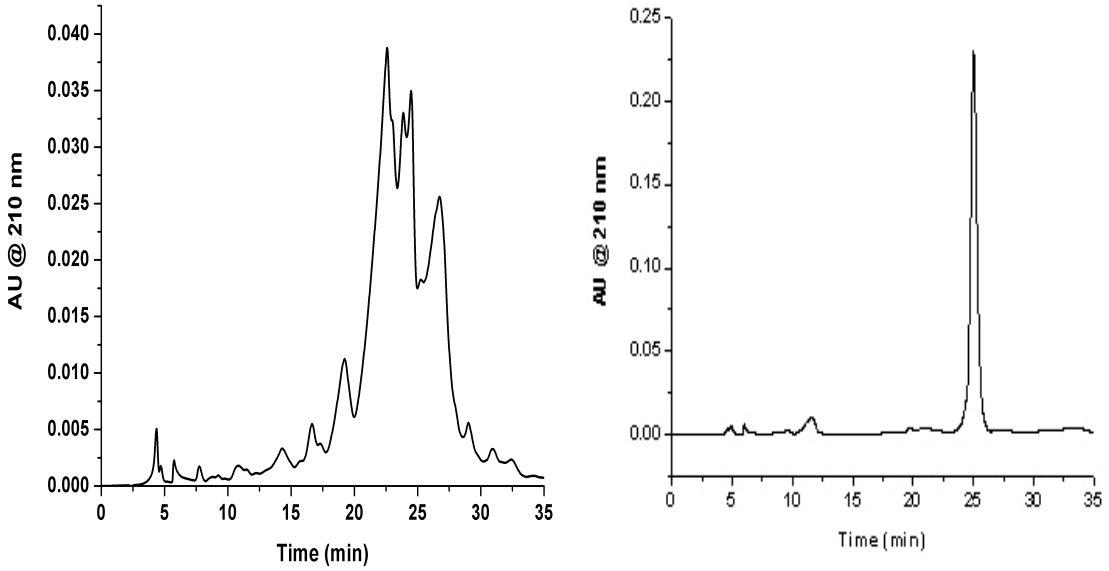

Figure 37. (Left) HPLC of identified problem region synthesized as individual peptide. (Right) Same peptide synthesized utilizing pseudoproline and Hmb schemes.

Pseudoproline Incorporation: The standard FMOC protocols described above were not adequate to produce sufficient quality and quantities of the HR-1 and HR-2 peptides **(Figure 37)**. To isolate the onset of aggregation, the larger LearnCoil-VMF sequences were broken into overlapping 15-mers and synthesized individually on custom resin. A 13 residue stretch (PEDQFNVALDQVF) that was difficult to synthesize was identified as an individual peptide within the HR-2 domain **(Figure 38)**. Therefore the strategy of pseudoproline and Hmb insertion discussed in Chapter I was employed. Pseudoproline dipeptide acids (Nova Biochem) were activated for 20 minutes in DMF in the presence of DIC (1 eq.), DIEA (2 eq), and Hobt (1 eq.) to achieve active esters. Next, three

equivalents, with respect to resin substitution, of the active ester derivative were then added to the resin and allowed to mix for 24 hours. The reaction was tested via the Kaiser test to ascertain completion.

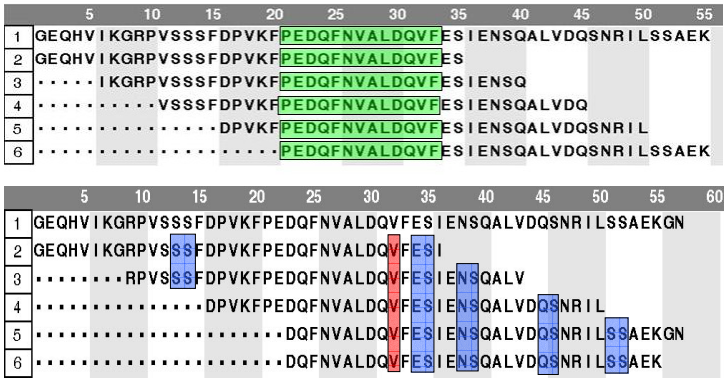

Figure 38. (Top) Overlapping 35-mer sequences derived from HR-2 used to identify problematic regions in synthesis. (Bottom) Location of pseudoproline coupling (blue) and valine HMB (red) used to overcome aggregation challenges

Hmb Incorporation: Hmb-protected amino acid derivatives were purchased from Nova Biochem already in activated pentafluorobenzyl ester form. The active esters were dissolved in DMF with 2 equivalents (with respect to resin substitution) Hobt and added to the resin. The reaction was allowed 24 hours for completion as determined via the Kaiser test. The subsequent amino acid was coupled via 10 equivalents of symmetrical anhydride. The anhydrides were synthesized in cold DCM by the addition of 20 equivalents of amino acid and 10 equivalents DIC. The result was a white precipitate which was added to the resin as a slurry and allowed to mix for 24 hours. This process was repeated as necessary until a negative Kaiser test was achieved.

Results

To compare the hMPV F protein to the F proteins of related paramyxoviruses, the sequences of 12 F proteins were aligned to that of hMPV using a PAM250 scoring

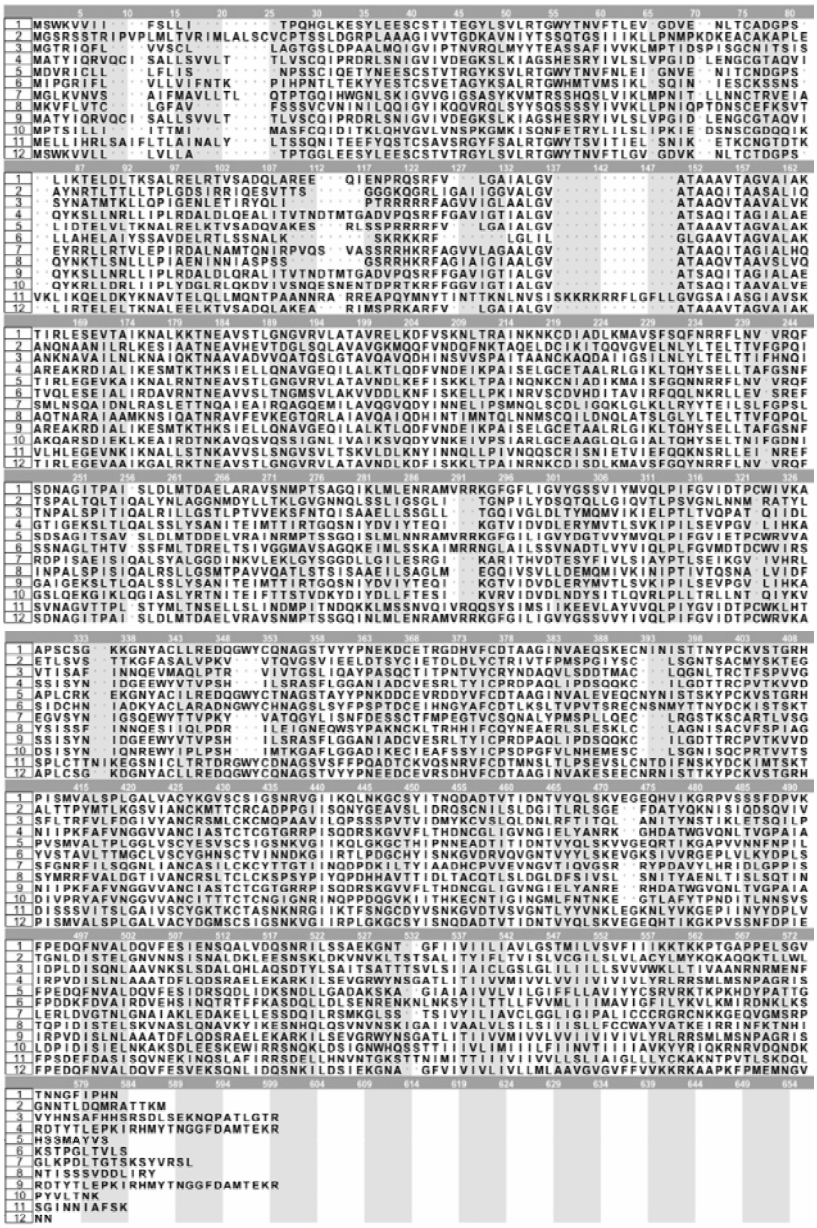

Figure 39. 12 paramyxovirus fusion proteins aligned using a PAM250 matrix with a gap start penalty of 10 and an extend penalty of 1. (1) hMPV (2) NDV (3) SV5 (4) Sendai (5) TRT (6) PVM (7) Measles (8) Mumps (9) PIV1 (10) PIV3 (11) hRSV (12) APV

matrix.[34] Results indicate that hMPV had several key local alignments, including the predicted α helical structures in the suspected HR regions **(Figure 39)**. The HR regions then were aligned locally using a Blosum80 matrix,[35] revealing a 3-4-4-4-3 stutter pattern characteristic of paramyxoviruses **(Figure 40)**.[32,36] The cysteine alignment patterns for the 12 sequences revealed eight conserved cysteines found to be involved in disulphide bonds within the PIV3 fusion protein.[12] Within the pneumoviruses, five of the sequences (hMPV, RSV, PVM, APV, and TRT) displayed an additional conserved cysteine pattern of six cysteine residues. These alignments suggested that the hMPV F protein has similar structure and function to previously studied paramyxovirus F proteins.

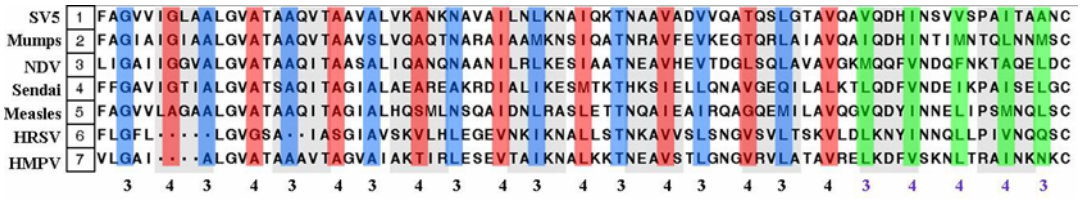

Figure 40. Alignment of 7 paramyxovirus HR-1 sequences displaying a 3-4-4-4-3 stutter pattern in the HR-1 region. This stutter is postulated to be present in all the paramyxovirus HR-1 regions.

To generate a computational model of the hypothesized hMPV fusion core, a suitable template was identified. The available hexameric crystal structures were examined for sequence similarity with hMPV's heptad repeat regions.[6,8,12,13,32,33,37] The hMPV F protein showed the greatest homology with RSV F protein HR regions (50% in HR-1 and 35% in HR-2; **Figure 41**). These values exceed the reasonable threshold of 25% sequence identity commonly employed to obtain reasonable homology models.[38]

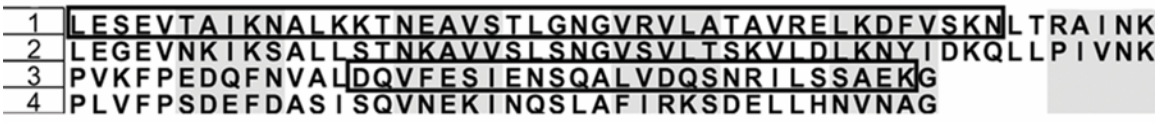

Figure 41. Sequence alignment of the HR regions of RSV and hMPV. RSV sequences obtained from crystal structure (PDB ID: 1G2C). The HR-1 region shows an identity of 50% between the two viruses while the HR-2 region has 35% identity. (1) hMPV HR-1 (L130 to K179) (2) RSV HR-1 (3) hMPV HR-2 (P448 to G487) (4) RSV HR-2. LearnCoil-VMF generated sequences for hMPV are boxed.

Several models were produced in the modeler package of InsightII. Subsequently, these models were scrutinized for overall energy and probability density function values to isolate the most stable model intermediate. This intermediate underwent further rigorous minimization for a final model of the hMPV fusiogenic core **(Figure 42)**. The model displayed several features akin to those of other hexameric

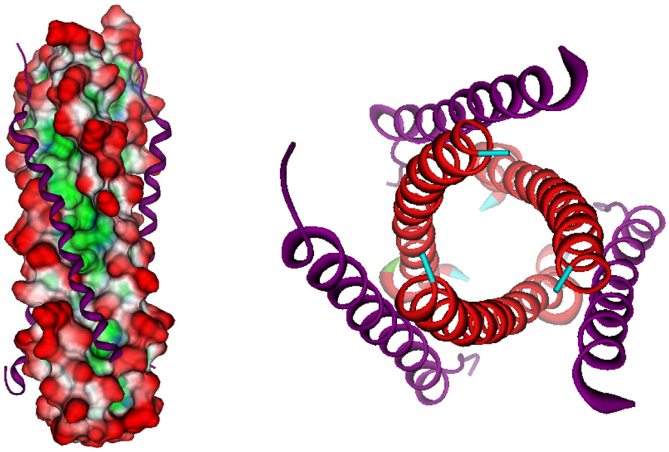

Figure 42. Shown is the modeled hexameric fusion core of hMPV. The sequence of the RSV fusion core crystal was subjected to a strong local alignment with the hMPV sequence to determine appropriate homology sequences for the hMPV fusion core model. The alignment produced two hMPV peptides with 50% (HR-1) and 30% (HR-2) identity with the RSV peptides. Using the RSV structure as a template, the hMPV peptides were grafted onto the RSV Cα backbone and allowed to minimize. (Left) Shown is the surface of the HR-1 trimeric stalk (red: solvent exposed, blue: hydrophilic, green: hydrophobic) with the HR-2 (purple ribbons) filling the hydrophobic grooves. (Right) Axial view of the hexameric core. This hexameric coiled-coil formation is the major structural feature of the F protein's post-fusion conformation.

fusion cores. Three HR-1 peptides form an inner helical bundle that presents three long hydrophobic grooves along the ~72 Å stalk. Corresponding HR-2 peptides assume helical structure offering a hydrophobic face that packs in an anti-parallel fashion into the HR-1 hydrophobic grooves. This configuration would allow for the fusion peptide, found near the N-terminus of the HR-1 stalk, to be in close proximity with the transmembrane anchor located at the C-terminus of the HR-2 peptide. The presence of a hydrophobic pocket and key salt bridges also were identified. The hydrophobic pocket of the hMPV model is comprised of residues V162, L165, V169 from one HR-1 peptide and A161, L165, and F168 of a second HR-1 fragment **(Figure 43)**. Lining the immediate exterior of the pocket are several polar residues contributed from HR-1 (R163, K166, D167, S170, and K171 with E164 from a second HR-1 fragment). The polar residues likely

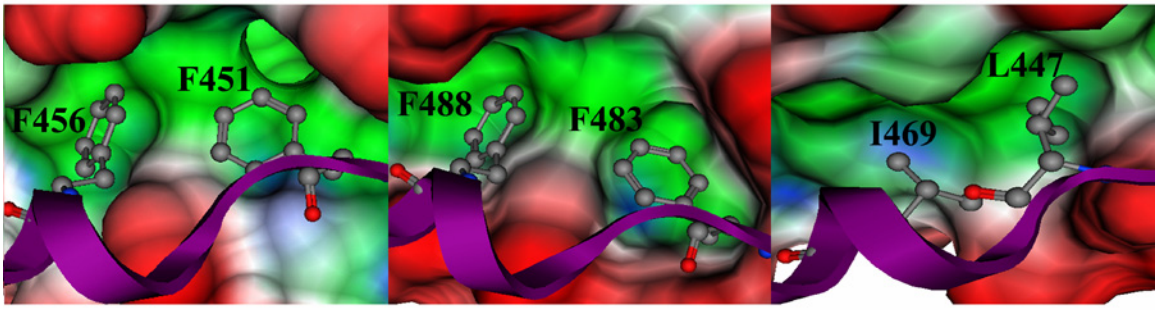

Figure 43. hMPV model images. (Left) Surface image of the hMPV hydrophobic pocket filled by phenylalanines 451 and 456 of the HR-2 peptide (red: solvent exposed, green: hydrophobic). (Center) RSV Phenylalanines 483 and 488 complimenting the hydrophobic cavity. (Right) Congruent leucine 447 and isoleucine 449 of SV5 packing a hydrophobic pocket. Images produced using MOE 2005.06 (Chemical Computing Group).

contribute specificity among HR sequences,[22,33] as seen by the formation of a strong ionic network between K166 and K171 from HR-1 and E453 of HR-2. Overall, the hMPV

fusion core model was consistent with other hexameric cores found in type I viral fusion proteins. The final refined hMPV model was superimposed upon the RSV fusion core crystal structure which has already been shown to be structurally similar to other paramyxovirus cores.[33] The overlayed C_α and backbone nitrogen of the RSV and hMPV HR-1 peptide strands reveals an RMSD of 0.53 Å, and the HR-2 strands have an average of 0.45 Å. Using the same superimposition technique, RSV and SV5 HR-1 peptides have an RMSD of 1.5 Å, and the HR-2 peptides result in a 2.78 Å RMSD. In comparison, hMPV and SV5 HR-1 peptides show a 1.48 Å RMSD, while the HR-2 peptides have a 3.55 Å RMSD. The combined molecular surface of the hMPV model and RSV crystal structure showed the same hydrophobic cavity filled by the phenylalanine residues of the RSV and hMPV HR-2 peptides (RSV: F483 and F488; hMPV: F451 and F456). Overall, the hMPV fusion core model is consistent with known type I fusion protein core structures.

In the absence of available hMPV F protein, peptide sequences for synthesis and study had to be determined by methods other than commonly used protein degradation.[15,33,39] The homology model of the hMPV heptad repeat regions yielded peptides of 50 and 40 amino acids in length for HR-1 and HR-2 respectively. To refine the critical regions of the HR peptides, the hMPV F protein sequence was analyzed using LearnCoil-VMF.[40,41] Originally developed to predict HR regions within viral fusion proteins, LearnCoil-VMF predicted a HR-2 of the HIV gp41 protein that mediates fusion, in which 80% of the overall sequence was identical to the 36-mer anti-viral, Enfuvirtide (La Roche). Similarly, a predicted HR-2 from RSV had a sequence overlap of 71.4% with the fusion inhibitor T-118.[23] For hMPV, LearnCoil-VMF suggested an optimal

43-mer peptide sequence (residues 130-172) within the HR-1 region and a 33-mer (33A; residues 454-486) peptide within the HR-2 region. 33B, a HR-2 33-mer shifted 5 amino acids to the N-terminus of the LearnCoil-VMF 33-mer, was synthesized to better complement the hydrophobic pocket within the fusion core model developed above.

The target peptides were synthesized and their solution-phase secondary structure was examined using circular dichroism spectroscopy in 0.15M PBS (pH 7.4) at 25 °C. Unexpectedly, the HR-1 peptide showed a lack of helical structure (< 25%). Previous HR-1 peptides from other viral fusion proteins have been shown to contain a significant α-helical content.[15,22-24,32,42,43] The spectra of 33A and 33B also displayed little secondary structure content consistent with previously reported HR-2 peptides. When the HR-1 and HR-2 peptides were combined at a 1:1 molar ratio, an additive spectrum was obtained indicative of no higher order complex formation **(Figure 44)**.

Based upon the fusion model and sequence analysis above, the HR-1 peptide should possess a propensity to adopt an α-helical structure. Trifluoroethanol (TFE) and thermal modulation [44] provide avenues for inducing the targeted helix confirmation. The HR-1 peptide showed a strong helical spectrum with as little as 2.5% (v/v) TFE that plateaued at 5% additive. In contrast, HR-1 showed no increase in observed intensity at 224 nm following a freeze/thaw cycle. The HR-2 peptides were unaffected by the addition of small volumes of TFE (up to 5% (v/v)) or thermal cycling.

Peptides from both HR regions were mixed in the presence of 5% TFE, and the intensity at 224 nm was greater than the additive spectra of the individual peptides in TFE. Such an enhancement of helicity indicates the formation of the desired coiled-coil

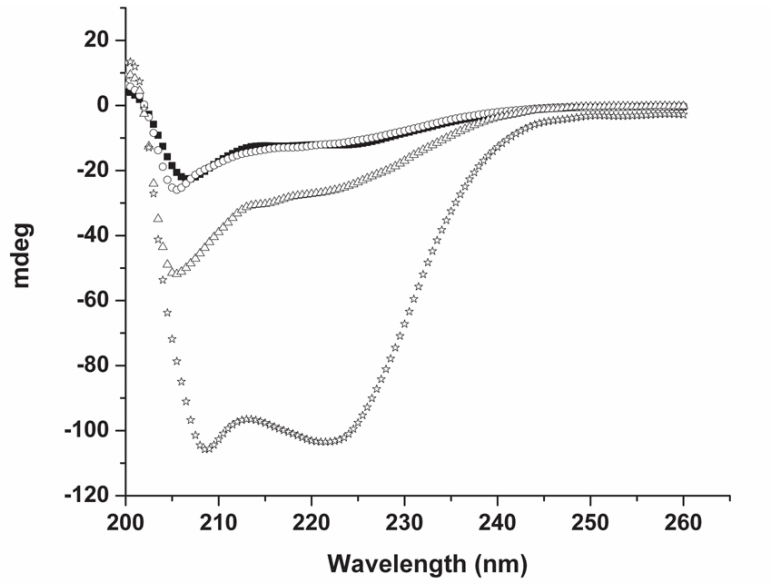

Figure 44. Circular Dichroism of Coiled-Coil Both the HR-1 and HR-2 (33A) peptides show little secondary structure at 25°C (HR-1 43-mer (O), HR-2 33A (■)). Mixing of the two HR peptides produced only an additive spectrum indicative of no interaction (equimolar mixture at 25°C (△)). The same equimolar mixture at 25°C following a freeze / thaw cycle adopted the putative coiled-coil (☆).

assembly. The use of more than 5% TFE did not cause an additional change in the 224 nm signal, suggesting that the maximal amount of peptide had transitioned to the putative hexameric core. After thermal cycling of an equimolar mixture of HR-1 and 33A, the CD spectrum exhibited the expected enhanced coil-coiled trace similar to that of the mixture in the presence of TFE **(Figure 44)**. A mixture of HR-1 peptide and 33B showed similar behavior.

The known viral F protein cores have been shown to have unusually high melting temperatures compared to similar length helical bundles.[6,8,15,24,33,45] The melting curve of the hexameric core of hMPV formed by HR-1 and 33A, obtained from a freeze/thaw cycle, gave a $T_m \sim 90$ °C **(Figure 45)**. This is consistent with the previously reported T_m

of 88 °C for the RSV F protein hexameric core.[33] The melting temperature obtained from the 33B and HR-1 complex was found to be ~ 85 °C.

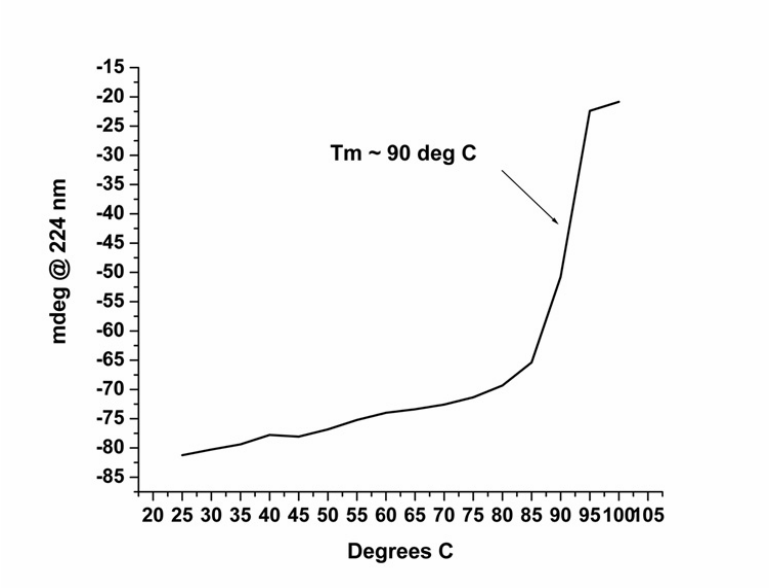

Figure 45. Melting point curve for the HR-1 and 33A peptides following a freeze/thaw cycle.

To investigate the aggregation state of the putative hexameric core, the induced peptide structure was examined by size-exclusion chromatography. The chromatograms of the peptide solutions yielded two pronounced and well resolved peaks. The major peak corresponded to a mass of 24,802 g/mol $\pm$ 135 (retention time: 26.1 min $\pm$ 0.02). The theoretical mass of the hexameric core formed from the LearnCoil-VMF peptide sequences is 24,933 g/mol. Furthermore, given the mass difference between the HR-1 and HR-2 peptides, non-hexameric structures and structures with a ratio other than 1:1 for HR-1 to HR-2 would fall outside of the standard deviation of the experiment. The second peak at 23.4 min. ($\pm$ 0.03) corresponded to a mass consistent with 12 peptides in a 1:1 ratio of the HR peptides. The fractions containing the hexameric and dodecameric

peptide assemblies were isolated and both were found to contain helical content consistent with the coiled-coil core. Additionally, the relative composition of the sample was found to shift towards the dodecamer over a 24-hour period, suggesting slow dimerization of the hexameric core.

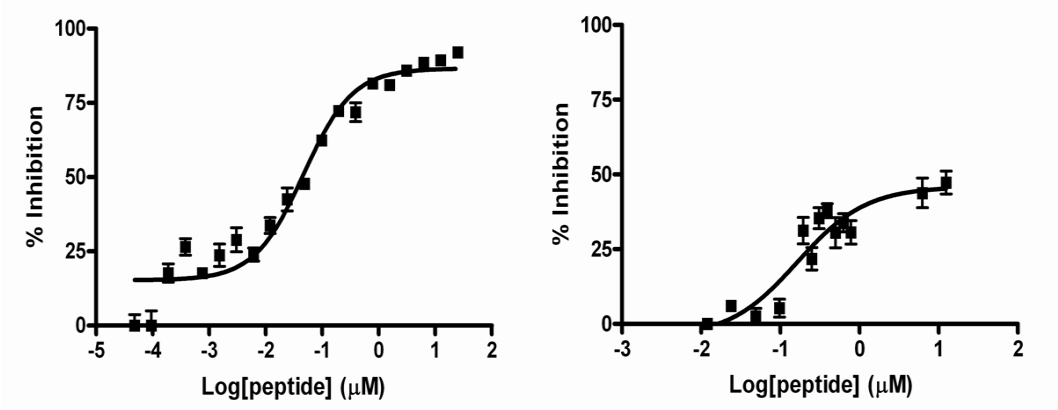

Figure 46. Dose Response Curve Data of the HR peptides was obtained by adding virus and peptide to confluent cells for 1hr. A layer of methyl cellulose was added and maintained the peptide concentration. Anti-hMPV guinea pig primary antibodies were then utilized followed by an anti-guinea pig secondary antibody linked to horseradish peroxidase in order to detect foci. Data was fit using the Hill-Slope model. The HR-1 peptide was found to be a very potent inhibitor (EC50 ~ 46 nm) comparable with reported HR-2 peptides. 33A was never able to achieve > 50% activity.

Peptides corresponding to the HR sequences of other hexameric F protein cores have been shown to be potent inhibitors of viral propagation.[6,15,19-25,32,43,46,47] The hMPV F protein HR sequences predicted by LearnCoil-VMF and the 33B peptide were tested and shown to inhibit viral growth. Peptide 33B mediated very little inhibition at the maximum test concentration of 25μM. Peptide 33A caused significant viral inhibition with an EC_{50} ~ 165 nm.[27,43] Surprisingly, the HR-1 peptide showed exceptional inhibition with an EC_{50} ~ 46 nM , at least 1000 times more potent than previously reported HR-1 peptides **(Figure 46)**.[27,28,48]

Discussion

The recently discovered paramyxovirus hMPV is one of the most common causes of serious lower respiratory tract illness in infants and children.[1,2] The studies described above show that the fusion protein of hMPV possesses a high level of homology at the nucleotide sequence level and at the level of predicted protein structure to other type I integral membrane viral fusion proteins. Peptides from the HR regions of the hMPV F protein inhibited virus-cell fusion, bolstering the hypothesis that the hMPV F protein functions through a HR peptide-sensitive membrane fusion mechanism similar to that of SV5,[32] RSV,[15] and HIV-1.[21]

Homology modeling suggested the presence of key electrostatic contacts and a hydrophobic pocket akin to that seen in the SV5, RSV, and hPIV3 F proteins that are characterized structurally.[12,32,33] Within the hMPV fusion core model, several polar groups line the hydrophobic cavity. Analogous residues in related paramyxoviruses appear to convey specificity among virus-derived HR-2 peptides.[22,33] The hydrophobic pocket proposed by the hMPV F protein model is complemented by two phenylalanines (F451 and F456) of a HR-2 strand, and exhibits homology with the hydrophobic F483 and F488 residues found in RSV F protein and the L447 and I449 residues of SV5 F protein. Docking of small-molecule antagonistic drugs within the hydrophobic cavity or interference with critical ion pairs has been shown previously to inhibit fusion of hMPV.[49]

LearnCoil-VMF was employed as a tool to analyze the hMPV F protein to determine potential target peptides for physical characterization of the fusion core. LearnCoil-VMF is similar to generic helical dimer and trimer prediction algorithms such

as PairCoil [50] and MultiCoil,[51] but it is biased to hexameric coiled-coil assemblies from viral membrane F proteins. Based on the ability of LearnCoil-VMF to predict sequences that encompass sequences of well-studied fusogenic core peptides, the HR-1 43-mer and 33A peptides were selected for synthesis. The homology fusion core model also suggested study of peptide 33B in order to examine any potential advantages of targeting the hydrophobic cavity.

Characterization of HR-1 and HR-2 peptide interaction is consistent with a hexameric coiled-coil fusion core for hMPV. Following helical induction, assembly of the hexameric coiled-coil resulted in CD spectra containing α-helical content substantially greater than the additive spectra of the individual peptides. This α-helical species also was determined to have a melting temperature ($T_m \sim 90$ ˚C) consistent with that of other described viral fusogenic cores.[6,8,15,32,33] SEC determined the mass of the induced samples to be consistent with the expected hexameric moiety in a 1:1 HR-1 to HR-2 ratio. This ratio is consistent with analytical sedimentation analysis, described by Lawless-Delmedico *et al.* of peptides derived from HR regions of RSV.[15] The sedimentation analysis of the RSV peptides found evidence of monomers, HR-1 trimers, and a hexameric structure with a 1:1 ratio of RSV's HR-1 and HR-2 peptides.[15] In contrast, the peptides of hMPV did not exhibit self-trimer aggregation by SEC analysis, consistent with the absence of α-helical content observed for HR-1.

Requisite induction of the hMPV HR-1 peptide from a predominantly random conformation to an α-helix illustrates subtle differences between experimentally determined HR sequences and those identified by LearnCoil-VMF. One such difference between previously reported HR-1 peptides determined from enzymatic footprinting

experiments and the hMPV LearnCoil-VMF HR-1 peptide is the lack of helical structure or aggregation of the hMPV HR-1 peptide.[15,22,32,33] A small volume of TFE produced a strong α-helix signal from the HR-1 solution, thus demonstrating the propensity for aggregating into the three-helix bundle comprising the inner stalk of the fusion core. The subsequent addition of a HR-2 peptide caused the hexameric assembly to form. These data suggest that the HR-1 helical transition prior to exposure to HR-2 peptides contributes significantly to the mechanism of the fusion process.

Fusion of paramyxoviruses with their target cellular membrane requires protein-driven cellular docking, activation of the pre-fusion F protein, and a conformational change of the F protein into the post-fusion state containing a hexameric coiled-coil.[9,47,52] Following activation, the HR-1 peptides of the trimeric F protein aggregate into the central helical bundle of the hexameric core. The membrane targeting fusion peptide presents on the tip of the trimeric HR-1 peptide bundle. The fusion peptide inserts itself into the target cellular membrane, resulting in a pre-"hairpin" intermediate **(Figure 47.1)**. This intermediate presents the hydrophobic grooves of the HR-1 bundle to the HR-2 peptides for binding in an anti-parallel fashion, resulting in the formation of a thermostable hexameric coiled-coil core. This conformational juxtaposition of the HR regions results in close proximity of the viral membrane to the target host cell, which facilitates subsequent fusion of the virus and cell membranes. The conversion from the pre-fusion to post-fusion structures has become a popular target of peptidyl anti-fusion antagonists.

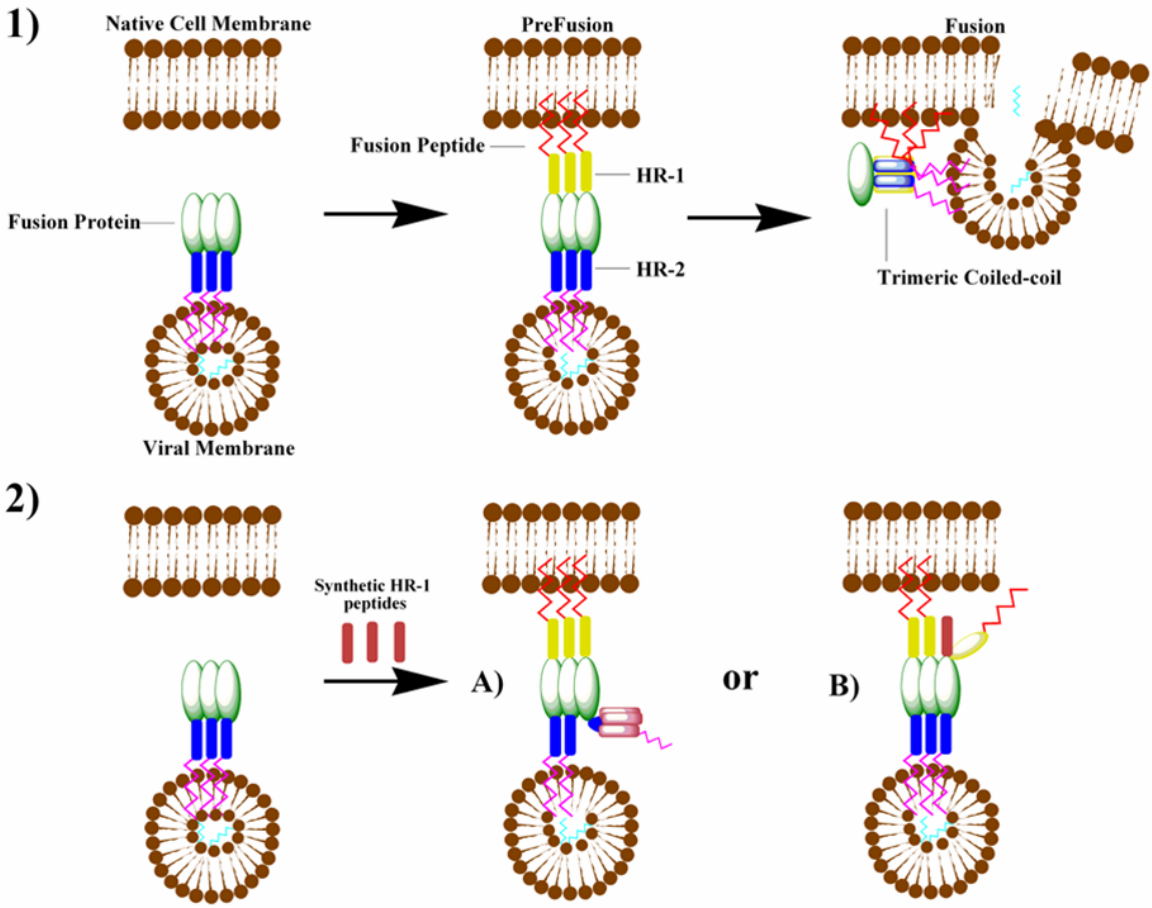

Figure 47. (1) Proposed mechanism between type I fusion proteins and cellular membranes. Following cellular docking, a transient prehairpin complex arises as a result of a conformational change in the F protein. This results in the insertion of the fusion peptide into the cellular membrane and the exposure of the HR-1 trimer. The previously constrained and sequestered HR-2 peptides migrate to pack hydrophobic channels of the HR-1 trimer resulting in the coiled-coil complex and membrane fusion. (2) Possible routes of inhibition by utilization of synthetic HR-1 peptides: (A) monomers aggregate into a synthetic trimer sequestering a native HR-2 peptide, and (B) monomeric synthetic units of HR-1 intercalating into native trimer stalk

Recent work involving type I integral membrane fusion protein inhibition has focused on peptides derived from HR-2 regions due to their remarkable potency against viral fusion.[47] The postulated mechanism of inhibition for the HR-2 peptides involves binding of the helical monomers to the hydrophobic groove presented along the surface of the HR-1 bundle. Binding of the synthetic HR-2 peptides prevents native HR-2

peptides from reaching their target. The synthetic peptides thus are able to arrest the fusion protein intermediate. The hMPV HR-2 peptides, 33A and 33B, failed to achieve anti-fusion activity comparable to optimal HR-2 peptides previously described.[20-24] While peptide 33B did not affect fusion, the LearnCoil-VMF predicted peptide 33A exhibited a titratable response that failed to reach >50% inhibition up to 25 μM. While the final sequences used in this study were taken directly from LearnCoil-VMF, previous work has shown significant fluctuations in anti-fusion activity between peptides offset by as little as a single residue in the HR sequence. In studying the HR-2 region of the RSV F protein, Lambert *et al.* examined a single offset scanning library of potential inhibitors and found, for example, EC_{50} values differing more than fivefold between the consecutive peptides T-106 and T-107 respectively.[22] Current work towards development of an optimal peptide inhibitor for hMPV involves investigation of a more exhaustive set of peptides from the HR-2 region.

The current paradigm for HR-1 peptide inhibition suggests that the synthetic HR-1 peptides present as a helical trimer and then ensnare one or more of the native HR-2 peptides **(Figure 47.2A)**.[20,27,43,53] Prior to this study, HR-2 peptides always have been reported to exhibit fusion-inhibiting activity that is orders of magnitude more potent than HR-1 peptides. It has been hypothesized that strong HR-1 aggregation is partly responsible for the weak inhibitory properties of HR-1 based peptides, as such interactions would create steric complications and require at least 3 times the concentration of HR-1 peptides relative to HR-2 peptides, which are thought to inhibit in a monomeric state.[48] For this to be true in this study, a required helix inducer would need to be present on the cellular or viral surface. While the present research does not

rule out the involvement of such an inducer, the phenomenon would likely depend on concentration; but this prediction is not supported by the strong fit of the Hill-Slope response model.[54]

An alternate inhibition mode for HR-1 peptides postulates that monomeric HR-1 peptide could insert and substitute for a native HR-1 peptide in the trimeric bundle. Indeed, the body of evidence in this study suggests a possible intercalation of the HR-1 peptide into the fusion protein prior to or during fusion **(Figure 47.2B)**. The absence of interaction amongst the HR-1 and HR-2 peptides in the CD analysis suggests that the HR-1 peptide does not inhibit as a dimeric or trimeric unit with an ensnared HR-2 peptide. Furthermore, the SEC data does not indicate the presence of the HR-1 helical bundle, unlike the trimeric HR-1 bundle seen in RSV sedimentation data.

Yin *et al.* recently solved the pre-fusion structure of the parainfluenza virus 5 F protein, previously mentioned.[11] The crystal displays the HR-2 peptides in a helical bundle associating the transmembrane domain with the viral membrane. The HR-1 and fusion peptide sequences are sequestered within the globular head. This structure suggests a possible intermediate target for an intercalating HR-1 peptide. In order to expose the fusion peptide for insertion in the target membrane, the HR-1 peptides must extend into a helical bundle outward from the viral membrane. During stalk extension, incorporation of a synthetic HR-1 peptide is not unreasonable. This would result in failure of the fusion peptide to reach its final position within the target membrane, and would likely arrest subsequent folding and fusion.

The compilation of data in this study provides evidence for the structural and functional relationship of the hMPV F protein to that of other paramyxoviruses. The

study identifies the first HR-1 derived peptide with potent fusion-inhibition activity. While previous research concluded that HR-1 peptides could be effective inhibitors of type I integral membrane fusion proteins when constrained and presented as trimeric helical bundles,[27,43] the data in this study suggests that intercalation of individual HR-1 peptides can lead to effective viral inhibition. To find the optimal peptidyl anti-fusion agent, synthesis and testing of a scanning HR-1 library combined with the ongoing HR-2 library should isolate the ideal peptide length and sequence for further modification. Dye transfer experiments, intermediate capture experiments and peptide labeling will help to elucidate which critical intermediates and functions are being arrested by the hMPV HR-1 peptide inhibitor and will shed new light on the mechanism of action of viral fusion proteins.

Current and Future Work

Preliminary work with hMPV HR offers encouragement that an optimized peptide based anti-viral can be identified and tested. LearnCoil-VMF identified the first generation of HR peptides for study, but weak inhibitory properties associated with the HR-2 peptide demand further refinement and optimization to reach an effective EC and $IC_{50.}$ The unexpected inhibition and the physical properties of the HR-1 peptide open a new avenue, previously disregarded, for peptide based inhibitors for all type I membrane bound fusion proteins. The known F protein crystallographic data as well as computer modeling will be used to generate structural, functional, and inhibitory information from a second generation of HR-2 and HR-1 based inhibitors.

The extension of the 33-mer predicted to include E453 is likely to convey an increase in anti-fusion activity. Extending the HR-2 sequence 3 residues towards the N-terminus will include the contact point predicted by the hMPV model. This will also give a length commonly associated with HR-2 fusion inhibitors. Overall helical content has shown a correlation with anti-fusion activity in HIV. Therefore, work continues to modify the termini of the second generation HR-2 peptides with one of several helix promoters that have been shown to be effective in fusion inhibiting peptides. The ability of these modifications, such as N-terminal succinyl and acetyl groups in conjunction with C-terminal amide formation, to induce α helix conformations is thought to reside in their hydrogen bonding ability.[22,42,43] These extra bonding sites likely reduce the entropic penalty to helix formation for the four terminal residues on either end of the peptide. This would be particularly useful in the extended HR-2 peptide where E453 would likely be included near the N-terminus. It has also been shown that constraining the HR-2 peptides into rigid helical structures confers increased activity against viral-fusion.[19,55] This method, discussed above, has been accomplished previously by the careful addition of glutamine residues into the HR-2 peptide followed by covalently linking the amide sidechains via a short hydrocarbon linker. This constraint helps lock helical loops into the desired conformation. To improve the inhibitory activity of the HR-2 peptides, conformational constraints and helical-inducing terminal modifications will be added to the peptides.

Preliminary results with the LearnCoil-VMF HR-1 sequence of hMPV offer a new avenue for mechanistic studies and peptide inhibitor design for type I fusion proteins. Previously, only HR-1 peptides isolated from enzymatic degradation and other

biophysical experiments designed to isolate stable protein domains were tested as inhibitors. These HR-1 peptides were found to be ~ 1000 times less potent than their HR-2 counterparts.[21,27,28,56] The weak anti-fusion activity of HR-1 peptides is thought to come from aggregation into a trimeric helical bundle which subsequently ensnares a native HR-2 peptide. A required 3:1 ratio of HR-1 peptides to fusion protein and increased steric issues of a large helical bundle causing poor inhibition of fusion form a reasonable hypothesis. Therefore, many type I fusion proteins have had their HR-1 sequences ignored or unreported as part of a broad inhibitory peptide library.[22] The hMPV HR-1 peptide isolated by LearnCoil-VMF has distinctly different structural properties when compared to the enzymatically derived sequences in the literature. The most notable of these distinctions is the lack of helical content in solution. This conclusion is supported by CD data, absence of a HR-1 trimer in the size exclusion chromatograms, and the strong fit of the nanomolar inhibition data to the Hill-Slope model. These results strongly suggest the HR-1 peptide is inhibiting hMPV growth as a single monomeric peptide. If the hMPV LearnCoil-VMF 43-mer is indeed functioning as a monomeric unit, then it is likely to be inhibiting a different fusion protein intermediate than the HR-2 counterparts. Identifying a possible route of action for the hMPV HR-1 peptide was greatly enhanced by Yin *et al.* providing crystallographic data of type I fusion proteins in both the pre-fusion and post-fusion conformations.[11,12]

A critical step in fusion protein activity is the extension of several short helical domains outward from the globular head of the pre-fusion protein in order to create the native, trimeric HR-1 stalk. This 'stalk extension' is likely the target of a monomeric HR-1 peptide inhibitor. It can be hypothesized that the hMPV 43-mer is able to

intercalate into this critical structure during stalk extension. This would result in an improperly folded and inactive fusion protein. Given the effectiveness of an unmodified, first generation HR-1 inhibitor, it is reasonable to assume an optimized sequence with effective modifications will likely surpass HR-2 peptides in anti-fusion activity. Therefore, two experimental methodologies are being explored to identify new HR-1 based inhibitors. The first approach is aimed at locating a shorter, easier to synthesize segment from the current LearnCoil-VMF HR-1 43-mer. Additionally, this experiment will be designed to also isolate critical regions within the HR-2 region. A second, and novel, approach to HR based inhibitors is a rational design to the creation of second generation HR-1 peptide inhibitors based on computer modeling and available crystallographic data. This could avoid costly and time consuming production of lengthy difficult peptide libraries as a means to optimize a sequence for inhibition.

Preliminary work in the first approach, identifying a short, effective peptide from within the HR-1 43-mer, has demonstrated early success. The experimental design is based upon taking an expanded sequence from each HR region and dividing them into relatively easy to produce 21-mers **(Figure 48)**. Given the critical requirement of helical content discussed throughout this chapter, these peptides were analyzed for helical content and propensity **(Table 3)**. Additionally, concentration dependent conformations were analyzed at 25uM, 50uM, and 100uM of the peptide in order to assess self assembly commonly seen with HR-1 peptides. One notable observation was the aggregation of several segments when the concentration was raised from 50uM to 100uM. Furthermore, each of the HR-1 21-mers was mixed individually with all the members of the HR-2 21-mers. N21B, from the N-terminal HR (SEVTAIKNALKKTNEAVSTLG), has been

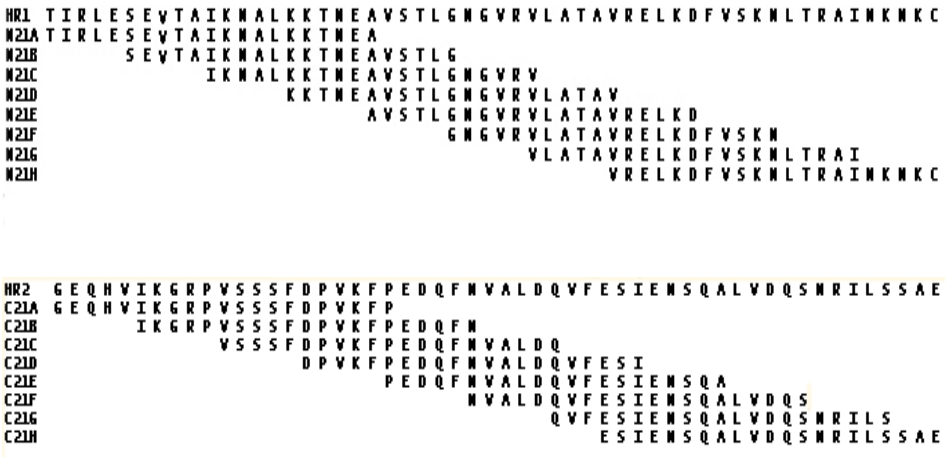

Figure 48 Sequences of extended LearnCoil-VMF HR regions and the 21-mers synthesized. Sequences of N-HR (top) and C-HR (bottom).

Table 3. Helicity of overlapping 21-mer peptides in buffer and TFE.

Peptide	Buffer(0.01M PBS)		50% TFE	
	θ_{224}	$\theta_{224}/\theta_{210}$	θ_{224}	$\theta_{224}/\theta_{210}$
N21A	-2263	0.49	-8564	0.82
N21B	-1400	0.51	-15958	0.87
N21C	-633	0.41	-3835	0.75
N21D	-1455	0.43	-7217	0.70
N21E	-1370	0.46	-7584	0.69
N21F	-209	0.36	-3752	0.79
N21G	-1455	0.43	-7217	0.70
N21H	-1334	0.54	-9293	0.81
C21A	-665	0.36	-1115	0.52
C21B	-1277	1.5	-2538	2.5
C21C	-959	0.45	-1965	0.71
C21D	-663	0.37	-2330	0.77
C21E	-1148	.413	-7909	.854
C21F	-745	0.39	-3852	0.82
C21G	-1374	0.51	-6640	0.81
C21H	-695	0.45	-3295	0.75

* θ in units of deg·cm^2/dmole

identified as being most reactive with the C-terminal HR peptide segments. N21B mixtures containing 1:1 ratios of C21E, C21G, and the full length LearnCoil-VMF 33-mer all display an increase in helical content that is greater than the simple addition of the two peptides in solution. The large increase in the 224 nm band coupled with the loss of the 210 nm band indicates a tightly constrained and stable helical species **(Figure 49)**. At the time of this writing, the 21-mers are being tested as fusion inhibitors.

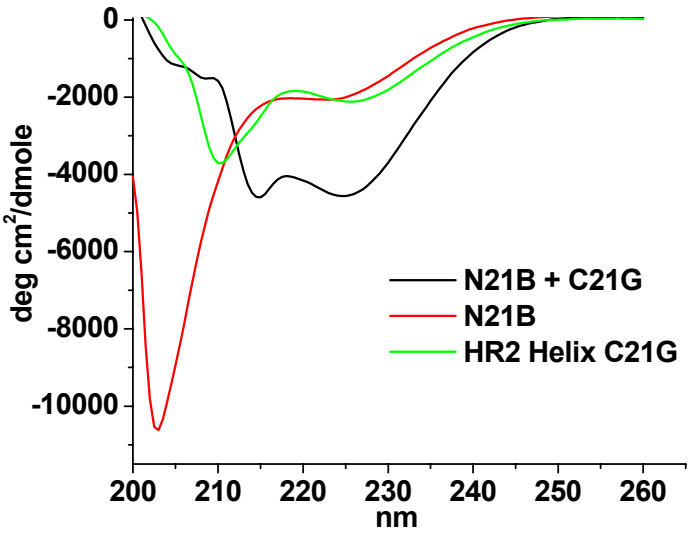

Figure 49. CD spectra of 21-mer N21B and 21-mer C21G mixture. These shorter peptides display a propensity to interact and form higher order structures such as a hexameric coiled-coil.

The experimental design of the second approach will be based on the SV5 pre-fusion crystal (PDB ID: 2B9B) and the current hMPV fusion core model. There are several helical subunits located within the globular head of the pre-fusion SV5 structure **(Figure 26, p. 57)**. These units make up a large portion of the hexameric SV5 post-fusion core structure (PDB ID: 1SVF). Additionally, LearnCoil-VMF predicts a 47 residue sequence (129-175) also found in these helical subunits. It can be hypothesized

that hMPV's pre-fusion structure also contains congruent helical subunits which undergo stalk extension during the fusion process, and exposure of the protein to monomeric

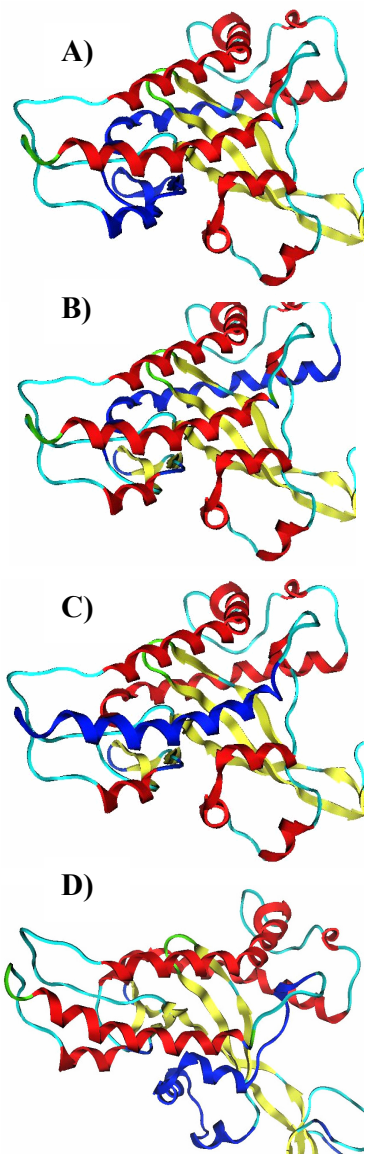

Figure 50. Stalk extension inhibitors (blue) based on (A) the LearnCoil-VMF HR-1 peptide (#6), (B) Peptide (#9) overlapping the fusion core peptide with near region of stalk, (C) Peptide (#10) helix from the mid-region of the extended stalk, (D) Peptide (#X11 helix-coil from the head region of the stalk). Note: All peptides undergo dramatic conformational shift assuming a strong helical conformation in the post-fusogenic form of the F protein.

HR-1 peptide inhibitors containing these sequences will interfere with stalk extension rendering an inactive fusion protein **(Figure 50)**. By effectively aligning the hMPV sequence and fusion core model to identify the likely sequences of these helical subunits, they can be tested individually for anti-fusion activity **(Table 4)**. This will also increase the likelihood of isolating a shorter, easier to synthesize peptide inhibitor. Furthermore, the previously discussed helical-promoting elements can be used to trigger HR-1 aggregation typically seen in proteolytically derived sequences. These experiments will likely lower the ability of the peptide to inhibit fusion. The data gained from an intercalating peptide sequence being converted to a less effective helical aggregate will provide insight into peptidyl anti-viral drug design as well as illustrate a new path for mechanistic intermediate arrest and study.

Table 4. Peptide inhibitors to be examined in this study

Peptide	Residues	HR Inhibitor	Description
1	454-486	HR 2	LC-HR-2 Sequence
2	451-486	HR 2	Computer homology model HR 2
3	451-488	HR 2	LC + 3 N-Term. Res. + helix inducer termini
4	451-486 : 454 X 461	HR 2	**2** + covalent helix constraint
5	Unknown	HR 2	Defined by F-protein footprinting
6	130-172	HR 1	LC Sequence
7	130-179	HR 1	Computer homology model HR 1
8	Unknown	HR 1	Defined by F-protein footprinting
9	114-144	HR 1	Stalk Inhibitor
10	178-204	HR 1	Stalk Inhibitor
11	209-236	HR 1	Stalk Inhibitor

REFERENCES

(1) Van den Hoogen BG, D. J., Groen J *et al. Nat. Med.* **2001**, *6*, 719.

(2) Williams, J. V.,Harris, P. A.,Tollefson, S. J.,Halburnt-Rush, L. L.,Pingsterhaus, J. M.,Edwards, K. M.,Wright, P. F.,Crowe, J. E., Jr. *N. Engl. J. Med.* **2004**, *350*, 443.

(3) Van den Hoogen BG, *e. a. Virology* **2002**, *295*, 119.

(4) Lamb, R. A. a. K., D. *Paramyxoviridae: the viruses and their replication.*; 3rd ed.; Raven Press: New York, 1996.

(5) Carr, C. M., and Kim, P.S. *Cell* **1993**, *73*, 823.

(6) Malashkevich, V. N., Kim, P.S., et al. *Proc. Nat'l. Acad. Sci.* **1998**, *95*, 9134.

(7) Lu, M., et al. *Nat. Struct. Bio.* **1995**, *2*, 1075.

(8) Malashkevich, V. N.,Schneider, B. J.,McNally, M. L.,Milhollen, M. A.,Pang, J. X.,Kim, P. S. *Proc. Nat'l. Acad. Sci.* **1999**, *96*, 2662.

(9) Hernandez, L. D., et al. *Ann. Rev. Cell Dev. Bio.* **1996**, *12*, 627.

(10) Melikyan, G. B.,Markosyan, R. M.,Hemmati, H.,Delmedico, M. K.,Lambert, D. M.,Cohen, F. S. *J. Cell Bio.* **2000**, *151*, 413.

(11) Yin, H.-S.,Wen, X.,Paterson, R. G.,Lamb, R. A.,Jardetzky, T. S. *Nature* **2006**, *439*, 38.

(12) Yin, H.-S.,Paterson, R. G.,Wen, X.,Lamb, R. A.,Jardetzky, T. S. *Proc. Nat'l. Acad. Sci.* **2005**, *102*, 9288.

(13) Chen, L.,Gorman, J. J.,McKimm-Breschkin, J.,Lawrence, L. J.,Tulloch, P. A.,Smith, B. J.,Colman, P. M.,Lawrence, M. C. *Structure* **2001**, *9*, 255.

(14) Lu, M.,Blacklow, S. C.,Kim, P. S. *Nat. Struct. Bio.* **1995**, *2*, 1075.

(15) Lawless-Delmedico, M. K. *Biochemistry* **2000**, *39*, 11684.

(16) Chan, D. C.,Fass, D.,Berger, J. M.,Kim, P. S. *Cell* **1997**, *89*, 263.

(17) Xun Zhao, et. al. *Proc. Nat'l. Acad. Sci.* **2000**, *97*, 14172.

(18) Chan, D. C.,Chutkowski, C. T.,Kim, P. S. *Proc. Nat'l. Acad. Sci.* **1998**, *95*, 15613.

(19) Samuel K. Sia, et al. *Proc. Nat'l. Acad. Sci.***2002**, *99*, 14664.

(20) Wild, C., et al. *Proc. Nat'l. Acad. Sci.* **1992**, *89*, 10537.

(21) Wild, C., et al. *Proc. Nat'l. Acad. Sci.* **1994**, *91*, 9770.

(22) Lambert, D. M.,Barney, S.,Lambert, A. L.,Guthrie, K.,Medinas, R.,Davis, D. E.,Bucy, T.,Erkckson, J.,Merutka, G.,Petteway, S. R., Jr. *Proc. Nat'l. Acad. Sci.* **1996**, *93*, 2186.

(23) Yao, Q.,Compans, R. W. *Virology* **1996**, *223*, 103.

(24) Wang, X.-J.,Bai, Y.-D.,Zhang, G.-Z.,Zhao, J.-X.,Wang, M.,Gao, G. F. *Arch. Biochem. Biophys.* **2005**, *436*, 316.

(25) Young, J. K.,Hicks, R. P.,Wright, G. E.,Morrison, T. G. *Virology* **1997**, *238*, 291.

(26) Reay G. Paterson, C. J. R., and Robert A. Lamb *Virology* **2000**, *270*, 17.

(27) Charles J. Russell, T. S. J. a. R. A. L. *EMBO Journal* **2001**, *20*, 4024.

(28) Wang, E.,Sun, X. o.,Qian, Y.,Zhao, L.,Tien, P.,Gao, G. F. *Biochem. Biophys. Res. Commun.* **2003**, *302*, 469.

(29) Wild, C.,Shugars, D. C.,Greenwell, T. K.,McDanal, C. B.,Matthews, T. J. *Proc. Nat'l. Acad. Sci.* **1994**, *91*, 9770.

(30) Wild, C., et al. *Proc. Nat'l. Acad. Sci.* **1992**, *89*, 10537.

(31) Samuel K. Sia, P. A. C., Andrea G. Cochran, Vladamir N. Malashkevich, and Peter S. Kim *Proc. Nat'l. Acad. Sci.* **2002**, *99*, 14664.

(32) Baker, K. A., et al. *Mol. Cell* **1999**, *3*, 309.

(33) Xun Zhao, et al. *Proc. Nat'l. Acad. Sci.***2000**, *97*, 14172.

(34) Dayhoff, M., Schwartz, R.M., and Orcutt, B.C. *A Model of Evolutionary Change in Proteins*; National Biomedical Research Foundation: Silver Springs, Maryland, 1978; Vol. 5 (suppl 3).

(35) Henikoff, S.,Henikoff, J. G. *Proc. Nat'l. Acad. Sci.***1992**, *89*, 10915.

(36) Brown, J. H.,Cohen, C.,Parry, D. A. *Proteins* **1996**, *26*, 134.

(37) Brian J. Smith, et al. *Prot. Eng.* **2002**, *15*, 365.

(38) Rost, B. *Prot. Eng.* **1999**, *12*, 85.

(39) Joshi, S. B.,Dutch, R. E.,Lamb, R. A. *Virology* **1998**, *248*, 20.

(40) Berger, B.,Singh, M. *J. Comput. Bio.* **1997**, *4*, 261.

(41) Singh, M., et al. *J. Mol. Bio.* **1999**, *290*, 1031.

(42) Root, M. J.,Kay, M. S.,Kim, P. S. *Science* **2001**, *291*, 884.

(43) Eckert, D. M.,Kim, P. S. *Proc. Nat'l. Acad. Sci.* **2001**, *98*, 11187.

(44) Lee, M. S.,Wood, G. G.,Jacobs, D. J. *J. Phys.: Cond. Mat.* **2004**, *16*, S5035.

(45) Lamb, R. A.,Joshi, S. B.,Dutch, R. E. *Mol. Membr. Bio.* **1999**, *16*, 11.

(46) Sergel, T. A.,McGinnes, L. W.,Morrison, T. G. *J. Virol.* **2001**, *75*, 7934.

(47) Kim, D. M. E. a. P. S. *Ann. Rev. Biochem.* **2001**, *70*, 777.

(48) Lu, M.,Blacklow, S. C.,Kim, P. S. *Nat. Struct. Bio.* **1995**, *2*, 1075.

(49) Ernst, J. T.,Kutzki, O.,Debnath, A. K.,Jiang, S.,Lu, H.,Hamilton, A. D. *Angew. Chem. Int. Ed.* **2002**, *41*, 278.

(50) Berger B., et al. *Proc. Nat'l. Acad. Sci.* **1995**, *92*, 8259.

(51) Wolf E., et al. *Prot. Sci.* **1997**, *6*, 1179.

(52) Lamb, R. A. *Virology* **1993**, *197*, 1.

(53) Weng, Y.,Weiss, C. D. *J. Virol.* **1998**, *72*, 9676.

(54) Whiting, B.,Kelman, A. W. *Clin. Sci.* **1980**, *59*, 311.

(55) Skelton, N. J.,Chen, Y. M.,Dubree, N.,Quan, C.,Jackson, D. Y.,Cochran, A.,Zobel, K.,Deshayes, K.,Baca, M.,Pisabarro, M. T.,Lowman, H. B. *Biochemistry* **2001**, *40*, 8487.

(56) Zhao, X.,Singh, M.,Malashkevich, V. N.,Kim, P. S. *Proc. Nat'l. Acad. Sci.* **2000**, *97*, 14172.

CHAPTER III

AMINE-TERMINATED DENDRIMERS AS BIOMIMETIC TEMPLATES FOR PROTEIN ENCAPSULATION WITHIN SILICA NANOPARTICLES

Introduction

Biologically active molecules are being used as tools in an increasingly diverse set of research fields ranging from synthetic organic chemistry to physics and materials development. Many uses for biomolecules such as biologically active materials, organic synthesis reagents, and reaction reporter, have been hindered by the reality that many biological reagents and components require additional separation procedures and have a poor shelf life. Previous work has shown that materials containing functional enzymes within a silica matrix offer increased stability over time and improved strategies for product recovery.[1,2] Unfortunately, many active silica materials are plagued by limitations stemming from inefficient loading and the limited scope of biomolecules that survive typical encapsulation reaction conditions.[3-10] Some recent approaches are able to achieve increased encapsulation efficiencies for a wider array of biomolecules, but require lengthy and laborious processing.[11-14]

Other recent attempts to stabilize biomacromolecules encased in silica using methods inspired by natural biomineralization processes have been reported to offer a rapid benchtop approach.[2,15-18] One biomimetic solution is to encapsulate the biomolecule in silica nanoparticles via a class of peptides related to the silaffins discussed in Chapter I. Silaffin peptides function in a self-assembled template to catalyze the formation of silica nanoparticles into the intricate biological structures of oceanic

diatoms.[19] The native silaffin peptides are highly post-translationally modified, having phosphorylated serines and modified lysines containing ε-N-dimethyllysine, phosphorylated ε-N-trimethyl-δ-hydroxylysine, or long chain N-methyl derivatives of polypropylenimine. Isolated silaffin inspired peptides have been able to produce spherical mesoporous silica nanoparticles of various sizes from hydrolyzed silicic acid.[20] Indeed, this biomimetic approach has been adopted with a variety of amine sources providing a wide range of encapsulated molecules.[21-23]

Silica Precipitating Peptides: Chapter I discussed the process of mitosis undertaken by oceanic diatoms. Formation of the frustule requires transportation, condensation, and deposition of silicic acid in the SDV. In one of the first studies of this biomineralization, Kröger *et al.* showed that diatoms employ specific peptides and polyamines for the biogenic synthesis of silica. The silaffin peptide extracted from the frustle of *C. fusiformis* was shown to moderate the direct precipitation of silica from a silicic acid solution.[24] Terminal amino acid degradation revealed a large amount of homology between all of the silica precipitating peptides generated from *C. fusiformis*. SSKKSGSYSGSKGSKRRIL was finally determined to be the critical amino acid sequence for silica precipitation. This peptide, deemed the R5 peptide, contained many post-translational modifications to the lysine and serine residues. The lysines were affixed with highly branched chains of polyamines, mostly by methylated polypropylenimine, while the serines were phosphorylated **(Figure 51)**. Mass spectrometry confirmed the post-translational modification structural analysis. [24,25]

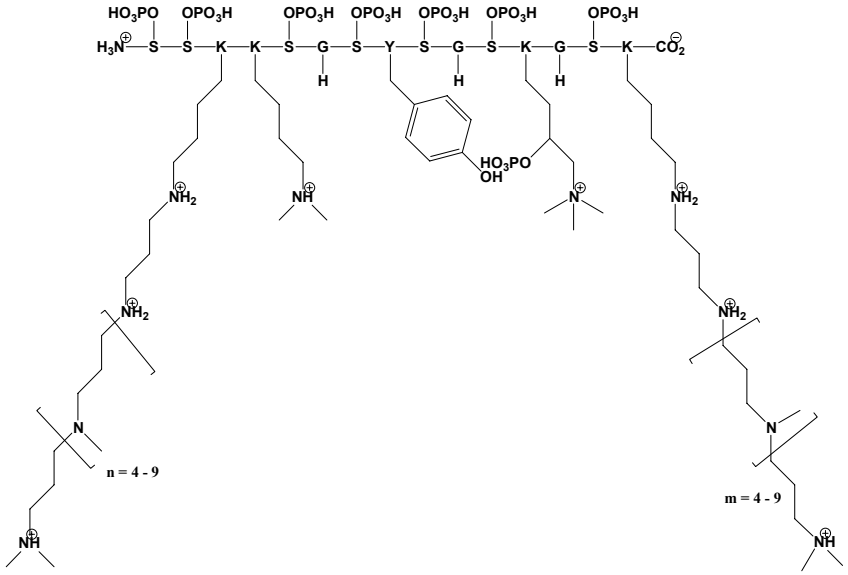

Figure 51. natSil-1a with alkylated lysine residues and phosphorylated serines.

As Frigeri *et al*. demonstrated, the post-translational modifications of the lysine and serine residues of the silaffin peptides are of particular importance.[26] Studies from multiple species have exposed these modifications to be species specific.[24,25] Many of the free polyamines are strongly associated with the frustule and have been shown to precipitate silica *in vitro* from solutions of silicic acid.[27] One reasonable series of events would occur via interactions of the amine moieties with the silicic acid driving the hydrolysis of the precursor into the formation of silica **(Figure 52)**.

Due to the significance of sidechain modifications, one of the key aspects to diatom research revolves around the extraction technique. Extracting the peptides from the cell frustule under harsh conditions, such as hydrofluoric acid exposure, cleaves the phosphate group, leaving only the hydroxyl groups of the serine residues. Under identical reaction conditions capable of precipitating silica in the presence of native

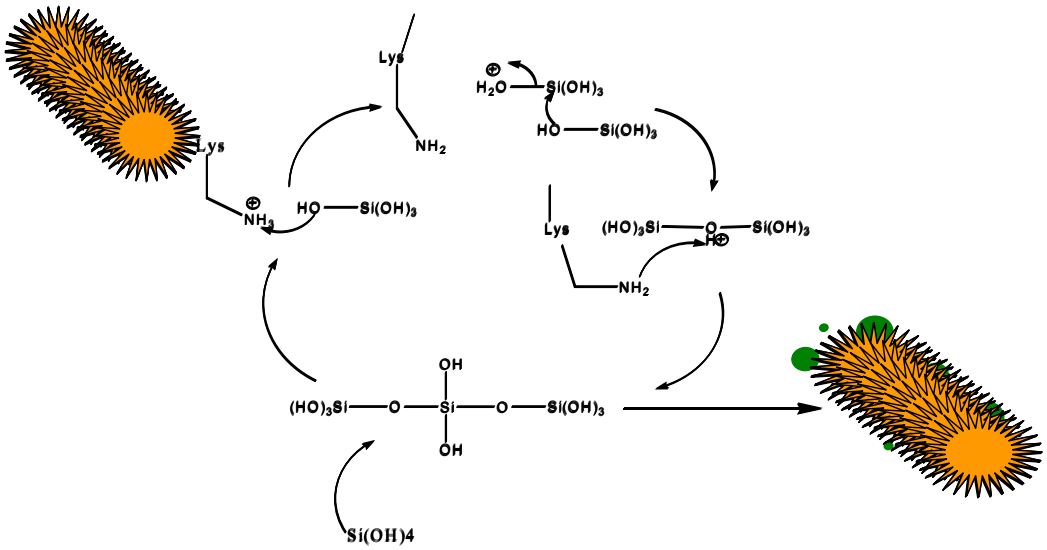

Figure 52. Amine mediated condensation of silicic acid. R5 peptide aggregate is representated in orange and nascent silica nanoparticles in green. Provided by Sarah Sewell.

silaffins, the dephosphorylated peptides produced little or no silica production. Charging these dephosphorylated peptide solutions with various concentrations of phosphate induces silica production in a linear dependence which plateaus once activity matches that of native silaffins at a concentration of 30 mM phosphate **(Figure 53)**.[24,25] Phosphate addition reconstitutes the ionic crosslinkage network to form aggregates capable of biosilification. This further supports the hypothesis of phosphate groups associated with the serine residues promoting an electrostatic assembly of multiple silaffin units to form a supramolecular assembly. This moiety would generate the locally high concentration of polyamine to drive silica precipitation.[25] Indeed, an ionic network created by phosphorylated serines was finally confirmed by ^{31}P NMR experiments showing peak broadening due to the aggregation in solution at pH 5.5. Extrapolation of

the peak broadening reveals that approximately 700 peptide sequences can self assemble into a network.[25]

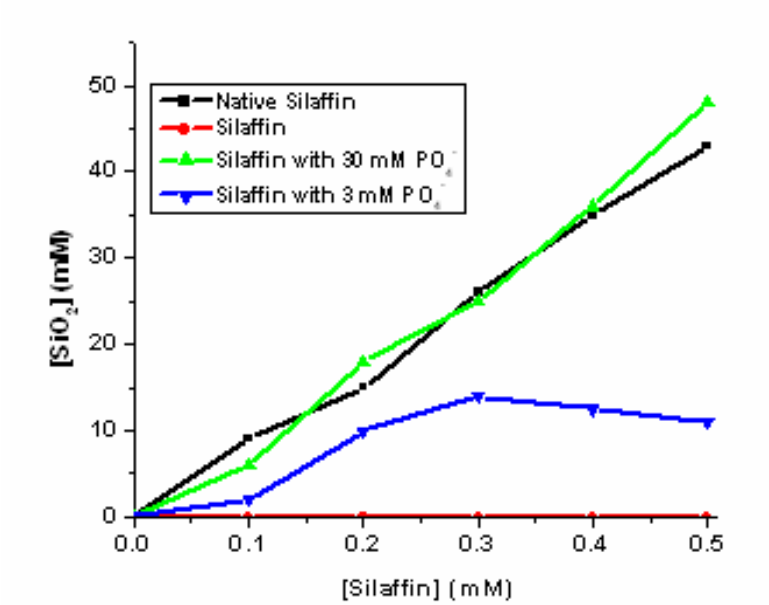

Figure 53 . Phosphate dependence of the non-phosphorylated silaffin; Provided by Dr. Marc Knecht

An interesting observation noted by Kröger *et al*. was the ability of the synthetic, unmodified R5 peptide to precipitate silica. This was unexpected considering the absence of the polyamine-to-lysine adducts as well as phosphorylation of the serines. Further analysis revealed a significant difference in the pH profiles for silica deposition between silaffin and the unmodified synthetic R5 peptide from *C. fusiformis.* One substantial difference between native silaffins and the unmodified R5 peptide was the difference in pH required to produce the maximum amount of silica particles. The non-modified R5 peptide precipitated silica with a maximum activity at pH 7.0, but silaffins have been shown to have optimal silica precipitation activity at pH 5.0 **(Figure 54)**.[24]

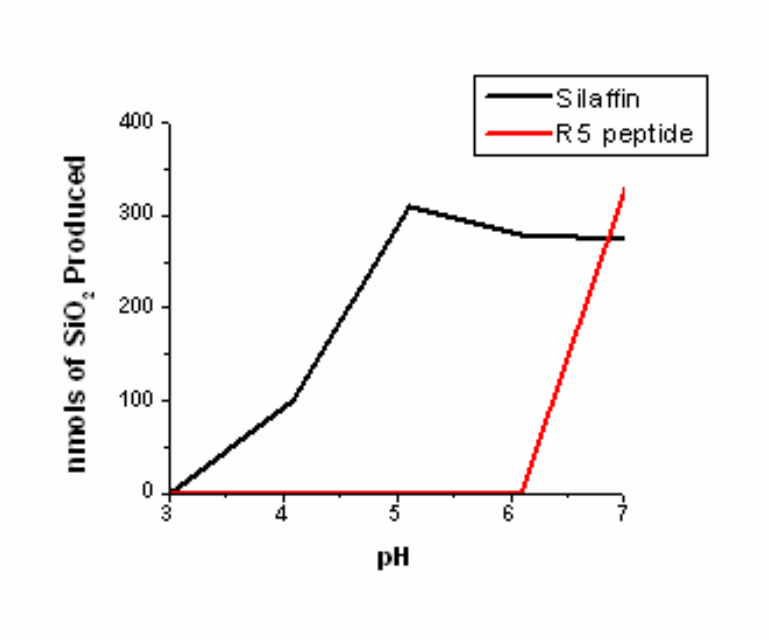

Figure 54. pH dependencies of silaffin and the R5; Provided by Dr. Marc

Table 5. The silica precipitating truncate and mutant peptides and their activities. *Specific activity listed as nmol of silica/(nmol peptide * min). Provided by Dr. Marc Knecht

Number	Sequence	Specific Activity*	Particle Size (nm)
1	SSKKSGSYSGSKGSKRRIL	3.59 ± 0.2	250 – 450
2	SSKKSGSY	0.08 ± 0.05	N/A
3	SGSKGSKRRIL	3.35 ± 0.3	180 – 400
4	KSGSYSGSKGSKRRIL	3.29 ± 0.2	125 – 200
5	SGSKGSKRR	2.70 ± 0.2	150 – 300
6	SSKKSGSYSGSKGSK	1.29 ± 0.2	85 – 130
7	LIRRSSKKSGSY	3.17 ± 0.2	60 - 300
8	SSKKSGSYRRIL	2.88 ± 0.3	60 - 300
9	SGSKGSKAAIL	0.24 ± 0.2	N/A
10	SGSKGSKEEIL	0.17 ± 0.1	N/A
11	SGSKGSKNNIL	0.16 ± 0.1	N/A

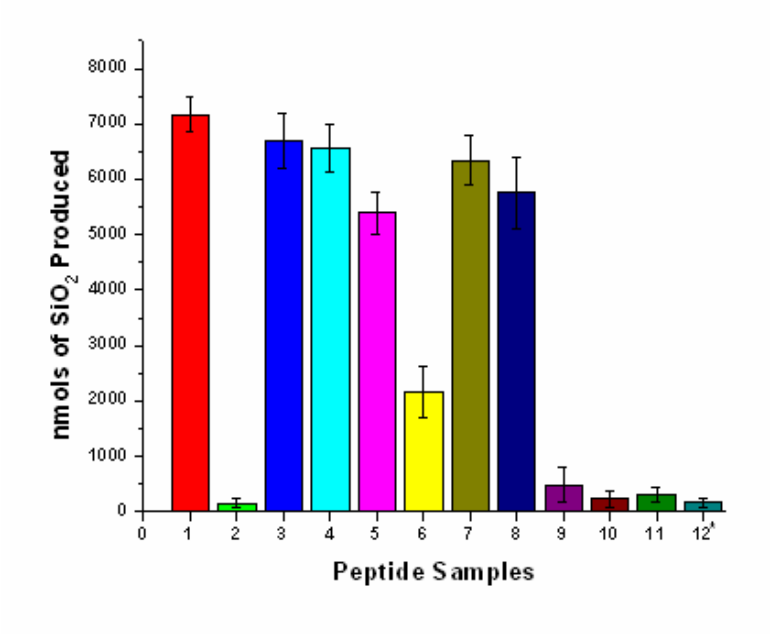

Figure 55. Silica production from the mutant and truncate peptides at concentrations of 2 mM. 12* refers to a blank measurement. Provided by Dr. Marc Knecht

This unexpected enigma of silica production from unmodified synthetic R5 was investigated by Knecht *et al.* Their mutational study **(Table 5; Figure 55)** of R5 revealed a critical C-terminal RRIL motif that serves as an organizing element for supramolecular formation of peptide assemblies observable by dynamic light scattering.[28] This complex also offers a locally high concentration of primary amine side chain residues to drive *in vitro* silica condensation. Again, the formation of silica dioxide from silicic acid solutions is driven by the formation of a complex aggregation of amino acid based molecules to achieve a locally high amine concentration.

Recent work with a variety of polyamines such as poly-L-lysine,[29] pentapropylenehexamine[30] or poly-allylamine hydrochloride[31,32] reveals that silica condensation can be driven by a variety of sources rich in amine moieties. One such study was performed by Manfred Sumper and associates in 2004.[31] The researchers

wanted to determine the role of anions and the effect of poly-allylamine hydrochloride (PAA) aggregation on silica precipitation. PAA exhibits a long chain polyamine structure similar to the silaffins isolated from diatoms. Previously, PAA had been shown to precipitate silica from silicic acid.[33,34] The investigators discovered that without at least 0.3 $[P_i]/[ru]$ of phosphate, silica would not precipitate from the PAA and silicic acid solution. They reasoned that in the absence of sufficient phosphate concentrations, PAA would fail to aggregate into large moieties lending locally high amine concentrations. To test this hypothesis, dynamic light scatter was used to determine the PAA moiety's size as a function of phosphate concentration **(Figure 56).** They found a direct correlation between the amount of phosphate in solution and the size of the PAA aggregates.

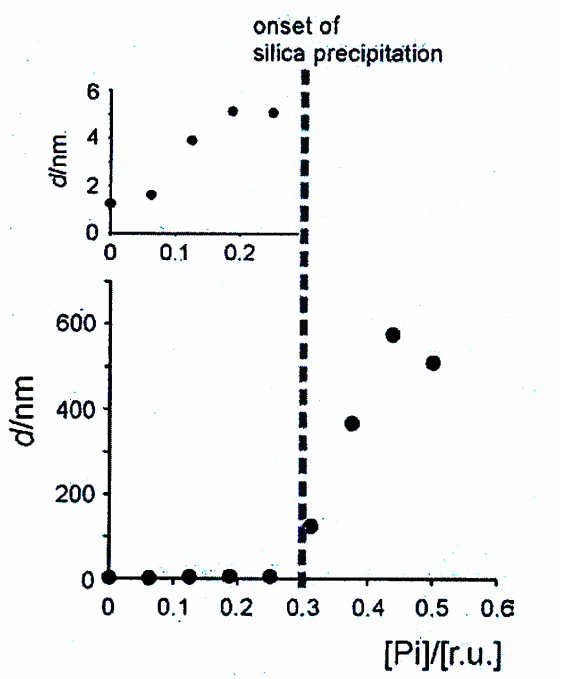

Figure 56. Diameter, *d,* of PAA aggregates determined by dynamic light scattering as a function of phosphate concentration per repeating unit (ru) of PAA. Dashed line indicates the minimum phosphate concentration required for silica precipitation.[31]

Additionally, the required 0.3 $[P_i]/[ru]$ of phosphate produced significant PAA aggregates. Indeed, the solutions containing the larger aggregates began to display a cloudy mixture consistent with the presence of ever larger PAA aggregates. NMR analysis showed that PAA concentration in the supernatant of the cloudy mixtures experienced a decrease as more phosphate was added. Therefore, it was not unexpected to observe that solutions with greater than 0.5 $[P_i]/[ru]$ failed to produce silica. They concluded from these experiments that microscopic phase separation was a requirement for the biomimetic silification from primary amine sources.

Their hypothesis of requisite PAA aggregation in order to condense silicic acid was further supported by the increase in size of the silica nanoparticles produced as the concentration of phosphate increased. This would be expected because the organic scaffolds used by diatoms to template biogenic silica are incorporated into the silica as discussed in Chapter I. Therefore, larger PAA aggregates being engulfed by silica would be expected to produce larger silica particles. Furthermore, these trends were found to be identical when sulfate was substituted for phosphate. However, chloride, a monovalent ion, failed to precipitate silica from the silicic acid mixture at its highest concentration (20 [Cl]/[ru]). Dynamic light scattering showed that chloride mediated aggregates reached a maximum diameter of 9 nm, two orders of magnitude smaller than divalent mediated aggregates of 600 nm **(Figure 57)**. Since macroscopic phase separation did not occur with the chloride and PAA mixtures, it was concluded that monovalent anions fail to attract sufficient quantities of PAA to achieve moieties necessary to achieve locally high amine concentrations.

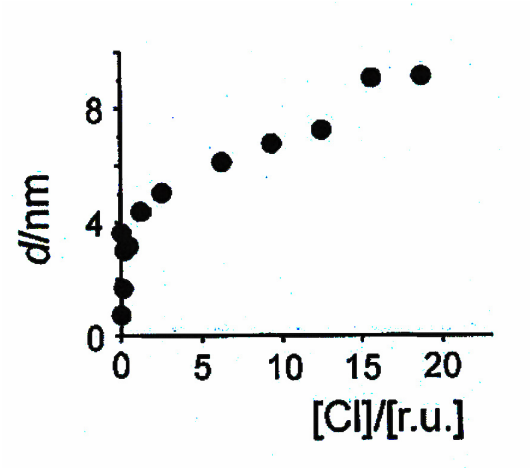

Figure 57. Diameter, *d,* of PAA aggregates as a function of chloride per repeated units (ru) of PAA[31]

Similar to the R5 peptide, systems such as PAA require the self assembly of the active catalyst. This assembly process and maintenance could potentially limit the scope of molecules incorporated into novel silica materials. Potential new components to silica materials may interfere with the suprastructure of the amine moiety and severely hinder silica precipitation. This could be particularly true with enzymes because of their large number of charged surface groups. One class of molecules that presents itself as a possible remedy to self-assembly requirements is the dendrimer family. Indeed, a plethora of nanoparticles, including sol-gel composites, have been patterned and stabilized from the use of dendrimers.[35-39]

Biomimetic Dendrimers: The observation of protein and peptide sequences with little homology having a shared ability to precipitate silica, provided they can generate a required local amine concentration, encourages biomimetic template exploration. Templates enriched with amines do not need to be peptide based, and therefore could be obtained more cheaply and easily than natural or synthetic silaffin. An abundant supply

of templating material opens doors for inexpensive novel materials produced under ambient conditions. Ambient conditions used for production would allow researchers to investigate biomolecules as components to the new materials.

Dendrimers are unimolecular polymer templates which offer a wide array of functionality and optimization stemming from the control of branching elements and terminal groups. Dendrimers have been used for molecular recognition, micellular generation, and formation of host-guest complexes (see reference 40 for a review of dendrimer literature). These polymeric supports represent well -defined templates to

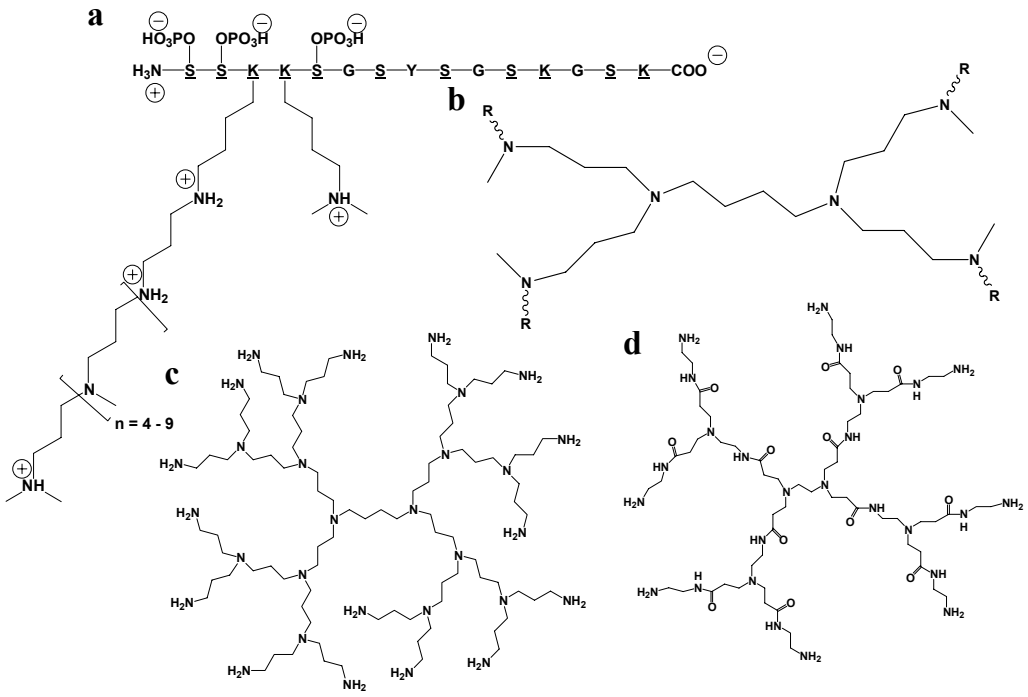

Figure 58. Chemical structures of silaffin derived and biomimetic dendrimer precipitating amines. (a) Silaffin peptide isolated from *C. fusiformis*, underscored residues are post translationally modified *in vivo*. Of note, the repeating N-methylpropylenimine units critical for providing sufficient amine concentration to drive silica condensation. (b) Poly N-methylpropylenimine extracted from *S. turris,* where R indicates a repeating N-methylpropylenimine unit of n = 15-21. (c) G-3 PPI dendrimer. (d) G-1 PAMAM.[41]

provide sufficiently high local amine concentrations to drive biomimetic silica nanosphere formation.[41] Polypropylenimine dendrimers (PPI) are composed of repeating propylenimine units similar to the major post-translational modification found in the lysines of the silaffins. PAMAM dendrimer branches terminating in primary amines are similar to the unmodified lysines of the R5 peptide **(Figure 58)**.

Table 6. Silica Condensation Activity for Amine-Terminated Templates [41]

Template	Template Diameter (Å)	Surface Amines	Specific Activity*	Nanosphere Diameter (nm)
G1 PPI	8.8	4	ND	180 ± 27
G2 PPI	13.8	8	ND	169 ± 45
G3 PPI	18.6	16	ND	242 ± 76
G4 PPI	23.2	32	7.47 ± 1.2	219 ± 91
G5 PPI	27.8	64	23.7 ± 2.6	258 ± 76
G0 PAMAM	15	4	ND	95 + 25 350 ± 50
G1 PAMAM	22	8	ND	130 ± 20 400 ± 40
G2 PAMAM	29	16	8.1 ± 0.7	380 ± 40
G3 PAMAM	36	32	17.2 ± 2.2	360 ± 75
G4 PAMAM	45	64	46.1 ± 4.4	292 ± 73
G5 PAMAM	54	128	63.0 ± 8.7	275 ± 105
G6 PAMAM	67	256	108.3 ± 19.3	334 ± 80
*nmols SiO_2 per minute per nmol dendrimer; ND not determined due to template interference.				

Knecht *et al.* demonstrated that an amine-terminated dendrimer can serve as an effective alternative to the self-assembled silica precipitating structure of the R5 peptide.[20,41,42] A series of dendrimers (PPI G1-G5 and PAMAM G0-G6) were probed for

their capabilities to rapidly precipitate silica nanospheres from a solution of metastable silicic acid **(Table 6)**. Each dendritic template assayed was active, and produced silica nanospheres of expected morphology. The β-silico-molybdate assay was employed to quantify the silica upon removal of the interfering dendrimer from the dissolved silica solution.[43] Further confirmation of the crucial role of amines was given by the lack of silica production from analogous hydroxyl-terminated PAMAM dendrimers.

Functional Silica Nanocomposites: Many applications are being developed based upon the genesis of composite materials with hybrid organic-inorganic composition. Functional building blocks for heterogeneous catalysis,[44,45] biological labeling and detection,[46,47] and components of electronic devices are some examples of real world application.[48] Typical synthetic methods for these materials include vapor deposition, self assembly,[49,50] and electrodeposition.[51,52] These techniques give the formation of a nearly homogenous material containing unique activities that can be manipulated through careful selection of the ratios of the respective materials. A complication to some of these techniques is the overly complex and strictly controlled reaction conditions necessary to produce them. Indeed, many of these synthetic routes limit the functionality and diversity of the materials. A biomimetic approach functioning rapidly under ambient conditions would open many doors to novel, functional materials.

Nanocomposite materials comprised of encased functional species in silica matrices[47,53-58] offer flexible routes for the tuning of nanoparticle properties, enhancing stability,[56] and a pliable surface for subsequent conjugation for additional functionality.[47] Methods currently employed in nanoparticle silica encapsulation include the Stöber method[53,54,56,57] and microemulsion techniques.[47,55,58] These techniques do in fact

encapsulate nanoparticles, but they either demand further synthetic work to induce silica formation or they function at extreme pH. As mentioned above, the ambient conditions required for amine terminated dendrimers to induce silica formation represent a versatile alternative to these often harsh methods. A diverse range of nanoparticles, including sol-gel composites, have been previously patterned and stabilized from the use of dendrimers.[35-39] Other approaches have relied on the host guest properties of dendrimers to stabilize nanoparticles.[56] Utilizing these attributes, PAMAM dendrimers have been employed as a multifunctional framework, performing dual roles as both the host for nanoparticle synthesis and a template for silica condensation under ambient conditions.[42] These composites were characterized by a variety of methods and demonstrate a robust method for the preparation of heteronanosphere composites derived from a biomimetic approach to the encapsulation of nanoparticles within a mesoporous silica framework.

To demonstrate this application, Knecht *et al.* were able to incorporate gold nanoparticles into silica spheres by utilizing the previously mentioned dendritic approach.[42] Dendrimer encapsulated gold nanoparticles were produced as described by literature procedures.[36,42,59] Fifteen minutes of incubation allowed for the coordination of Au^{3+} ions to amines associated with the G4 PAMAM dendrimers.[50] Reduction by $NaBH_4$ yielded the Au^{o} nanoparticles, displaying a fingerprint plasmon absorbance band at 513 nm. The nanoparticles were then lyophilized **(Figure 59)**. Subsequent transmission electron microscopy (TEM) analysis of the powder displayed a mean gold particle size of 4.1 ± 1.1 nm. These nanoparticles were either trapped within the interior of the dendrimer or surface passivated by select dendrimers, as determined by TEM analysis. This leaves surface primary amines of the dendritic template available for silica

condensation reactivity. The dendritic Au^{o} nanoparticle powders suspended in phosphate buffer and diluted to give a primary amine concentration of 20 mM shown to be optimal for silica condensation[41] were reacted with monosilicic acid.

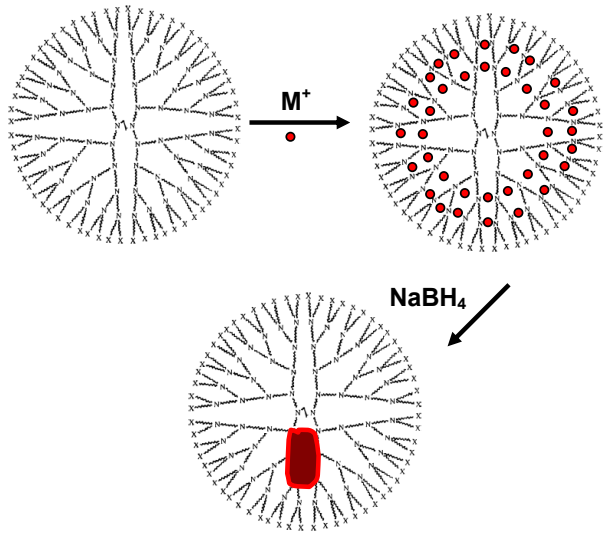

Figure 59 Synthetic scheme of the synthesis of zero-valent noble metal nanoparticles using dendrimeric templates.[42]

When compared to the empty G4 PAMAM template, slightly less activity and a linear dependence on the concentration of surface primary amines was observed from the silica formation activity profile of the dendritic Au^{0} nanoparticles.[38] This infers a heterogeneous mixture of *inter*- and *intra*-dendrimeric nanoparticles.[59,60] The nascent negatively charged silicates align along the positively charged template and finally ripen to form nanospheres of silica that encapsulate the dendrimer. Thus, multiple siliceous particles ripen to yield larger structures. Eventually a critical size is reached, and the silica nanosphere becomes insoluble and precipitates.[24,28,41]

Upon reaction of the nanoclusters/dendrimer composite with monosilicic acid, a dark red siliceous pellet was evident following centrifugation, giving visual evidence to the silica encapsulation of the dendrimer-supported Au^0 nanoparticles. The resulting multicomponent nanocomposite was analyzed using a variety of techniques that demonstrated the encapsulation of the Au^0-dendrimer composite within the silica nanoparticle.[42] Additionally, treatment with potassium cyanide proved that there was significant solvent access to the gold nanoparticles as evinced by the cyanide mediated degradation of the Au^0 cluster. This result suggests that such silica nanocomposites may have applications in heterogeneous supported catalysis.

Biocomposites: Biologically active molecules are being used as tools in an increasingly diverse set of research fields ranging from synthetic organic chemistry to medicine to materials science. Great interest is held for biomolecules as novel, functional materials, reagents for organic synthesis, and reporters for biological activity. Traditional approaches have been hindered by the stringent conditions of a biological reaction including lengthy purification procedures and poor stability. Previous reports state that materials containing functional enzymes within a silica matrix offer improved stability as a function of time and simplified strategies for product recovery.[1,2,12] Older techniques for the production of active silica materials are plagued by limitations of inefficient loading and the limited scope of biomolecules that survive typical encapsulation reaction conditions.[3-10] Recent advances have increased the loading efficiencies in sol-gel composites, but at the expense of extensive and precise synthetic processing.[12] The biomimetic technique, based on the silaffin chemistry discussed above, promises reasonable encapsulation efficiencies in a rapid, inexpensive, and bench top environment.

When compared to traditional sol-gel methods of encapsulation, the use of a biomimetic approach improved the preparation of bio-silica composites. Using the unmodified R5 peptide of *Cylindrotheca fusiformis* (H_2N-SSKKSGSYSGSKGSKRRIL-CO_2H), Luckarift *et al.* reported an encapsulation efficiency improvement up to a reported 20% relative to the typical 0.1%-5% (w/w) with other sol-gel techniques.[2,4] The improvements in silica encapsulation were attributed to reaction conditions more amenable to biological molecules. Furthermore, due to the mild conditions, a much larger array of biologically active molecules could be potential targets for silica encapsulation. Compared to more efficient sol-gel methods based on sodium silicates,[12] the R5 encapsulation reaction was performed on the benchtop on the order of minutes in contrast to the multi-day and thermally sensitive silicate sol-gel synthesis.

This chapter focuses on a novel use of PAMAM dendrimers to drive the encapsulation of enzymes in silica spheres with high loading efficiency and excellent long term stability. Consequently, the requirement of generating a supramolecular complex of the silica precipitating moiety in order to achieve locally high amine concentrations has been eliminated. Furthermore, electrostatics of the enzyme, buffer, and dendrimer are shown to play a crucial role in the encapsulation efficiency.

Experimental

Peroxidase Encapsulation and Activity: Horseradish peroxidase (HRP; EC 1.11.1.7) from Sigma (181 units/mg Type II from Horseradish) was encapsulated into silica particles using a generation 4 PAMAM dendrimer (Sigma; 10 wt% in MeOH) as a nucleating template. An aliquot of 200 μL from HRP stock solution (220 units/mg) was

charged with dendrimer to give a final dendritic amine concentration of 20mM. HCl (aq) hydrolyzed 1M tetramethylorthosilicate (TMOS) was added (20 μL) resulting in rapid precipitation of white silica nanoparticles. The particles were centrifuged at 10,000 RPM and washed with water three times. General protein content was quantitated using the Bradford assay from a standard curve of known amounts of HRP. Specific HRP activity was determined via a H_2O_2 and 3-3'-5-5' tetramethylbenzidine TMB assay kit (Sigma).[61]

Glucose Oxidase Encapsulation and Activity: Encapsulation proceeded as above for HRP. Glucose Oxidase (EC 1.1.3.4) from Fluka (220u/mg) was dissolved in water at pH 7. O-dianisidine (0.1 mL of a 1% solution) was added to 12mL of 0.1M phosphate buffer at pH 6 for dye reagent. From this dye reagent, 192 μL was added to 25 μL of 18% β-D-glucose solution. HRP (8.35 μL of 200 μg/mL) was then added, followed by 25 μL of glucose oxidase test solution. The reaction was allowed to run for 5 minutes and terminated with 50 μL of 2M sulfuric acid. Absorbance was read at 460 nm (Agilent Technologies model 8453 UV-Vis).

TMB Assay: HRP was dissolved in either water pH 7 or 0.1M phosphate buffer pH 7. A test sample of 100 μL from the enzyme solution was mixed with 100 μL of 3,3',5,'-tetramethylbenzidine liquid substrate and allowed to sit at room temp for 10 minutes. 2M sulfuric acid was added to terminate the reaction. Absorbance was read at 420 nm.

β-Galactosidase Activity Assay: β-Galactosidase (Fluka) was suspended at 2 mg/mL. Encapsulation proceeded as above for HRP. Activity was determined via UV-VIS spectrophotometry as previously described.[62] Briefly, 1 mL of phosphate buffer was charged with 0.3 mL of 1.0M 2-mercaptoethanol, 0.5 mL of 0.014M *o*-Nitrophenyl-β-D-

galactopyranoside (ONPG), and 1 mL of pure water. This mixture was then charged with the enzyme and the absorbance was monitored at 420 nm.

Nitrilase Activity Assay: Nitrilase (Biocatalytics) was suspended at 2 mg/mL in 25mM phosphate buffer at pH 7.5. Encapsulation proceeded as above for HRP. Activity was determined by a fluorometric assay previously described.[63] Briefly, nitrilase was charged with 50mM 3-cyanopyridine and an aliquot of the nitrilase and substrate mixture was removed and added to an alcoholic *o*-phthaldialdehyde (Fluka) solution (3.75 mM) in the presence of alcoholic 2-mercaptoethanol (Sigma; 3.6 mM). This solution was allowed to mix for 35 minutes, and was excited at 412 nm. The emission was monitored at 467 nm (Biotek Synergy HT). NMR analysis was performed on a Bruker DPX-300 at room temperature. NMR samples were prepared by performing encapsulation and enzymatic activity assay in deuterated 25 mM phosphate buffer.

Bradford Assay: Quantification of protein mass was performed by adding 160 μL of enzyme test solution to 40 μL of BioRad Protein Assay solution concentrate and mixing for 15 minutes and monitored via UV-Vis at 595 nm. Calibration curves were produced for each enzyme studied between the ranges 0.8 μg/mL and 80 μg/mL.

Silica Quantitation: Silica was quantified following the β- Silicomolybdate method described by Iler.[43] Individual samples were dissolved in 0.5 M NaOH and incubated at 95 °C for 30 minutes. Following incubation, the liberated dendrimers were removed from solution by Centricon filtration (American Centricon filtration devices, Millipore Inc.), as they interfered with the molybdate assay. Samples with templates of molecular weights greater than 3000 were quantitated. Molybdate reagent was added (1:4 silicic acid/molybdate) to the filtered solutions to initiate the formation of the bright yellow

product monitored by UV-Vis spectrophotometry at 410nm and quantitated from a standard curve of silicate standards.

Scanning Electron Microscopy: Silica samples were suspended in ethanol and pipetted onto the surface of an aluminum SEM sample stage (Ted Pella Inc.) to dry. Each sample was sputter-coated with a thin layer of gold by use of a Pelco Model 3 Sputter Coater (Ted Pella Inc.). Once sputtered, samples were imaged on a Hitachi S4200 scanning electron microscope operated at variable voltage.

Results and Discussion

Biogenic Silica Morphology: Biogenic silica is utilized to create a myriad of intriguing shapes and morphologies, although *in vitro* silica produced from synthetic silaffins is spherical. The nascent silica spheres aggregate together to form larger particles with a size distribution of 500-700 nm **(Figure 60)**.[24,27] These nanospheres of amorphous silica are the building blocks of the cell wall frustule which will be templated for the final intricate design.

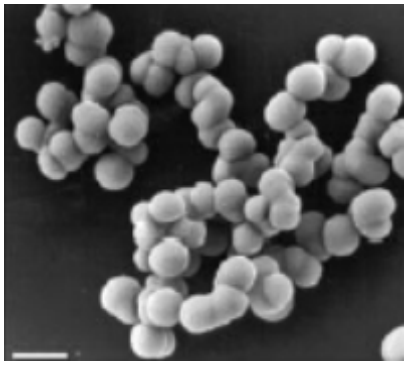

Figure 60. Biogenic silica produced *in vitro*. Bar (lower left) = 1 μm[27]

The spherical morphology of biomimetic silica produced *in vitro* can be dramatically altered by the addition of external forces to the reaction mixture, such as changing the anionic species in solution. For example, extended arched, interconnected, pearl-like silica structures of ornate morphology have been generated by bubbling nitrogen through the reaction mixture. Further changes were observed when shear stress was added to the reaction vessel, resulting in the formation of lengthy ropelike structures **(Figure 61)**.[64] Charging the reaction with hydroxylated glycerol induced the formation of networks of aggregated silica particles, while addition of electrostatic and hydrodynamic variants created plate and dendritic like siliceous structures.[65] These physical changes likely perturb the reaction at the templating level of silica formation.

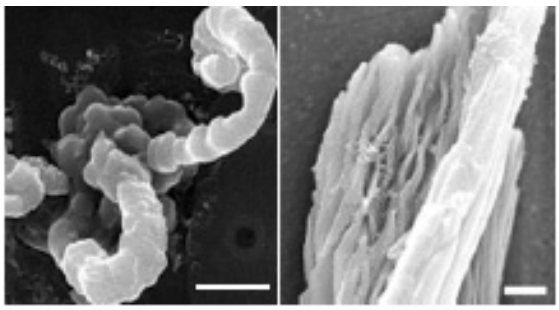

Figure 61. Modified silica morphologies. (Right) Silica produced following constant nitrogen bubbling. (Left) Silica produced as a function of shear stress being applied during the reaction. Bar = 1 μm.[64]

Changes to silica morphology have also been observed from the addition of various anionic species to the reaction. Previous work has shown the relationship between polyanions and silica production.[25,31,66] Silica deposition along these anionic molecular scaffolds is key for the formation of novel multi-dimensional silica structures.

With the addition of short chain DNA, formation of strings of silica nanospheres were reported, most likely templated along the phosphate backbone. Surfactant addition also changed the silica morphology such that the formation of sponge-like siliceous structures were obtained.[66]

Previously, the use of amine terminated dendrimers to catalyze the condensation and precipitation of silica nanoparticles from monosilicic acid has been reported.[41,42,67] Synthesis of novel silica composites that incorporate CdSe/ZnS and Au^0 nanoparticles into the framework of dendrimers has also been reported.[42] This approach has been extended to encapsulate PAMAM dendrimers and biomolecules within silica nanospheres. At physiological pH, interactions between the enzyme surface and cationic surface of the PAMAM dendrimers are hypothesized to play an important role in forming a supramolecular complex between the enzyme and dendrimer (**Figure 62**). To examine

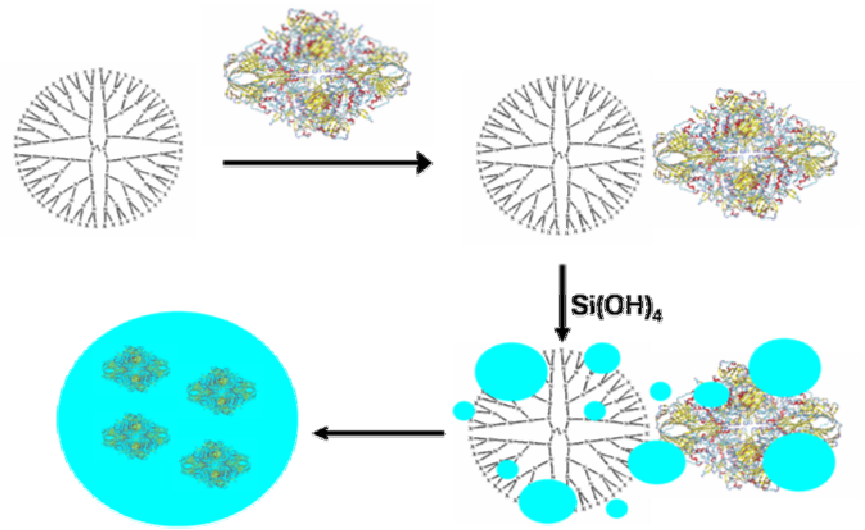

Figure 62. Proposed scheme for enzyme encapsulation within silica nanoparticles. The complimentary electrostatics associated with the cationic dendritic amines are likely to associate with the acidic residues along the enzyme surface. This effect is more influential in an unbuffered media.

the effects of electrostatics between the protonated dendrimer (pKA ~ 9.5) and the surface of enzymes with different pI values as a potential methodology for achieving maximum loading efficiency, encapsulation of horseradish peroxidase (HRP; pI ~ 8.9), glucose oxidase (GO; pI ~ 4.2), and ß-galactosidase (ß-gal; pI 4-6) was examined in both 0.1M phosphate buffer and water (both at pH 7).

A solution of HRP 0.1M phosphate at pH 7 was charged with enough PAMAM dendrimer to achieve a 20 mM primary amine concentration. To this mixture, 1 M hydrolyzed TMOS was added to be condensed into silica. Following the rapid precipitation of silica from the reaction mixture, the supernatants and washes were tested for enzyme activity and protein content. Analysis of the supernatants and washes gave significant enzyme activity, suggesting inefficient encapsulation of HRP **(Table 7)**. Enzyme presence in the supernatant and washes was confirmed using the Bradford assay, and was consistent with ~ 30% encapsulation. A subsequent wash with 200 mM KCl failed to yield additional activity suggesting that the enzyme was not weakly adsorbed to the surface of the silica nanoparticles. Using the ß-silicomolybdate assay,[43] the amount of silica produced in each reaction averaged 0.42 mg (± 0.06), and was consistent with previously published yields.[41]

Table 7. Percentages of active enzyme within silica nanoparticles

Enzyme	0.1M Phosphate Buffer (pH 7)			Water (pH 7)		
	0.5 mg/mL	1 mg/mL	2 mg/mL	0.5 mg/mL	1 mg/mL	2 mg/mL
HRP	32.38±12.63	21.84 ± 1.74	26.35 ± 8.34	39.04±12.24	13.02 ±6.80	27.22±13.86
GO	7.57 ± 5.67	4.32 ± 2.84	5.50 ± 1.85	47.27 ± 8.46	52.76 ± 7.92	53.90 ± 5.31

The same experiment was repeated in water (pH 7). Testing revealed a similar encapsulation efficiency for HRP. A corresponding enzyme activity and concentration were found in the supernatant and washes. These results suggested that there is little electrostatic interactions between the dendrimer and HRP, undoubtedly a result of the predominately positive surface of HRP repelling the postively charged dendritic amines at pH 7. Under both conditions, the enzyme was likely trapped nonspecifically in the aggregating silica matrix as the particles precipitated from solution. The loading efficiency is similar to previous reports of R5 encapsulation (20%)[2] in phosphate buffer. Furthermore, the encapsulated enzymes showed no loss of enzyme content through diffusion into the storage solution over several days. This is analogous to the previously reported stability for butylcholinesterase encapsulated in silica by the R5 peptide.[2]

Glucose oxidase (GO) was subjected to the same encapsulation procedures as described above for HRP. With GO's more acidic pI, an increase in encapsulation was hypothesized given the reciprocating charge on the surface of the cationic dendrimer. Initial encapsulation in 0.1M phosphate buffer gave a small percentage of active enzyme encased in the silica particles **(Table 7)**. The remaining enzyme activity was accounted for in the supernatants and the first two of three water washes. Despite having a complementary charge to the cationic dendrimer, GO in a buffered environment exhibited lower encapsulation efficiencies. This may be due to the higher ionic strength buffer masking the negative surface of GO from the cationic dendritic surface.

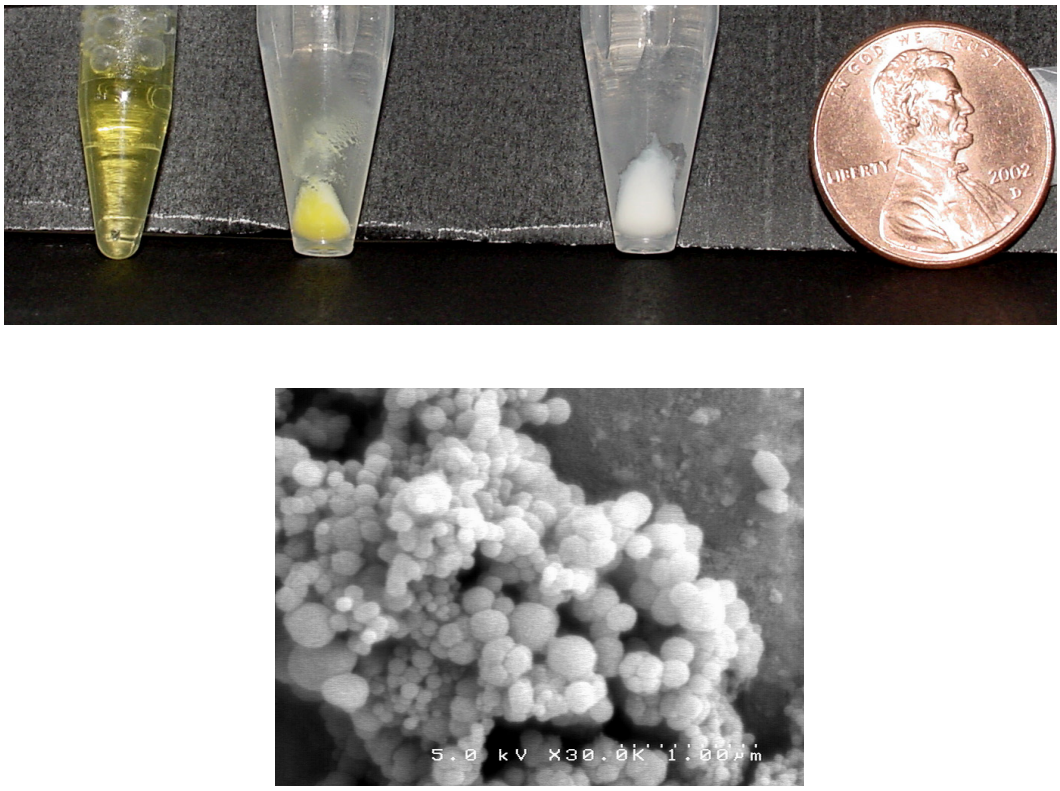

Figure 63**.** (Top) Visual confirmation of GO encapsulation. (Left) 6 mg/mL GO solution used in silica synthesis. (Center) Silica prepared and washed in water showing encapsulated GO. (Right) Silica prepared in the presence of GO and 0.1M phosphate buffer. (Bottom) SEM image of silica particles formed in water and containing GO.

When GO was encapsulated in water (pH 7), the silica particles **(Figure 63)** were found to incorporate quantitative amounts of enzyme. Of note, both the enzyme activity assays and Bradford assay failed to detect any GO in the supernatant of the condensation reaction or subsequent washes. Activity of encapsulated enzyme via direct testing of the nanoparticles led to an observed retained activity of 53.90% ($\pm$ 5.31) **(Figure 64)** with the 2 mg/mL stock and a maximum loading by mass (wt / wt%) with the 6 mg/mL stock **(Figure 65)**. The 6 mg/mL stock resulted in 446.48 ug ($\pm$ 53.50) of active enzyme in the average 426 ug of silica nanoparticles, thus giving

quantitative loading (wt/wt). The decline of the enzyme's specific activity by 50% during the encapsulation process could be explained by unfavorable orientations of the enzymatic active sites within the growing silica nanoparticle.

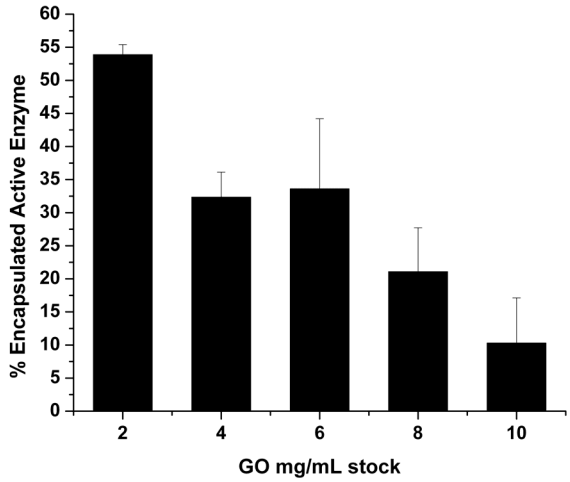

Figure 64. Encapsulation efficiency of GO as a function of initial GO concentration. 200 µL of the buffer free enzyme stock was charged with PAMAM dendrimer followed my hydrolyzed TMOS. The resulting silica contained ~ 50% of the initial enzyme activity until a stock solution of greater than 2mg/mL was used.

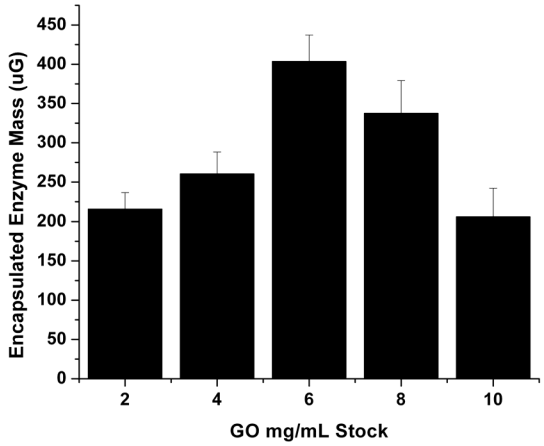

Figure 65. Loading capacity by mass of GO in silica particles as a function of initial GO concentrations. Measurements were obtained from the specific activity assay for GO. Using a 6mg/mL stock solution of GO resulted in the maximum mass of active enzyme

ß-galactosidase underwent encapsulation in the same fashion as HRP and GO. The Bio-Rad assay for protein content and specific activity assays failed to detect any enzyme in the supernatent produced from the encapsulation process. Unfortunately, no enzymatic activity was detected within the silica nanoparticles following collection and washing. In order to investigate the fate of the ß-galactosidase, stock solutions of the enzyme were charged with relevant concentrations of the PAMAM G4 dendrimer and tested for activity as a function of time. It was determined that the G4 dendrimer was a significant inhibitor to ß-galactosidase activity. Dilution studies indicated that the G4 dendrimer was able to inhibit activity at a concentration of 35 μM. There are 64 amine functional groups on each molecule of the G4 dendrimer demonstrating that the PAMAM G4 dendrimer inhibits ß-galactosidase activity at 2.7 mM amine, 10 fold less than the 20mM required to achieve maximum silica production.

This phenomenon was further investigated by a larger array of PAMAM dendrimers. Generations 1-6 of PAMAM dendrimers were tested as ß-galactosidase activity inhibitors at a 35 μM concentration of the dendrimer molecule **(Figure 66)**. Generations 1 and 2 were found to be less effective as inhibitors than the larger dendritic molecules. This could be the result of the PAMAM dendrimers affinity to the enzyme surface near the active site. This would result in occlusion prior to encapsulation and also promote silica precipitation over the active site. Another possible scenario could be the disruption of required subunit interactions, resulting in encapsulation of inactive subunits. This could explain the lack of protein content in the supernatant following encapsulation, while rendering inactive silica nanoparticles.

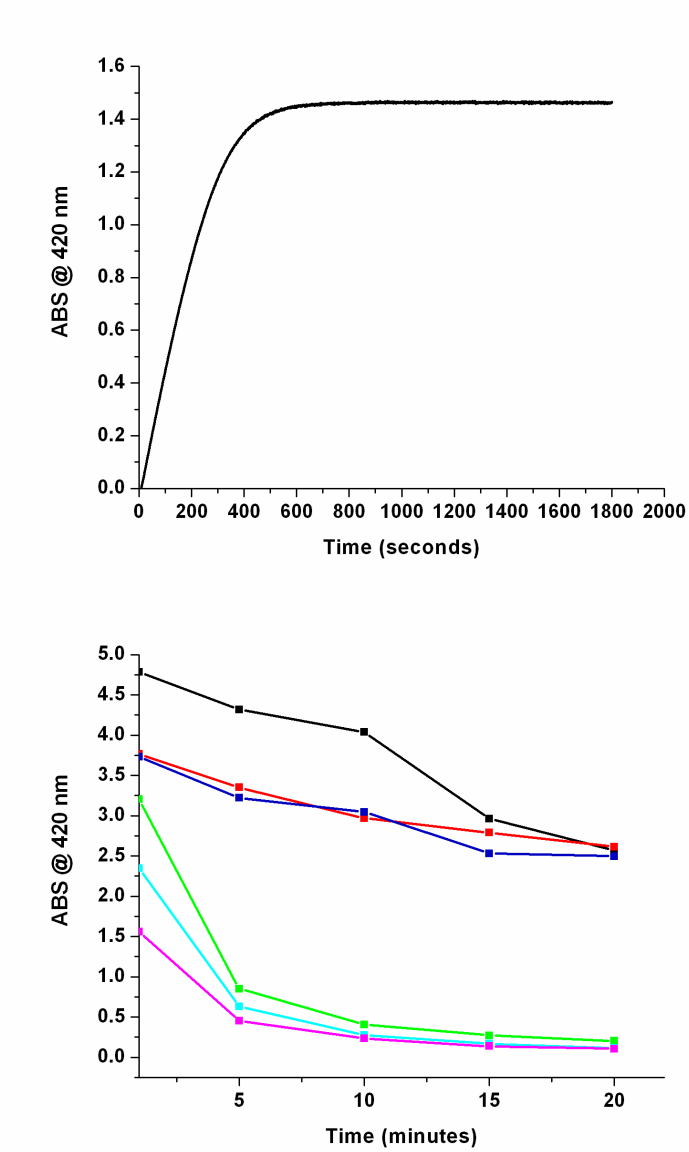

Figure 66. (Top) Initial ß-galactosidase activity. (Bottom) Activity following exposure to 0.035 mM PAMAM dendrimer G1(black), G2(red), G3(blue), G4 (green), G5 (light blue), and G6 (purple).

Enzyme Kinetics of Encapsulated HRP and GO: While specific activity measurements suggest the amount of folded and functioning enzyme, questions pertaining to substrate and product dynamics and the newly created locally high enzyme concentrations require a broader examination of enzyme function. Comparisons between the kinetic parameters

of the free enzyme and enzyme encapsulated in silica nanoparticles revealed that the encapsulated enzyme experiences a slight shift in the K_m values to a lower concentration **(Figure 67)**. GO's K_m was decreased by one fold (13.51mM for free GO and 6.25mM for encapsulated GO) following encapsulation, while encapsulated HRP's K_m was found

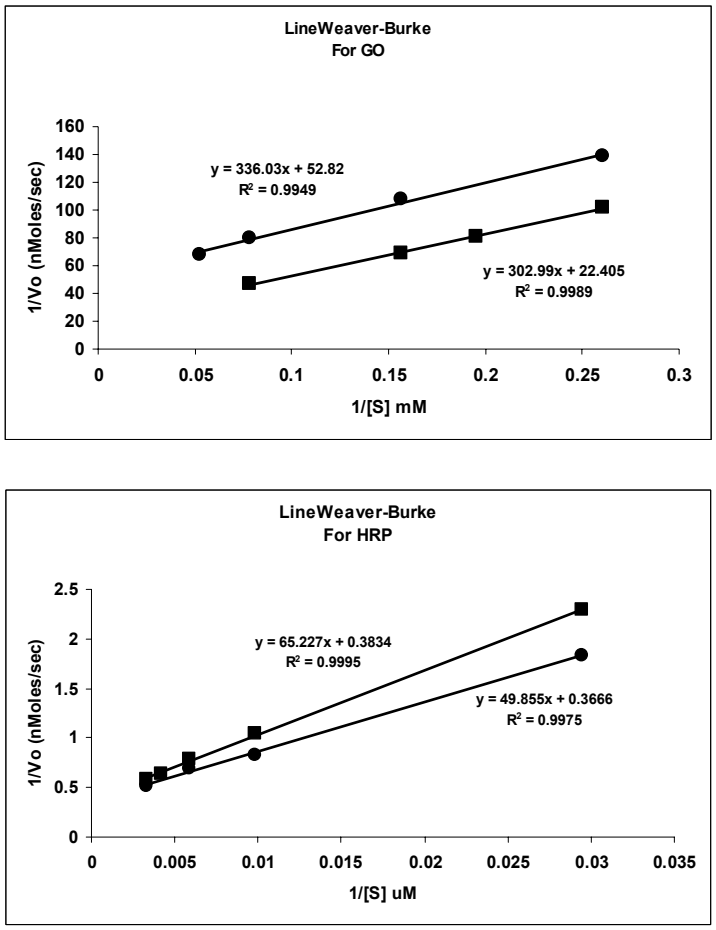

Figure 67. (Top) Kinetic plots for GO. (■) Free Glucose Oxidase (●) Encapsulated Glucose Oxidase (Bottom) Kinetic plots for HRP (■) Free Horseradish Peroxidase (●) Encapsulated Horseradish Peroxidase

to shift by less than one fold (0.170mM for free HRP and 0.130mM for encapsulated HRP). Previous reports for sol-gel encased HRP report a 6-fold increase in K_m (0.163mM for free HRP and 0.985mM for encapsulated HRP),[12] while HRP based electrodes have even shown significantly higher K_m values.[14,68,69] This suggests the silica nanoparticle is not significantly hindering the enzyme's access to substrate or release of product by creating a diffusion barrier. In theory, lower K_m values could result from affinity of the silica nanoparticles to the different substrates, or alternatively, enzymes restricted in their movement within the bulk solution may be reaching V_{max} sooner due to competition of several constrained enzymes in close proximity within the silica nanoparticle. This constraint would create a locally high concentration of enzyme within the nanoparticles and may no longer maintain sufficient substrate concentrations to satisfy steady state Michaelis-Menten analysis. Additionally, enzyme kinetics may also be affected by a basic silica surface[70,71] perturbing the enzymes' local environments. This may be especially true for GO where it is known to be optimally active at ~ pH 6.[72,73] Assuming Michaelis-Menten steady state kinetics, the active enzyme components within the composite are functioning kinetically similar to the free enzyme. Consequently, the loss of 50% of the absolute GO activity is most likely due to occlusion of the active site by silica during the encapsulation process.

Silica Nanoparticle Size: Previously, dendrimer mediated silica nanospheres were scrutinized by scanning electron microscopy.[67] PPI dendrimers G1 and G2 produced spherical silica particle sizes ranging from 170-180 nm, and G3-G5 produced particles with diameters from 220-260 nm. Silica formed by PAMAM G0 and G1 dendrimers yielded a bimodal population with smaller particle diameters averaging 95 and 130 nm

and larger diameter particles of 350 and 400 nm, respectively. In contrast to the smaller dendrimers, PAMAM dendrimers G2-G6 show average silica particles ranging from 275 to 390 nm. Comparing PPI and PAMAM dendrimers with the same number of amines (i.e. PPI GX vs. PAMAM G(X-1)) shows that the ratio of the template diameter correlates with the ratio of silica nanosphere diameters, suggesting that the silica encapsulated dendrimer is the aggregating unit of silica growth. These silica nanosphere sizes were consistent with those produced from native silaffins,[24] the R5 peptide as reported by Naik *et al*.[64] and a series of R5 truncates reported by Knecht *et al*.[28] While the simpler dendrimer system produces silica nanoparticles at a rate comparable to the R5 peptide, the observed particle size distributions data suggests that monodispersity of nanoparticles represents a challenge in this approach.

Ion Effect on Nanoparticle Size: One of the largest hurdles facing the biomimetic synthesis of materials is acquiring the desired degree of dimensional and spatial control. Given that a particle's size plays a vital role in reactivity, methods resulting in a more monodispersed product need to be developed. Typical reaction conditions for biomimetic silica synthesis provide for continual growth and ripening, resulting in the formation of larger nanospheres with diameters on the order of 200 – 600 nm.[24,25] Studies of biogenic silica formation with polyamine templates implicated phosphate ions associated with the buffer system as crucial players for *in vitro* growth of silica nanospheres.[31,66] Thus it is difficult to differentiate the nanosphere formation mechanism from the template assembly, due to the phosphate-dependent self-assembly process. Indeed, by using a monomolecular dendrimer template Knecht *et al.* were able to separate these steps and

show evidence that the cation choice and concentration can be a critical factors in nanoparticle size.[67]

Their work highlighting the use of PAMAM and PPI dendrimers as monomolecular templates allowed for the expansion of the biomimetic silica production reaction conditions, yielding a more robust synthesis allowing for size selective precipitation of silica nanospheres. Utilizing defined concentrations of phosphate buffer or main group metal chloride salts, it was shown that the dendrimer mediated biomimetic silica growth process was governed by cationic neutralization of the anionic silica nanosphere surface. Establishing a charge double-layer around the nanoparticle results in neutralization, thus minimizing electrostatic repulsions and favoring agglomeration and continued ripening of nanospheres to the order of 250 – 300 nm in diameter. By modulating the concentrations of cations, one can judiciously precipitate silica nanospheres of desired dimensions between 30 and 300 nm without negatively affecting the template's activity or the overall reaction yield.

One of the goals of biomimetics is to simplify complicated biologically pathways and processes in order to increase robustness and feasibility. To further investigate the role of the buffer ions and any dependence on sodium phosphate in particular, Knecht *et al.* obtained silica particles from a G4 PAMAM dendrimer template where phosphate was replaced with individual salt solutions (0.255 mM to 400 mM, pH 7.5).[67] Particle size followed a linear increase in diameter as salt concentrations increased up to 100 mM. Silica also precipitated from LiCl, NaCl and KCl. All gave nanospheres with a maximum size of approximately 235 nm at concentrations higher than 100 mM. RbCl and CsCl produced particles of smaller diameter, 210 nm and 195 nm respectively **(Figure 68)**.

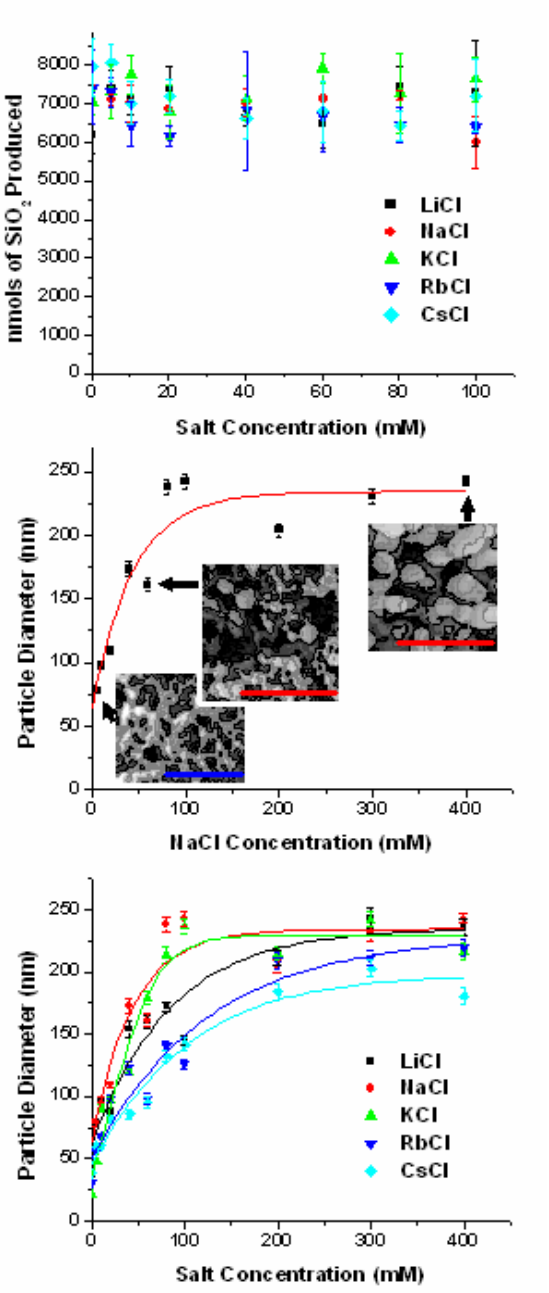

Figure 68. G4 PAMAM dendrimer mediated silica as a function of main group metal chloride salt concentrations. (a) Normal silica production at 20 mM primary amine. (b) Typical size distributions and micrographs of nanospheres generated by the G4 PAMAM dendrimer at various sodium chloride concentrations (scale bars: blue – 500 nm, red = 1000 nm). (c) Typical size distributions for silica nanospheres generated from PAMAM dendrimers. Error bars illustrate the error associated with the sample size investigated for particle size distributions.[67]

The difference in nanosphere sizes may be attributed to the atomic radii of each cation studied. The smaller cations having radii between 90 pm and 152 pm,[74,75] preferentially bind a single silanol group at the surface of the ripening clusters, resulting in a stronger affinity to the growing silica structures and effective charge neutralization of the particle. The cations greater than 166 pm[74,75] are more likely to bridge between several silanol groups, resulting in inefficient surface charge neutralization and more rapid flocculation, the consequence being diminished particle sizes. This study suggests an important difference between biologically derived templates and a unimolecular template. Silaffin based templates require both polyvalent anions, particularly phosphate, for self assembly of an active template and cations for nanoparticle solubilization, but a unimolecular template does not require self-assembly. Unimolecular templates require only cations for nanoparticle stabilization. The ability of a cation to promote the solubility of the nascent silica surface for an extended time gives rise to larger particles and in many cases bimodal distribution through the agglomeration of smaller particles. In contrast to Sumper's work discussed in the introduction to this chapter, this body of work concludes that the size of the isolated silica nanoparticles is determined by the period of ripening prior to precipitation from solution. Consequently, a potential advantage of the use of polymeric biomimetics is improved robustness of the system.

Physical characterization of the HRP and GO active silica nanoparticles was performed via SEM. The HRP particles gave an average particle size of 162 $\pm$ 92 nm when aggregated from water. For comparison, low ionic strength water control particles displayed an average of 39 $\pm$ 14nm which is consistent with previously published values.[41] Particles containing HRP produced in 0.1M phosphate buffer revealed a

bimodal distribution, as a result of particle necking, with average sizes centered at 232 ± 97 nm and 721 ± 113 nm size compared to the 244 ± 106 nm and 745 ± 102 nm averages of control silica produced in phosphate buffer. Similar patterns were observed for

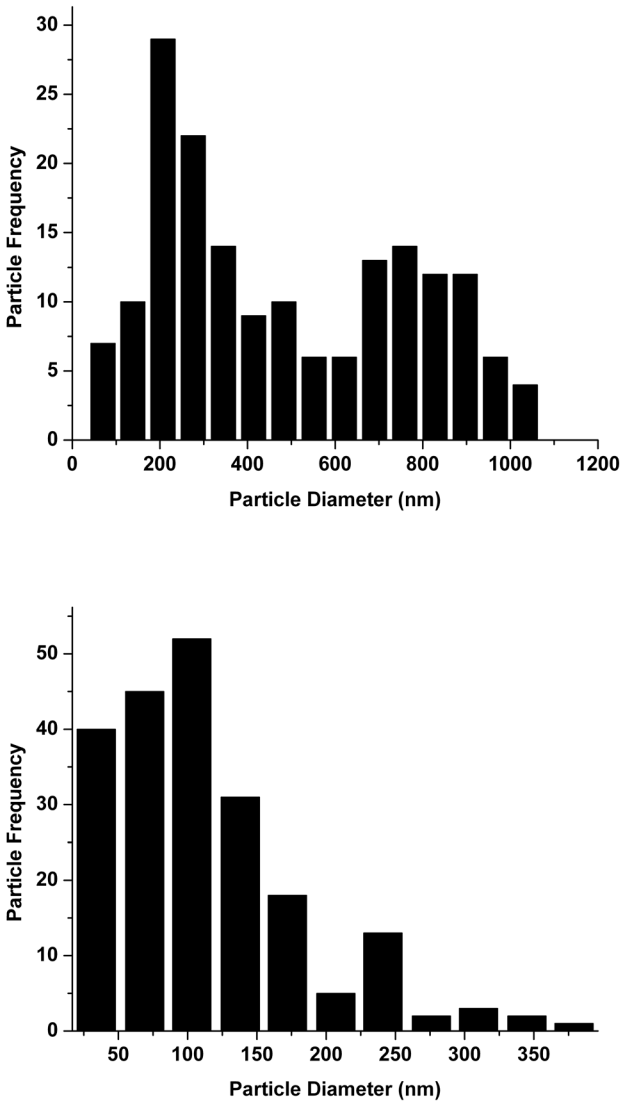

Figure 69. (Top) Size distribution of GO containing silica nanoparticles generated in 0.1M phosphate buffer. Ripening and necking of growing particles allows for a bimodal distribution. (Bottom) Size distribution of GO containing silica particles formed in water. Absence of cations results in early particle precipitation due to inefficient surface charge masking the growing nanoparticle.

average particle sizes and distribution in the case of silica particles containing GO. GO in unbuffered water gave rise to silica particles with an average size of 113 $\pm$ 60 nm. Particles produced in 0.1M phosphate buffer resulted in average particle sizes of 269 $\pm$ 113 nm and 784 $\pm$ 130 nm for the two modes **(Figure 69)**.

The particle sizes suggest that both GO and HRP were able to self-buffer the growing nanoparticles when encapsulated in a water environment. In the case of GO, the electrostatics in the hybrid supramolecular system result in having the positively charged dendrimer in close proximity to the enzyme's surface (due to the overall acidic pI leading to an overall negative charge) while the cationic sidechains substitute for the missing cations in the aqueous environment.

The shelf life of some enzymes has been shown to increase upon silica encapsulation relative to storage in solution.[2] The long term stability of the encapsulated GO was examined. The GO composite, stored under a variety of conditions (citrate, succinate, PBS, sodium chloride, and phosphate buffers at pH 6) for 30 days, demonstrated no loss of activity **(Figure 70)**. One reason may be the inability of microorganisms commonly found in aqueous mixtures to penetrate the porous silica cage around the enzymes.[2]

One of the potentials of biologically active, stable silica materials is their use in organic chemistry. The physical characteristics and shelf life described above would be desirable properties in a biologically active reagent. Enzymes as organic reagents would be particularly useful because of their efficiency and specificity. Another drawback to enzyme use has been enzyme regeneration following use. Enzyme immobilized within

silica nanoparticles offers a solution to this problem through the use of standard filtration or centrifugation.

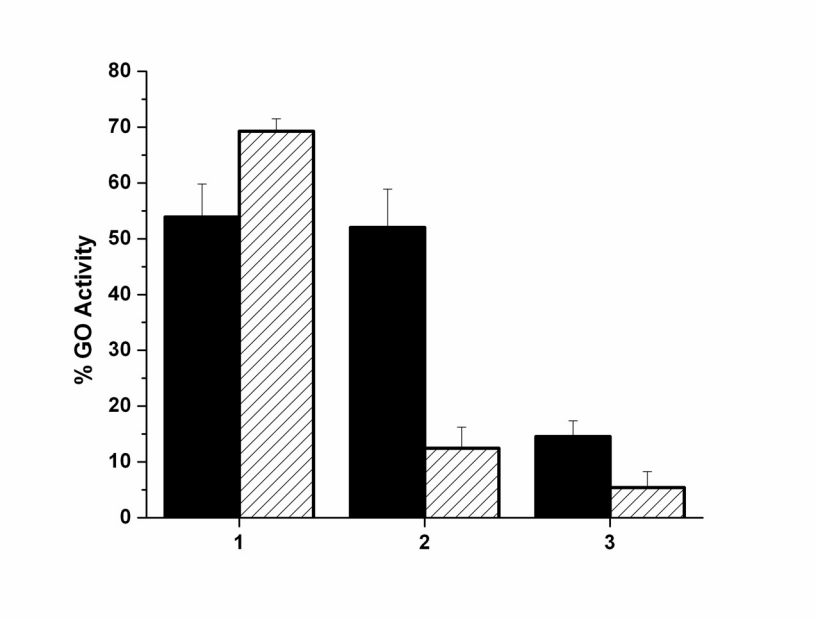

Figure 70. Stability of encapsulation. (1) GO encapsulated in water and stored in phosphate buffer (solid: day 1, slash: day 30). (2) Encapsulated in water and stored in water. (3) Encapsulated in phosphate buffer and stored in phosphate buffer. No leeching of enzyme was detected in the storage media and the silica was found to retain the activity of the encapsulated GO for at least 30 days.

Chemical transformation of nitriles into carboxylic acids is of significance due to the relative ease of organic nitrile production. Organonitriles can be produced by the addition of cyanide to alkyl halides,[76] the Strecker reaction,[77] reaction of aryl halides with copper cyanide,[78] and the dehydration of amides.[79] Unfortunately, the hydrolysis of nitriles typically involves harsh conditions, such as strong base and high temperatures, or laborious and expensive catalysis.[80-83] Due to the desire to utilize organonitriles, the use of whole cells containing nitrilase enzymes to produce hydrolyzed organonitriles has become well established.[84-86]

In order to produce a simpler, biomimetic approach, we chose to encapsulate isolated and purified nitrilase was encapsulated using the methods established and studied above, using 200 µL of a 2 mg/mL stock solution of nitrilase. The goal of the experiment was to evaluate a synthetically desirable enzyme encapsulated in silica nanoparticles as a potential reagent. The conversion of 3-cyanopyridine was chosen as an initial substrate because the hydrolyzed product (nicotinic acid; vitamin B_5) is of biologically and commercial interest. The specific activity test used in this study for nitrilase detects the production of the ammonia byproduct, and the presence of nicotinic acid was confirmed via NMR **(Figure 71).** The nitrilase purchased from Biocatalytics has a theoretical pI of 5-7. This should promote some level of dendrimer interaction with the enzyme moiety. It was determined that nitrilase performed poorly in unbuffered water, unlike GO, but was found to achieve sufficient activity with 25mM phosphate buffer pH 7.5 – 7.8. The requirement of ions is likely due to the activity of nitrilase being linked to subunit association.[87]

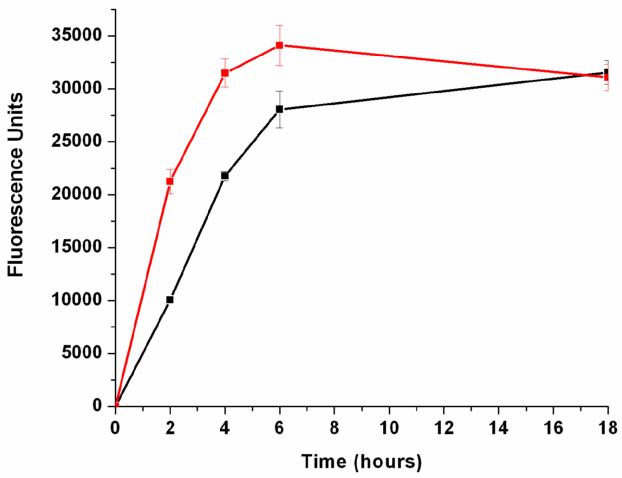

Figure 71. Conversion of 3-cyanopyridine to nicotinic acid by nitrilase containing silica nanoparticles as a function of time. Red = stock nitrilase solution of 2 mg/mL and black is silica containing nitrilase.

Following nitrilase encapsulation, silica nanoparticles analogous with GO and HRP containing particles discussed above were collected. The protein mass was assessed in the supernatant and found to be ~ 20% of the initial enzyme mass. However, the supernatant failed to display significant activity with the 3-cyanopyridine substrate. Further investigation revealed a small inhibitory effect attributed to continued exposure of nitrilase to the PAMAM dendrimer, similar to the ß-galactosidase discussion above, but far less potent than in the case of ß-galactosidase. Again, this is most likely to interference with the aggregation of nitrilase subunits necessary for activity. Unlike the ß-galactosidase, however, significant activity was retained within the silica nanoparticles in the case of nitrilase**.** The conversion from nitrile to carboxylic acid and ammonia is near completion at six hours for the 50 mM substrate concentration. Additionally, this activity did not diminish over a four day period.

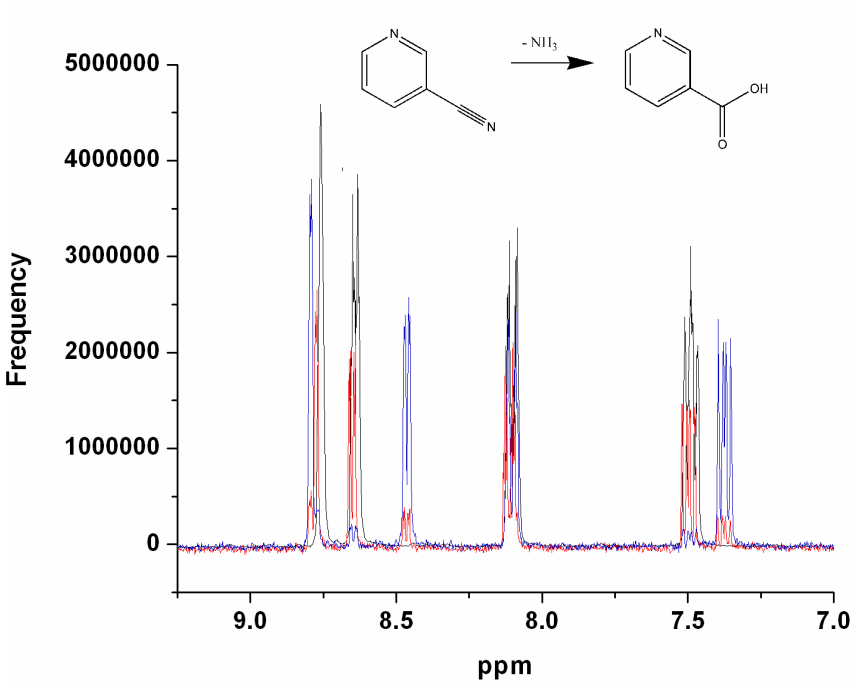

Figure 72. NMR spectra following the conversion of 3-cyanopyridine to nicotinic acid. Time points are overlayed where black is initial, red is 3 hours, and blue is 36 hours.

Physical characterization of freshly prepared silica nanoparticles with enzymatic activity may not be ideal conditions to gauge more likely uses in everyday organic synthesis. For example, despite a six hour reaction time, many practical uses of nitrilase containing silica would involve leaving the reaction running overnight. The activity assay data shows an 18 hour time point, and the NMR data shows a 36 hour spectrum **(Figure 72)**. Furthermore, the 36 hour NMR spectrum does not contain signal from nitrilase, suggesting that the nitrilase is not leeching out over the course of the reaction.

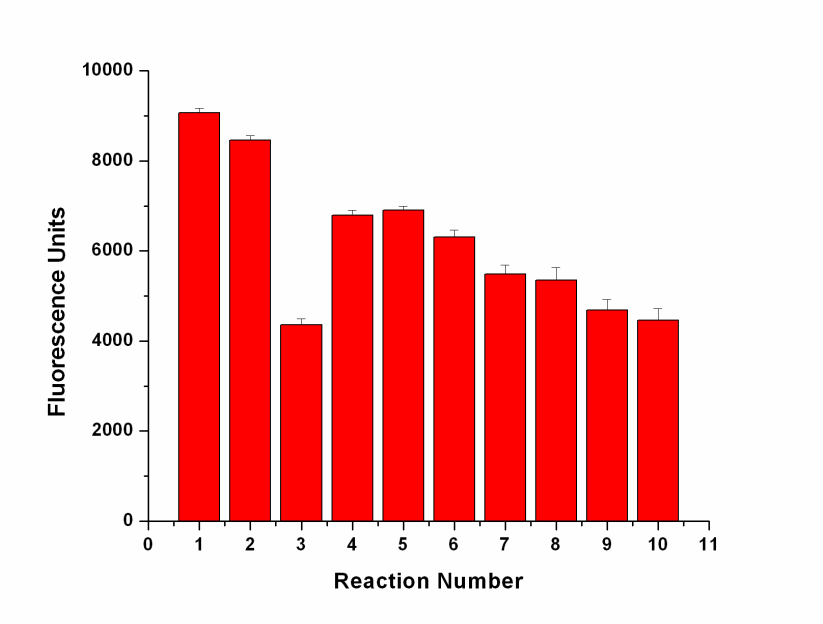

Figure 73. Consecutive experiments performed on a single triplicate batch of silica. 50 mM 3-cyanopyridine was added and time points taken at 6 hours. Silica was washed 3 times between experiments and stored at room temperature over 8 consecutive nights. Activity was below 50% of first run by run ten.

The recycling and reuse of the nitrilase containing silica particles is a critical improvement over traditional use of enzymes in solution. Recycling was performed by either filtration or centrifugation of the reaction mixture followed by washing the active silica particles **(Figure 73)**. The silica was given 10 consecutive 50 mM substrate

solutions, over an eight day period, and displayed consistent loss likely associated with silica loss due to washing between trials. The loss of activity on trial 3 was contributed to oxidizing thiols in the test solution. Test solutions were prepared fresh thereafter. Further testing is underway to determine a maximum number of uses of individual particle preparations, but the ten consecutive uses already demonstrated compensate for any enzymatic activity lost during the encapsulation process.

Conclusions

The entrapment of HRP, quantitative encapsulation of GO, and significant nitrilase activity inside silica nanoparticles by utilizing an amine terminated dendritic template was performed. Improvements over harsh traditional sol-gel chemistry allow a wide array of proteins and other sensitive molecules to be explored as potential targets for encapsulation. Newer sol-gel techniques offer an improved array of potential biomolecules, but are slow and cumbersome compared to the reported method. This improved strategy utilizes a water soluble biomimetic template, PAMAM dendrimer, to catalyze the condensation of $Si(OH)_4$ while trapping an enzyme within the mesoporous framework. This technique is rapid, achieving the final isolated product in a few minutes. Furthermore, the role of pI and ionic strength within the encapsulation environment has a strong influence on encapsulation efficiencies. When placed in a low ionic strength environment, GO's acidic pI has the complementary charge to the amine terminated dendrimer, encouraging formation of a supramolecular complex capable of condensing silica. This resulted in a quantitative amount of GO being trapped inside the silica nanoparticles. However, encapsulations performed in a high ionic strength or with

peroxidase's non-complimentary pI gave significantly lower encapsulation efficiencies. These results suggest that the electrostatic manipulation of a rapid and strong supramolecular silica precipitating complex has the potential of adding a vast array of chemical and biological activity to hybrid composite materials.

Further manipulation of electrostatics should lead to multi-layered complexes offering even more diverse materials. Another avenue to be explored is the surface functionalization of the biologically active nanocomposite materials. These new biologically active composite materials have the potential of finding applications in fields as diverse as microbiology, clinical diagnostics, electronic devices, and organic synthesis. Microbiologists can begin to develop 'smart' assays capable of reproducing entire biological systems via the incorporation of heterogenous composite materials consisting of many different enzymes and detection probes. With the incorporation of fluorescent probes and proteins, clinically relavent diagnostics capable of rapid and early detection of infectious agents are now within reach. Merging the fields of materials, semi-conductors (such as the CdSe quantum dots[42]), and biochemistry opens the door to researching sophisticated electronic sensors and circutry. Organic chemists interested in utilizing enzyme specificty and catalysis as reagents for delicate synthetic routes will find easy to filter and long lasting 'biosand' a valuable tool. Combining all these disciplines affords the potential of a single silica wafer capable of simulating a cellular or disease pathway while simultaneously providing a fluorescent detection or tagging mechanism can open new doors in biology and disease detection and prevention.

REFERENCES

(1) Avnir, D., Braun, S., Lev, O. & Ottolenghi, M. *Chem. Mater.* **1994**, *6*, 1605.

(2) Luckarift, H. R., Spain, Jim C, Naik, Rajesh R & Morley O Stone *Nat. Biotech.* **2004**, *22*, 211.

(3) Dave, B. C., Miller, J.M. & Dunn, B., Valentine, J.S. & Zink, J.I. *J. Sol-Gel Sci. Technol.* **1997**, *8*, 629.

(4) Gill, I., Ballesteros, A. *J. Am. Chem. Soc.* **1998**, *120*, 8587.

(5) Mann, S. J. *J. Mater. Chem.* **1995**, *5*, 935.

(6) Oliver, S., Kuperman, A., Coombs, N., Lough, A. & Ozin, G. *Nature* **1995**, *378*, 47.

(7) Monnier, A. et al. *Science* **1993**, *261*, 1299.

(8) Zhao, D. Y. et a.l *Science* **1998**, *279*, 548.

(9) Kresge, C. T., Lenowicz, M.E., Roth, W.J., Vartuli, J.C. & Beck, J.S. *Nature* **1992**, *359*, 710.

(10) Ying, J. Y., Mehnert, C.P. & Wong, M.S. *Angew. Chem. Int. Ed.* **1999**, *38*, 56.

(11) Yu, A.,Wang, Y.,Barlow, E.,Caruso, F. *Adv. Mater.* **2005**, *17*, 1737.

(12) Bhatia, R. B., Brinker, Jeffrey C., Gupta, Alok K., and Singh, Anup K. *Chem. Mater.* **2000**, *12*, 2434.

(13) Li, Y.,Yip, W. T. *J. Am. Chem. Soc.* **2005**, *127*, 12756.

(14) Liu, Y.,Shi, L.,Wang, M.,Li, Z.,Liu, H.,Li, J. *Green Chem.* **2005**, *7*, 655.

(15) Vrieling, E. G., Beelen, T.P.M., van Santen, R.A. & Gieskes, W.W.C. *J. Biotechnol.* **1999**, *70*, 39.

(16) Morse, D. E. *Trends in Biotechology* **1999**, *17*, 230.

(17) Simpson, T. L. V., B.E. *Silicon and Siliceous Structures in Biological Systems*; Springer: New York, 1981.

(18) Kröger, N., Lehmann, G., Rachel, R. & Sumper, M. *Eur. J. Biochem.* **1997**, *250*, 99.

(19) Kroger, N., Deutzmann, R. & Sumper, M. *Science* **1999**, *286*, 1129.

(20) Knecht, M. R. W., D.W. *Chem. Comm.* **2003**, *24*, 3038.

(21) Delak, K. M. S., N. *Chem. Mater.* **2005**, *17*, 3221.

(22) Jian-Jun, Y. R.-H., J. *Advanced Materials* **2005**, *17*, 885.

(23) Roth, K. M.,Zhou, Y.,Yang, W.,Morse, D. E. *J. Am. Chem. Soc.* **2005**, *127*, 325.

(24) Kröger, N.,Deutzmann, R.,Sumper, M. *Science* **1999**, *286*, 1129.

(25) Kröger, N.,Lorenz, S.,Brunner, E.,Sumper, M. *Science* **2002**, *298*, 584.

(26) Frigeri, L. G.,Radabaugh, T. R.,Haynes, P. A.,Hildebrand, M. *Mol. Cell. Prot.* **2006**, *5.1*, 182.

(27) Kröger, N.,Deutzmann, R.,Bergsdorf, C.,Sumper, M. *Proc. Nat'l. Acad. Sci.* **2000**, *97*, 14133.

(28) Knecht, M. R.,Wright, D. W. *Chem. Comm.* **2003**, *24*, 3038.

(29) Patwardhan, S. V. M., N.; Clarson, S. J. *J. Inorg. Organomet. Polym.* **2001**, *11*, 193.

(30) Noll, F.,Sumper, M.,Hampp, N. *Nano Lett.* **2002**, *2*, 91.

(31) Brunner, E.,Lutz, K.,Sumper, M. *Phys. Chem. Chem. Phys.* **2004**, *6*, 854.

(32) Patwardhan, S. V.,Clarson, S. J. *Mat. Sci. Eng. C* **2003**, *23*, 495.

(33) Patwardhan, S. V.,Mukherjee, P.,Clarson, S. J. *Silicon Chem.* **2002**, *1*, 47.

(34) Mizutani, T.,HNagase, H.,Fujiwara, N.,Ogoshi, H. *Bull. Chem. Soc. Jpn.* **1998**, *71*, 2017.

(35) Crooks, R. M.,Zhao, M.,Sun, L.,Chechik, V.,Yeung, L. K. *Acc. Chem. Res.* **2001**, *34*, 181.

(36) Gröhn, F.,Bauer, B. J.,Akpalu, Y. A.,Jackson, C. L.,Amis, E. J. *Marcromol.* **2000**, *33*, 6042.

(37) Balogh, L.,Tomalia, D. A. *J. Am. Chem. Soc.* **1998**, *120*, 7355.

(38) Larsen, G.,Lotero, E.,Marquez, M. *J. Phys. Chem. B.* **2000**, *104*, 4840.

(39) Larsen, G.,Lotero, E.,Marquez, M. *J. Mat. Res.* **2000**, *15*, 1842.

(40) Baars, W. P. L. M. M., E.W. *Top. Curr. Chem.* **2000**, *210*, 132.

(41) Knecht, M. R.,Wright, D. W. *Langmuir* **2004**, *20*, 4728

(42) Knecht, M. R.,Wright, D. W. *Chem. Mater.* **2004**, *16*, 4890.

(43) Iler, R. K. *The Chemistry of Silica*; Wiley: New York, 1979.

(44) Zhou, Z. Q.,Xu, H. Y.,Ji, W. J.,Chen, Y. *Cat. Lett.* **2004**, *96*, 221.

(45) Yu, K. M. K.,Thompsett, D.,Tsang, S. C. *Chem. Comm.* **2003**, *13*, 1522.

(46) Luckarift, H. R.,Spain, J. C.,Naik, R. R.,Stone, M. O. *Nat. Biotech.* **2004**, *22*, 211.

(47) Gao, X.,Kerry, K. M.,Tam, K. Y.,Tsang, S. C. *Chem. Comm.* **2003**, *24*, 2998.

(48) Ditchek, B. M. *Isr. J. Tech.* **1988**, *24*, 433.

(49) Yamaguchi, A.,Uejo, F.,Yoda, T.,Uchida, T.,Tanamura, Y.,Yamashita, T.,Teramae, N. *Nat. Mat.* **2004**, *3*, 337.

(50) Corma, A.,Chane-Ching, J. Y.,Airiau, M.,Martinez, C. *J. Catyl.* **2004**, *224*, 441.

(51) Chang, W.,Skandan, G.,Danforth, S. C.,Kear, B. H.,Hahn, H. *Nanostruct. Mat.* **1994**, *4*, 507.

(52) Dierstein, A.,Natter, H.,Meyer, F.,Stephan, H. O.,Kropf, C.,Hempelmann, R. *Scripta Mater.* **2001**, *44*, 2209.

(53) Liz-Marzán, L. M.,Giersig, M.,Mulvaney, P. *Langmuir* **1996**, *12*, 4329.

(54) Ung, T.,Liz-Marzán, L. M.,Mulvaney, P. *Langmuir* **1998**, *14*, 3740.

(55) Li, T.,Moon, J.,Morrone, A. A.,Mecholsky, J. J.,Talham, D. R.,Adair, J. H. *Langmuir* **1999**, *15*, 4328.

(56) Radloff, C.,Halas, N. J. *App. Phys. Letts.* **2001**, *79*, 674.

(57) Mine, E.,Yamada, A.,Kobayashi, Y.,Konno, M.,Liz-Marzán, L. M. *J. Col. Int. Sci.* **2003**, *264*, 385.

(58) Vestel, C. R.,Zhang, Z. J. *Nano Letters* **2003**, *3*, 1739.

(59) Kim, Y.-G.,Oh, S.-K.,Crooks, R. M. *Chem. Mater.* **2004**, *16*, 167.

(60) Garcia, M. E.,Baker, L. A.,Crooks, R. M. *Anal. Chem.* **1999**, *71*, 256.

(61) Frey, A., Meckelein, B., Externest, D. & Schmidt, M.A. *J. Immunol. Methods* **2000**, *233*, 47.

(62) Craven, G.,Steers, E.,Anfinsen, C. *J. Biol. Chem.* **1965**, *240*, 2468.

(63) Banerjee, A.,Sharma, R.,Banerjee, U. C. *Biotechnol. Appl. Biochem.* **2003**, *37*, 289.

(64) Naik, R. R.,Whitlock, P. W.,Rodriguez, F.,Brott, L. L.,Glawe, D. D.,Clarson, S. J.,Stone, M. O. *Chem. Comm.* **2003**, *2*, 238.

(65) Rodriguez, F.,Glawe, D. D.,Naik, R. R.,Hallinan, K. P.,Stone, M. O. *Biomacromol.* **2004**, *5*, 261.

(66) Sumper, M.,Lorenz, S.,Brunner, E. *Angew. Chem. Int. Ed.* **2003**, *42*, 5192.

(67) Knecht, M. R., Sewell, S.L. & Wright, D.W. *Langmuir* **2005**, *21*, 2058.

(68) Qian, J., Liu, Yongcheng, Liu, Haiying, Yu, Tongyin, Deng, Jiaqi *J. Electroanal. Chem.* **1995**, *397*, 157.

(69) Li, J., Tan Ngin, Swee, Ge, Hailin *Anal. Chim. Acta* **1996**, *335*, 137.

(70) Shaw, A. M., Hannon, Theresa E., Li, Fuping, & Zare, Richard N. *J. Phys. Chem. B* **2003**, *107*, 7070.

(71) Ong, S., Zhao, Xiaolin, & Eisenthal, Kenneth B. *Chem. Phys. Lett.* **1992**, *191*, 327.

(72) Bright, H. J.,Appleby, M. *J. Biol. Chem.* **1969**, *244*, 3625.

(73) Weibel, M. K.,Bright, H. J. *J. Biol. Chem.* **1971**, *246*, 2734.

(74) Shannon, R. D. *Acta Crystal. A* **1976**, *A32*, 751.

(75) Shannon, R. D.,Prewitt, C. T. *Acta Crystal. B`* **1969**, *25*, 925.

(76) *The Chemistry of the Cyano Group*; Wiley-Interscience: New York, 1970.

(77) Strecker, A. *Liebigs. Ann. Chem.* **1850**, *75*, 27.

(78) Clarke, H. T.,Read, R. R. *J. Am. Chem. Soc.* **1924**, *46*, 1001.

(79) Harrison, C. R.,Hodge, P.,Rogers, W. J. *Synthesis* **1977**, 41.

(80) DiBiase, S. A.,Wolak, R. P.,Dishong, D. M.,Gokel, G. W. *J. Org. Chem.* **1980**, *45*, 3630.

(81) Bennet, M. A.,Yoshida, T. *J. Am. Chem. Soc.* **1973**, *95*, 3030.

(82) Paraskewas, S. *Synthesis* **1974**, 574.

(83) Chin, J.,Kim, J. H. *Angew. Chem.* **1990**, *102*, 580.

(84) Arthaud, I.,Chatel, S.,Chauvin, A. S.,Bonnet, D.,Kopf, M. A.,Leduc, P. *Coord. Chem. Rev.* **1999**, *190-192*, 577.

(85) Thompson, L. A.,Knowles, C. J.,Linton, E. A.,Wyatt, J. M. *Chem. Brit.* **1988**, *24*, 900.

(86) Nagasawa, T.,Yamada, H. *Biocatalysis*; Van Nostrand Reinhild: New York, 1990.

(87) Nagasawa, T.,Wierser, M.,Tetsuji, N.,Hitomi, I.,Toyokazu, Y.,Gekko, K. *Eur. J. Biochem.* **2000**, *267*, 138.

CHAPTER IV

INITIAL EVALUATION OF ROOM TEMPERATURE IONIC LIQUIDS AS POTENTIAL SOLVENTS TO IMPROVE SYNTHESIS OF DIFFICULT PEPTIDES

Introduction

Since Merrifield introduced solid-phase peptide synthesis (SPPS) in the early 1960s,[1] it has become one of the most important synthetic methodologies in biochemical research. Examples demonstrating the power of this technique can be seen in the production of biologically active proteins such as ribonuclease A,[2] fragment P_2 of *Staphylococcus aureus* nuclease T,[3] and the acyl carrier protein.[4] However, despite these noted accomplishments, many synthetic peptides are still unattainable in sufficient yields and purities.

The first comprehensive study investigating difficulties associated with some peptide sequences during SPPS was published by Pillai and Mutter in 1981.[5] The confirmation of a peptide is determined by the intramolecular, noncovalent interactions between various amino acid groups and by the growing peptide's interaction with the solvent medium. The latter interactions had previously limited experimental investigation of peptide and protein interactions due to the limited solubility in appropriate solvents.[6] Therefore, Pillai and Mutter utilized a liquid-phase method whereby the C-terminal macromolecule, polyoxyethylene (POE), is solubilized in order to allow a more facile approach to investigate growing peptide chain interactions. This design effectively simulates SPPS in an environment suitable for biophysical analysis, such as CD, UV, and NMR spectroscopy.

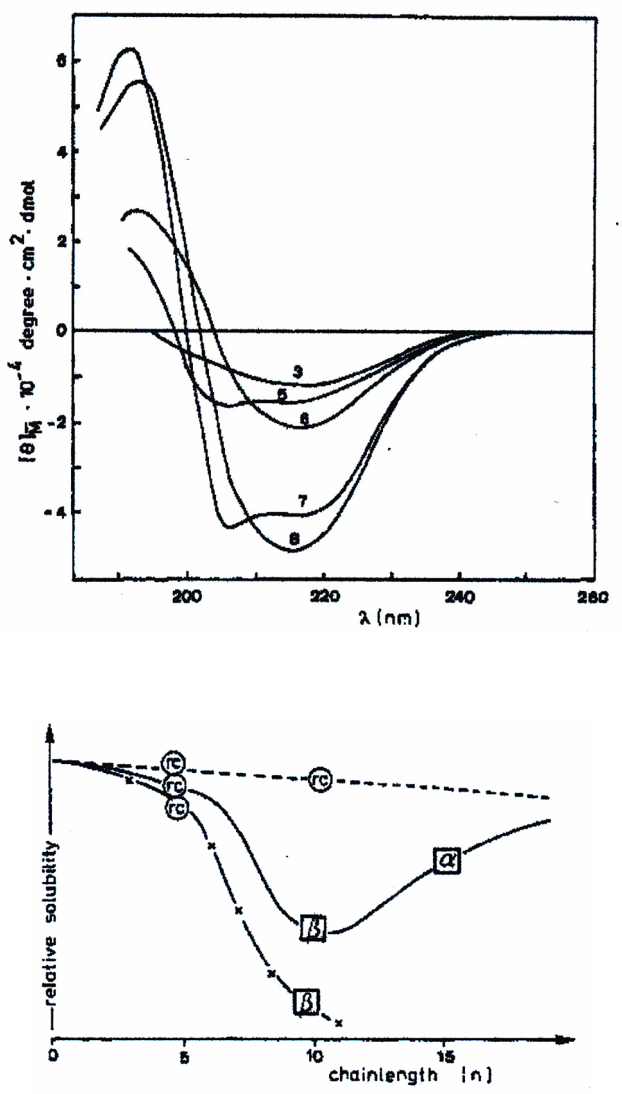

Figure 74. CD and solubility experiments examining the relationship between β-sheet onset and solubility of the peptide. (Top) CD spectra of oligoisoleucine as a function of increasing chain length. (Bottom) Solubility of peptides as a function of their chain length and secondary structure where rc = random coil, β = beta sheet, and α = helix.[5]

It was determined that a direct correlation is present between the onset of secondary structure in the growing peptide chain and the insolubility of the growing peptide chain. Insoluble intermediates result in incomplete coupling of subsequent amino acid residues. Insufficient couplings produce truncated peptide sequences which

complicate crude product purification and drastically decrease yields. The onset of ß-sheet structure for a variety of homooligomers was monitored by CD **(Figure 74)**. Homooligoisoleucine was shown to adopt a ß-sheet conformation by the 6th residue, and similar patterns were observed for a 7-mer of oligoalanine and a 8-mer oligovaline. It was further determined that the 8-mer oligoisoleucine was still in a ß-sheet structure at a concentration as low as 0.02 mg/mL. This remarkable stability would be expected in an intramolecular ß-structure containing intramolecular hydrogen bonding of ß-bends. Unfortunately, such stability proved to be detrimental to peptide synthesis. The transition from random coil to ß-sheet initiated precipitation of the growing peptide chain **(Figure 74)**. Additionally, it was observed that particular peptides such as $[Glu(OBzl)]_n$ were able to increase in solubility, as a transition from ß-sheet to α-helix was noted for increased chain length. This underscores the idea that each peptide could potentially have its own intrinsic 'difficult' sequence regions.

As discussed in Chapter I, one remedy to the onset and subsequent precipitation of a ß-sheet structure during peptide synthesis is the Hmb backbone protection scheme **(Figure 75)**. While this method has brought some remarkable successes, synthetic and practical obstacles prevent the Hmb protection scheme from finding widespread acceptance. *FMOC Solid Phase Peptide Synthesis: A Practical Approach,* edited by Chan and White,[7] identifies the problems associated with Hmb protection:

- Synthetic protocols associated with the synthesis of the active ester residue containing the protective N-(2-hydroxy-4-methoxybenzyl) group and the insertion of the residue into the peptide chain are lengthy and low yielding.
- Protection must be utilized on a residue prior to the onset of aggregation.

- Backbone protection is implemented at a maximum of every sixth residue.
- Hmb protection cannot be used on a residue that is to be followed by a ß-branched residue, because the subsequent coupling will not be quantitative due to steric hindrance.
- Aspartyl bonds susceptible to base-catalysed transformations require specific protection.

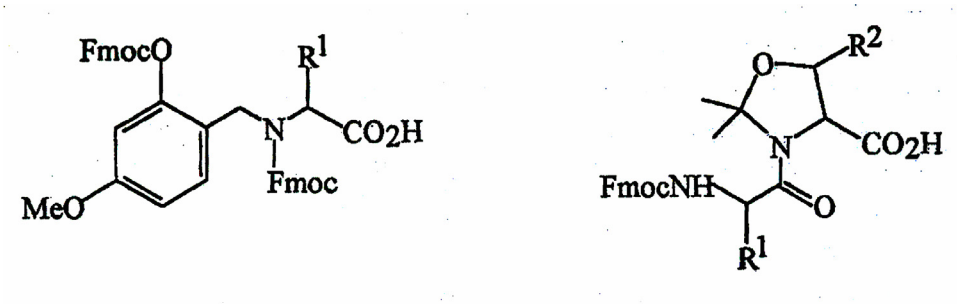

Figure 75. (Left) structure of the Hmb amide backbone protection unit. R1= residue sidechain. (Right) Pseudoproline protection unit. R1 = residue sidechain and R2 = Methyl.

An example of a difficult peptide that failed to respond to Hmb protection has been reported by Keller and Miller.[8] They were interested in chaperonin 60.1 because of its role in human monocyte expression of IL-1ß and IL-6 genes, key mediators of inflammation. Enzymatic digestion had isolated a 25 residue sequence (195-217) with significant biological activity. The subsequent SPPS synthesis of H-KGFLSAYFVTDFDNQQAVLKEDALI-OH using an Hmb protection scheme resulted in low coupling yields and undesirable side products. However, they were able to employ the pseudoproline protection scheme to acquire acceptable purity and yield. Pseudoproline dipeptides (FMOC-Val-Thr($\psi^{Me,Me}$ pro)-OH and FMOC-Leu-Ser($\psi^{Me,Me}$

pro)-OH) were inserted at S199 and T204, and it was noted that neither dipeptide was able to sufficiently delay the onset of aggregation alone. The successful synthesis of the previously unattainable chaperonin subunit demonstrates the distinct differences between the Hmb and pseudoproline methodologies and further highlights proper study and planning required when choosing a synthetic peptide strategy.

The success of pseudoproline dipeptides where Hmb backbone protection has failed was further illustrated by Nicholas Ede and associates in a report of direct comparison between the two methods.[9] Their experimental design was simply to evaluate crude product purities from known difficult peptide sequences following standard HBTU coupling, HBTU coupling aided by Hmb protection, and HBTU coupling aided by pseudoproline insertion. The peptide H-PKYLQNTLKLATGMRNVPEKQTT-OH (underscore represents point of insertion of Hmb or pseudoproline residues) was evaluated, and the HPLC profiles resulting from the various synthetic methodologies are given **(Figure 76)**. Ala was incorporated as FMOC-(FMOC-Hmb)Ala-OH and as FMOC-Ala-Thr($\psi^{Me,Me}$ pro)-OH. The standard HBTU coupling procedures was only able to produce a 24% yield of the desired peptide. The Hmb amide backbone protection generated 43% of the peptide. The best method proved to be the pseudoproline insertion as it was able to yield 78% of the desired product. The authors conclude that pseudoproline insertion is superior to the Hmb backbone protection scheme in both synthetic preparation of the derivatized residues and overall quality of the resulting crude product.

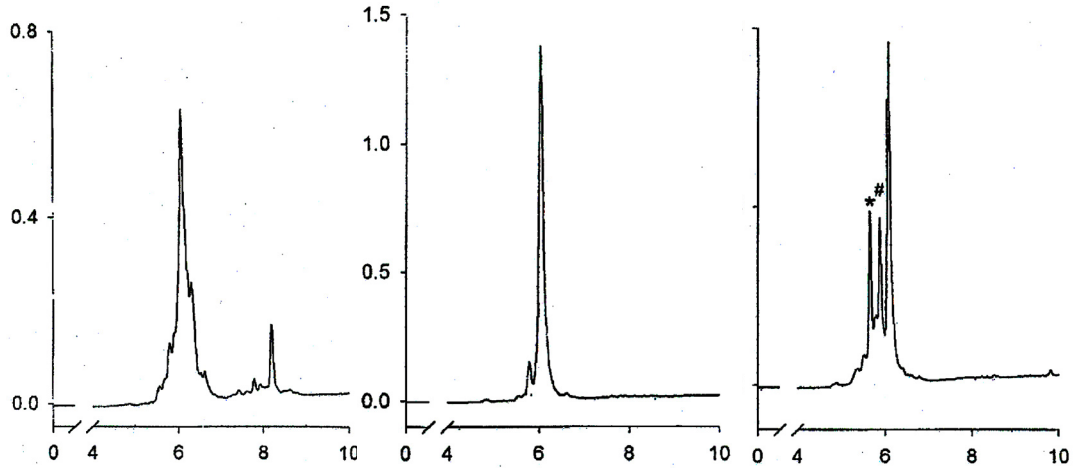

Figure 76. (Left) HPLC of difficult peptide following standard FMOC synthesis protocols. (Center) Same peptide following pseudoproline protection scheme. (Right) Same peptide following Hmb amide backbone protection scheme where # = lysine deletion and * = leucine deletion.[9]

Many chemical research laboratories are capable of utilizing standard FMOC based SPPS. However, difficult peptide synthesis limits the scope of peptides produced. Alleviation of the ß-sheet onset and subsequent insoluble peptide during synthesis can be achieved by the methods discussed above, but the expertise needed to implement the Hmb backbone protection is a limiting factor. Additionally, the simpler pseudoprolines have the substantial drawback of only being applicable if the difficult sequence desired happens to have a Ser, Thr, or Cys in an appropriate location in the sequence. One reason for this hurdle is that both methods require they be implemented prior to the onset of aggregation. Prior knowledge of this phenomenon is typically the result of multiple failed synthesizes adding cost and time to the production of the desired peptide. Therefore, many peptides may still be unattainable and require a more universal and simplistic solution to difficult peptide synthesis.

Recent attempts to deliver a simple, universal remedy to difficult peptide sequences have focused on changing the environment in which the peptide is being synthesized. The rationale is that a change in the environment could either dissolve or disrupt the ß-sheet structures. Two such methods involve the use of dimethyl sulfoxide (DMSO) as either an additive or substitute solvent for traditional DMF or N-methylpyrrolidinone (NMP) and the addition of chaotropic salts, such as LiCl. Hyde *et al.* demonstrated the potential of DMSO by alleviating aggregation associated with a decamer from the acyl carrier protein. This peptide (H-VQAAIDYING-OH) is known to aggregate just prior to the final valine. Typical yields are between 80 and 90% **(Figure 77).** DMSO allowed for a near quantitative yield and has been proven to potential be kinetically superior to traditional dipolar aprotic solvents for ester activation of acid residues.

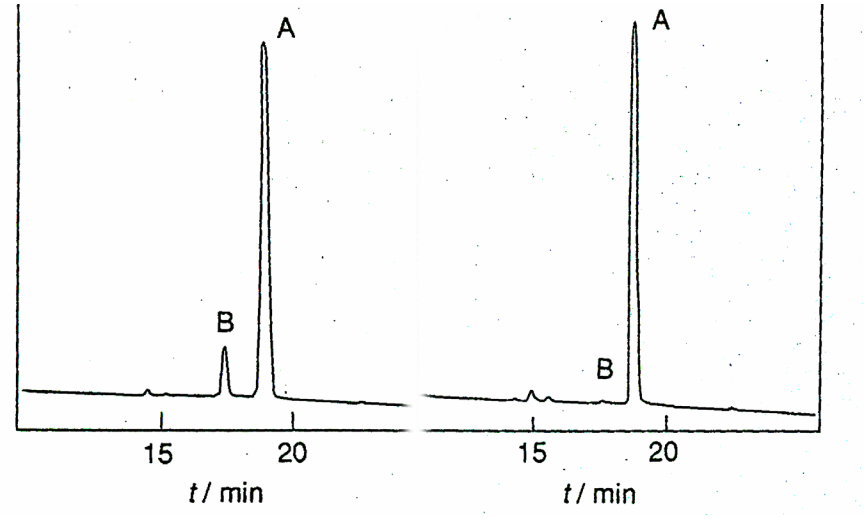

Figure 77. Comparison of traditional polar aprotic solvents and dimethyl sulfoxide during acyl carrier protein peptide synthesis. (Left) traditional solvent where A is the desired decamer and B is des-valine. (Right) Same peptide synthesized in 100% dimethyl sulfoxide.[7]

It was also noted in Hyde's study that LiBr, a chaotropic salt, was effective in delaying or disrupting β-sheet formation. Thaler *et al.* published a more thorough investigation of lithium salts as potential coupling additives in 1991.[10] They chose to test the peptide $(Ala)_nPhe$ with n ranging from 5 to 12. This peptide is known to adopt a β-sheet structure at $n \geq 5$ even in a TFA solution.[11] They tested three different resin matrices, poly(ethylene oxide) on polystyrene (PEO-PS), a poly(N,N-dimethylacrylamide) on 'Kieselgur' (PDMAA-KG), and a classical polystyrene (PS) support. They reported that lithium salts can exhibit a strong influence in peptide coupling reactions. Increased yields were seen for the n = 6 peptide, such as a 16% increase in a 1:1 DMF:DCM mixture and a 5% increase in NMP. This was attributed to the increased swelling of the resin matrix, which increases the solubility of short peptides and the distance between growing peptide chains. The latter is similar to using a lower substituted resin which has fewer peptide elongation sites for the same surface area. The best results were observed with the more polar PEO-PS and PDMAA-KG resins in either NMP or 1,3-dimethyl-3,4,5,6-tetrahydro-2(1H)-pyrimidinone (DMPU) solvent systems.

One intriguing approach to try and gain the advantages of both polar solvents and ionic disruption of the β-sheet structure was Vallette *et al.*'s use of a room temperature ionic liquid (RTIL) as the primary solvent.[12] ILs are molten salts below 100°C with poorly coordinated ions.[13] Those ILs which are liquid at room temperature are referred to as room temperature ionic liquids (RTILs). ILs have previously been used in a variety of organic reactions such as hydroformulations,[14] Heck reactions,[15] and aromatic nitration reactions.[16] ILs display a wide range of solubility properties and are charged ionic species that have the potential to strongly disrupt hydrogen bonding networks, similar to

the above mention lithium salts. Vallette found marginal success with dipeptide synthesis using 1-butyl-3-methylimidazolium hexafluorophosphate [BMIM]PF_6. One disadvantage noted was the large increase in reaction times. Typical peptide couplings in traditional dipolar aprotic solvents are near quantitative conversion within an hour, but the [BMIM]PF_6 system was on the order of days depending on the amino acids used. However, an advantage to the ionic liquid system was an increase in crude product purity. Both of these observations could be explained by stabilization of the charged species in the RTIL. The stabilization would likely slow the kinetic rate for the nucleophilic attack of the N-terminal amine from the peptide to the activated ester. Additionally, this could provide a more selective pathway for the reaction. This was the first report of peptide bond formation in a RTIL system, but key aspects critical to SPPS were left untested. First, the reactions were not performed on a solid support, which adds additional extraction techniques that could result in yield reduction, and removes solvent-matrix interactions discussed above. Second, the 'peptides' produced were all dipeptides consisting of unnatural amino acids, leaving the question of solubility during chain elongation still unanswered. Third, the researchers investigated only one RTIL and a single traditional solvent, DCM, as a control. This was an unusual choice given that most SPPS is not performed in DCM, but rather dipolar aprotic solvents. Finally, the time required to achieve modest product yields would be a large obstacle to widespread usage for SPPS. The time may be comparable to the Hmb protection scheme, but would still require prior knowledge to aggregation onset if used during specific coupling steps.

This chapter investigates 5 RTILs as potential solvents for SPPS. In particular, the solubility of the pre-activated amino acid residue as well as the protected peptide

present during chain elongation is tested. Additionally, the coupling efficiencies achieved by the RTILs are compared to a variety of traditional solvents. Once a suitable liquid is discovered to achieve reasonable coupling kinetics and efficiencies, the potential of an RTIL being used as a simple, effective alternative in the chemical toolbox against difficult peptide aggregation can be determined **(Figure 78)**.

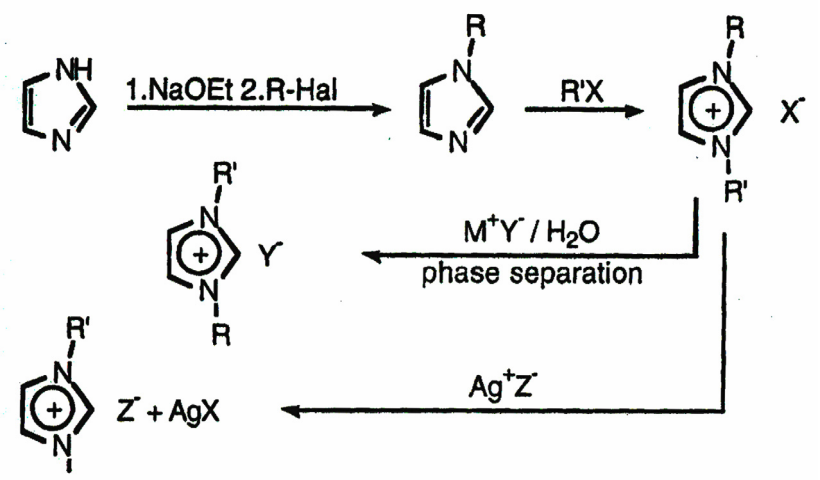

Figure 78. General scheme for ionic liquid synthesis.

Experimental

Preparation of 1-methy-3-butylimidazolium and 1-Butyl-1-methylpyrrolidinium chloride salts: Salts were prepared as previously described.[17] Briefly, a schlenk flask was covered in aluminum foil, flushed with nitrogen, and then charged with dried acetonitrile and either dried 1-methylimidazolium or dried 1-methylpyrrolidinium. The mixture was cooled with ice and charged with a 1 molar equivalence, with respect to the methylated rings, of 1-chlorobutane dropwise. This mixture was slowly brought to room temperature and then refluxed for 16 hours at 80 ˚C. The resulting yellow, orange liquid

was cooled and allowed to solidify. The supernatant was aspirated and the solid was reheated to 80 ˚C and then dripped into an excess of cold ethyl acetate. The white precipitate was collected by filtration. Care should be taken as the precipitate is very hygroscopic. The white powder was washed with fresh ethyl acetate and then dried under vacuum for 48 hours.

1-Butyl-1-methylpyrrolidinium bis-(trifluoromethansulfonyl)imide, [BMPY]N(Tf)$_2$: In a schlenk flask flushed with nitrogen, a 1:1 molar mixture of 1-methylpyrrolidinium chloride and lithium bis-(trifluoromethansulfonyl)imide were suspended in DCM. It was later found that 1-methylpyrrolidinium chloride was readily soluble in DCM, but the lithium salt was not. The vessel was protected from light and allowed to mix under nitrogen for 72 hours and then filtered. The resulting cake was washed with further aliquots of DCM and the aliquots were then pooled and washed with water until the washes tested negative for halides (silver nitrate test). Care should be taken to keep the volume of the water washes at least 10 times smaller in volume than the organic layer, because the product is miscible in both. The organic layer was then removed *in vacuo* and the resulting liquid was charged with activated charcoal and mixed for 24 hours. This mixture was then filtered over basic alumina to yield the final ionic liquid as a near colorless liquid. The liquid was then dried at 110 ˚C *in vacuo* for at least 48 hrs. or until no loss of volume over time.

1-Butyl-1-methylpyrrolidinium Trifluormethansulfonate, [BMPY]OTF: The same procedures were followed as described above for [BMPY]N(Tf)$_2$ with the exception that lithium trifluoromethansulfonate was used in place of lithium bis-(trifluoromethansulfonyl)imide.

1-methy-3-butylimidazolium Tetrafluoroborate, [BMIM]BF_4 : The same procedures were followed as described above for [BMPY]$N(Tf)_2$ with the exception that silver tetrafluoroborate was used in place of lithium bis-(trifluoromethansulfonyl)imide.

1-methy-3-butylimidazolium Trifluormethansulfonate, [BMIM]OTF: The same procedures were followed as described above for [BMPY]$N(Tf)_2$ with the exception that lithium trifluoromethansulfonate was used in place of lithium bis-(trifluoromethansulfonyl)imide.

1-methy-3-ethylcyanoimidazolium bis-(trifluoromethansulfonyl)imide, [EMIMCN] $N(Tf)_2$: The cation produced from the initial reflux reaction of 1-methylimidazole and 3-chloropropionitrile was a stand-alone ionic liquid. The mixture was then charged with 1 equivalence (eq.), with respect to the theoretical amount of 1-methy-3-ethylcyanoimidazolium produced, lithium bis-(trifluoromethansulfonyl)imide chloride was dissolved in a minimal amount of acetonitrile and added to the yellow, viscous 1-methy-3-ethylcyanoimidazolium chloride. The resulting product was collected in as described above.

UV-Analysis of Solubilized FMOC: Traditional gravimetric analysis would not be sufficient to analyze the mass of reagents dissolved in RTILs, because of their extremely low vapor pressure. Traditionally, undissolved solid material from the initial mass of solute would be separated by filtration or centrifugation followed by a drying process. The resulting mass would be weighed and subtracted from the initial mass. The thermal stability and low vapor pressure would not be conducive to achieving sufficient drying and would thus interfere with accurate measurement. Therefore, a spectrometric approach was developed.

All the solutes tested had a primary amine protected by FMOC. The design calls for the solid solute to be allowed 20 minutes to dissolve in the liquid being tested, followed by filtration through celite and paper plug. From the filtrate, 100 μL was added to a mixture of DMF and piperidine (3:1) to achieve a total volume of 1 mL. This solution was allowed to react for 25 minutes in order to remove any FMOC protecting groups dissolved, and further diluted to 3 mL. The biphenylfullvene released (see Chapter I for a more thorough discussion of FMOC removal) can then be measured at 290 nm. A calibration curve was generated in DMF, and subsequent reactions were evaluated and normalized to DMF.

Peptide Synthesis: Peptides were synthesized on an Apex 396 (Advanced Chemtech) equipped with a 96-well reaction block capable of vortex mixing. Customized tentagel resin was swollen in Dichloromethane (Fisher) prior to synthesis. 9-Fluorenylmethoxycarbonyl (FMOC) amino acids (Synpep) were coupled using O-Benzotriazole-N,N,N',N'-tetramethyl-uronium-hexafluor-phosphate (HBTU; 5 eq. with respect to resin; Synpep), 1-hydroxybenzatriazole (Hobt; 5 eq.; Synpep), diisopropylethylamine (DIEA; 10 eq.; Advanced Chemtech) in N,N-dimethylformamide (DMF; Fisher). Peptides were cleaved with 95% (v/v) trifluoroacetic acid and 5% triisopropylsilane and desalted on a G-25 sephadex column before final purification on a C4 semi-prep reverse phase HPLC column using water and acetonitrile gradients. The final Leu was coupled by dissolving 3 (eq.) of the pre-activated pentafluorophenyl ester derivative, and then addition of this solution to the resin. Three hours of vortex or mechanical stirring followed. Peptide containing FMOC and side chain protection

elements were collected by exposure of the 2-chlorotrityl polystyrene resin to 3% TFA in DCM for 5 minutes followed by precipitation with cold diethyl ether.

Results and Discussion

Ionic liquids (ILs) are defined as salts that melt near or below 100 ˚C due to poor coordination between ions, and room temperature ionic liquids (RTILs) are liquids at 25 ˚C or below. They have currently been used in a wide array of organic reactions.[18] Their enduring popularity exists for several reasons. They are often referred to as nontoxic, 'Green' solvents. This label comes from their vanishingly small vapor pressures under ambient and typical reaction conditions. This is of particular importance for reclaiming and recycling the solvent. Several groups have reported reactions showing an increase in crude purity that saves enough time in purification to offset typically longer reaction times. Given the large number of potential combinations of cations and anions, researchers can customize solvents to particular reactions to greatly increase efficiency and yields. Therefore, the study of basic properties associated with ionic liquids and the reactants for a given reaction is of particular interest.

ILs display a wide range of solubility properties and are charged ionic species that have the potential to strongly disrupt hydrogen bonding networks. Recently, Tom Welton and colleagues have been able to apply ILs as manipulators of nucleophilicity and reaction rates for amine bases in charge-neutral reactant reactions **(Figure 79)**.[19] This work noted that the reaction conditions follow Hughes-Ingold[20] and Kamlet-Taft[21-23] rules and parameters. By following the UV-Vis transition of Tri-^{n}butylamine, they were able to conclude that if initial reactants are charge -neutral and the generation of an

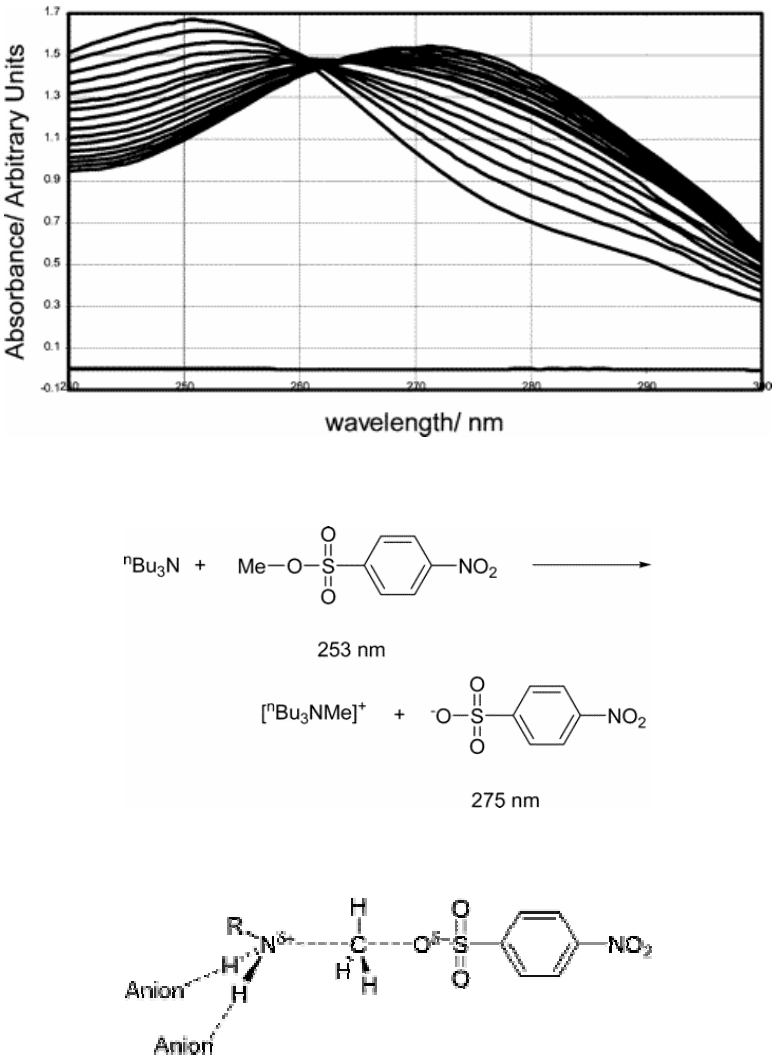

Figure 79 (Top) UV-VIS analysis of tri-^{n}butylamine with methyl-*p*-benzesulfonate. (Center) Scheme for the methylation of tertiary amines. (Bottom) Stabilization of high energy intermediate by the hydrogen bond acceptor of the ionic liquid anion.[19]

activated complex includes charge formation, then the reaction rates will increase in an ionic liquid solvent system. This conclusion suggests that ILs should be investigated as synthetic solutions to peptide chain insolubility and aggregation. Furthermore, the reaction rates could potentially surpass those where traditional solvents are utilized.

Judicious selection of the ion pair of the RTIL should allow for the selection of possible solvents to achieve ideal reaction conditions for SPPS **(Figure 80)**.

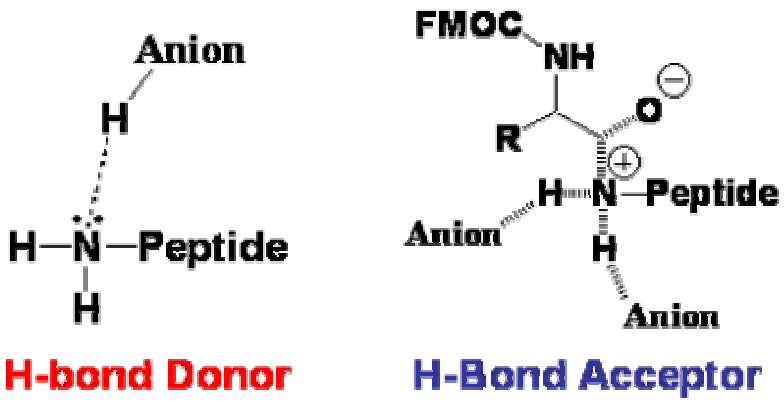

Figure 80. Theoretical hydrogen bonding affects. (Left) Hydrogen bond donors would likely slow kinetics by inhibiting the primary amine lone pair from performing a nucleophilic attack. (Right) Congruent with the analysis of Welton, designed anions could be capable of stabilizing the high energy intermediate during amide bond formation.

The observation of increased nucleophilicity by Welton is encouraging for the idea of using RTILs in peptide synthesis, because the same general reaction is at the heart of peptide bond formation **(Figure 80)**. The RTILs chosen as the first to be evaluated for SPPS compatibility were [BMPY]OTF, [BMIM]OTF, [BMIM]BF_4, [BMPY]$N(Tf)_2$, and [EMIMCN]$N(Tf)_2$. The latter two liquids are hydrophobic in order to assure that trace amounts of water often found in the extremely hygroscopic ILs were not interfering with amide bond formation. All of these anions should be capable of accepting a hydrogen bond, and thus stabilizing the charged intermediate formed during amide bond formation. However, given the large number of potential ion pairs capable of being hydrogen bond acceptors, the experiments designed herein also test general parameters with an eye

towards possibly developing a rapid, combinatorial approach to identifying the ideal IL for SPPS. The parameters chosen were coupling efficiency, active ester solubility, and protected peptide solubility.

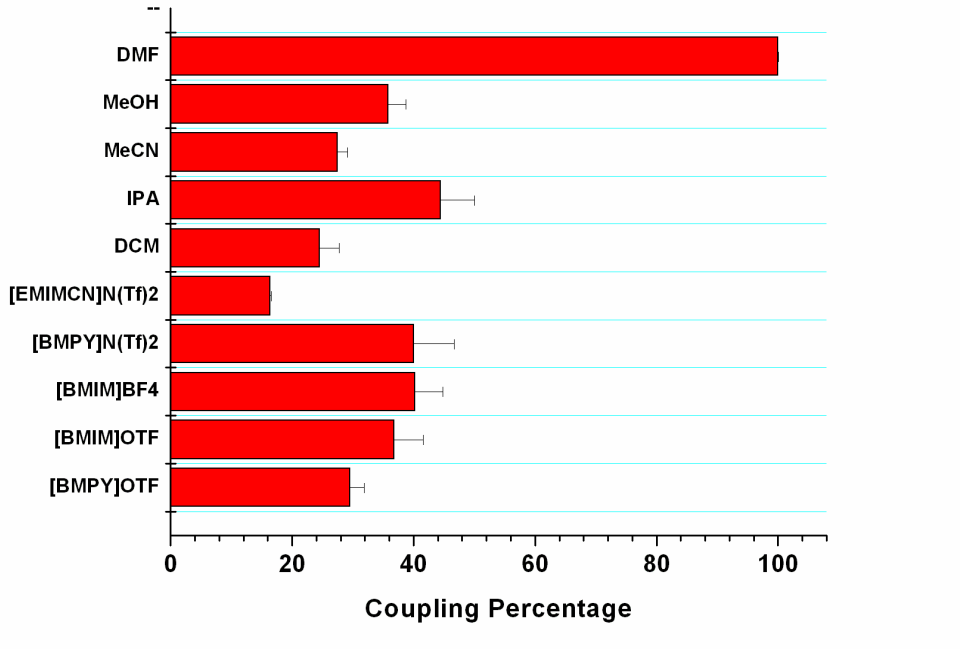

Figure 81. Bar graph showing relative percentage of coupling efficiency as a function of solvent Reaction proceeded for 3 hours at room temperature under vortex or mechanical mixing.

The peptide chosen to study in these experiments was H-LAPEGRS-OH. This peptide was designed to be water soluble for simple purification and analysis, and provides a reasonable test for two common side chain protection schemes employed in modern SPPS (i.e. butyl associated with Ser and Glu and N‘-2,2,4,6,7-pentamethyldihydrobenzofuran-5-sulfonyl (PBF) on Arg). Standard protocols were utilized to synthesize the first six residues on a 2-chlorotrityl polystyrene resin. The final residue, Leu, was coupled via FMOC-Leu-OPfP (activated pentafluorophenyl ester) in

the test liquids for three hours. The pre-activated residue was chosen to simplify the coupling reaction. HBTU and DIC couplings require additional additives, such as Hobt, and demand an initial activation reaction take place in order to generate an active ester.

The coupling efficiencies, as determined by HPLC analysis, are shown in **Figure 81**. The results following a three hour reaction time with both vortex and mechanical mixing were less than desired. All of the RTILs failed to achieve 50% conversion as compared to DMF, which was quantitative. Additionally, no significant change in conversion was observed upon heating the reaction to 60 °C or following a 24 hr. reaction time.

One of the barriers to widespread industrial use of ILs is the absence of knowledge pertaining to how the structure of the IL affects solvent strength and physical properties. Two parameters which may warrant further investigation are the viscosity of the RTIL and the polarity of the RTIL. The RTILs were observed to be very viscous, comparable to glycerine following visual inspection. Indeed, [BMIM]BF_4's viscosity was recently determined to be 279.86 η/mPa•S at 298 K, as compared to water (1 η/mPa•S), benzene (0.604 η/mPa•S), and glycerol (934 η/mPa•S).[24] The viscosity of the solvent medium could interfere with the movement of the polystyrene resin beads. A single molecule moving in a liquid has to escape the forces of attraction associated with its neighboring molecules. Design of the ionic liquid allows for reasonable control of physical properties, such as viscosity. There are two key structural components to an IL that govern viscosity: the charge localization of the anion and the length of the alkyl chain associated with the cation. Anions that fail to delocalize the negative charge throughout its structure tend to be more viscous and often experience a transition from

glass to liquid above room temperature. This is expected as the localized negative charge strengthens the coordination of the ion pair, thus beginning to resemble a traditional salt. The alkyl chains attached to the cation have been shown to increase viscosity through what is believed to be Van der waals forces. This too might be expected in the RTILs used in this chapter due to their ring and planar structures being able to stack.

The polarity of ILs is a topic being investigated by several research groups. Traditional calculations led to early misconceptions of the polarity of RTILs. For example, the program Chem3D can accurately predict the polarity of traditional solvents within 10% of accepted values. DMF was predicted to be 3.97 debyes and the accepted value is 3.82 debyes. [BMPY]OTF was predicted by Chem3D to be 15.21 debyes. These misconceptions have been recently been debunked, and even led to publications such as 'How polar are room-temperature ionic liquids?'.[25] Most attempts at determining polarity for these new solvents involve solvatochromic probes.[26,27] These probes have λ_{max} values that shift as a function of the solvents polarity. From this, researchers are able to calculate energy values and polarity approximations. They have determined that many of the imidazolium and pyrrolidinium ILs have polarities between methanol and ethanenitrile. One variant in using solvatochromic dyes is that they measure values from an excited state. Earle *et al.* later confirmed these approximations for [BMIM]BF_4 and [BMIM]OTF in the ground state by using keto-enol tautomerism as a gauge for polarity **(Figure 82)**.[28] The nucleophilic attack and the subsequent high energy intermediate associated with amide formation would be predicted to be greatly influenced by the polarity of the solvent according to the Hughes-Ingold rules discussed above.

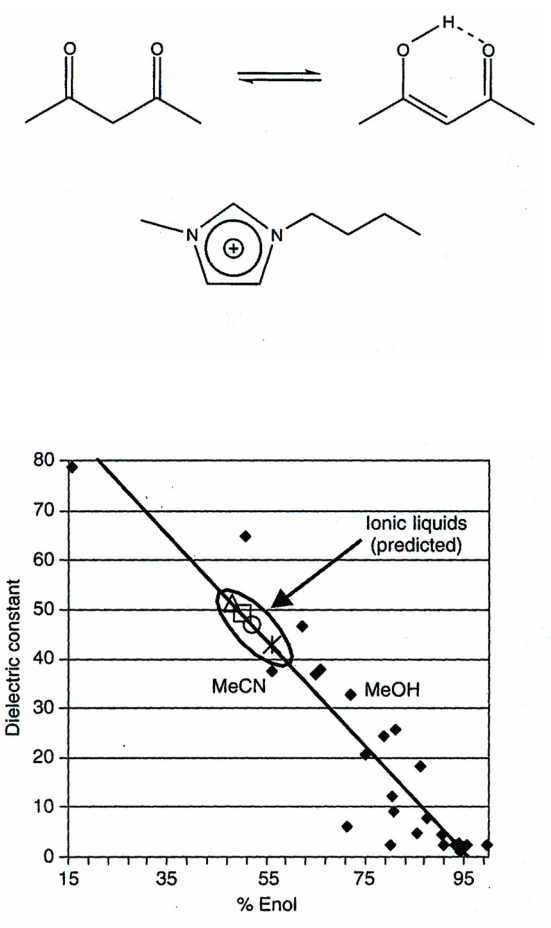

Figure 82 (Top) Keto-enol tautomerization and the cation of the ionic liquids tested. (Bottom) Graph of dielectric points from 30 different solvents.[28]

During the investigation of coupling efficiency it was observed that the RTILs were unable to dissolve 3 molar equivalents (34 mg; with respect to theoretical number of growing peptide chains on 50 mg of 0.4 mmol/g of substituted resin) of the active FMOC-Leu ester. UV-VIS analysis of the biphenylfullvene released during base catalyzed removal of the FMOC protecting group showed distinct solvent strengths in the RTILs **(Figure 83)**. All of the RTILs save [EMIMCN]$N(Tf)_2$ achieved $\leq$ 1 molar equivalence dissolved. This is likely a contributing factor to the poor yields discussed

above. Curiously, [EMIMCN]N(Tf)$_2$ was found to be the least effective solvent tested for amide bond formation. Either one of the physical properties such as viscosity or polarity are inhibitive of amide bond formation, or the solvent was nearing saturation as may be the case for all of the RTILs tested.

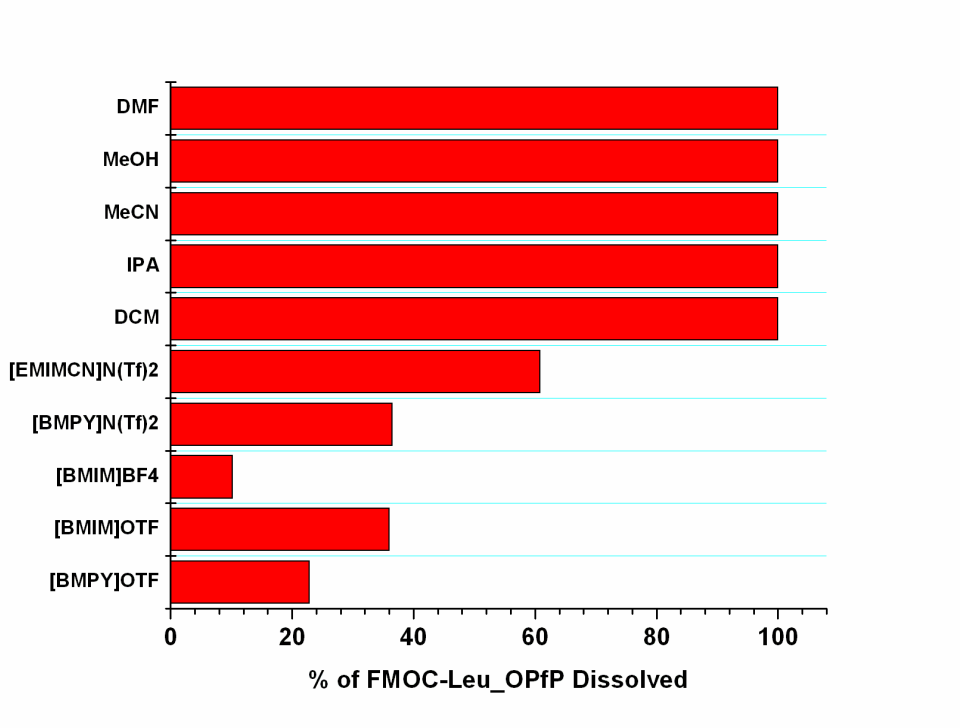

Figure 83. Bar graph representing the percentage of active ester solubilized in the selected solvents. 34 mg (65 μM) is equivalent to 100%.

The poor solubility of the active ester led to the investigation of whether the protected peptide chain on the surface of the resin was soluble in RTILs. The 6-mer peptide was collected with all of the side chain protecting groups as well as the N-terminal protecting FMOC group. UV-Vis analysis revealed that all of the RTILs, save [BMPY]N(Tf)$_2$, dissolved the theoretical amount of peptide in the reaction (24 mg). [BMPY]N(Tf)$_2$ was found to only dissolve 36% of the 24 mg. However, [BMPY]N(Tf)$_2$

was one of the more efficient solvents for the amide bond formation. It maybe the case that [BMPY]N(Tf)$_2$ has certain properties conducive to amide bond formation, but has overall poor solvent strength limiting the reaction yield. Further investigation, and likely a combinatorial approach, into the properties and design of RTILs suitable for SPPS is warranted.

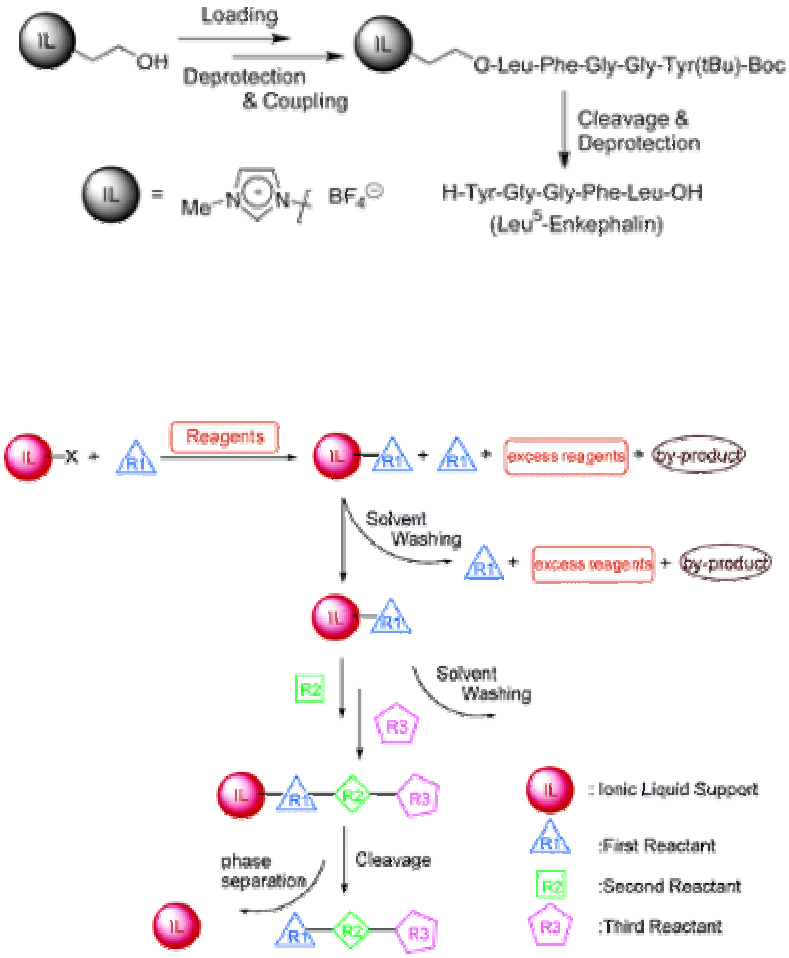

Figure 84. Peptide synthesis scheme utilizing an ionic liquid support as proposed by Chan.[29]

Future work in the area of RTIL mediated SPPS involves testing solubility limits for the active ester in concert with the protected peptide. Careful addition of reagent quantities should lead to ideal solubility properties in order to better isolate the physical properties of the RTILs governing the amid formation reaction. This suggests that a liquid phase reaction may prove to be a more effective method for peptide synthesis in a RTIL. During the time of this research, a group led by Tak-Hang Chan synthesized a biologically active 5-mer in a liquid phase reaction involving an ingenious use of an RTIL **(Figure 84).**[29] Their approach appears to be well thought out and efficient, and would be predicted as a potential success by the data presented in this chapter. One of the questions raised by the researchers was how many residues could be added to the peptide chain before solubility or glass transition becomes a problem. This present research shows that in fact, many RTILs are powerful solvents for at least six residues and likely several more amino acids.

Critical analysis of their approach does leave some unanswered questions that need to be addressed. First, they chose to use the older N-terminal BOC protection scheme (discussed in Chapter I). This requires the use of a 1:1 DCM:TFA solution to deprotect the N-terminal primary amine as opposed to 3:1 DMF:piperidine used in FMOC synthetic protocols. This could be due to an unreported immiscibility with either DMF or piperidine and may present a problem as an overall method for peptide synthesis because most modern side chain protecting groups are acid labile. Acid labile protection schemes are preferred due to their removal and easy cleanup during the peptide's cleavage from the support. They were able to incorporate a butyl protected Tyr residue,

but this was the final residue in the 5-mer and would not have been compatible with a subsequent elongation step.

In conclusion, RTILs and possibly other ILs show potential as peptide synthesis mediums. Further investigation into the physical properties of individual ILs can aid in the careful selection of the proper solvent. However, a combinatorial approach which tests specific parameters such as reagent solubility, viscosity, and polarity could prove to identify an ideal IL for peptide synthesis more rapidly. By either approach, the potential offered by a 'green,' easily recycled, and non toxic solvent for the growing field of peptide synthesis is worth investigating.

REFERENCES

(1) Merrifield, R. B. *J. Am. Chem. Soc.* **1963**, *85*, 2149

(2) Gutte, B.,Merrifield, R. B. *J. Biol. Chem.* **1971**, *246*, 1922.

(3) Ontjes, D. A.,Anfinsen, C. B. *Proc. Nat'l. Acad. Sci.* **1969**, *64*, 428.

(4) Hancock, W. S.,Prescott, D. J.,Nulty, W. L.,Weintraub, J.,Vagelos, P. R.,Marshall, G. R. *J. Am. Chem. Soc.* **1971**, *93*, 1799.

(5) Pillai, V. N. R.,Mutter, M. *Acc. Chem. Res.* **1981**, *14*, 122.

(6) Naider, F.,Goodman, M. *Bioorg. Chem.* **1977**, *3*, 179.

(7) *FMOC Solid Phase Peptide Synthesis: A Practical Approach*; Oxford University Press: New York, 2000.

(8) Keller, M.,Miller, A. D. *Bioorg. Med. Chem. Lett.* **2001**, *11*, 857.

(9) Sampson, W. R.,Patsiouras, H.,Ede, N. J. *J. Pept. Sci.* **1999**, *5*, 403.

(10) Thaler, A.,Seebach, D.,Cardinaux, F. *HeIv. Chim. Acta* **1991**, *74*, 628.

(11) Mutter, M.,Pillai, V. N. R.,Anzinger, H.,Bayer, E.,Toniolo, C. In *Proceedings of the 16th European Peptide Symposium*; Brunfeldt, K., Ed.: Copenhagen, 1981, p 660.

(12) Vallette, H.,Ferron, L.,Coquerel, G.,Gaumont, A.,Plaquevent, J. *Tetrahedron Lett.* **2004**, *45*, 1617.

(13) Keim, P. W. A. W. *Angew. Chem. Int. Ed.* **2000**, *39*, 3772.

(14) Yves Chauvin, L. M., Helene Olivier *Angew. Chem. Int. Ed.* **1995**, *34*, 2698.

(15) D.E. Kaufmann, M. N., H. Henze *Synthesis Lett.* **1996**, *11*, 1091.

(16) Llopis-Mestre, N. L. L. a. V. *Chem. Comm.* **2003**, 2812.

(17) Lorna Crowhurst, N. L. L., Juan M. Perez Arlandis, and Tom Welton *J. Am. Chem. Soc.* **2004**, *126*, 11549.

(18) *Ionic Liquids in Synthesis*; VCH-Wiley: Weinheim, 2002.

(19) Lorna Crowhurst, N. L. L., Juan M. Perez Arlandis, and Tom Welton *J. Am. Chem. Soc.* **2004**, *126*, 11549.

(20) Ingold, E. D. H. a. C. K.; University College: London, 1934, pp 244.

(21) R.W.Taft, M. J. K. a. *J. Am. Chem. Soc.* **1976**, *98*, 377.

(22) R.W.Taft, M. J. K. a. *J. Am. Chem. Soc.* **1976**, *98*, 2886.

(23) Mortimer J Kamlet, J. L. A., and RW Taft *J. Am. Chem. Soc.* **1977**, *99*, 60276038.

(24) Kim, S.,Shin, B.,Lee, H. *Korean J. Chem. Eng.* **2004**, *21*, 1010.

(25) Aki, S. N. V. K.,Brennecke, J. F.,Samanta, A. *Chem. Comm.* **2001**, 413.

(26) Fletcher, K. A.,Pandey, S. *App. Spec.* **2002**, *56*, 1498.

(27) Carmichael, A. J.,Seddon, K. R. *J. Phys. Chem.* **2000**, *13*, 591.

(28) Earle, M. J.,Engel, B. S.,Seddon, K. R. *Aust. J. Chem.* **2004**, *57*, 149.

(29) Miao, W.,Chan, T. H. *J. Org. Chem.* **2005**, *70*, 3251.

APPENDIX A

HPLC DATA FROM HMPV PEPTIDES AND SIZE EXCLUSION DATA FROM THE HMPV FUSION CORE

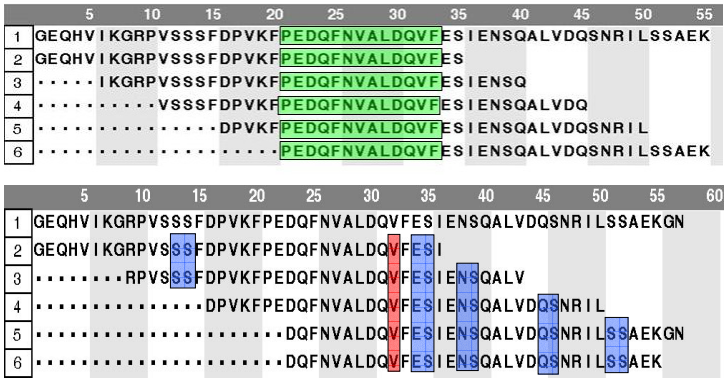

Figure 85. (Top) Overlapping 35-mer sequences derived from HR-2 used to identify problematic regions in synthesis. (Bottom) Location of pseudoproline coupling (blue) and valine HMB (red) used to overcome aggregation challenges

Peptide synthesis of peptides 2-6 **(Figure 85)** was performed as described on page 73. Pseudoproline addition was achieved as described on page 75, and Hmb incorporation as described on page 76. Peptides were produced on custom resin described on page XX to achieve a C-terminal amide group. N-terminal succinyl groups were added by an additional HBTU, DIEA, and HOBT mediated coupling of mono-*tert*-butyl succinic acid following final FMOC removal. These peptides are the next generation of HR-2 peptides from hMPV to be optimized and tested.

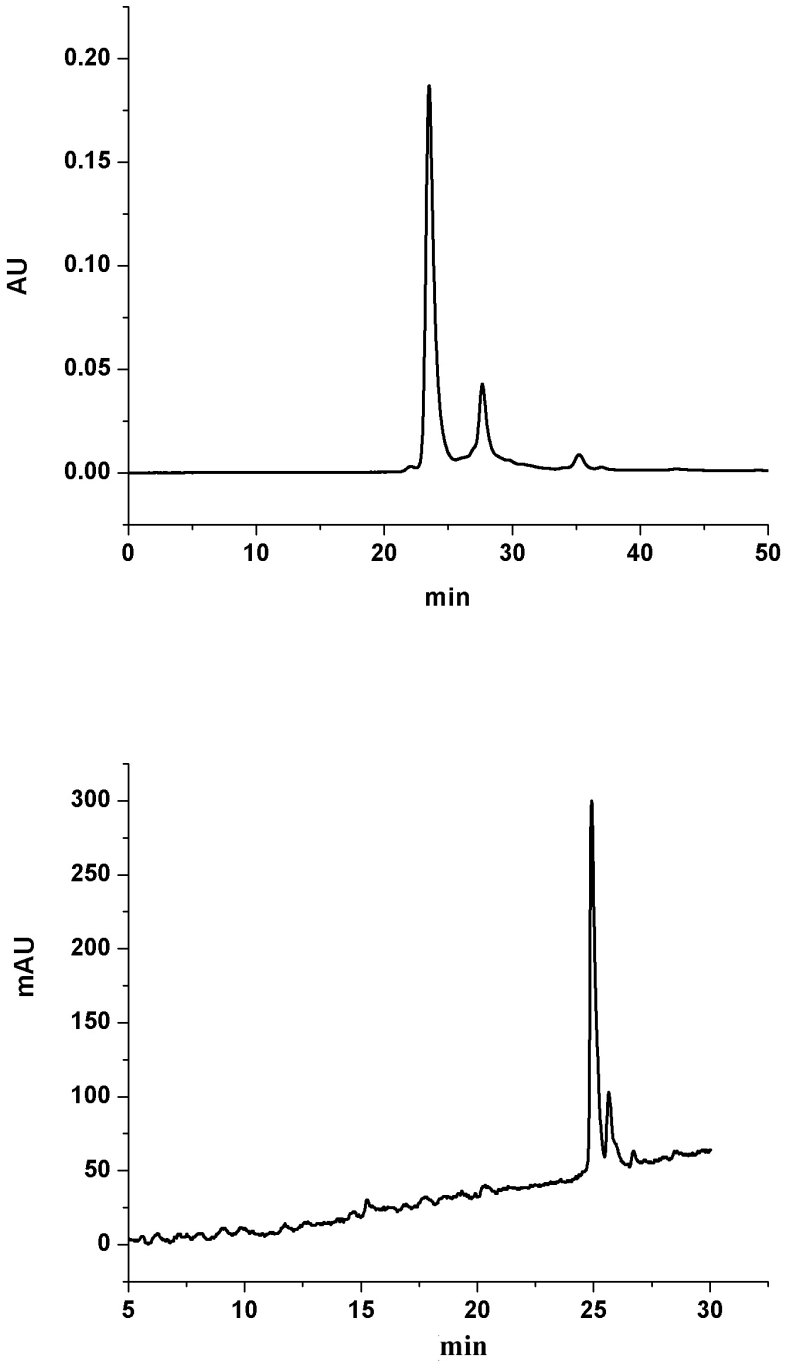

Figure 86. HPLC data for purified LearnCoil-VMF sequences discussed in Chapter II. (TOP) 33A (Bottom) HR-1 43-mer

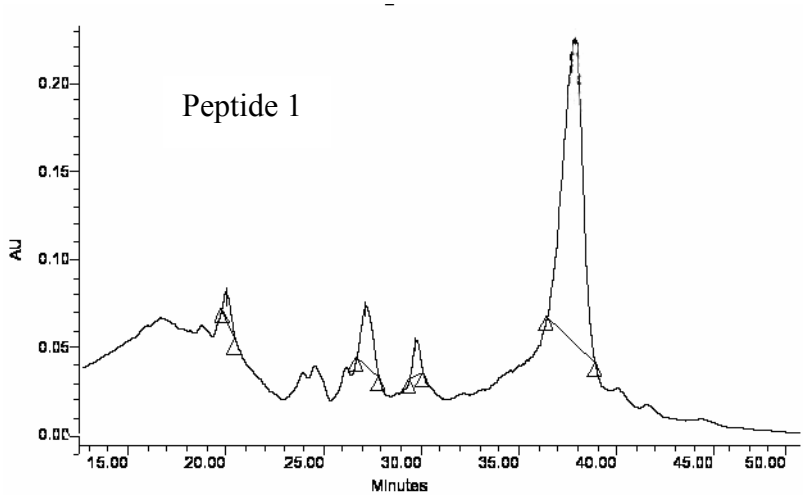
Peptide 1
AU
Minutes

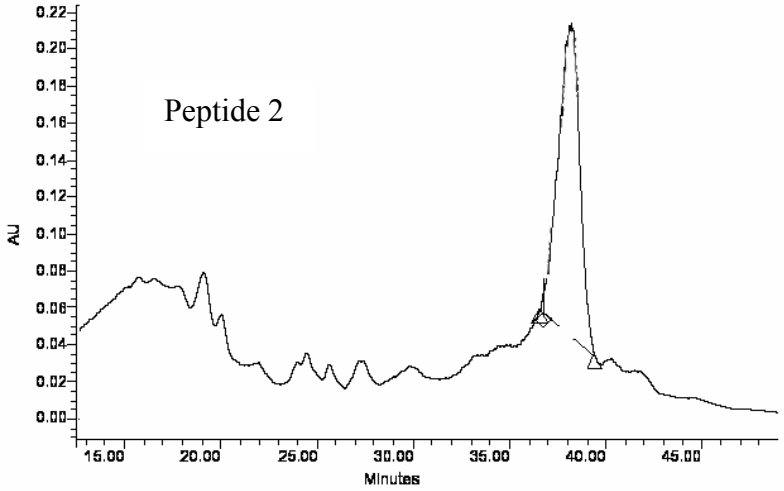
Peptide 2
AU
Minutes

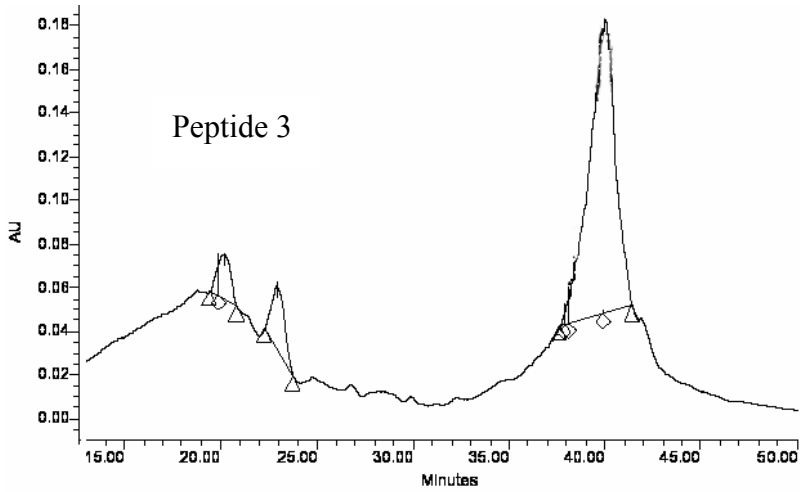
Peptide 3
AU
Minutes

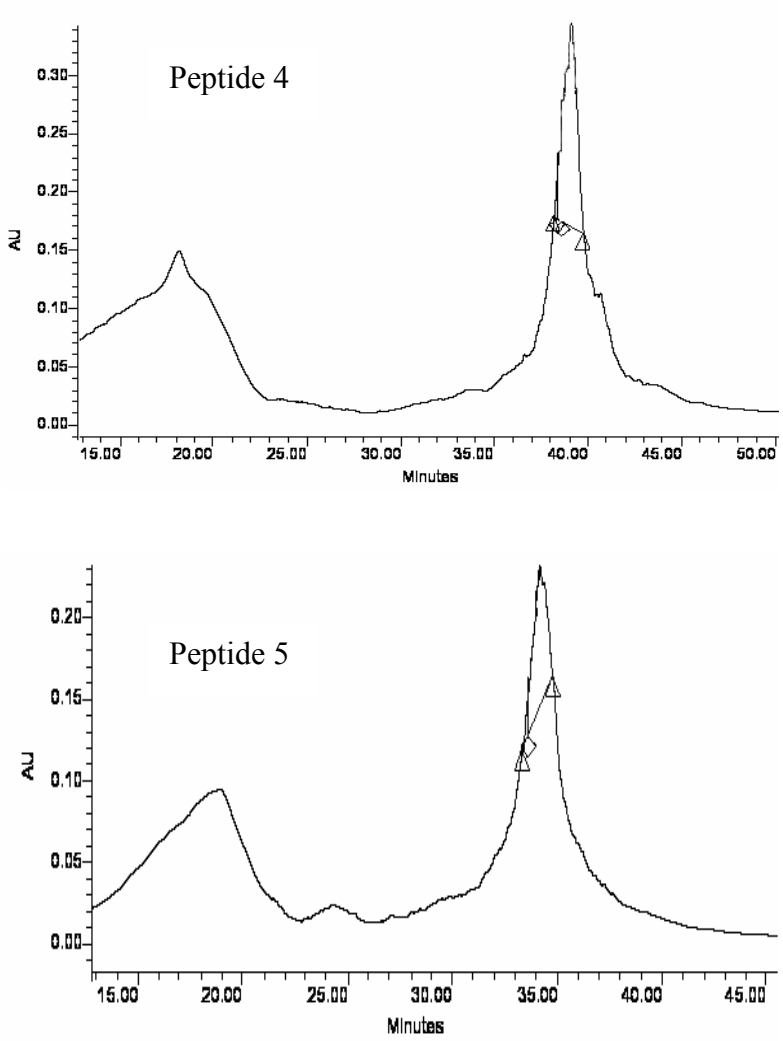

Figure 87—cont. Crude HPLC data for the HR-2 peptides listed in Figure 85 above. Peaks with largest area under the curve were confirmed to contain the desired peptides via MALDI-TOF.

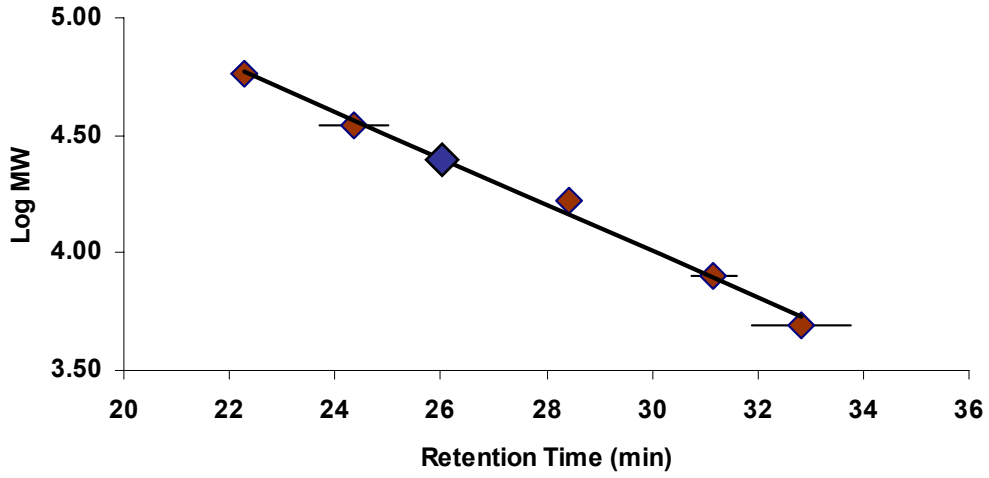

Figure 88. Size exclusion chromatography data (discussed in Chapter II) of the hMPV fusion core following a freeze/thaw cycle of the HR peptide mixture. The polymeric weight standards are shown in brown, and the fusion core sample is purple.

APPENDIX B

SELECTED PEPTIDE LIBRARY

The following library of overlapping 15-mers is being used to elicit immune system response. The resulting data set will produce a linear epitope map of the human metapneumovirus F protein. The crude peptides were synthesized and collected as described on page 73. Purification was performed on a 20 mL Sephadex G-15 column. Highlighted sequences were purified on a Waters C_{18} HPLC system with degassed solvents to avoid intramolecular disulfide bond formation. Identities were confirmed by MALDI-TOF.

Table 8. Linear peptides currently being evaluated to produce a linear epitope map of the hMPV F protein.

M	S	W	K	V	V	I	I	F	S	L	L	I	T	P
K	V	V	I	I	F	S	L	L	I	T	P	Q	H	G
I	I	F	S	L	L	I	T	P	Q	H	G	L	K	E
S	L	L	I	T	P	Q	H	G	L	K	E	S	Y	L
I	T	P	Q	H	G	L	K	E	S	Y	L	E	E	S
Q	H	G	L	K	E	S	Y	L	E	E	S	C	S	T
L	K	E	S	Y	L	E	E	S	C	S	T	I	T	E
S	Y	L	E	E	S	C	S	T	I	T	E	G	Y	L
E	E	S	C	S	T	I	T	E	G	Y	L	S	V	L
C	S	T	I	T	E	G	Y	L	S	V	L	R	T	G
I	T	E	G	Y	L	S	V	L	R	T	G	W	Y	T
G	Y	L	S	V	L	R	T	G	W	Y	T	N	V	F
S	V	L	R	T	G	W	Y	T	N	V	F	T	L	E
R	T	G	W	Y	T	N	V	F	T	L	E	V	G	D
W	Y	T	N	V	F	T	L	E	V	G	D	V	E	N
N	V	F	T	L	E	V	G	D	V	E	N	L	T	C
T	L	E	V	G	D	V	E	N	L	T	C	A	D	G
V	G	D	V	E	N	L	T	C	A	D	G	P	S	L
V	E	N	L	T	C	A	D	G	P	S	L	I	K	T
L	T	C	A	D	G	P	S	L	I	K	T	E	L	D
A	D	G	P	S	L	I	K	T	E	L	D	L	T	K
P	S	L	I	K	T	E	L	D	L	T	K	S	A	L
I	K	T	E	L	D	L	T	K	S	A	L	R	E	L
E	L	D	L	T	K	S	A	L	R	E	L	R	T	V
L	T	K	S	A	L	R	E	L	R	T	V	S	A	D
S	A	L	R	E	L	R	T	V	S	A	D	Q	L	A

R E L R T V S A D Q L A R E E
R T V S A D Q L A R E E Q I E
S A D Q L A R E E Q I E N P R
Q L A R E E Q I E N P R Q S R
R E E Q I E N P R Q S R F V L
Q I E N P R Q S R F V L G A I
N P R Q S R F V L G A I A L G
Q S R F V L G A I A L G V A T
F V L G A I A L G V A T A A A
G A I A L G V A T A A A V T A
A L G V A T A A A V T A G V A
V A T A A A V T A G V A I A K
A A A V T A G V A I A K T I R
V T A G V A I A K T I R L E S
G V A I A K T I R L E S E V T
I A K T I R L E S E V T A I K
T I R L E S E V T A I K N A L
L E S E V T A I K N A L K K T
E V T A I K N A L K K T N E A
A I K N A L K K T N E A V S T
N A L K K T N E A V S T L G N
K K T N E A V S T L G N G V R
N E A V S T L G N G V R V L A
V S T L G N G V R V L A T A V
L G N G V R V L A T A V R E L
G V R V L A T A V R E L K D F
V L A T A V R E L K D F V S K
T A V R E L K D F V S K N L T
R E L K D F V S K N L T R A I
K D F V S K N L T R A I N K N
V S K N L T R A I N K N K C D
N L T R A I N K N K C D I A D
R A I N K N K C D I A D L K M
N K N K C D I A D L K M A V S
K C D I A D L K M A V S F S Q
I A D L K M A V S F S Q F N R
L K M A V S F S Q F N R R F L
A V S F S Q F N R R F L N V V
F S Q F N R R F L N V V R Q F
F N R R F L N V V R Q F S D N
R F L N V V R Q F S D N A G I
N V V R Q F S D N A G I T P A

R Q F S D N A G I T P A I S L
S D N A G I T P A I S L D L M
A G I T P A I S L D L M T D A
T P A I S L D L M T D A E L A
I S L D L M T D A E L A R A V
D L M T D A E L A R A V S N M
T D A E L A R A V S N M P T S
E L A R A V S N M P T S A G Q
R A V S N M P T S A G Q I K L
S N M P T S A G Q I K L M L E
P T S A G Q I K L M L E N R A
A G Q I K L M L E N R A M V R
I K L M L E N R A M V R R K G
M L E N R A M V R R K G F G F
N R A M V R R K G F G F L I G
M V R R K G F G F L I G V Y G
R K G F G F L I G V Y G S S V
F G F L I G V Y G S S V I Y M
L I G V Y G S S V I Y M V Q L
V Y G S S V I Y M V Q L P I F
S S V I Y M V Q L P I F G V I
I Y M V Q L P I F G V I D T P
V Q L P I F G V I D T P C W I
P I F G V I D T P C W I V K A
G V I D T P C W I V K A A P S
D T P C W I V K A A P S C S G
C W I V K A A P S C S G K K G
V K A A P S C S G K K G N Y A
A P S C S G K K G N Y A C L L
C S G K K G N Y A C L L R E D
K K G N Y A C L L R E D Q G W
N Y A C L L R E D Q G W Y C Q
C L L R E D Q G W Y C Q N A G
R E D Q G W Y C Q N A G S T V
Q G W Y C Q N A G S T V Y Y P
Y C Q N A G S T V Y Y P N E K
N A G S T V Y Y P N E K D C E
S T V Y Y P N E K D C E T R G
Y Y P N E K D C E T R G D H V
N E K D C E T R G D H V F C D
D C E T R G D H V F C D T A A
T R G D H V F C D T A A G I N
D H V F C D T A A G I N V A E

F C D T A A G I N V A E Q S K
T A A G I N V A E Q S K E C N
G I N V A E Q S K E C N I N I
V A E Q S K E C N I N I S T T
Q S K E C N I N I S T T N Y P
E C N I N I S T T N Y P C K V
I N I S T T N Y P C K V S T G
S T T N Y P C K V S T G R H P
N Y P C K V S T G R H P I S M
C K V S T G R H P I S M V A L
S T G R H P I S M V A L S P L
R H P I S M V A L S P L G A L
I S M V A L S P L G A L V A C
V A L S P L G A L V A C Y K G
S P L G A L V A C Y K G V S C
G A L V A C Y K G V S C S I G
V A C Y K G V S C S I G S N R
Y K G V S C S I G S N R V G I
V S C S I G S N R V G I I K Q
S I G S N R V G I I K Q L N K
S N R V G I I K Q L N K G C S
V G I I K Q L N K G C S Y I T
I K Q L N K G C S Y I T N Q D
L N K G C S Y I T N Q D A D T
G C S Y I T N Q D A D T V T I
Y I T N Q D A D T V T I D N T
N Q D A D T V T I D N T V Y Q
A D T V T I D N T V Y Q L S K
V T I D N T V Y Q L S K V E G
D N T V Y Q L S K V E G E Q H
V Y Q L S K V E G E Q H V I K
L S K V E G E Q H V I K G R P
V E G E Q H V I K G R P V S S
E Q H V I K G R P V S S S F D
V I K G R P V S S S F D P V K
G R P V S S S F D P V K F P E
V S S S F D P V K F P E D Q F
S F D P V K F P E D Q F N V A
P V K F P E D Q F N V A L D Q
F P E D Q F N V A L D Q V F E
D Q F N V A L D Q V F E S I E
N V A L D Q V F E S I E N S Q
L D Q V F E S I E N S Q A L V

V F E S I E N S Q A L V D Q S
S I E N S Q A L V D Q S N R I
N S Q A L V D Q S N R I L S S
A L V D Q S N R I L S S A E K
D Q S N R I L S S A E K G N T
N R I L S S A E K G N T G F I
L S S A E K G N T G F I I V I
A E K G N T G F I I V I I L I
L I A V L G S T M I L V S V F
V L G S T M I L V S V F I I I
S T M I L V S V F I I I K K T
I L V S V F I I I K K T K K P
S V F I I I K K T K K P T G A
I I I K K T K K P T G A P P E
K K T K K P T G A P P E L S G
K K P T G A P P E L S G V T N
T G A P P E L S G V T N N G F
P P E L S G V T N N G F I P H N

APPENDIX C

NUCLEAR MAGNETIC RESONANCE SPECTRA OF ROOM TEMPERATURE IONIC LIQUIDS

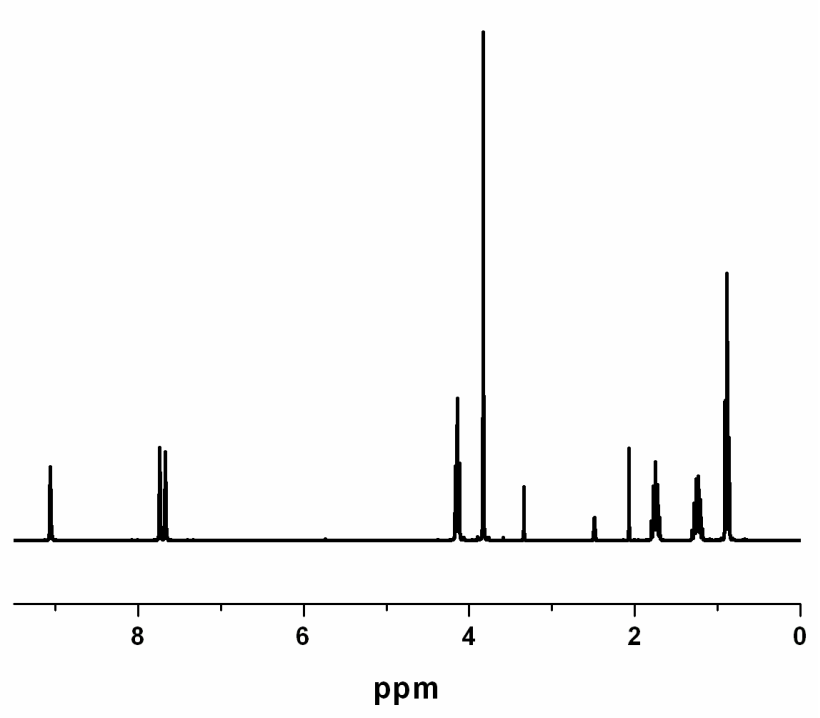

Figure 89. 1H NMR spectrum of [BMIM]BF_4

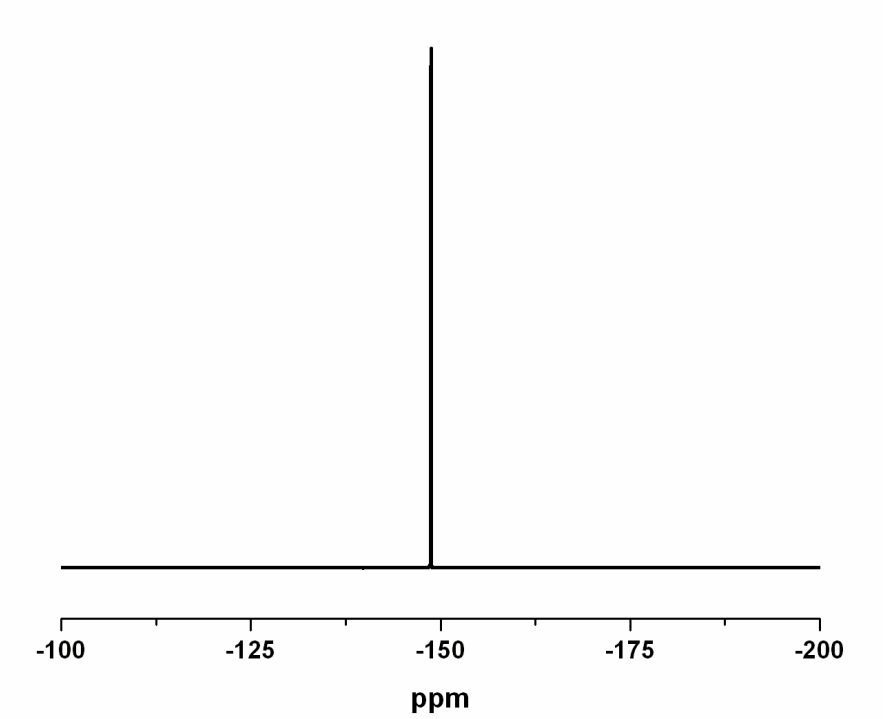

Figure 90. 19F NMR spectrum of [BMIM]BF_4

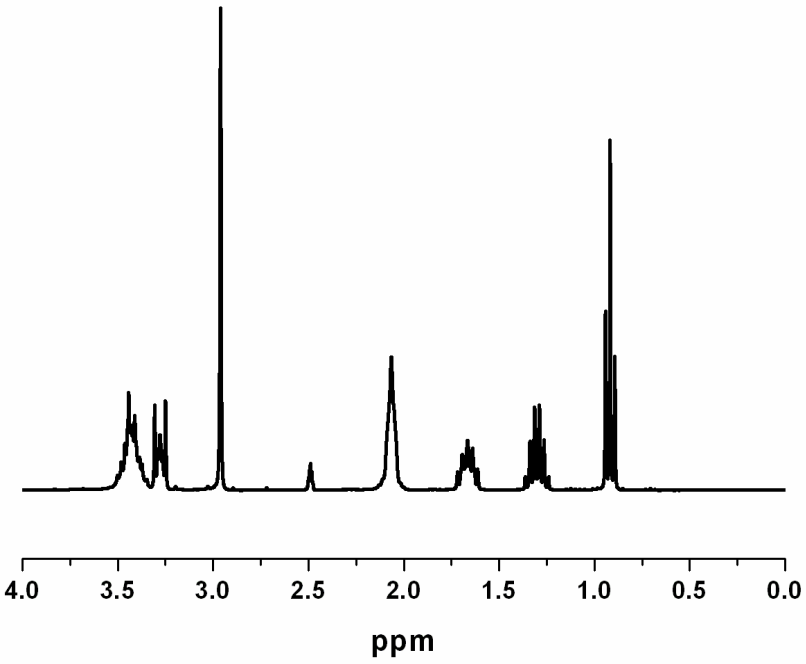

Figure 91. 1H NMR spectrum of [BMPY]OTF

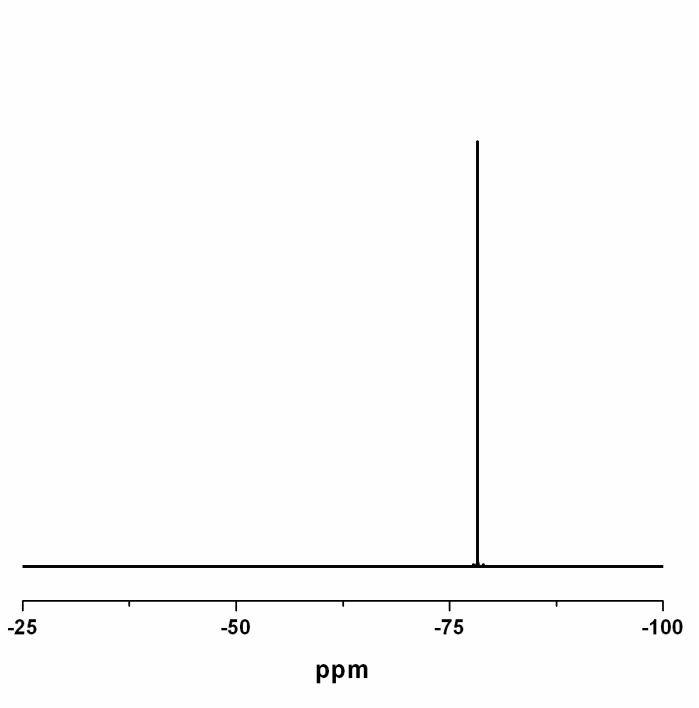

Figure 92. 19F NMR spectrum of [BMPY]OTF

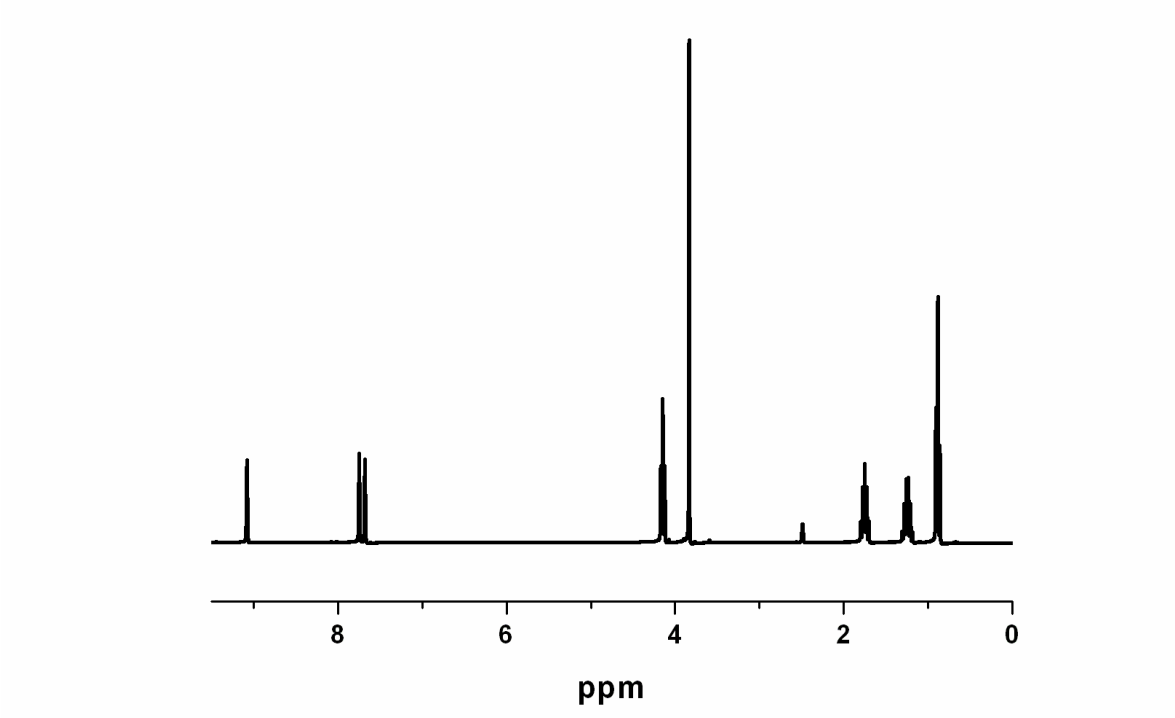

Figure 93. 1H NMR spectrum of [BMIM]OTF

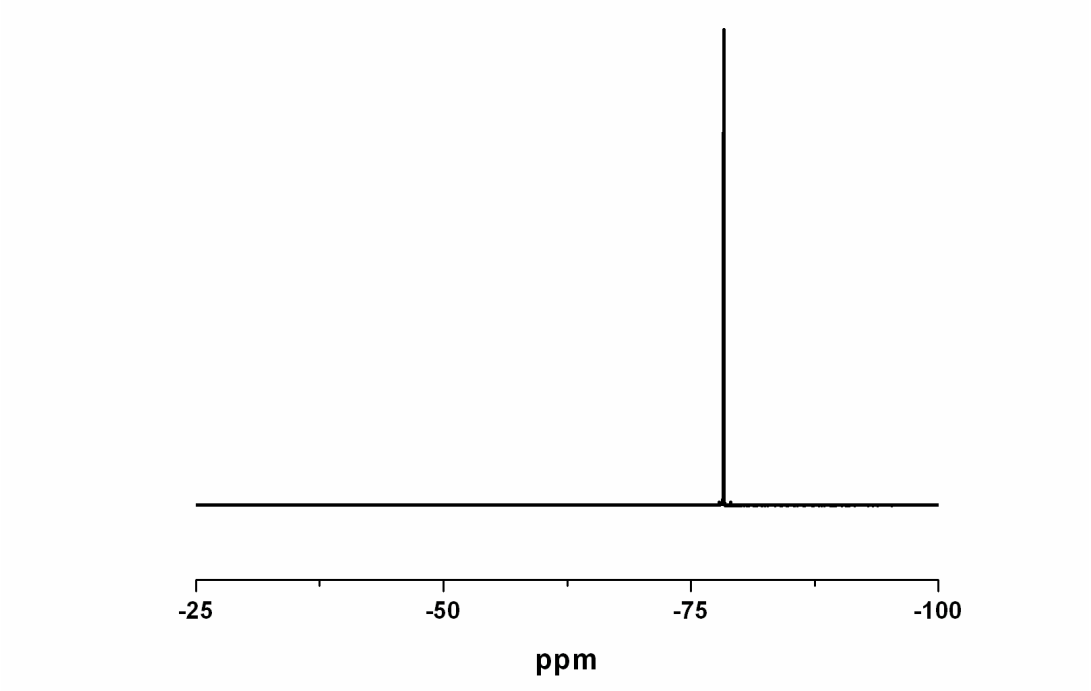

Figure 94. 19F NMR spectrum of [BMIM]OTF

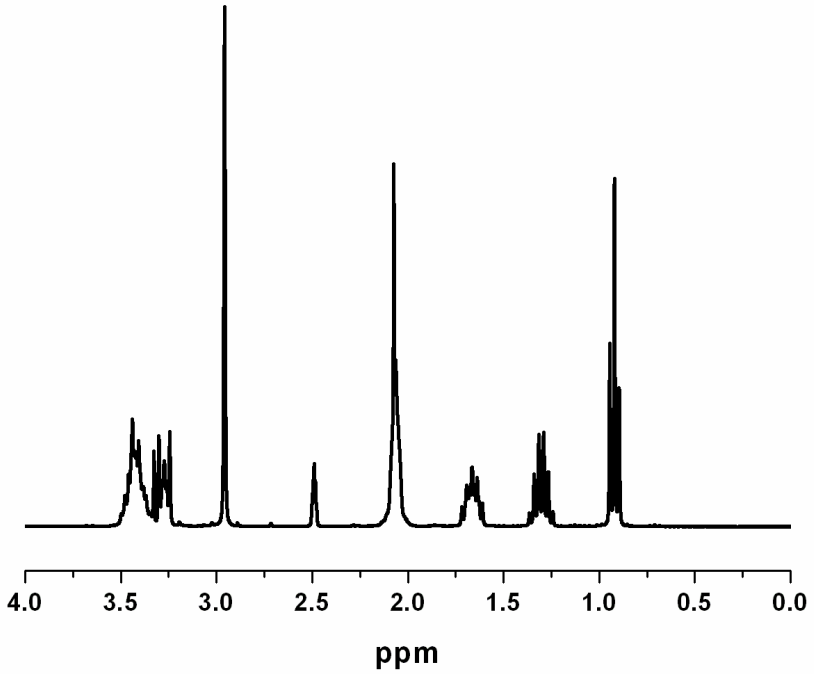

Figure 95. 1H NMR spectrum of [BMPY]N(Tf)$_2$

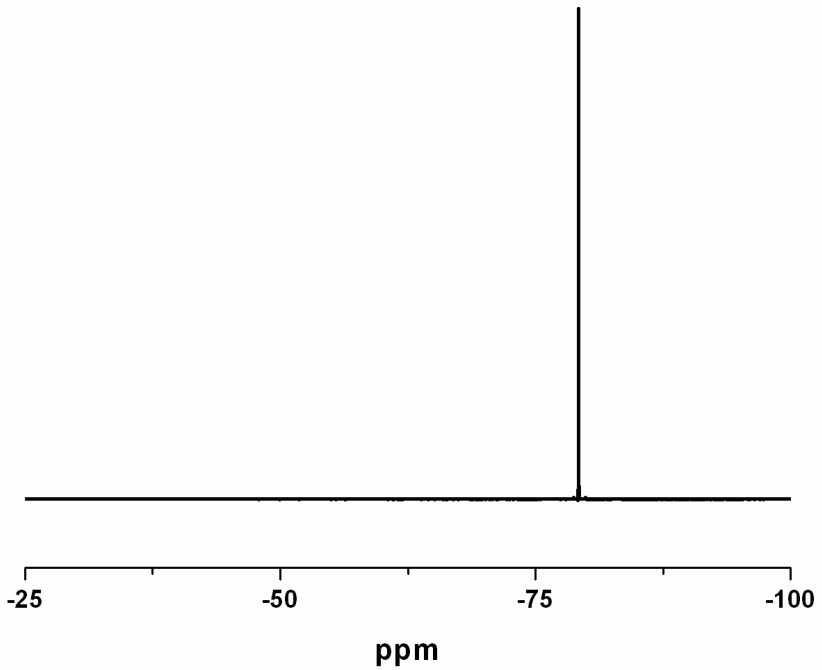

Figure 96. 19F NMR spectrum of [BMPY]N(Tf)$_2$

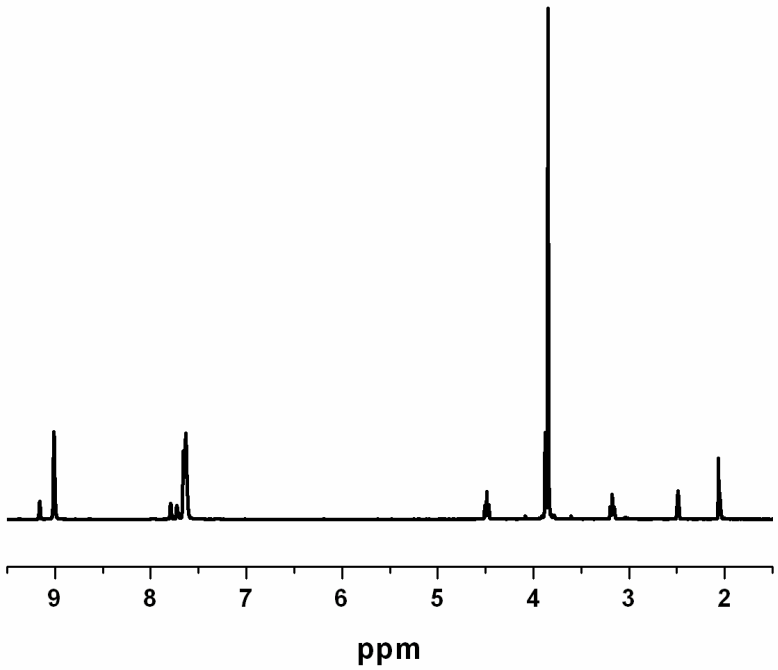

Figure 97. 1H NMR spectrum of [EMIMCN]N(Tf)$_2$

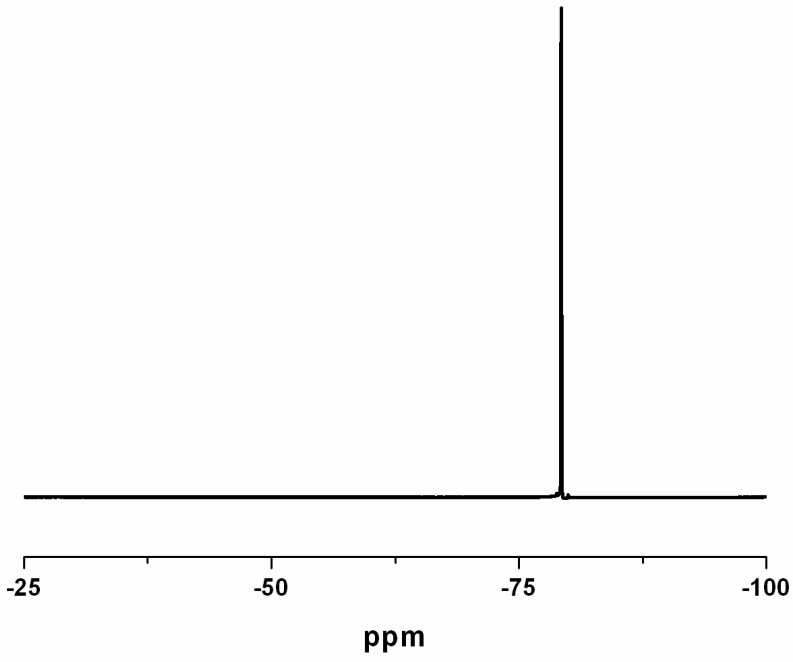

Figure 98. 19F NMR spectrum of [EMIMCN]N(Tf)$_2$

APPENDIX D

CUSTOM RESIN AND SELECTED CUSTOM PEPTIDES

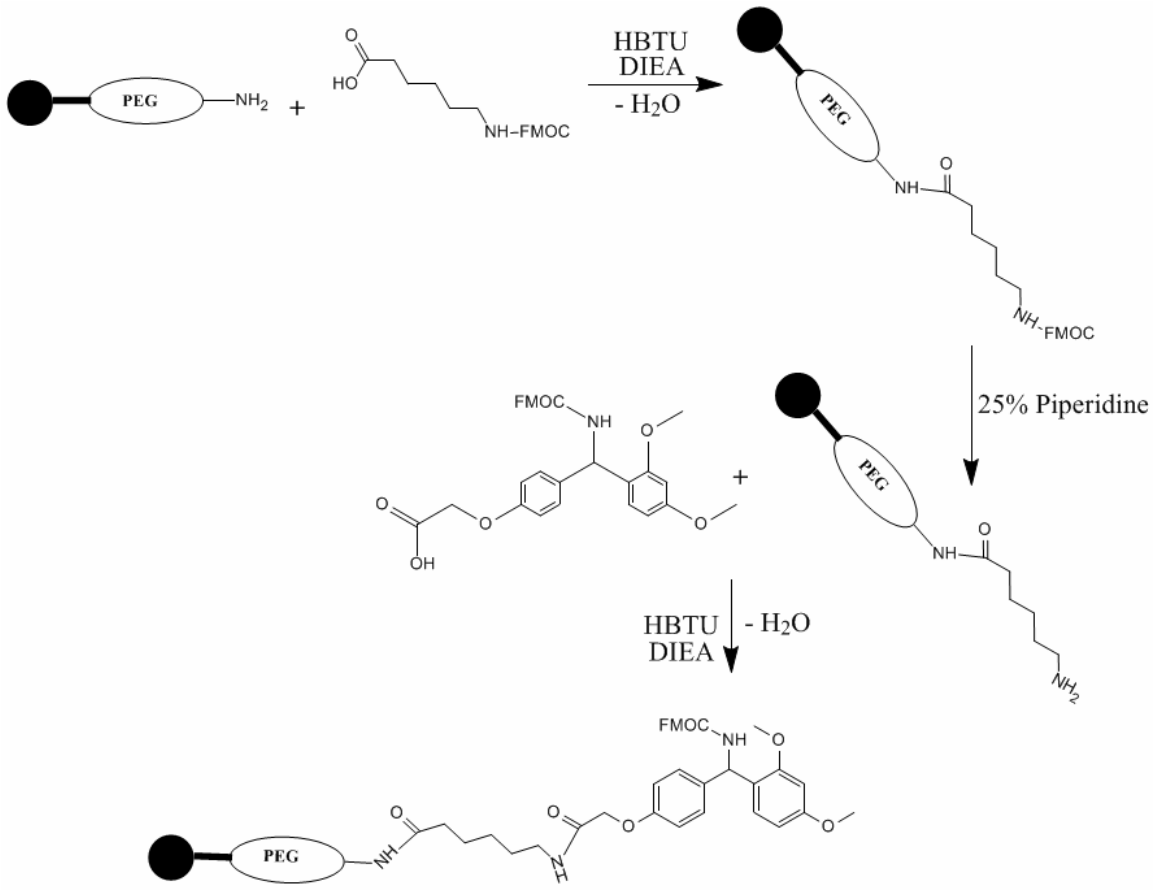

Figure 99. Synthetic scheme used to produce the custom resin utilized during HR peptide synthesis. Briefly, 6-(amino)-caproic acid (Sigma) was coupled to tentagel resin (Synpep). FMOC was removed by the use of piperidine. The Knorr linker (4-[(2, 4-Dimethoxyphenyl)(FMOC-amino)methyl]-Phenoxyacetic Acid; Advanced Chemtech) was coupled to the resin to produce final amidated peptides. Note: 33A and HR-1 43-mer from Chapter II substituted a 2-chlorotrityl linker (Advanced Chemtech) in place of the Knorr linker to produce carboxy terminal peptides.

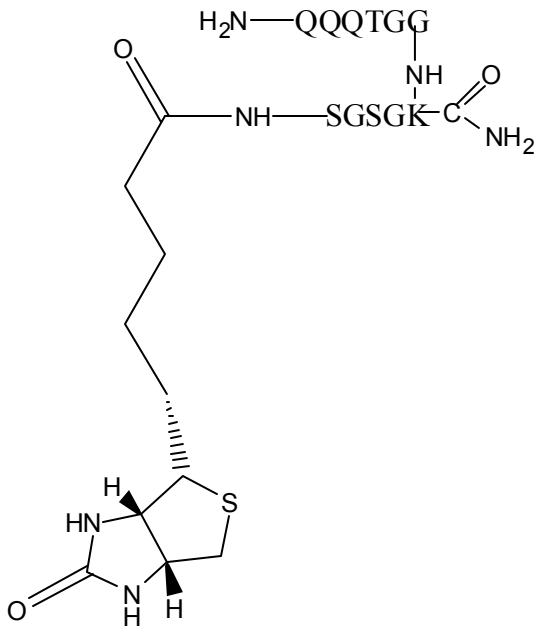

Figure 100. Custom peptide created at the request of Dr. Daniel Liebler.

Briefly, the peptide **(Figure 100)** was synthesized on Rink Amide MBHA resin (Anaspec) and needed to be ≥ 95% pure. SGSGK was created with K having the sidechain amine protected with a trityl protecting group. The final FMOC was removed as described in Chapters I and Chapter II. D-biotin (Anaspec) was added via a standard HBTU, DIEA, and HOBT coupling with a 24 hour mixing time. The trityl group on K was then removed with a 3 minute exposure to 3% trifluoroacetic acid in dichloromethane. Additional residues were coupled sequentially to the K sidechain amine by standard chain elongation protocols. The final Q contained an N-terminal benzyloxycarbonyl (Cbz) protecting group. The Z group was inserted to avoid pyroglutamate formation of the N-terminal Q during acidylosis. The peptide was collected as described in Chapter II and purified via HPLC. The Z group was then removed via hydrogenation catalyzed by 10% palladium on carbon in an aqueous

medium. The mixture was filtered and purified via HPLC to produce ≥ 95% pure product as confirmed by MALDI-TOF.

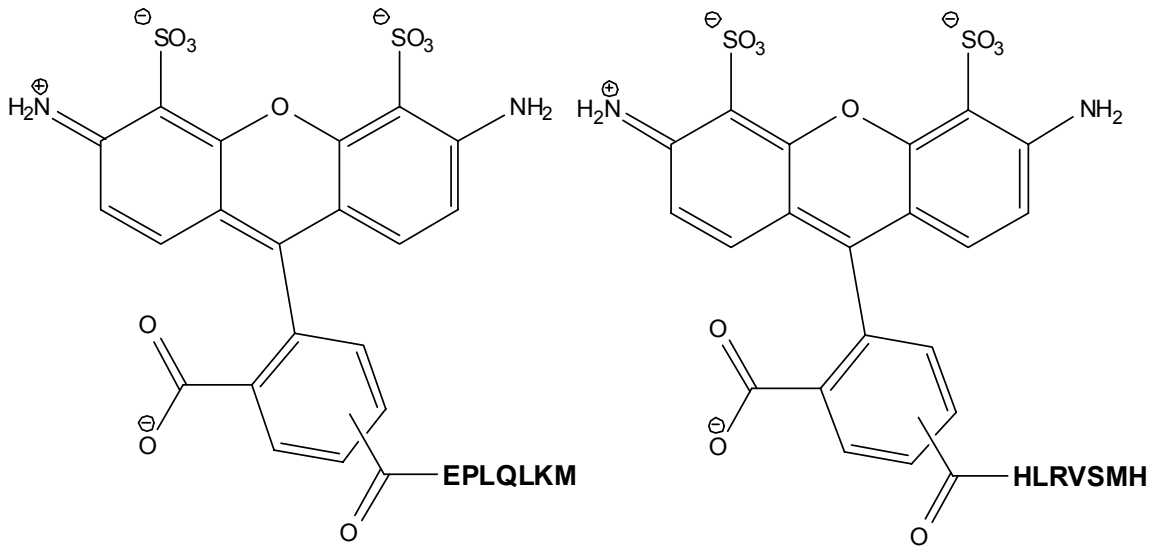

Figure 101. Custom peptides produced at the request of Dr. Todd Giorgio.

Peptides **(Figure 101)** were synthesized following normal protocols described in Chapter II. Following collection and purification, the peptides were dissolved in carbonate buffer (pH 9). Care was taken to avoid K sidechain adduction by carefully monitoring solution pH to allow for a greater concentration of N-terminal amines in a deprotonated neutral state (sidechain pKA ~ 10.3 and N-terminal amine pKA ~ 8.9). 1.5 equivalents of Alexa Fluor^{TM} 488 tetrafluorophenyl ester (Molecular Probes, Inc.) were added to the individual peptide solutions. The reaction was allowed 4 hours to react. Final purification was then performed via HPLC. The desired peptides gave off an intense green color by visual inspection. The green color turned to light red during the freezing of the peptide solutions. Final products were confirmed via MALDI-TOF analysis.

APPENDIX E

CURRICULUM VITA

Scott A. Miller

Research Associate
Vanderbilt University
Scott.A.Miller.1@Vanderbilt.edu

331 Bridgewalk Place
Nashville, TN 37209
Phone: (615) 293-8177

Citizenship: US

Department of Chemistry
Vanderbilt University
7370 Stevenson Center
Nashville, TN 37235
Phone: (615) 322-5516
Fax: (615) 343-1234

Employment Goal

Expand and apply expertise in chemical biology in the development of novel materials, drug design, and drug delivery.

Education and Experience

Education

Ph.D. Chemistry, Vanderbilt University, Nashville, TN, May 2006
B.S. Chemistry, University of South Alabama, Mobile, AL, 2001

Additional Training

Biohazard Level 2 Training
Sterile Technique in Cell Culturing
Radiation Safety

Related Experience

Instructor for General Chemistry Laboratory
Supervisor and Trainer of Undergraduate Researchers
Organic Chemistry Tutor
Undergraduate researcher maintaining cell cultures and radio-labeling proteins

Instrumentation Experience

- Advanced Chemtech Apex 396 and Model 90 Peptide Synthesizers
- Mattson Research Series FTIR
- Agilent UV-Vis
- Waters Analytical and Semi-Prep HPLC Systems
- Insight II, MOE, Amber 7, and MultiAlign computer software packages
- Applied Biosystems Voyager MALDI-TOF
- Aviv Model 215 Circular Dichroism Spectrophotometer
- Bruker 300, 400, and 500 NMR instruments
- Biotek Synergy Fluorometer

Doctorial Thesis

Peptides and Proteins: Anti-Virals to Novel Materials

Brief Description of Doctoral Work: The fusion protein of the recently discovered human metapneumovirus was shown to be a homolog of previously characterized type I integral membrane fusion proteins. Computer models were generated to study structural aspects of the fusion protein and identify potential antagonists. Synthetic peptides from the heptad repeat regions were also shown to possess anti-viral activity. The synthesis of several hundred peptides for collaborative endeavors and the 'difficult' sequences of the heptad repeat regions led to the study of ionic liquids as potential solvents to address aggregation and other synthetic hurdles currently cleared by expensive and labor intensive methods. Concurrently, new biologically active materials comprised of functional enzymes encapsulated in SiO_2 were synthesized and characterized with an eye towards these novel materials being used as synthetic reagents.

Research Interests

Developing methods to improve peptides as possible materials, drugs, drug delivery, and tools for protein structure/function elucidation

- Improving methods of synthesis for 'difficult' peptide sequences
- Modifying amino acid sidechains and termini to offer useful properties for drug and materials research and deliver
- Designing peptide and small molecule anti-viral and anti-cancer agents

Development of Novel Biologically and Chemically Active Materials

- Designing clinical diagnostic devices
- Improving stability and adding functionality to novel biologically active materials

Publications

Doctoral Dissertation

Peptides and Proteins: Anti-Virals to Novel Materials

Refereed Articles

Geoffrey H. Chew, Lamar C. Galloway, Neil R. McIntyre, Laura Aaron Schroder Karla M. Richards, **Scott A. Miller**, David W. Wright, David J. Merkler **"Ubiquitin and Ubiquitin-Derived Peptides as Substrates for Peptidylglycine α-Amidating Monooxygenase";** *FEBS Letters* (2005), 579(21) 4678-4684

Scott A. Miller and David W Wright "**Dendrimer Nanocomposite Materials";** *Polymer News* (accepted)

Miller, Scott A., Hong, Edmund, & D. Wright, David.W. (2005) "**Rapid and Efficient Enzyme Encapsulation in a Dendrimer Silica Nanocomposite";** (submitted to *Langmuir*)

"**The Human Metapneumovirus Fusion Protein Mediates Fusion Through a Coiled-Coil Complex That Can Be Inhibited By Potent Synthetic Heptad Repeat Region 1 Peptides**"; (submitted to *The Journal of Biological Chemistry*)

"**Relative Affinities of Neutral Ligands for CpRu(Ph2(CH2)nPPh2))+ Determined by IR Multiphoton Dissociation FT-ICR Mass Spectrometry**"; (to be submitted to *Inorganic Chemistry*)

"**Determination of Relative Binding Strengths of Isosteric p-Benzoate Anions for trans-Rh(PPh3)2(CO)+ via the Rh-NCS/Rh-O2C(p-benzoate) Equilibrium**"; (to be submitted to *Organometallics*)

"**Determination of Relative Binding Strengths of Aliphatic and Substituted Aliphatic Carboxylate Anions for trans-Rh(PPh3)2(CO)+ via the Rh-NCS/Rh-O2C(carboxylate) Equilibrium**"; (to be submitted to *Organometallics*)

Public Talks and Presentations at Meetings

Principal Presenter

"Relative Affinities of Carboxylate Anions for *trans*-$Rh(PPh_3)_2(CO)^+$ Measured by Metathesis Equilibrium with Isothiocyanate Ion," American Chemical Society National Meeting, New Orleans, Aug. 1999 (presented by Scott A. Miller)

"Relative Affinities of Carboxylate Anions for *trans*-$Rh(PPh_3)_2(CO)^+$ Determined Quantitatively via Metathesis Equilibrium with Isothiocyanate Ion," American Chemical Society National Meeting, San Francisco, CA, Mar. 2000 (presented by Scott A. Miller)

"Characterization of A New Paramyxovirus Fusion Protein via Models and Synthetic Peptides," Southeast Regional Meeting of the American Chemical Society, Atlanta, Nov. 2003 (presented by Scott A. Miller)

"Rapid and Efficient Enzyme Encapsulation in a Dendrimer Silica Nanocomposite," Southeast Regional Meeting of the American Chemical Society, Memphis, Nov. 2005 (presented by Scott A. Miller)

Contributed

"Molecular Modeling & Crystal Structures of Rhodium (I) Vaska Complexes of Tricyclohexylphosphine and Other Bulky Phosphines," American Chemical Society National Meeting, Dallas, Mar. 1998

"Steric Interactions in *trans*-$Rh(PR_3)_2(CO)O_2CCR$ Modeled by Semi-Empirical Methods," Southeastern Theoretical Chemistry Association Meeting, Memphis, TN, Mar. 1999

"Determination of Relative Activation Energy for Metal-Ligand Bond Breaking by IR Multiphoton Dissociation Mass Spectrometry," American Society of Mass Spectroscopists, Nashville, TN, May 2004.

"Relative Activation Energies for Metal-Nitrile Bond Breaking in $CpRu(dppn)(NCR)^+$ via IR Multiphoton-Dissociation Mass Spectrometry," Gordon Research Conf. on Organometallic Chemistry, Newport, RI, July 2004.

"Ligand Affinity for Ru(II) by IR Multiphoton Dissociation FT-ICR Mass Spectrometry," ACS National Meeting, San Diego, CA, Apr. 2005.

"Effect of Bite Angle in Cyclopentadienyl-Diphosphine Ruthenium Complexes on Binding Neutral Ligands," ACS National Meeting, San Diego, CA, Apr. 2005.

"Ligand Affinity for Ru(II) Determined by IR Multiphoton Dissociation FT-ICR Mass Spectrometry," 5th North American FT-ICR MS Conference, Key West, FL Apr. 2005.

"Steric Interactions in Square-Planar Rhodium(I) Complexes Containing Bulky Triorganophosphines," Southeastern Theoretical Chemistry Association Meeting, Memphis, TN, Mar. 1999

"Semiempirical Modeling & Crystal Structures of Rhodium (I) Vaska Complexes with Bulky Phosphines," American Chemical Society National Meeting, New Orleans, Aug. 1999

"Intramolecular Oxidative Addition of the Carbon-Halogen Bond in Rh(I) Vaska *o*-Halobenzoates," American Chemical Society National Meeting, San Diego, CA, Apr. 2001

"^{19}F NMR Reporter Ligands in Anion-Metathesis Equilibrium Studies of Rh(I) Systems," American Chemical Society National Meeting, Washington, DC, Aug. 2000